Microscale Bioprocessing Platform for the Evaluation of Membrane Filtration Processes for Primary Recovery

A thesis submitted to

University College London

for the degree of

Doctor of Philosophy

by

Andrea Chielou May Elumbaring Rayat

Department of Biochemical Engineering
University College London
Torrington Place
London WC1E 7JE

Declaration

'I, Andrea Chielou May Elumbaring Rayat, confirm that the work presented in this thesis is my own. Where information has been derived from other sources, I confirm that this has been indicated in the thesis.'

Signed 25th August 2011

Abstract

An automated microscale bioprocessing platform for membrane filtration processes was established to identify key process issues early and aid the rapid design of robust and scaleable filtration processes. To demonstrate the utility of this platform, it was used to investigate the impact of upstream operations on microfiltration performance. The primary recovery of humanised antibody Fab' fragments from *Escherichia coli* (supplied courtesy of UCB Celltech) were used as a case study to evaluate the microfiltration methodologies and devices created in this work.

Initially, the methodology associated with the microscale dead-end filtration device previously created and investigated by Jackson et al. (2006) has been improved by reducing the required volume by 50% (~500 μL). This improved method demonstrated reproducibility and sensitivity to changes in feed preparation. The method was then applied in the study of the influence of various cell disruption operations on subsequent solid-liquid separation and hence, Fab' product recovery. Results showed that the heat extracted cells showed better dead-end microfiltration performance in terms of permeate flux and specific cake resistance. In contrast, the cell suspensions prepared by homogenisation and sonication showed more efficient product release but with lower product purity and poorer microfiltration performance. Having established the various microscale methods, the linked sequence was automated on the deck of the Tecan™ robotic platform and used to illustrate how different conditions during thermo-chemical extraction impacted on the optimal performance of the linked unit operations of product release by extraction and subsequent recovery by microfiltration.

The microscale approach was then extended for crossflow operations. A microscale crossflow filtration device was designed to enable integration also within the Tecan™ platform for automated processing. The device has an effective membrane area of 0.001 m^2, which is a hundred-fold smaller than the larger scale Pellicon-2™ membrane module used for scale translation studies, and has two independent membrane channels for parallel analysis. The device was first characterised by determining the normalised water permeability (NWP) of a Poly(vinylidene fluoride) membrane and compared this with the NWP of the membrane by dead-end filtration. NWP is an inherent membrane property and as expected, the NWP values derived from crossflow filtration experiments match the values derived from dead-end filtration to within 90%. For scale translation studies, two types of feeds were used: a model feed, which is resuspended active dry yeast and Bovine Serum Albumen in phosphate buffer, and the antibody fragment expressing *E. coli* strain. Results showed, that at matched optimal shear rates and transmembrane pressure, the percentage differences between microscale and large scale values were up to ± 25% for the permeate flux, ± 10% for Fab' and total protein yields. These scale-up predictions were achieved with a ten-fold reduction in feed material requirement for crossflow operation.

Overall, the results illustrate the power of microscale techniques to identify and enable the understanding of key process performance attributes in a bioprocess sequence. The broader implications derived from using these microscale membrane devices, further applications and recommendations for future research are also discussed.

Acknowledgement

I sincerely thank my supervisor, Prof. Gary J Lye, for his tremendous support and guidance in relation to my PhD work and to my stay here in the UK as a foreign student. He has given me the freedom to seek and carry out things on my own, and yet has not faltered in mentoring, encouraging or in providing me a sense of direction when needed. I am grateful to my advisor, Dr. Martina Micheletti, for her all her help and advice on how to organise my research, and in particular, for her expert opinion on fluid flow. It was a real pleasure to be under their tutelage, from which I have drawn inspiration to aspire to do things well and also share the same with others.

This thesis, in general, was an independent endeavour. However, I am obliged to many people who have shared their time through training, conceptual input, assistance in certain areas of the experimental work or even just by making the curious life of a PhD student much more interesting. In this regard, I would like to especially mention the following people: Dr. Simyee Kong, Dr. Jean Aucamp, Dr. Bangaru Balasundaram, Alan Craig, Dr. Gareth Manall, Dr. Yuhong Zhou, Dr. Diana Hernandez, Dr. Steven Branston, Nigel Jackson, Andrew Brown, Wasim Domah, Guijun Ma, Paul Beckett, Razwan Hanif, Affaro Affandy, Alisa Wong, Shahina Ahmad, Alison Tang, Claire Burden, Pat Morris and Adriana Lopes.

I am grateful to Dhushy Stanislaus, Technical Manager, and my colleagues in the automation lab, Dr. Naveraj Gill and Jasmin Baboo, for sustaining the efficiency of the lab where most of the experimental work in this thesis was performed.

My attendance here at UCL Biochemical Engineering would not have been possible if not for the financial support of the then Overseas Research Students Award Scheme (ORSAS) and the department through an IMRC studentship. I am truly indebted and thankful for this support. Many thanks to Prof. Nigel Titchener-Hooker, Director of the IMRC programme, for endorsing my scholarship application four years ago and for the continued support and encouragement during my studies.

I very much appreciate the moral support, advice and confidence bestowed upon me by my colleagues and friends, especially Adriana, Andy, Pat, Farah, Vetja, Jason, Sheila, Rica, Bon, and Tara.

I have been blessed, as it has always been, by my family's kind support and constant understanding. I am grateful to my parents, Chito and Andrelina, my siblings, especially Cheryl Grace, and my in-laws.

Most of all, I am very thankful to my husband, Glenn, for always being there for me and our son, Gian. His steadfast love and support is my strength and comfort.

To

Glenn & Gian

In memory of Nanay Gulang

Table of Contents

Section

Abstract **3**

Acknowledgement **4**

Table of Contents **7**

List of Figures **13**

List of Tables **17**

Nomenclature **19**

Abbreviations **21**

1. Introduction **22**

1.1 Background and motivation of the project 22

1.2 Overview of biopharmaceutical product development 28

1.2.1 Biopharmaceuticals and the drug development process 28

1.2.2 Biopharmaceutical manufacturing process 32

1.3 Opportunities in biopharmaceutical manufacturing 35

1.3.1 Monoclonal antibody therapies 35

1.3.2 Emerging therapies: antibody fragments 37

1.3.3 Lean manufacturing and single-use systems 41

1.4 Membrane filtration for biopharmaceutical processes 42

1.4.1 System design and mode of operation 43

1.4.2 Theories and models of membrane filtration 46

1.4.2.1 Hagen-Poiseuille flow through a membrane pore: ideal flux 48

1.4.2.2 Flux modelling based on flow resistances 48

1.4.2.3 Theories of concentration polarisation 54

1.4.2.4 Application to biological materials recovery and purification 61

1.5 Overview of microscale (scale down) unit operations 63
1.6 Aims of the project 69

2. Materials and Methods 73
2.1 Materials 74
2.2 Pilot-scale production of antibody fragments 74
2.2.1 20 L Fermentation vessel 74
2.2.2 *E. coli* fed-batch fermentation 74
2.2.3 Cell harvest by laboratory scale centrifugation 75
2.2.4 Cell harvest by pilot scale centrifugation 75
2.2.5 Storage of cell paste 76
2.3 Methods for Fab' release 76
2.3.1 Fab' release by continuous homogenisation 76
2.3.2 Fab' release by batch homogenisation 76
2.3.3 Fab' release by thermo-chemical treatment 77
2.3.4 Fab' release by sonication 77
2.3.5 Fab' release by adaptive focused acoustics 78
2.4 Microwell automation platform: Tecan Genesis™ 78
2.5 Microscale dead-end microfiltration 79
2.5.1 Microscale dead-end filtration device 79
2.5.2 Water flux experiments by dead-end filtration 79
2.5.3 Microfiltration of disrupted *E. coli* cells 79
2.6 Laboratory scale crossflow filtration 82
2.6.1 Laboratory scale CFF module 82
2.6.2 Laboratory scale CFF operation 82
2.7 Microscale crossflow filtration 83
2.7.1 Microscale CFF device design 83
2.7.2 Microscale CFF operation 85
2.8 Quantification of filtration performance 87
2.8.1 Membrane resistance 87
2.8.2 Normalised water permeability 87
2.8.3 Membrane solids rejection 87
2.8.4 Transmission 88
2.8.5 Apparent transmission 88
2.9 Analytical methods 88
2.9.1 Quantification of biomass concentration (Dry cell weight) 88

2.9.2 Quantification of biomass concentration (Optical density) 89
2.9.3 Quantification of total protein concentration 89
2.9.4 Quantification of antibody Fab' fragment concentration 89
2.9.5 SDS PAGE analysis of proteins 90
2.9.6 DNA sample purification 90
2.9.7 DNA gel analysis 90
2.9.8 Nucleic acid quantification 91
2.10 Physical methods 91
2.10.1 Particle size measurement by laser diffraction 91
2.10.2 Viscosity measurement 92

3. Creation of an Improved Microscale Dead-end Filtration Methodology 93
3.1 Introduction and aims 93
3.2 Experimental approach 94
3.3 Results and discussion 96
3.3.1 Quantification of clean membrane resistance 96
3.3.2 Observations on calculated clean membrane resistances 105
3.3.3 Improved cake resistance quantification: (1) single plate method 105
3.3.4 Application of the single plate microscale filtration method 111
3.3.5 Improved cake resistance quantification: (2) steady-state method 112
3.3.6 Observations on actual R_m and α values of biological feeds 115
3.4 Conclusions 117

4. Evaluation of Microscale Filtration Methodology for Primary Recovery of Antibody Fragments 119
4.1 Introduction and aims 119
4.2 Experimental approach 122
4.3 Results and discussion 123
4.3.1 Impact of Fab' cell disruption technique on filtration performance 123
4.3.2 Impact of disruption conditions on Fab' recovery by microfiltration 130
4.3.2.1 Influence of cell concentration and extraction pH 130
4.3.2.2 Influence of extraction temperature and time 137
4.3.3 Impact of filtration conditions on Fab' recovery by 139

microfiltration
4.3.3.1 Influence of membrane material 142
4.3.3.2 Influence of transmembrane pressure 144
4.4 Conclusions 147

5. Design and Evaluation of a Novel Microscale Crossflow Filtration Device 148
5.1 Introduction and aims 148
5.2 Microscale CFF design criteria 151
5.3 Experimental approach 153
5.4 Results and discussion 155
5.4.1 Design considerations 155
5.4.2 Preliminary experiments 159
5.4.3 Steady state flux determination 162
5.4.4 Characterisation of the fluid dynamics in the membrane systems 168
5.4.5 Scale comparison of the crossflow microfiltration of Baker's yeast 172
5.5 Conclusions 175

6. Microscale Technology Evaluation of the Impact of DNA Hydrolysis on Primary Recovery Operations 176
6.1 Introduction and aims 176
6.1.1 Background microscale information 176
6.1.2 Selection of Fab' extraction method 177
6.1.3 DNA hydrolysis for process feedstock conditioning 178
6.1.4 Aim and specific objectives 179
6.2 Experimental approach 181
6.2.1 *E. coli* strains and ferementation 181
6.2.2 Fab' extraction and DNA digestion 181
6.2.3 Fab' recovery 183
6.2.3.1 Microscale dead-end microfiltration 183
6.2.3.2 Crossflow microfiltration 184
6.2.3.3 Pilot scale centrifugation 184
6.2.4 Characterisation of process streams 184
6.3 Results and discussion 185
6.3.1 DNA hydrolysis in homogenised *E. coli* strains 185
6.3.1.1 Effect of nuclease digestion on DNA fragments 185

6.3.1.2 Effect of process shear on DNA fragments 186
6.3.1.3 Influence of cell age on DNA hydrolysis 186
6.3.1.4 Influence of cell concentration on DNA hydrolysis 188
6.3.2 Impact of DNA hydrolysis on viscosity of *E. coli* homogenates 188
6.3.2.1 Effect of nuclease digestion on viscosity 188
6.3.2.2 Influence of cell age 189
6.3.2.3 Influence of cell concentration 193
6.3.3 Impact of DNA hydrolysis on Fab' and protein release 194
6.3.3.1 Influence of DNA digestion on Fab' release 194
6.3.3.2 Influence of cell age on Fab' release 194
6.3.3.3 Total protein content of E. coli homogenates 195
6.3.3.4 Fab' and HCP content of *E. coli* with co-expressed Staphylococcal nuclease 196
6.3.4 Comparison of microscale and large scale CFF performance 196
6.3.5 Microscale CFF study of *E. coli* homogenates: flux behaviour 199
6.3.5.1 Impact of DNA hydrolysis on flux 199
6.3.5.2 Impact of transmembrane pressure on flux 202
6.3.6 Microscale CFF study of *E. coli* homogenates: Fab' recovery 204
6.3.6.1 Impact of DNA hydrolysis on Fab' transmission 204
6.3.6.2 Impact of transmembrane pressure on Fab' transmission 205
6.3.7 Microscale CFF study of *E. coli* homogenates: total protein recovery 207
6.3.8 Microscale CFF study of *E. coli* homogenates: DNA removal 209
6.3.9 Comparison of clarification methods for *E. coli* Fab' homogenates 212
6.4 Conclusions 214

7. Conclusions and Future Work 217
7.1 Summary and overall conclusions 217
7.2 Broader implications and applications 220
7.2.1 Enabling whole bioprocess analysis 220
7.2.2 Enabling deeper understanding of microfiltration processes 222
7.3 Recommendations for future research 224

References **229**

Appendices **237**

Appendix 1.1 Fermentation profile during production of antibody Fab' fragments from *E.coli*. 237

Appendix 1.2 Sample Tecan Gemini™ program for the automated operation of the vacuum separator (Te-VacS) on the deck of the Tecan. 238

Appendix 1.3 Optical density measurements corresponding to dry cell and wet cell concentrations. 239

Appendix 1.4 Typical total protein calibration curve. 239

Appendix 1.5 Typical chromatograms of: (A) Fab' standard prepared by and according to Tustian (2008); (B) blank sample composed of the binding buffer 20 mM sodium phosphate at pH 7.4 ; and (C) Fab' lysate from thermo-chemical extraction. 240

Appendix 1.6 Typical calibration curve of the Fab' standard. 241

Appendix 1.7 Typical shear stress-shear rate curve showing a linear relationship (r^2>0.95) which depicts Newtonian fluid behaviour. 241

Appendix 2.1 Estimation of Pellicon-2™ dimensions 242

Appendix 2.2 Momentum balance to derive Equation 5.13 243

Appendix 3.1 Agarose gel showing the hydrolysis by Benzonase® of chromosomal DNAs in freeze-thawed homogenised (30% w/w) *E. Coli* cells 245

Appendix 3.2 Agarose gel showing the hydrolysis by Benzonase® of chromosomal DNAs in freeze-thawed homogenised (15% w/w) *E. Coli* cells 245

Appendix 3.3 An example of a shear stress-strain plot used as basis for determining absolute viscosities in Figure 6.4. 246

Appendix 3.4 Typical permeate flowrate data from lab-scale crossflow microfiltration experiments withSNase. 246

Appendix 3.5 Cumulative permeate data from microscale crossflow microfiltration experiments with SNase (Channel 2). 247

List of Figures

Figure Title		Page
Figure 1.1	Two-dimensional representation of bioprocess development	25
Figure 1.2	Relationship between the different concepts of microscale bioprocessing, high throughput bioprocess development, and ultimately whole bioprocess analysis	27
Figure 1.3	Overview of the drug development process	31
Figure 1.4	Typical process flowsheet for manufacturing monoclonal antibodies	33
Figure 1.5	Typical primary recovery strategies for the large-scale production of monoclonal antibodies	36
Figure 1.6	Overview of process sequences in the industrial production and purification of antibody fragments expressed in *E. coli*	40
Figure 1.7	Classification of membrane filtration of biological and other common materials according to membrane pore sizes or molecular weight cut-off	44
Figure 1.8	Schematic illustration of the different modes of membrane filtration operation typically used in biopharmaceutical production	47
Figure 1.9	Schematic representation of flow through membrane pores to model permeate flux by the Hagen-Poiseuille equation.	49
Figure 1.10	Schematic representation of the different situations showing flow through resistances in series for membrane filtration processes	51
Figure 1.11	Schematic diagrams of the particle concentration distribution and fluid flow field in the steady state situation during crossflow microfiltration.	60

Figure 1.12	Application of the microscale bioprocessing platform for membrane filtration for the investigation of bioprocess routes for the primary recovery of antibody Fab' fragments	72
Figure 2.1	Tecan Genesis^{TM} automation platform.	80
Figure 2.2	Microscale devices for automated microfiltration studies	81
Figure 2.3	Laboratory module used in larger scale CFF experiments	84
Figure 2.4	Microscale crossflow microfiltration device	86
Figure 3.1	Application of microscale bioprocessing platform for membrane filtration for the investigation of bioprocess routes	95
Figure 3.2	Typical pressure profile obtained by setting the pressure difference at 20 kPa for a period of 1600s using the Tecan vacuum manifold	97
Figure 3.3	Typical pressure profile obtained by setting the pressure difference at 35 kPa for a period of (A) 30s and (B) 60s using the Tecan vacuum manifold	98
Figure 3.4	Typical pressure profile obtained by setting the pressure difference at maximum (70 kPa) for a period of 2000s using the Tecan vacuum manifold	99
Figure 3.5	Measured membrane resistances of individual membrane inserts containing 0.22 μm PVDF membranes on different vacuum block positions	100
Figure 3.6	Details of the two plate orientations used in water flux experiments on a single plate indicating position relative to vacuum source	102
Figure 3.7	Measured membrane resistances for individual membrane inserts obtained by performing water flux experiments on a single plate with inserts arranged according to	103
Figure 3.8	Schematic representation for a single well of the two-step microscale dead-end filtration process	107
Figure 3.9	Quantification of permeate flux versus time for dead-end microfiltration of thermo-chemically extracted *E. coli* cells	109
Figure 3.10	Comparison of calculated specific cake resistances (α) of thermo-chemically extracted *E. coli* cells by the two- plate method	110
Figure 3.11	Comparison of calculated specific cake resistances of thermo-chemically extracted *E. coli* cells by the single plate method	116
Figure 4.1	Application of microscale bioprocessing platform for membrane filtration for the investigation of bioprocess routes	120

Figure 4.2	Quantification of specific cake resistance following different *E. coli* cell disruption methods	125
Figure 4.3	Particle size distribution of disrupted *E. coli* cells	127
Figure 4.4	SDS PAGE analysis of *E. coli* suspensions following different cell disruption operations	128
Figure 4.5	Microscale process sequence for automated evaluation of impact of Fab' thermo-chemical extraction conditions on subsequent microfiltration performance of disrupted *E. coli* cells	131
Figure 4.6	Impact of cell concentration during extraction on Fab' release from the periplasm of thermo-chemically extracted *E. coli* cells	132
Figure 4.7	Impact of cell concentration on (A) calculated specific cake resistance and (B) apparent permeate transmission of thermo-chemically extracted *E.coli* cells	133
Figure 4.8	Particle size distribution of cell suspension after thermo-chemical treatment	136
Figure 4.9	Impact of heat extraction temperature and time on Fab' and total protein release from the periplasm of thermo-chemically extracted *E. coli* cells	140
Figure 4.10	Impact of heat extraction temperature and time on calculated specific cake resistance of thermo-chemically extracted *E.coli* cells	141
Figure 4.11	The effect of transmembrane pressure on specific cake resistance (α) values.	146
Figure 5.1	Application of microscale bioprocessing platform for membrane filtration for the investigation of bioprocess routes	150
Figure 5.2	The laboratory module used in larger scale crossflow filtration experiments	152
Figure 5.3	Microscale crossflow microfiltration device	154
Figure 5.4	Typical flux data from water flux experiments	160
Figure 5.5	Typical permeate flowrate data from lab-scale crossflow microfiltration experiments with baker's yeast and BSA	164
Figure 5.6	Typical permeate flowrate data from microscale crossflow microfiltration experiments with baker's yeast and BSA	165
Figure 5.7	Effect of ΔP_{TM} during crossflow microfiltration of Baker's yeast with BSA in phosphate buffer	170
Figure 6.1	Application of microscale bioprocessing platform for membrane filtration for the investigation of bioprocess routes for the primary recovery of antibody Fab' fragments	180

Figure 6.2	Bioprocesss flowsheet used in the study of crossflow microfiltration process as an option for primary recovery of antibody Fab' fragments in *E. coli*	182
Figure 6.3	Agarose gel showing the hydrolysis of chromosomal DNAs in homogenised *E. coli* cells as described in Table 6.1	187
Figure 6.4	Absolute viscosity (μ_i) of *E. coli* feedstocks as defined in Table 6.1	190
Figure 6.5	Rheological properties and apparent viscosity of selected homogenised *E. coli* process feedstocks	191
Figure 6.6	Ratio of absolute viscosity (μ_i) of *E. coli* feedstocks to the absolute viscosity (μ_o) of the Control.	192
Figure 6.7	Comparison of crossflow microfiltration performance of *E. coli* Fab feedstocks using the lab-scale Pellicon 2 Mini - Millipore TFF System and the novel microscale CFF device	198
Figure 6.8	Steady state permeate fluxes during microscale crossflow microfiltration of *E. coli* Fab homogenates	201
Figure 6.9	Fab' transmission levels obtained during microscale crossflow microfiltration of *E. coli* Fab homogenates	206
Figure 6.10	Total soluble protein transmission obtained during microscale crossflow microfiltration of *E. coli* Fab homogenates	208
Figure 6.11	DNA transmission obtained during microscale crossflow microfiltration of *E. coli* Fab homogenates	210
Figure 6.12	Agarose gel showing chromosomal DNAs from the different process streams following crossflow microfiltration of *E. coli* homogenate feedstocks as defined in Table 6.1	211

List of Tables

	Table Title	Page
Table 1.1	Marketed monoclonal antibodies and related protein	29
Table 1.2	Common membrane filters for biopharmaceuticals processing	45
Table 1.3	Key concentration polarisation models and their assumptions	55
Table 1.4	Previous studies on microscale filtration system	66
Table 1.5	Commercial filter modules for miniature or automated tangential flow filtration	67
Table 1.6	Available miniature filtration systems or devices	68
Table 3.1	Calculated membrane resistances from microscale water flux measurements	104
Table 3.2	Application of the single plate, two-step microscale filtration method	112
Table 4.1	Impact of various laboratory and microscale *E. coli* cell disruption operations on protein composition of Fab' suspensions	124
Table 4.2	Specific cake resistances of cell disrupted *E. coli* cells using 0.45 μm PES filters	143
Table 5.1	Design attributes of the laboratory scale and microscale crossflow microfiltration systems	158
Table 5.2	Comparison of calculated membrane resistances from water flux experiments using microscale cross flow and dead-end filtration devices	161

Table 5.3 Sample calculation of the microfiltration data points in Figure 5.5 167

Table 5.4 Effects of ΔP_{TM} and crossflow rate on permeate flux during crossflow microfiltration of Baker's yeast with BSA in phosphate buffer using the microscale CFF device 171

Table 5.5 Summary attributes of the Pellicon–2^{TM} Mini crossflow filtration system (lab-scale) and the novel microscale crossflow filtration device 174

Table 6.1 Descriptions of the different bioprocess feedstocks used in this chapter 183

Table 6.2 Effect of a two-fold increase in cell concentration on viscosity of homogenised *E. coli* from frozen-thawed cell paste. Feedstocks as described in Table 6.1 193

Table 6.3 Comparison of clarified *E. coli* Fab' profiles from large scale experiments of crossflow microfiltration and centrifugation 213

Nomenclature

A_c	cross section area
A_m	membrane area
$C_{P,s}$	solids concentration in the permeate
$C_{R,s}$	solids concentration in the retentate
$C_{P,i}$	concentration in the permeate of either Fab or total soluble protein
$C_{R,i}$	concentration in the retentate of either Fab or total soluble protein
d_{ch}	Channel diameter or membrane pore size
D	Particle diffusivity
f	Fanning friction factor
F	temperature correction factor
g	acceleration due to gravity
h	channel height
J	permeate flux
$J_{\Delta t}$	Permeate flux at Δt
J_{ss}	steady state permeate flux
J_i	permeate flux at time i
K	Kozeny-Carman constant
k	Boltzmann's constant
l	Membrane thickness
L	channel length
m_c	Mass of cake
M	Mass of permeate
P_F	feed pressure
P_P	permeate pressure
P_R	retentate pressure
Q	volumetric flow rate
r	Particle radius
R_e	Reynolds number
R_m	membrane resistance
R_T	total hydraulic resistance
R_x	Hydraulic resistance where x can be: f for fouled membrane resistance; g for gel layer; bl for boundary layer; c for cake layer
S	circumference or wetted perimeter
S_m	Pore internal surface per unit volume

T	temperature
V^*	Permeate volume collected during t^*
V_n	Cumulative volume of permeate during t_n
V_s	Starting volume in membrane well
$V_{\Delta t}$	volume of permeate
v	velocity
w	channel width
ΔP_{axial}	axial pressure drop
ΔP_{TM}	transmembrane pressure drop
Δt	filtration time
t^*	Extended time during single plate filtration
t_n	Elapsed filtration time
α	Specific cake resistance
ε	Membrane porosity
ε_m	Membrane surface porosity
γ_{wall}	wall shear rate
μ	viscosity
μ_F	viscosity of feed
μ_P	viscosity of permeate
μ_{25C}	viscosity at 25^{o}C
ρ	density
ρ_F	density of feed
ρ_o	Dry mass of cake solids per volume of permeate
σ_s	solids rejection coefficient
ϕ_w	Particle volume fraction in the cake layer
ϕ_b	Particle volume fraction in the bulk layer

Abbreviations

AFA	Adaptive focused acoustics
BNase	homogenised *E. coli* feed added with Benzonase®
BP	Base pairs (also “bp”)
CFD	Computational fluid dynamics
CFF	Crossflow filtration
DEF	Dead-end filtration
DNA	Deoxyribonucleic acid
EDTA	Ethylenediaminetetraacetic acid
FDA	Food and Drug Administration
HCP	Host cell protein
kbp	Kilo base pairs
N.D.	Not detected
N.M.	Not measured
NWP	Normalised water permeability
PES	Polyethersulfone
PVDF	Poly(vinylidene fluoride)
RNA	Ribonucleic acid
rpm	Revolutions per minute
SNase	Homogenised *E. coli* with co-expressed Staphylococcal nuclease

1. Introduction

1.1 Background and motivation of the project

The need for more efficient approaches to speed up the discovery and development of manufacturing routes to new drug substances as well as to market such products is widely recognized. This has prompted the review of development routes and strategies in recent years (Lye et al., 2002; Dimasi et al., 2004). Traditionally, the focus of most development efforts were on drug discovery which aims to obtain knowledge on clinical efficacy and the parameters that may affect this. In recent years, efforts were directed towards early stage bioprocess development and drug manufacturing activities. This has emerged in line with strict regulatory requirements set by the United States of America's Food and Drug Administration (FDA). The FDA is the leading regulatory body for pharmaceuticals with the USA being one of the largest target markets. The significance of careful planning and experimentation during bioprocess development is well recognised. The information obtained will provide the basis for the creation of a scaleable process that meets the marketing and clinical needs of a biotherapeutic product. The unavailability of critical information causes delays in the actual plant start-up to manufacture such products (Goochee, 2002). These delays do not help the patients who would have otherwise benefited from the manufacture of these therapies. Furthermore, the delays translate to the rapid accumulation of millions of dollars of lost future revenue and diminished competitive advantage of the drug product.

Due to the increased number of new drug candidates, the need to acquire a critical mass of information for bioprocess development consequently becomes more acute. To avoid process development bottlenecks, the use of automated microscale bioprocessing techniques has been promoted to bring manufacturing process development in line with drug discovery operations (Lye et al., 2003). Product processing studies, may be accelerated and will benefit from the availability of microscale devices which allow processing of small quantities of feed as well as multiple or parallel analysis of different process conditions. Microscale bioprocessing provides a platform to explore a variety of process conditions using minimal amounts of material so that essential bioprocess information can be collected early in the process development stage, and therefore process scaleability may be improved (Micheletti and Lye, 2006).

A recent review highlighted the increasing awareness in the resource effectiveness of high throughput bioprocess development to obtain both bioprocess and product understanding (Bhambure et al., 2011). With this awareness is the acknolwedgement that it could potentially enable the application of Quality by Design (QbD) principles for the commercial development of biopharmaceuticals. Under the QbD approach, pharmaceutical quality is assured by the understanding and control of manufacturing and formulation variables (Yu, 2007). A shift in development objectives is now expected to focus on the understanding of the fundamentals of the unit operations since the positive impact of QbD will be realised more rapidly and broadly through the expansion of the knowledge space for manufacturing processes as a result of these investments in a better understanding of the current platform (Kelley, 2009).

Figure 1.1 is a schematic representation of bioprocess development for a new biopharmaceutical drug substance. Bioprocess development is depicted as a two-dimensional process where in one dimension there is the process flowsheet involving

the development of each unit operation and in the second dimension is the level or stage of development, usually corresponding to a certain scale, of these unit operations.

The development of primary recovery and purification processes during the early phase of development is difficult because the amount of material obtained from laboratory scale cell culture is not sufficient for screening downstream process conditions. As shown by Betts and Baganz (2006), most of the earlier microscale studies have mainly focused on upstream operations which reflects the traditional focus in the early development phase. In order to maximise the potential of the microscale bioprocessing approach, however, Jackson et al. (2006) underlined the need to establish more microscale downstream processing operations (shaded region in **Figure 1.1**) so that evaluation could be made early in the development phase.

An important aspect of the microscale bioprocessing approach promoted in this thesis is the link with laboratory robotics. This is central to the creation of high throughput process development platforms (Bhambure et al., 2011). Thus, it is important to create microscale or miniaturised unit operations for bioprocessing that mimics larger scale modules and which are compatible with standard laboratory automation platforms (Lye et al., 2003). The platforms allow modularisation of component unit operations enabling the study of linked process sequences. Automated whole bioprocess analysis is thus the ultimate aim of this philosophy whereby the development of each unit operation in the bioprocess sequence is analysed with respect to its impact on the entire bioprocess. This whole bioprocess approach will now enable the evaluation of different process and economic trade-offs in order achieve the required final product yield and quality in an optimised manner.

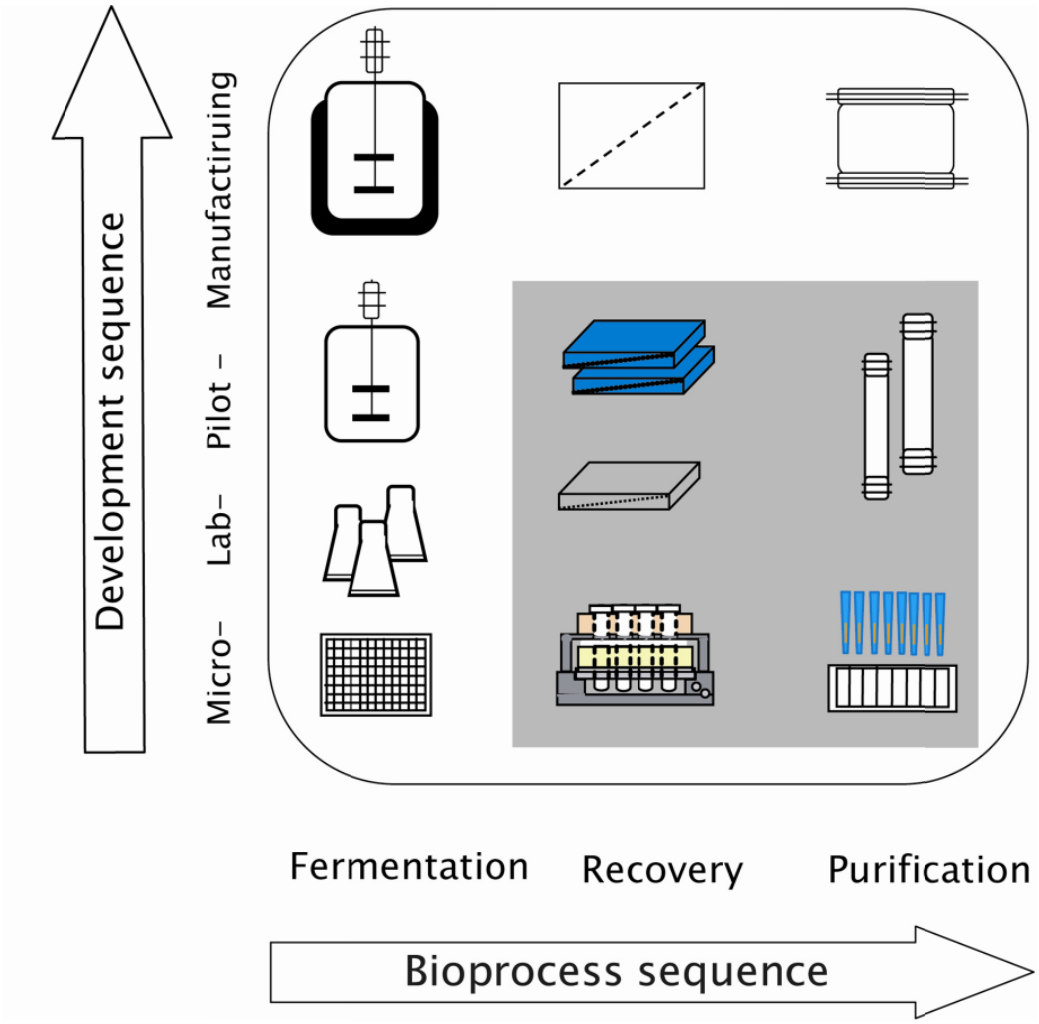

Figure 1.1 Two-dimensional representation of bioprocess development: on the abscissa is the bioprocess flowsheet and on the ordinate is the development of each unit operation (scale-down and scale-up) within the process flowsheet. Shaded region indicates the opportunities for establishment of microscale bioprocessing techniques. With the application of laboratory robotics this could enable automated whole bioprocess analysis.

Figure 1.2 illustrates the interconnection between the three concepts of microscale bioprocessing, high throughput process development and the whole bioprocess analysis approach. It shows that the creation of the different devices and tools for microscale unit operations will permit the growth of high throughput bioprocess development and is necessary to underpin microscale investigation of a whole bioprocess sequence.

Against this backdrop, the overall aim of this thesis is to establish microscale bioprocessing methods for the evaluation of membrane filtration processes. A review of literature on membrane filtration (Section 1.5) has revealed that no other work has been done on automated microscale membrane filtration since the initial work of Jackson et al. (2006). In order to appreciate the requirement for microscale processing for membrane filtration of biopharmaceuticals an overview is first given in Sections 1.2 and 1.3. The discuss the areas for growth and opportunities for expanding process development and manufacturing of emerging therapies. It also provides the basis for the selection of antibody Fab' fragments production as a case study in the application of membrane filtration as the key primary recovery unit operation. Section 1.4 provides a brief review of membrane filtration concepts in order to understand the opportunities available for development and optimisation of membrane filtration processes as applied to the primary recovery of biopharmaceuticals. Section 1.5 then outlines current knowledge on scale-down and microscale membrane filtration. Finally, the overall aim of this thesis and the specific objectives are stated in Section 1.6.

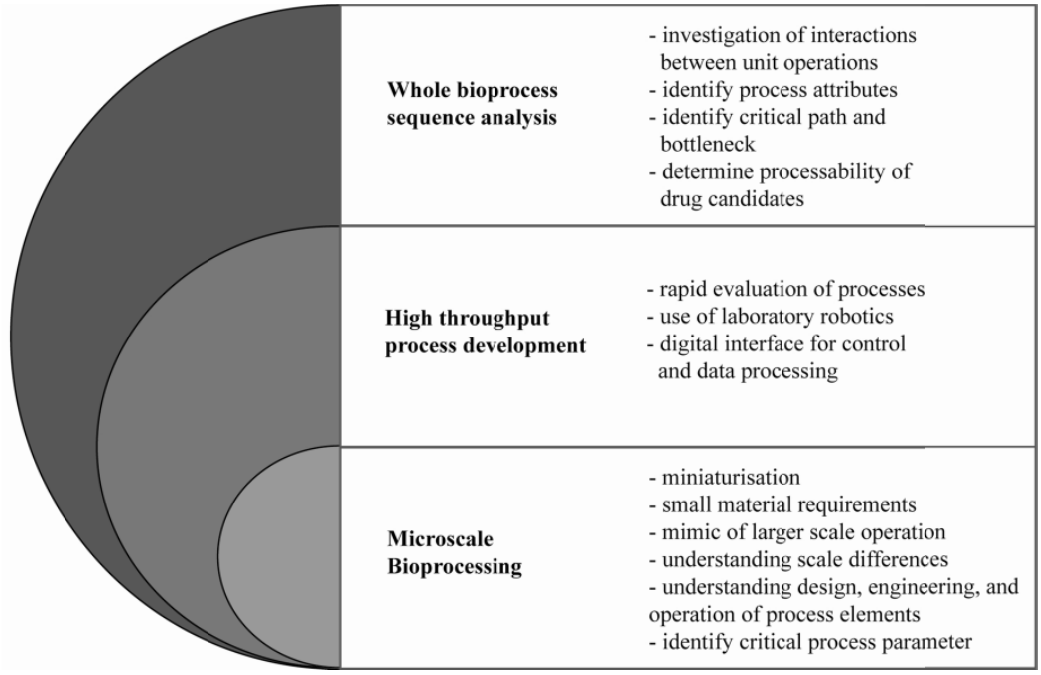

Figure 1.2 Relationship between the different concepts of microscale bioprocessing, high throughput bioprocess development, and ultimately whole bioprocess analysis.

1.2 Overview of biopharmaceutical product development

1.2.1 Biopharmaceuticals and the drug development process

Biopharmaceuticals are biologically based therapeutic products, typically recombinant macromolecules (Ho and Gibaldi, 2003). These biologics are not easily characterised and therefore refinement to achieve high purity is a difficult process. Therapeutic monoclonal antibodies (Mabs) are the fastest growing class of biologics and have the largest market share of approved biopharmaceuticals (Strohl, 2009). Currently, 30 Mabs and related proteins are on the market with additionally 150 Mabs either in pre-clinical, clinical trials or awaiting FDA approval (Shukla and Thömmes, 2010; Rao et al., 2011). Advances in antibody engineering technologies enabled the fast generation of high-affinity antibodies of defined specificity facilitating the development of a wide range of antibody-based molecules for use in indications such as oncology, inflammations and infectious diseases (Brekke and Løset 2003; Bowering, 2004). It is projected that the number of antibodies in the market will increase to about 50 by 2012 even if only 50% of Phase III candidates are successful (Strohl, 2009). **Table 1.1** shows a list of marketed Mabs and related proteins.

It is acknowledged that the rate at which therapeutic Mabs and other related proteins are identified and developed is so advanced that the impediment in launching these to market rests on the constraints of human effort and resources required to demonstrate the clinical efficacy and safety of these drug candidates (Ho and Gibaldi, 2003). The task of evaluating the information on the new drug candidate is performed by the FDA. **Figure 1.3** shows the schematic diagram of the drug development process which aims to demonstrate the effectiveness and safety of drug candidates before reaching the market.

Table 1.1 Marketed monoclonal antibodies and related proteins*

Year approved	U.S. Trade name® (Type, Protein Format)	Company (US$ Million Sales**)	Indication
1986	Orthoclone OKT3 (Murine, IgG)	Ortho Biotech/ now J&J(>$80)	Acute kidney transplant rejection
1994	ReoPro (Chimeric, Fab fragment)	Centocor/now J&J ($300)	Prevention of blood clot
1995	Panorex (Murine, IgG)	GlaxoSmithKleine (n.d.)	Colorectal cancer
1997	Rituxan (Chimeric, IgG)	Biogen-Idec/ Genentech ($ 3800)	Non-Hodgkin's lymphoma, rheumatoid arthritis
	Zenapax (Humanised, IgG)	PDL/ Roche (>$80M)	Acute kidney transplant rejection
1998	Synagis (Chimeric, IgG)	MedImmune (n.d.)	Respiratory synctial virus (infant)
	Remicade (Chimeric, IgG)	Centocor/now J&J ($ 3800)	Rheumatoid arthritis
	Herceptin (Humanised, IgG)	Genentech ($ 3000)	Breast cancer
	Enbrel (FC fusion protein)	Immunex/now Amgen ($ 4400)	Rheumatoid arthritis, psoriasis, ankylosing spondylitis
	Simulect (Chimeric, IgG)	Novartis (>$ 80)	Prophylaxis of acute organ transplant rejection
2000	Mylotarg (Humanised, IgG)	Wyeth ($115)	Leukemia
2001	Campath-1H (Humanised, IgG)	ILEX-Millenium/now Takeda (>$ 80)	Leukemia
2002	Zevalin (Murine, IgG)	Biogen-Idec (>$ 80)	Non-Hodgkin's lymphoma
	Humira (Human, IgG)	CAT/Abbott ($ 2000)	Rheumatoid arthritis, Crohn's disease
2003	Amivive (FC fusion protein)	Biogen (>$ 80)	Psoriasis
	Xolair (Humanised, IgG)	Genentech ($500)	Asthma
	Bexxar (Murine IgG)	Corixa/ now GSK (>$ 80)	Non-Hodgkin lymphoma

* Adapted from Strohl (2009) and Shukla and Thömmes (2010)

** in 2006, rounded up to nearest hundreds

n.d. – no data

Table cont'd overleaf

Table 1.1 ***Continued***

Year approved	U.S. Trade name® (Type, Protein Format)	Company (US$ Million Sales**)	Indication
2004	Erbitux (Chimeric, IgG)	ImClone/Bristol-Myers Squibb (Eli Lilly) ($ 1100)	Colorectal cancer
	Avastin (Humanised, IgG)	Genentech ($ 2400)	Colorectal cancer
	Tysabri (Humanised, IgG)	Biogen(-Idec)/Elan (> $ 80)	Multiple sclerosis
2005	Orencia (FC fusion protein)	Bristol-Myers Squibb ($ 100)	Rheumatoid athritis
2006	Lucentis (Humanised, Fab fragment)	Genentiech/Novartis $ 380	Age-related macular degeneration
	Vectibix (Humanised, IgG)	Amgen (> $80)	Colorectal cancer
2007	Soliris (Humanised, IgG)	Alexion Pharma	Paroxysmal nocturnal hemoglobinuria
	Arcalyst (Fc fusion protein)	Regeneron	Cryopyrin Associated Periodic Syndrome
2008	Cimzia (Humanised, Fab' fragment)	UCB/ Shwartz	Rheumatoid athritis
	Nplate (FC fusion protein)	Amgen	Thrombocytopenia
	Stelara (Human, IgG)	Centocor/ now J&J	Psoriasis
	Simponi (Human, IgG)	Centocor/ now J&J	Rheumatoid arthritis
	Actemra (Humanised, IgG)	Roche	Rheumatoid arthritis

* Adapted from Strohl (2009) and Shukla and Thömmes (2010)

** in 2006, rounded up to nearest hundreds

n.d. – no data

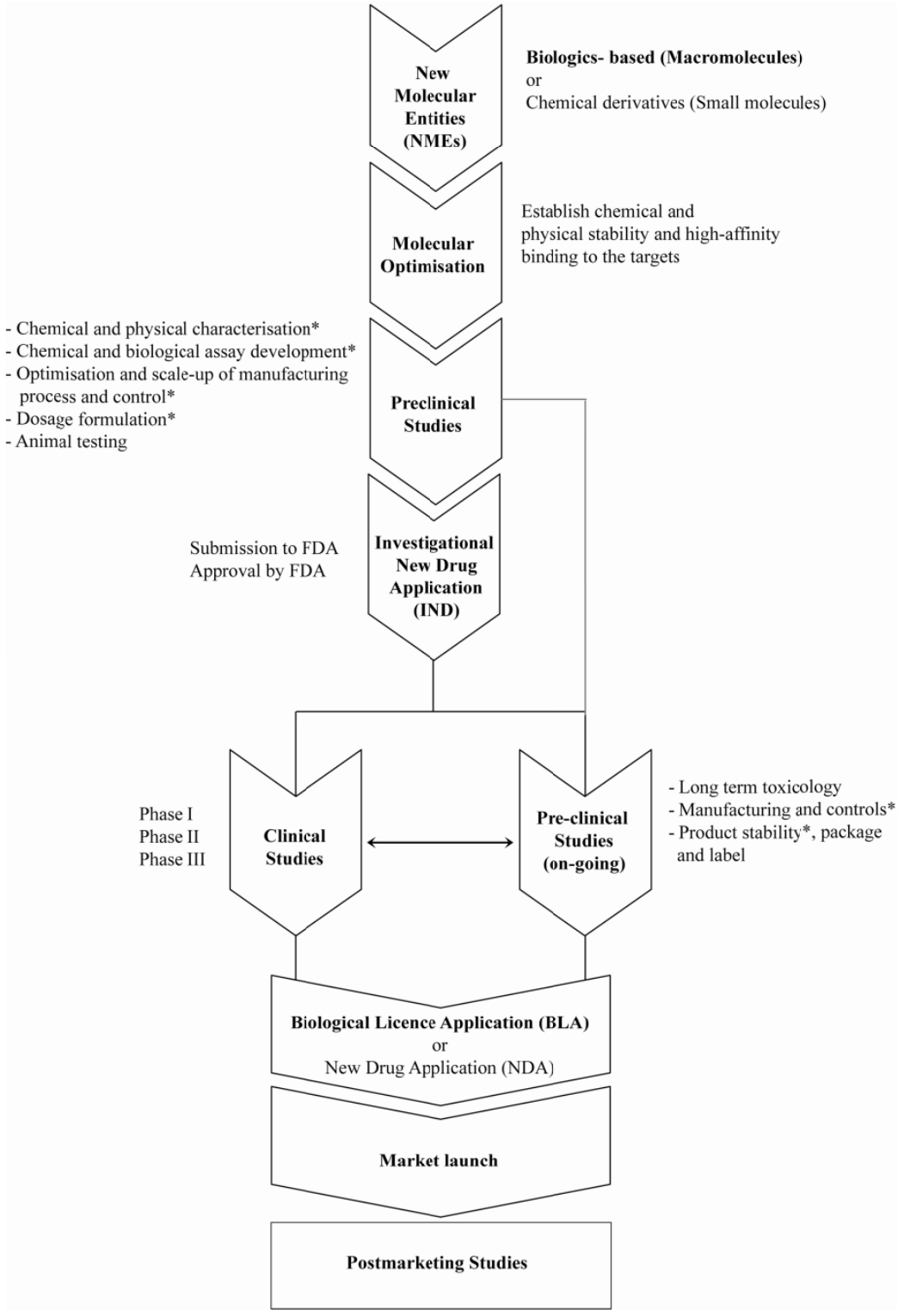

Figure 1.3 Overview of the drug development process. The asterisk (*) indicates process development and manufacturing-related activities. Adapted and modified from Ho and Gibaldi (2003).

Drug development activities, shown in **Figure 1.3**, are typically accomplished between 12-15 years with the clinical phase usually starting between the 6^{th}-8^{th} year (Ho and Gibaldi, 2003). Given this long development phase, the ability to develop and create the right process to manufacture the drug at the required scale is clearly in the critical path of the launch of the new drug. The advantage of being first to launch to market can be seen from the sales figures of 23 of the marketed antibodies shown in **Table 1.1** which had accumulated sales of US$23 Billion in the year 2006 (Strohl, 2009) and about $30 B in 2007(Liddell, 2009). Interestingly, 65% of these sales are from antibodies which have reached the market first. This has formed the basis for the drive to shorten the development timeline and enhance the drug development process.

Development activities related to manufacturing, highlighted with an asterisk (*) in **Figure 1.3**, are usually performed later in drug development which add to the criticality of process development activities. It is within this context of biopharmaceutical drug development process where the concept of accelerated bioprocess development, as illustrated by **Figure 1.2**, is expected to have a great impact.

1.2.2 Biopharmaceutical manufacturing process

The need to deliver new biopharmaceutical drugs to market in a tight timeline and consistently to high quality and reproducibility has resulted in a consensus manufacturing process, particularly for monoclonal antibodies (Kelley, 2009; Shukla and Thömmes, 2010). In both upstream cell culture and downstream primary recovery and purification, platform processes have become widely established. **Figure 1.4** shows a typical process flowsheet for manufacturing Mabs. Slight variations may be adapted by different companies but close similarities remain (Farid, 2006). The figure shows the typical unit operations (I) for each step of the process (II).

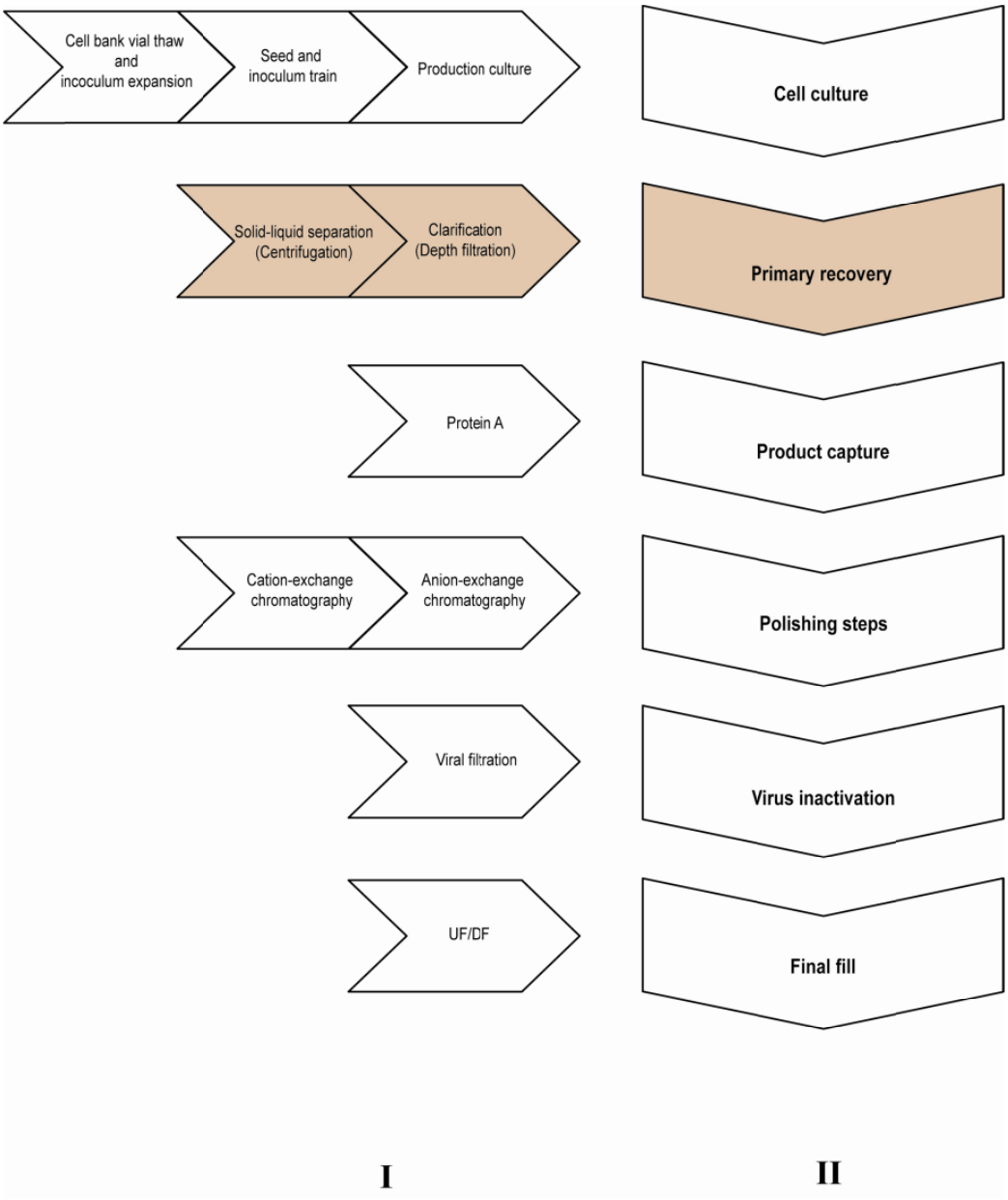

Figure 1.4 Typical process flowsheet for manufacturing monoclonal antibodies where (I) are the unit operations that seek to accomplish the functional steps in (II). Shaded elements are the unit operations which are the focus of this work (Shown in detail in Figure 1.5). Adapted and modified from Birch and Racher (2006), Kelley (2009), and Shukla and Thömmes (2010).

The expression system that is commonly used in commercial Mab processes are mammalian cells which produce the complex and large Mabs molecules with the correct glycan chain structure (Shukla et al., 2009). It is now widely known that the glycosylated structure is essential in maintaining the biological activity of these monoclonal antibodies (Jefferis, 2005).

"Primary Recovery" is highlighted in **Figure 1.4** since this is the main subject of this thesis. This step involves the removal of cells and cellular debris and the clarification of the broth suspension. Primary clarification is usually achieved by centrifugation while depth filtration is employed for further particulate removal as well as the removal of other undesired soluble components (Yigzaw et al., 2006; Birch and Racher, 2006). This primary recovery strategy is typical for Mabs production at production scale greater than 2000 L (**Figure 1.5**). Other common cell removal techniques are crossflow microfiltration and depth filtration. However, these are commonly used at scales less than 2000 L, with depth filtration only being used at scales of up to several hundred litres (about 400L) (Shukla and Kandula 2009; Kelley et al., 2009).

The rest of the process steps in **Figure 1.4** are aimed at purifying the recovered solution from the recovery steps. Affinity chromatography (Protein A) is the usual primary product capture step, with almost two-thirds of monoclonal antibodies captured by Protein A (Curling, 2009). Polishing steps follow such as bind-and-elute cation-exchange (CEX) chromatography and a flow-through mode anion-exchange (AEX). These ion exchange chromatography (IEX) steps are used to reduce host cell protein (HCP) levels, DNA and aggregates and to remove leached Protein A and endotoxins. A crossflow ultrafiltration/diafiltration (UF/DF) step may be employed to concentrate or exchange buffer as required by each chromatographic step to increase selectivity and binding of the desired protein.

As a result of the maturity and robustness of the technology, the use of the typical process flowsheet in **Figure 1.4** is common at many commercial scales of production. The adoption of this generic platform may result in cost savings in time and material resources when developing processes for several other Mabs for different indications. This can be achieved by, among others, streamlining process development efforts of cross-functional groups within a company, leveraging negotiations for reduced raw material costs, and by facilitating the application of modular approaches in process validation (Shukla et al., 2007). However, fine tuning of process flowsheets and process development strategies are still important undertakings as Mabs molecules and cell culture composition may widely vary in their biochemical identities which could affect the ease of which they could be processed and purified (Kelley, 2009).

1.3 Opportunities in biopharmaceutical manufacturing

1.3.1 Monoclonal antibody therapies

As the Mabs sector matures, quality and flexibility of development efforts are gaining attention as factors which could provide competitive advantage in addition to the traditional focus of speed to market (Farid, 2009). Issues regarding capacity utilisation have come into focus with increasing product titre. Titres of up to 5 g/L have left bioreactors under-utilised as fermentation volumes of about 4000 L can now achieve the same output which formerly required 20 000 L (Anicetti, 2009). A further increase to double digit titres may lead to production scales less than 2000 L. If this becomes a norm, crossflow microfiltration as a harvest step will become increasingly relevant (see **Figure 1.5**) as this is the current unit operation used for primary recovery at the intermediate scale.

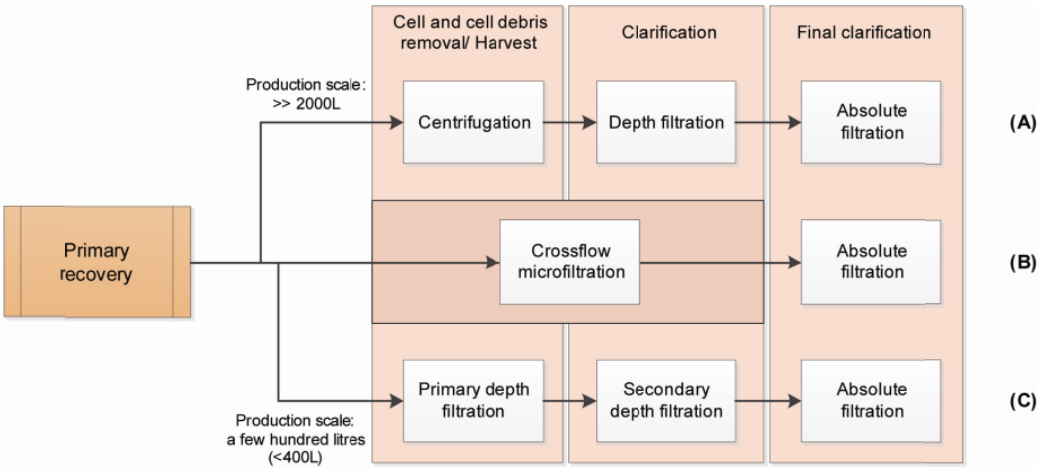

Figure 1.5 Typical primary recovery strategy for the large-scale production of monoclonal antibodies. Adapted and modified from Shukla and Kandula (2009).

Kelley (2009) has shown that there is excess production capacity in the foreseeable future and that efforts to reduce the cost of goods (COGs) are only highly applicable to Mab products intended for large therapeutic markets and not for all products in the pipeline. It was further explained that platform technologies will continue and new purification technologies may not provide the advantage these are expected to make in terms of reducing manufacturing costs. However, to keep manufacturing off the critical path, continuous improvement is important, particularly on product quality and process consistency which may greatly improve overall economics (Farid, 2009). Understanding the process fundamentals of the current platform will help achieve this especially when developing processes that are not based on mammalian cell culture. Recent advances in antibody engineering resulted in the production of full length IgGs in *Escherichia coli* and *Pichia pastoris* (Mazor et al., 2007; Potgieter et al., 2009). The production process using *E. coli* and *P. pastoris* may or may not require modifications of the current platform process. Certainly, development efforts are necessary to understand and scope the unique process requirements of these new Mabs expression systems.

1.3.2 Emerging therapies: antibody fragments

There are different antibody fragment formats which can be used for therapeutic use aside from the full length IgG. Currently, three of these antibody fragments are in the market (**Table 1.1**), at least eight antibody fragment products are in development and at least two of these are Fab' fragments (Liddell, 2009). When the effector functions of the Fc portion are expendable, requiring only the antigen-binding site, and when better tissue penetration to the specific target and rapid clearing from the body are just two of the specific instances when antibody fragments may have particular advantage over intact antibodies (Rowe et al., 2004). The latter is possible due to the characteristic short serum half-life of the antibody fragment. To improve the pharmacokinetic properties of the antibody fragments, protein engineering or chemical coupling of

antibody fragments with polyethyleneglycol (PEG) have been explored (Dennis *et al.*, 2002; Humphreys, 2003). Both methods were shown to increase serum half-life to approach that of native IgG. Another key advantage of using Fab' fragments is that these fragments hold the antibody property that stimulates a therapeutic response. Fab' fragments can therefore be used as therapuetic entity building blocks, making the design of therapeutic antibodies more flexible than using standard IgG (Bowering, 2004).

In the context of manufacturing, antibody fragments can be produced in microbial, usually *E. coli*, and eukaryotic systems (Andersen and Reilly, 2004). However, *E. coli* remains the main production system of choice for antibody fragments due to shorter, thus faster, drug development process, lower cost of goods, short fermentation time, large global fermentation capacity, as well as significant regulatory experience for therapeutic protein production which may be absent in novel expression systems (Humphreys, 2003; Liddell, 2009).

The biopharmaceutical industry is known to make conservative changes when it comes to the use of manufacturing equipment and operation largely due to the regulatory implication of process changes. This is understandable given the regulatory requirements a product has to go through before it is launched to market. However, for antibody fragment production, a defined process has yet to become widely established (Shukla and Thömmes, 2010). Antibody fragment production in *E. coli* has its own intricacies very different from intact Mab production. This is brought about by the nature of the expression system such that antibody fragments in *E. coli* are produced either as inclusion bodies in the cytoplasm or as soluble protein in the periplasm. Therefore, the production of antibody fragments presents an opportunity to develop process flowsheets that are different from the platform Mab process shown in **Figure 1.4**.

Figure 1.6 shows the process sequence for antibody fragment production in *E. coli*. As illustrated, there are different process options for antibody fragments production depending on their location in the cells and whether PEGylation is required or not. It is clear in **Figure 1.6** that the primary recovery of antibody fragments is more complex and now involves more unit operations than Mabs (**Figure 1.5**). This makes it ever more important to consider the strategies for process route selection since an increased number of process steps will result in a drop in the overall downstream processing yield (Farid, 2009).

In the production of antibody fragments, the solid-liquid separation and clarification steps are now two unit operations after fermentation (instead of just one) which means these steps are affected not only by the characteristics of the broth coming from fermentation but also by the impact of the product release methods. Product release is a relatively new step in biopharmaceutical manufacture. As discussed in Section 1.2.2, full length IgGs are secreted from the cell into the culture broth thereby not requiring product release strategies. Product release is usually done by disrupting the cells or causing permeability changes to the cell membranes (Balasundaram et al., 2009a). Most of these strategies have been applied to other biotechnological processes but are quite unusual in antibody production.

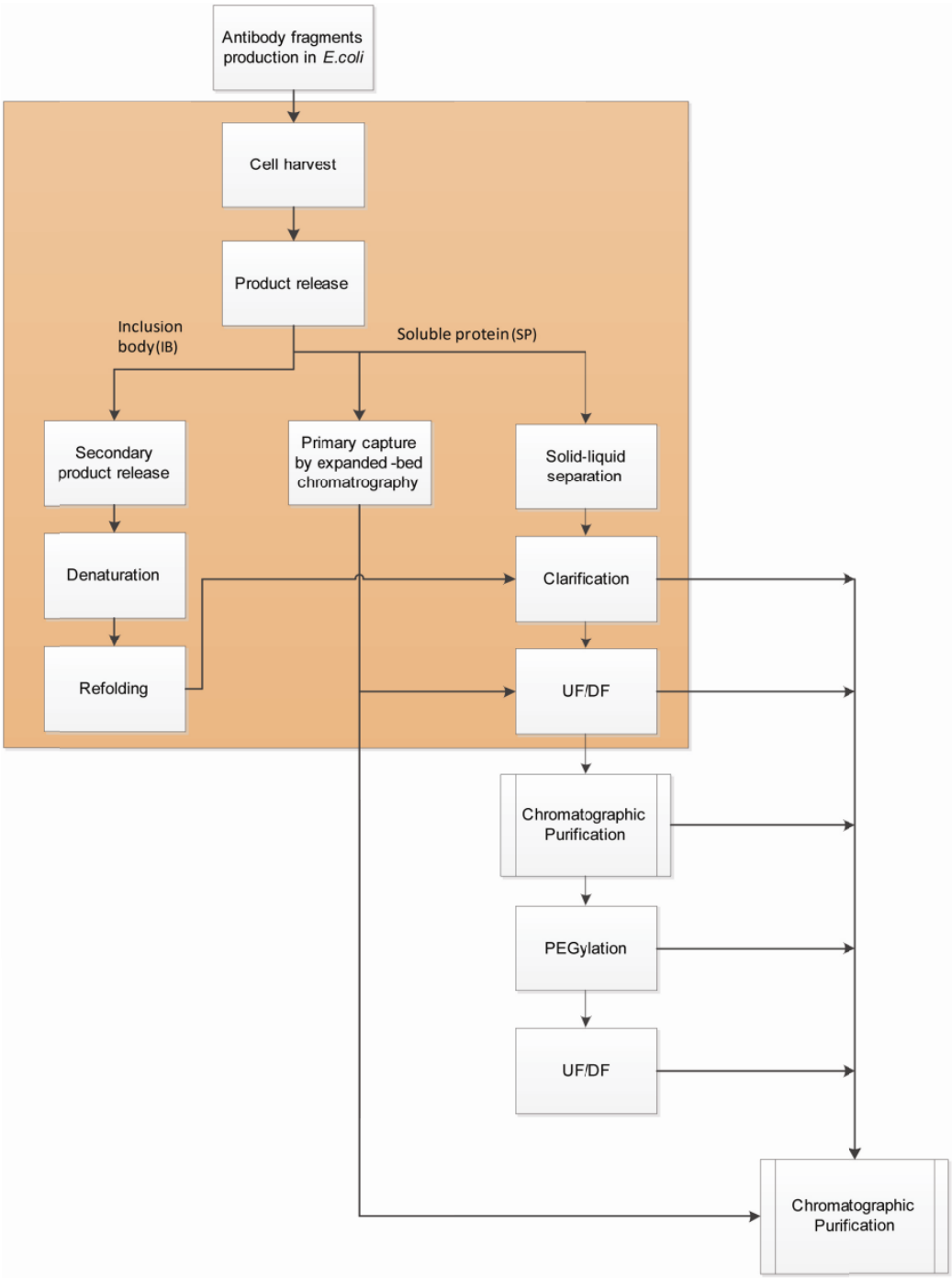

Figure 1.6 Overview of process sequences in the industrial production and purification of antibody fragments expressed in *E. coli*. Shaded region illustrates the primary recovery strategies for the different products. Inclusion bodies and soluble proteins are expressed in the cytoplasm and periplasm, respectively. (Adapted and modified from Spitali, 2009).

1.3.3 Lean manufacturing and single-use systems

Given the current situation in biopharmaceutical manufacture, particularly for Mabs as shown in Section 1.3.1, a direct consequence of increasing production titres is the decrease in manufacturing scale. The size of the unit operations in the production and recovery sections in **Figure 1.4** will decrease while size requirements for the chromatographic steps for product capture increases. To produce the same amount of Mab product, the total number of batches per year will also decrease thus resulting in a situation where a production facility may be underutilised unless multiple products are produced within the facility. There are, however, risks for a multi-product facility. An important one, particularly in regulatory and safety terms, is cross-contamination. In this regard, there has been an increased interest in lean and flexible manufacturing (Kelley, 2009). This requirement has been addressed in part by single-use systems, also known as disposable technologies. The use of disposables have been promoted to have numerous advantages such as reduced capital expenditure and risk; potential to downgrade room classifications; economic benefits in terms of downsizing water systems and simplifying the facility; regulatory impact: as the FDA supports the use of disposables due to less risk of cross contamination; speed-to-market (as a result of the ability to set-up new processes very quickly) and flexibility in production capacity and product changeovers (Sinclair and Monge 2010).

At present, available disposable systems include mixing systems, bioreactors, aseptic connectors, sampling systems, freezing, and fill-finish (Sinclair and Monge 2008). For primary recovery strategies including cell debris removal and clarification, as well as concentration and buffer exchange, membrane filtration systems are now mostly available as disposables. For example, the large membrane manufacturers such as GE Healthcare (Chalfont, UK), Merck Millipore (Massachusetts, USA), Novasep (Pompey, France), Pall (New York, USA), and Sartorius Stedim (New York, USA) all have disposable membrane filters specifically for crossflow filtration. Some have fully

integrated crossflow filtration systems like Millipore which has the Mobius^{TM} Flexible Filtration system which is marketed as out-of-the-box, modular and fully optimised assemblies for single-use crossflow filtration operation. In this regard, membrane filtration processes, unlike centrifugation, offer the possibility of choosing between the traditional stainless steel and disposable technologies to fill the requirement of manufacturing groups according to production requirements. In the next section, a focus on membrane filtration processes as applied to biopharmaceutical production is discussed.

1.4 Membrane filtration for biopharmaceutical processes

Membrane filtration, a pressure-driven separation process, is an established unit operation and has long been used to recover and concentrate biotechnological products (van Reis and Zydney, 2007). Although other novel separations are currently being investigated, membrane filtration remains a key unit operation in bioprocessing. In the case of large scale production of monoclonal antibodies for example, Kelley (2007) stressed that the conventional unit operations, including membrane filtration, still appear to be the separation processes of choice due to reduced risks in scale-up, technology transfer and process robustness.

Membrane filtration processes separate components according to size in which the primary role of the membrane is to act as a selective barrier for the different components of the feed stream. As opposed to conventional filtration processes, which are usually applied to the separation of fine and course particles greater than 10 microns, membrane filtration is a classification of filtration processes involving particles less than 10 microns using membrane filters that are usually less than 10 microns as well (Mulder, 1996). **Figure 1.7** illustrates the typical classification of

membrane filtration processes. This figure demonstrates that microlfiltration and ultrafiltration processes are applicable in biopharmaceutical manufacturing. Thus, concepts presented here are limited to these two filtration processes.

1.4.1 System design and mode of operation

The design of a membrane filtration process requires consideration of certain key process elements: (1) the size of the material that has to be retained on or be allowed to permeate through the membrane; (2) the type of filter required in terms of pore size, whether microporous filter or ultrafilter; and (3) the mode of operation of the separation process.

Although, historically, membrane filtration processes were mostly performed using ultrafiltration membranes, increased use of microfiltration membrane processing has become evident since the late 1990s (Cheryan, 1998; Foley, 2006a). **Table 1.2** shows some of the different membranes currently available for microfiltration and ultrafiltration of suspensions and solutions. When choosing membrane filters, the type of material of the membrane should be compatible to the feed stream which is going to be processed and that it could provide the desired separation. It is necessary that the membranes do not bind to the product as this will decrease recovery. Some of the membrane materials in **Table 1.2** are naturally hydrophobic (PVDF and PTFE). Therefore, modified versions of these membranes should be used. Most manufacturers will have hydrophilic PVDF membrane, for example, which is the suitable type of membrane for cell harvesting and clarification.

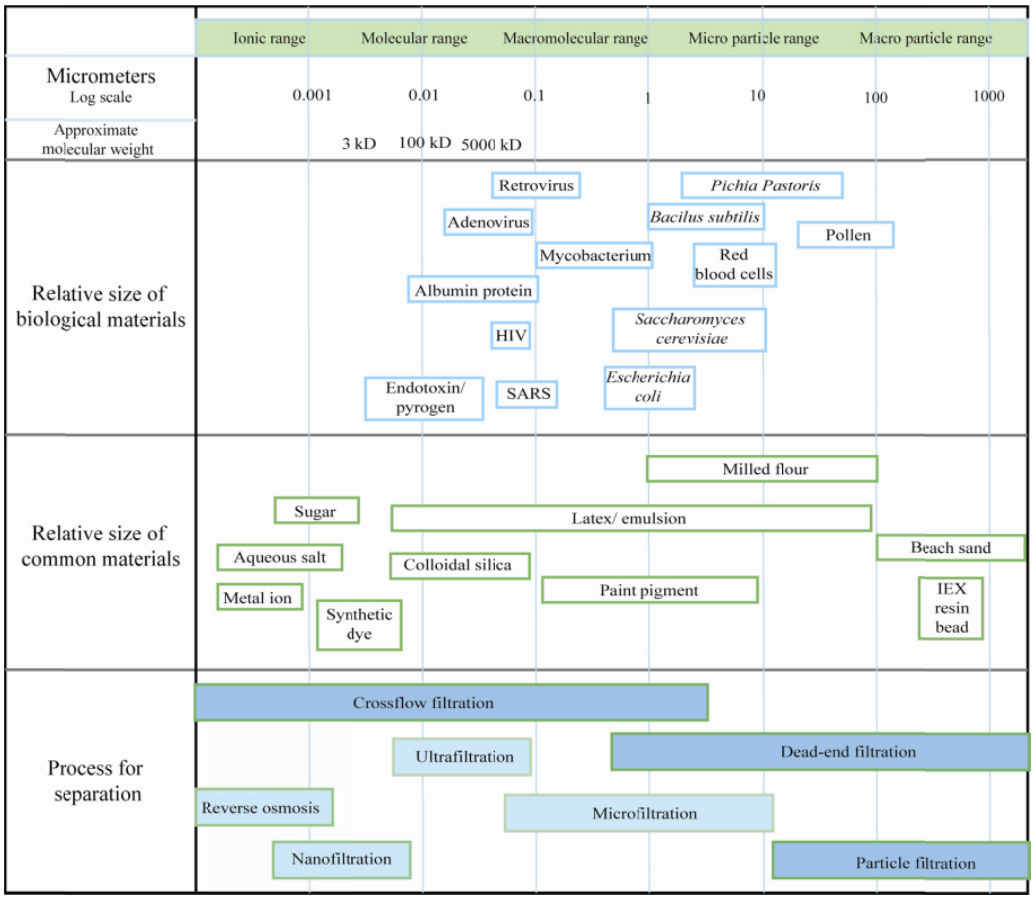

Figure 1.7 Classification of membrane filtration of biological and other common materials according to membrane pore sizes or molecular weight cut-off. (Adapted and modified from: www.gelifesciences.com)

Table 1.2 Common membrane filters for biopharmaceuticals processing*

Material	Microfiltration	Ultrafiltration
Polyvinylidene fluoride (PVDF)	X	
Polyethersulfone (PES)	X	X
Polytetrafluoroethene (PTFE)	X	
Regenerated cellulose (RC)		X
Polysulfone (PS)	X	X

*Material data from Cheryan (1998); application data cross-checked from online catalogue of different manufacturers

For their practical application, membranes are packaged according to the design of the equipment housing. Typical membrane filtration configurations in industrial bioseparation are as flat-sheet membranes in cartridges (similar to the plate-and-frame type for particulate filtration) or flat-sheets in spiral wound; and as bundles of hollow fibre membrane (Ladisch, 2001). In recent years, membrane separations in bioprocessing have mostly focused on the use of flat-sheet and hollow fibre membranes for cell harvest or cell debris removal (van Reis and Zydney, 2007). A survey of the online product catalogue of some of the large membrane suppliers revealed that flat-sheet membranes in cassette format is the most common format sold. However, not all the different membranes are available in the different formats sold by the manufacturer. It is therefore very important to select membrane formats which have available filtration systems at different scales of development, i.e., from laboratory to pilot and then to manufacturing scale.

The classical mode of operation of membrane filtration processes is via normal flow (NFF) or dead-end filtration (DEF). This has followed from conventional filtration processes which were also operated in this way (Cheryan, 1998). However, since dead-

end filtration results in low permeate flux, different strategies for increasing flux were developed. With the evolving understanding of the fundamentals of membrane separation, crossflow microfiltration has found more application in industrial bioseparation because of improved permeate fluxes (Belfort et al., 1994; Meltzer and Jornitz, 1998). **Figure 1.8** illustrates these two modes of operation. DEF is a process where the feed flows perpendicular to the membrane surface. As a result, retained components build up on the feed/retentate side and lead to membrane fouling and concentration polarisation. The permeate flux during dead-end filtration decreases over time. Tangential (TFF) or crossflow filtration (CFF) have the feed stream flowing parallel to the membrane. The feed flow then allows the retained components to be brushed off along the membrane surface and out of the CFF device.

1.4.2 Theories and models of membrane filtration

A key performance indicator of membrane filtration processes is the permeate flux, $J_{\Delta t}$, which is the measure of volume of liquid, $V_{\Delta t}$, which has permeated through the membrane of a certain area, A_m, for a certain period, Δt. Based on Equation 1.1, once the flux is known, the processing time for certain volume of material can be determined for a given membrane area, or if given a fixed processing time, the required membrane area can be determined. Thus, flux modelling has been an important undertaking in understanding membrane filtration processes. This section will present the common models for predicting flux as well as the theories behind these models.

$$J_{\Delta t} = \frac{V_{\Delta t}}{A_m \cdot \Delta t} \tag{1.1}$$

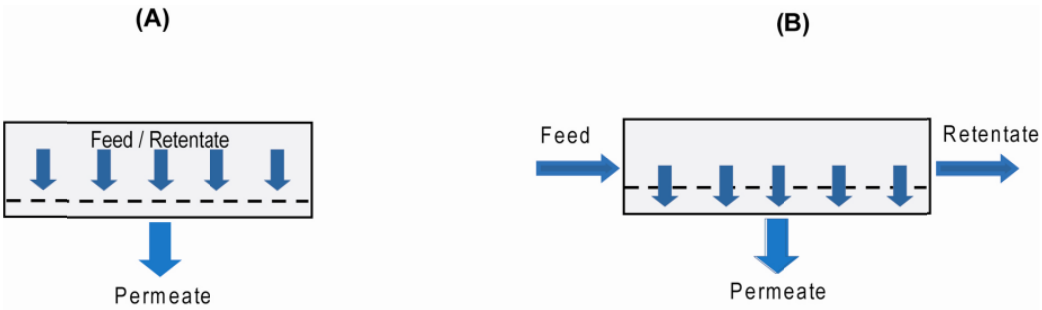

Figure 1.8 Schematic illustration of the different modes of membrane filtration operation typically used in biopharmaceutical production: (A) dead-end filtration; and (B) crossflow filtration.

1.4.2.1 Hagen-Poiseuille flow through a membrane pore: ideal flux

In the most ideal and simplest situation, flow through a membrane can be treated as a fluid flow situation analogous with viscous flow through pipes as in fluid transport problems (Bird et al., 2001). **Figure 1.9** is a schematic representation of this situation. If the Hagen-Poiseuille flow equation is applied to flow of fluid through a membrane pore, Equation 1.2 is derived.

$$J = \frac{\varepsilon \cdot d_{ch}^2 \cdot \Delta P_{TM}}{32 \cdot l \cdot \mu} \tag{1.2}$$

Where: J is the permeate flux; ε is the membrane porosity; d_{ch} is the channel diameter or membrane pore size; ΔP_{TM} is the transmembrane pressure; l is the membrane thickness; and μ is the viscosity of the fluid.

The Hagen-Poiseuille equation assumes that the fluid flows through a constant circular cross-section with the diameter that is very small compared to the length. Also, in this situation, the flow is viscous, incompressible and laminar. The fluid follows Newtonian law and that there is no slip of fluid particles at the boundary (Bird et al., 2001).

1.4.2.2 Flux modelling based on flow resistances

The determination of flux through a series of resistances is commonly encountered in heat transfer in the form of Fourier's law of conduction (Bird et al., 2001). Modelling flux by the resistance model takes the general form of:

$$\text{Flux} = \frac{\text{Driving force}}{\text{Total resistance}} \tag{1.3}$$

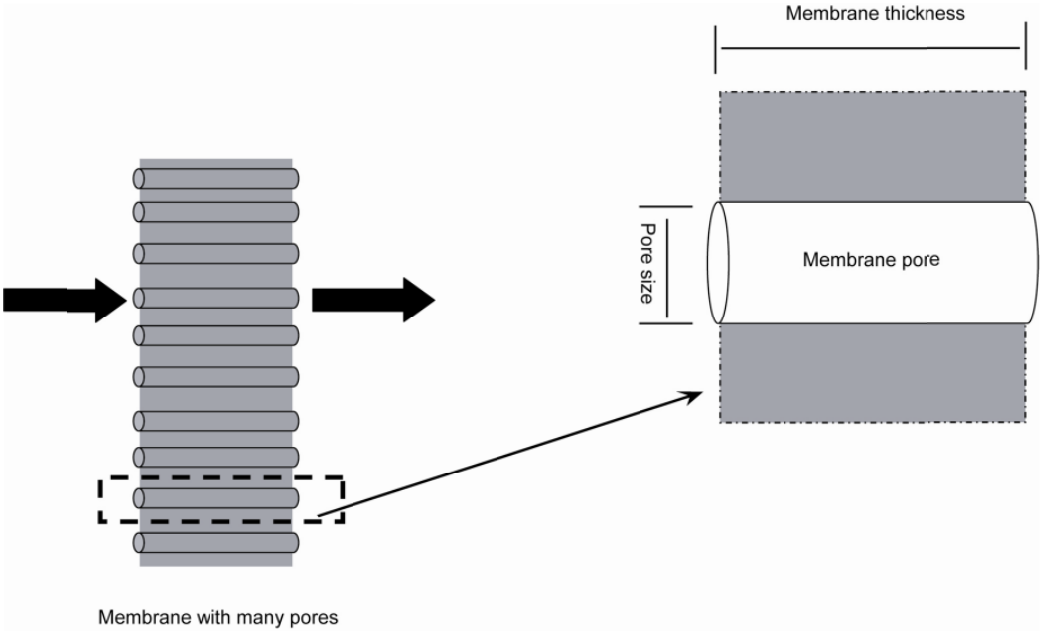

Figure 1.9 Schematic representation of flow through membrane pores to model permeate flux by the Hagen-Poiseuille equation.

Different resistances are considered for flows through a membrane filter (Mulder, 1996; Cheryan, 1998). **Figure 1.10** illustrates these which include: (A) the clean membrane; (B) the fouled membrane; (C) the fouled membrane with a gel layer; (D); the fouled membrane with a boundary layer; (E) the fouled membrane with a boundary layer and gel layer; and (F) the fouled membrane with a boundary , gel and cake layer. From **Figure 1.10**, it can be seen that the different levels of resistances should be determined if flux is to be known using the general equation in Equation 1.4. In the following paragraphs, the determination of these resistances is discussed.

$$J = \frac{\Delta P_{TM}}{R_T \cdot \mu_P} \tag{1.4}$$

Where: R_T is the total resistance which could be:

(A) the clean membrane

$$R_T = R_m \tag{1.5}$$

(B) the fouled membrane

$$R_T = R_m + R_f \tag{1.6}$$

(C) the fouled membrane with a gel layer

$$R_T = R_m + R_g \tag{1.7}$$

(D) the fouled membrane with a boundary layer

$$R_T = R_m + R_{bl} \tag{1.8}$$

(E) the fouled membrane with a boundary layer and gel layer

$$R_T = R_m + R_{bl} + R_g \tag{1.9}$$

(F) the fouled membrane with a boundary , gel and cake layer

$$R_T = R_m + R_{bl} + R_g + R_c \tag{1.10}$$

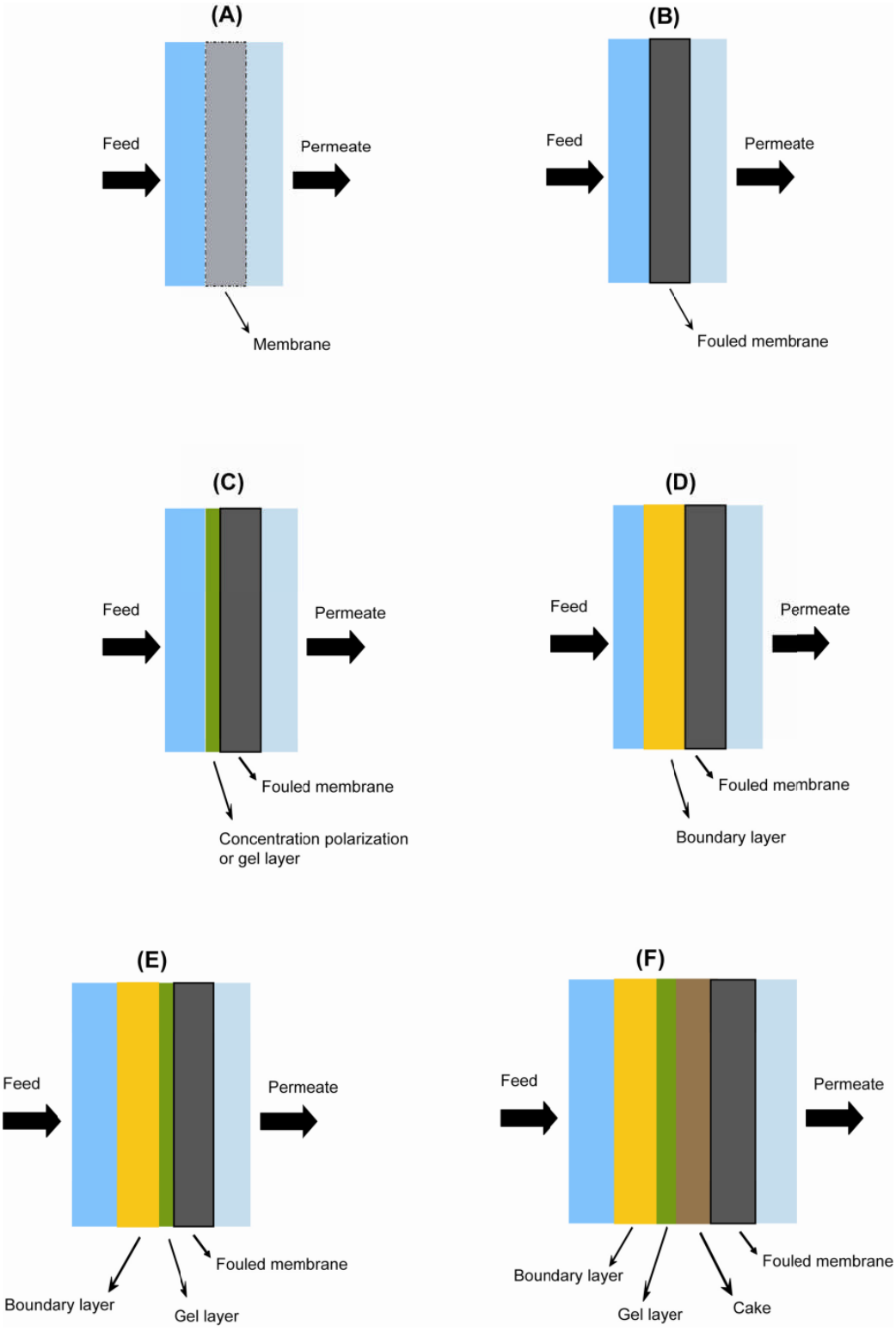

Figure 1.10 Schematic representation of the different situations showing flow through resistances in series for membrane filtration processes.

- **Membrane resistance**

Predicting a pure solvent flux, e.g. for water, is straightforward if the membrane resistance is known. R_m can be determined from experimental flux measurements and calculated by using Equation 1.4 and Equation 1.5. R_m can also be determined by employing the Kozeny-Carman equation in Equation 1.11 (Modise et al., 2005).

$$R_m = \frac{K(1-\varepsilon_m)^2 S_m^2 \Delta x_m}{\varepsilon_m^3} \tag{1.11}$$

In Equation 1.11, K is the Kozeny-Carman constant which depends on membrane morphology, ε_m is the membrane surface porosity, Δx_m is the membrane thickness and S_m is the pore internal surface area per unit volume. The membrane resistance can be estimated using the Kozeny-Carman equation under the assumption that each membrane consists of closely packed spheres. According to this equation, a small difference in porosity may have a significant effect on the calculated membrane resistance.

- **Fouled membrane resistance**

The fouled membrane resistance ($R_m + R_f$) is determined by performing the water flux experiment, as described above, before and after passing through to the membrane the feed suspension of interest. The first water flux experiment is to determine the clean membrane resistance, R_m, and the second to determine the total resistance R_T. From Equation 1.4 and Equation 1.6, R_f can be determined.

- **Boundary layer, concentration polarisation layer and gel layer**

The retention of certain components on one side of the membrane results in the phenomenon called concentration polarisation. At a certain distance from the membrane, the concentration of particles or solutes starts to deviate from the bulk concentration. This concentration increases, with the highest near the surface of the

membrane (Cheryan, 1998). For certain feeds, the concentration near the membrane becomes very high such that a layer of particles become viscous and gel-like, hence the term gel layer. This is schematically shown in **Figure 1.10**C. The resistance of the gel layer is calculated from Equation 1.4 and Equation 1.7.

The boundary layer on the other hand is formed at a distance away from the membrane where the concentration changes from the bulk concentration towards the highest (gel concentration) concentration near the membrane. This is schematically shown in **Figure 1.10**D. The resistance of the gel layer is calculated from Equation 1.4 and Equation 1.8. **Figure 1.10**E also illustrates a situation of concentration polarisation wherein the resistance is contributed by the resistances due to both the gel and the solutes within the boundary layer. This is also shown schematically in **Figure 1.11**A. Mulder (1996) has shown this differentiation between resistances of boundary layer and gel layer while Cheryan (1998) did not distinguish between the two and simply referred to this layer separate from the membrane as the concentration polarisation layer.

A disadvantage of this approach is the difficulty of distinguishing between these different layers. Okamoto et al. (2001) have shown a step by step determination of the different resistances of *E. coli* broth components. This type of investigation though is not practically applicable particularly when studying feed stocks that have interacting solutes and particles and with the interaction being different under actual filtration conditions.

- **Cake resistance**

Equation 1.11 is based on the classical cake filtration theory that was supported by the influential work of Grace (1953a). This was developed based on the Poiseuille law of viscous flow. It has become one of the most important equations in classical cake filtration which only assumes that aside from the membrane resistance, the other

contribution to resistance to flow is the cake which formed due to particles being deposited on the membrane surface. For membrane filtration, there has been no clear distinction between a “cake” layer, “gel” layer, “boundary” or “concentration polarisation” layer (Cheryan, 1998). It has been commonly applied to dead-end microfiltration analysis (Foley, 2006b).

$$\frac{dV}{dt} = \frac{A_m \cdot \Delta P_{TM}}{\left(\frac{\alpha \rho_o V}{A} + R_m \right) \cdot \mu} \tag{1.11}$$

Simple integration of Equation 1.11 yields the widely known parabolic law of constant-pressure filtration in Equation 1.12. From Equation 1.12, the average specific cake resistance, α, can be determined if ρ_o is known or can be estimated (Tien, 2008). α is a measure of how easily a feed can be filtered (Foley, 2006b). With Equation 1.13, and Equation 1.4, the permeate flux can be predicted if it could be assumed that the resistance is due to cake formation.

$$\frac{A_m \cdot t}{V} = \frac{\mu}{\Delta P_{TM}} \left(\frac{\rho_o \alpha}{2A_m} V + R_m \right) \tag{1.12}$$

$$R_T = R_C = \alpha \cdot m_C \tag{1.13}$$

1.4.2.3 Theories of concentration polarisation

In the previous section, the concept of concentration polarisation has been described. There are different theories that aim to describe this phenomenon although the basic premise of this is covered by the mass transfer film theory model (Belfort et al., 1994). Based on this model, the transport of solutes or particles towards the membrane is by convective transport mechanism due to permeate flow through the membrane while

transport away from the membrane may be by diffusion, inertia or shear forces (Romero and Davis, 1991). At steady state, these two opposing transport mechanisms reach a balance thus resulting in a steady flux. **Table 1.3** summarises the key theories for concentration polarisation and the inherent assumptions. Other models not included in the table were also reviewed by Ripperger and Altmann (2002). The models in **Table 1.3** are usually applied in CFF mode since this allows for the application of certain back transport mechanisms such as shear (Ripperger and Altmann, 2002). The classical models in this table were initially developed for ultrafiltration processes and their use extended in explaining microfiltration data (Song and Eiimelech, 1995). **Figure 1.11** illustrates the situations described by the models in **Table 1.3**. **Figure 1.11** A and C shows the concentration polarisation layer, either without (A) or with (C) cake formation, as stagnant or non-flowing and thus, the flow field shows the typical velocity flow field of most concentration polarisation models (e.g. Models 1, 2 and 5 in **Table 1.3**). **Figure 1.11** B and D illustrate a flowing concentration polarisation layer, beside a membrane (B) or a cake layer (C), as in Models 6 and 7 in **Table 1.3**.

Table 1.3 Key concentration polarisation models and their assumptions.

Model
[1] Film theory or *traditional* concentration polarization model *(Back transport by Brownian diffusion)* Porter (1972) in Belfort et al. (1994) $J = 0.81\left(\frac{\gamma_w D^{\ 2}}{L}\right)^{1/3} \ln\left(\frac{\phi_w}{\phi_b}\right)$ where $D = D_B = \frac{0.053kT}{\mu_F r}$

Table cont'd overleaf

Table 1.3 ***Continued***

Model
[1] Film theory or *traditional* concentration polarization model (*continued*) For dilute suspensions $\phi_b << \phi_w$ or $\phi_b < 0.1$ $$J = 1.31\left(\frac{\gamma_w {D_B}^2 \phi_w}{\phi_b L}\right)^{1/3}$$ **Key assumptions** ▪ strictly valid for only for very small permeate flux compared to longitudinal flux; ▪ no particle interaction ▪ cake is immobile ▪ laminar flow ▪ diffusivity is independent of shear rate
[2] Film theory or *traditional* concentration polarization model *(Back transport by Shear-induced diffusion)* Zydney and Colton (1986) in Belfort et al. (1994) $$J = 0.81\left(\frac{\gamma_w D^2}{L}\right)^{1/3} \ln\left(\frac{\phi_w}{\phi_b}\right) \qquad \text{where} \quad D = D_S = 0.03\gamma_w r^2$$ $$J = 0.078 \cdot \gamma_w \left(\frac{r^4}{L}\right)^{1/3} \ln\left(\frac{\phi_w}{\phi_b}\right)$$ For dilute suspensions $\phi_b << \phi_w$ or $\phi_b < 0.1$ $$J = 1.31\left(\frac{\gamma_w {D_S}^2 \phi_w}{\phi_b L}\right)^{1/3} \text{ or } J = 0.126 \cdot \gamma_w \left(\frac{r^4 \phi_w}{\phi_b L}\right)^{1/3}$$ **Key assumptions** ▪ strictly valid for only for very small permeate flux compared to longitudinal flux; ▪ no particle interaction ▪ cake is immobile ▪ laminar flow ▪ diffusivity is dependent of shear rate ▪ ignores viscosity effects

Table cont'd overleaf

Table 1.3 ***Continued***

Model
[3] Back transport by Shear-induced diffusion Romero and Davis (1988) $\int_0^{\delta_{fl}} u(\phi - \phi_b)\mathrm{d}y = \int_0^{L} J_{local}\phi_b \mathrm{d}L = Q$ $\qquad J_{local} = \frac{\Delta P_{TM}}{\mu_F\left(R_m + \delta_{fl}R_{fl} + \delta_{st}R_{st}\right)}$ (see number [4] for conditions)
[4] Back transport by Shear-induced diffusion Davis and Sherwood (1990) $J = C \cdot \gamma_w \left(\frac{r^4}{\phi_b L}\right)^{1/3}$ ▪ valid for very small permeate flux compared to axial flux; ▪ cake resistance dominates (low permeability) ▪ no particle interaction ▪ cake is immobile ▪ laminar flow ▪ dilute suspensions ▪ shear rate is dependent on particle concentration (ϕ) due to concentration dependence of viscosity ▪ diffusivity is dependent on particle concentration ▪ C = 0.0604 if particle concentrations between: $0 < \phi_b < 0.5$ and particles are monodisperse , rigid spheres in maximum random packing
[5] Film theory or *traditional* concentration polarization model *(Back transport by Inertial lift)* Drew *et al.*(1991) in Belfort et al. (1994) $J = 0.036\rho_F r^3 \frac{\gamma_w^2}{\mu_F}$ Reynolds number based on particle size is not negligible $\left(\frac{r}{2D_H}\right)^2 \cdot \mathrm{Re} << 1$ ▪ fast laminar flow ▪ immobile cake ▪ dilute suspensions ▪ independent of filter length and particle concentration

Table cont'd overleaf

Table 1.3 ***Continued***

Model
[6] Concentration polarization model *(Back transport by Brownian diffusion and shear induced diffusion)* Song and Eiimelech (1995) $$N_F = \frac{4\pi r^3}{3kT}\Delta P_P$$ if $N_F \leq 15$ $$J = \left(\frac{3}{2}D_B\right)^{2/3}\left(\frac{\gamma_w}{L}\right)^{1/3}\left(\frac{\Delta P_{TM}}{A_s(\theta^*)kTC_o}\right)^{1/3}$$ ▪ Defines a filtration number, N_F, which is the ratio of the energy needed to bring a particle from the membrane surface to the bulk suspension to the thermal (dissipative) energy of the particle.
[7] Non-equilibrium filtration (Cake formation) Song and Eiimelech (1995) From [6] if N_F >15, and resistance of the polarization layer dominates: $$J = \left(\frac{3}{2}D_B\right)^{2/3}\left(\frac{\gamma_w}{L}\right)^{1/3}(1+N_c)^{1/3}\left(\frac{\Delta P_P}{A_s(\theta^*_{\max})kTC_o}\right)^{1/3}$$ Assuming negligible membrane resistance: $$N_c = \frac{\Delta P_c}{\Delta P_c}\frac{A_s(\theta^*)}{A_s(\theta_{\max})}$$ From [6] if N_F >15, and resistance of the cake layer dominates $$J = \left(\frac{3}{2}D_B\right)^{2/3}\left(\frac{\gamma_w}{L}\right)^{1/3}\left(\frac{\Delta P}{A_s(\theta_{\max})kTC_o}\right)^{1/3}$$ ▪ Assumes immobile cake ▪ Fluid field in the channel is undisturbed by the cake layer ▪ N_c is the cake thickness factor which reflects the effect of the cake layer thickness on the accumulation of the retained particles in the polarization layer

Table cont'd overleaf

Table 1.3 ***Continued***

Model
[8] Back-transport with cake filtration Schulz and Ripperger (1989) For turbulent flow: $$J = K_T{}^{1/2}\left(\upsilon \cdot \rho_F \cdot \frac{(\rho_c - C_B)}{C_B}\right)^{1/2}\left(\frac{\Delta P}{\mu_F \alpha}\right)^{1/2}$$ For laminar flow: $$J = K_L{}^{1/2}\left(\frac{\upsilon}{h} \cdot \frac{(\rho_c - C_B)}{C_B}\right)^{1/2}\left(\frac{\Delta P}{\mu_F \alpha}\right)^{1/2}$$ ▪ Combines fluid transport treatment in the presence of cake that may cause resistance to flow.
[9] Suspension flow model Kromkamp *et al.*. (2005) Hydrodynamics components: $$\frac{\partial \rho}{\partial t} = \nabla \cdot \rho \mathbf{u}$$ $$\frac{\partial \rho \mathbf{u}}{\partial t} + \mathbf{u} \cdot \nabla \rho \mathbf{u} = -\nabla p + \upsilon \nabla^2 \rho \mathbf{u} + F$$ Suspension component (convection-diffusion): $$\frac{\partial \phi}{\partial t} + \mathbf{u} \cdot \nabla \phi = D \nabla^2 \phi$$ ▪ Flow model resolved by Lattice Boltzmann method by computational fluid dynamics ▪ Does not assume Poiseuille flow for pressure. ▪ Viscosity is a function of particle volume fraction (ϕ) ▪ Diffusion coefficient, D is $f(\phi)$

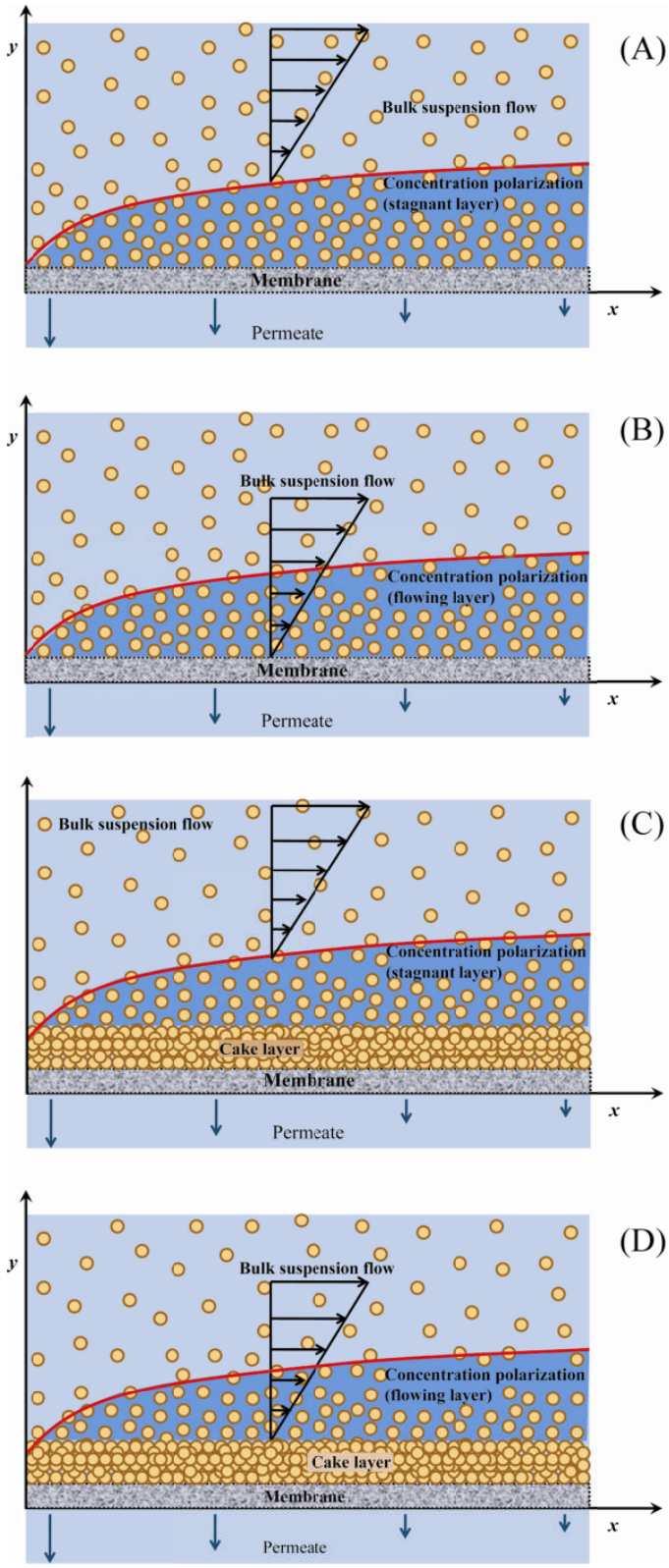

Figure 1.11 Schematic diagram of the particle concentration distribution and fluid flow field in the steady state situation during crossflow microfiltration.

1.4.2.4 Application to biological materials recovery and purification

The complicated nature of modelling filtration processes is obvious from **Table 1.3** and **Figure 1.11**. This is not surprising considering the dynamic nature of membrane filtration and with the many aspects to be considered which may affect the filtration process. Key here are the operating conditions such as crossflow velocity (shear-rate), and the transmembrane pressure; the properties of the membrane such as material, pore size; and the possible interactions of feed components (soluble or particles) with the membrane under filtration conditions (Russotti et al., 1995). Most of the models in **Table 1.3**, however, are still simplistic representation of actual membrane filtration processes involving complex biological solutions. For example, the classical models (e.g. Models 1-5 in **Table 1.3**) generally ignore the impact of cake formation, membrane fouling due to physico-chemical interaction, and adsorption of some of the soluble components in the feed suspension. Some of these models also do not take into account the resistance to permeate flow of the presence of a cake or gel, or even the resistance of a concentration polarisation layer. For particles greater than 0.1 μm, cake formation is known to dominate flux behaviour and that pressure dependence becomes weak with the presence of concentration polarisation and cake formation (Song and Eiimelech, 1995). Additionally, the classical models also do not include:

- any interactions between particles, solutes and the membrane or the fact that these interactions could change depending on operating conditions (Hodgson et al., 1993; Russotti et al., 1995; Keskinler et al., 2002);
- the effect of particle size in the preferential deposition on the membrane (Foley et al., 1995; Kromkamp et al., 2006);
- the effect of cake compressibility or the compressibility of the concentration polarisation layer (Reismeir and Kula, 1989; McCarthy et al., 1998); and
- the impact of pore blocking on flux (Song, 1998).

The general assumption in most of the classical models in **Table 1.3** is that bulk flow is fully developed Poiseuille flow with time-independent flowrate is not valid in actual filtration conditions due to, among others, the complex geometry of the flow path (e.g. presence of turbulence promoter) or with the variation of cake layer height along the channel length (Kromkamp et al., 2005). Furthermore, these models were derived from a single mass balance equation with the permeate velocity and particle concentration distribution over the membrane as the unknowns, thus, as is often made, it is assumed that the concentration of the stagnant layer along the membrane is constant (Song and Eiimelech, 1995). More accurate modelling is therefore promoted to cover the complexities of membrane systems. An accurate and detailed solution of the flow field is now possible with the use of computational fluid dynamics (CFD) as was shown by Wiley and Fletcher (2003), Kromkamp et al. (2005), and Ghidossi et al. (2006). Recently, Foley (2006a) cited that the complexities of the crossflow microfiltration processes can be captured from small, targeted experimental data and together with dimensional analysis can provide useful empirical correlation to explain and predict crossflow microfiltration data. Dimensional analysis has been traditionally applied to describe the complex relationships in fluid flow, heat and mass transfer in chemical engineering processes (Foley, 2006a).

Belfort et al. (1994) has stressed the difficulty in modelling crossflow filtration processes. Even with CFD, it is still necessary to assess the CFD models against actual crossflow filtration data. This could be done by retrospective analysis of previous studies or combining modelling studies with experimentation. Both of these have their drawbacks. First, on previous data, Foley (2006a) reviewed the data available in literature and concluded that while there are a large number of papers on crossflow microfiltration, only a few provide extensive information on the effect of process parameters on the steady state flux. Most studies were found to be on membrane fouling and flux decay. A similar conclusion has been reached in assessing the literature for this

thesis. Additionally, it could be said that the available data in literature on crossflow microfiltration were using feed systems that are simple (such as harvest broths or reconstituted Baker's yeast in buffer) and often times diluted or at low concentration. Very few reflect the kind of complexity which is inherent in biopharmaceutical feedstocks, for example high titre cell culture in complex media or cell lysates. Second, on experimentation, comprehensive experiments to cover extensive experimental space and conditions require a lot of feed material. The production of biopharmaceutical feedstock is inherently expensive making extensive experimentation impractical.

Given this background, it is proposed in this thesis to create microscale bioprocessing techniques for membrane filtration which will address the need to understand microfiltration processes. This membrane filtration platform will enable experimentation with real, complex feedstocks because the cost of performing experiments with the microscale approach is not prohibitive due to the relatively smaller feed requirements. In tandem with laboratory automation, the automated microscale approach has the potential to rapidly explore wider experimental space thus enabling in-depth analysis of the extensive microscale data to understand membrane filtration mechanism. In the subsequent section, the current microscale unit operations and the available membrane filtration systems are reviewed.

1.5 Overview of Microscale (Scale down) Unit Operations

Most of the earlier microscale studies in microscale processing have mainly focused on upstream operations particularly in high-throughput miniature bioreactors (Betts and Baganz, 2006). In order to maximise the potential of this approach, however, Jackson et al. (2006) identified the need to establish more microscale downstream processing operations. In this regard, Titchener-Hooker et al. (2008) highlighted in their review the

strong interaction between the complex biological materials and the engineering environment within the downstream process steps. A comprehensive analysis of the various micro-biochemical engineering design of downstream processes revealed that scale-down methods are available for a wide range of operations including disc and tubular centrifugation, dead-end microfiltration, leaf filtration, high pressure homogenisation, expanded bed adsorption and chromatography. In scaling down, the key effects that dominate the unit operation were maintained across the scales. For example, shear was found to play an important role in various process operations and its effects should be reflected at all scales. Other examples of criteria for scaling are linear velocity in chromatography and power per unit volume or volumetric mass transfer coefficient in bioreactors. This scale down method has been applied to a variety of systems (microbial fermentation, mammalian cell culture, precipitation, high cell density cultures) and recently applied to a centrifugation study using industrial process feedstocks (Zaman et al., 2009).

Coffman et al. (2008) developed a high-throughput screening methodology to investigate hydrophobic interaction and anion-exchange chromatographic separations using microwell filter plates. Chhatre et al. (2009) employed commercially available chromatographic pipette tips for the automated microscale investigation of column performance. Successful prediction of industrial scale clarification of mammalian cell broth have been obtained by Tait et al. (2009) using microwell technology in combination with ultra scale-down centrifugation techniques. Other downstream process technology developments include the use of Adaptive Focused Acoustics to simulate the product and contaminant profile produced by the larger-scale high pressure homogenization process (Wenger et al. 2008). Microplates have also been successfully employed in the optimization of protein freeze-drying formulations (Grant et al., 2009). Most of the reports on microscale downstream processes mentioned above are amenable for parallel experimentation and automation within a laboratory robotic

platform thereby increasing the number of experimental variables that could be investigated and facilitating studies on linked-process sequences.

Until the beginning of this work in 2007, very few filtration studies have been conducted at the microscale and most operate as dead-end filtration processes as summarised in **Table 1.4**. Low-volume tangential flow filtration modules are also commercially available. However, the modules are not readily adaptable into automated workstations and may not be easily used for parallel membrane testing or multiple feed processing. More recently, a miniature rotating disc device was used to simulate a larger scale diafiltration process (Guijun et al., 2010).

Table 1.5 describes the available commercial membrane modules which may be fitted in the filtration systems given in **Table 1.6**. Aside from the specified membrane modules, the membrane devices mentioned in **Table 1.6** can also be fitted with custom-made membrane modules. Among the available platforms, Jackson et al. (2006) were able to show quantitative parallel analysis of DEF processes within an automated environment. They were able to show that filtration processes at the microscale yield comparable data with standard laboratory membrane cells but with less amount of feed and with more ease and higher degree of reproducibility since their format also allows for parallel testing. Furthermore, a custom-made system integrated into an automated platform enabled the quantitative collection of process engineering data.

Table 1.4 Previous studies on microscale filtration system

[Ref.] Format	Operation/Application	Filter area (cm^2)
[1] 96-well plate syringe filter discs	Dead-end filtration/ microfiltration	0.28 to 4.26
[2] 16-well filter discs (custom-made)	Dead-end filtration/ nanofiltration	12.6
[3] 8 to 24-well filter discs (custom-made)	Dead-end filtration/ microfiltration	0.79

Ref.: [1] Chandler and Zydney (2004); [2] Vandezande et al. (2005); [3] Jackson et al. (2006)

Table 1.5 Commercial filter modules for miniature or automated tangential flow filtration

Manufacturer and product	Membrane material	Operating pressure	Hold-up volume	Remarks
Millipore (www.millipore.com) Pellicon® XL 50 Cassette (membrane area = 50 cm^2)	1. Polyethersulfone 2. Composite regeneratre cellulose 3. Hydrophilic PVDF	5600 kPa (maximum)	3.2 mL	The same path length and channel height exist for all filters of the Pellicon cassettes. This allows for linear scale-up.
PALL Life Sciences (www.pall.com) Minimate™ TFF Capsule (membrane area = 50 cm^2)	Modified polyethersulfone	4000 kPa (maximum)	1.6 mL	Allows for linear scale-up A limitation of this module is that it is only available in one type of membrane
GE Healthcare Life Sciences (www.gehealthcare.com) a.) Hollow fibre Start AXM Crossflow Cartridge (membrane area = 50 cm^2) b.) Hollow fibre Start AXH Crossflow Cartridge (membrane area = 40 cm^2) c.) MidGee™ Hoop Crossflow Cartridges (membrane area = 29-73 cm^2)	Polysulfone-based		1-1.5 mL (Lumen side) 1 mL (Shell side) < 1mL (Lumen or shell side)	A limitation of this module is that it is only available in one type of membrane

Table 1.6 Available miniature filtration systems or devices

Reference	Filter module	Flow rates/ Recirculation volume	Remarks
Millipore (www.millipore.com) Labscale™ TFF System	Pellicon XL 50	Feed flow rate: 10-100 mL/min Min Recirculation volume: 20 mL	The system can hold up to 3 Pellicon cassettes which makes it useful for simultaneous membrane testing. Has one feed reservoir.
PALL Life Sciences (www.pall.com) Minimate TFF System	Minimate TFF Capsule	Recirculation rate: 10-240 mL/min Min system working volume: < 5mL	The system can only hold 1 capsule. Has one feed reservoir.
GE Healthcare Life Sciences (www.gehealthcare.com) ÄKTAcrossflow™	Any modular membranes (commercial e.g. AXH/AXM Crossflow cartridges or even Pellicon XL 50 or Minimate TFF Capsule, or costum made)	Feed flow rates: 8.5 – 600 mL/min (depending on membrane format) Min working volume: 22 mL	Fully automated system. A software controls the process and allows some electronic data logging. Has one feed reservoir.
Petersen and Wolk (2007) US Patent/ European Patent Assigned to Millipore Corp. USA *Automated low-volume TFF device*	Any modular membranes (commercial e.g. Pellicon XL 50 or Minimate TFF Capsule, or costum made)	Min recirculation volume: < 20 mL	Fully automated system. Has a feed reservoir with distinct mixing zone. System allows for electronic data processing.

1.6 Aims of the Project

The overall aim of this thesis is to establish a microscale bioprocessing platform for the evaluation of both dead-end and crossflow filtration operations and the impact of upstream operations on filtration performance. The dead-end filtration studies will extend the previously published method of Jackson et al. (2006) described earlier in Section 1.5. Establishment of a microscale crossflow operation will require the design of a novel filtration device compatible with the automation platform on which linked fermentation – cell disruption – filtration sequences will be established.

The context of this work is within biopharmaceutical product development described in Sections 1.2 and 1.3 as well as industry collaborative studies within the UCL Innovative Manufacturing Research Centre (IMRC) for Bioprocessing. Where ever possible therefore, care has been taken to utilise products and expression systems that are representative of the complex biological feeds encountered by industry in this sector. In particular, an *E. coli* strain expressing humanised antibody Fab' fragments (kindly supplied by UCB Celltech) was used as a case study for evaluation of the microscale filtration methodologies. Given the potential of antibody Fab' fragments to be developed into novel therapeutic molecules and the new challenges brought about by being expressed inside microbial cells (Section 1.3.), this particular expression system (referred to from here on as *E. coli* Fab') was chosen to be an ideal system for process development studies using the microscale bioprocessing approach.

In order to achieve the overall project aim a series of objectives were defined as described below.

- Building on the work of Jackson et al. (2006), where a microscale dead-end filtration device was created and which was shown to produce comparable results

with larger scale dead-end filtration systems, the first objective was to further simplify and reduce the volumes of feed needed to perform microfiltration studies. A new method was thus developed and its suitability to investigate microfiltration performance was first assessed. This was to confirm reproducibility and show that the improved method could also capture differences in feed preparation and operating conditions. The results of this work are presented in Chapter 3 of this thesis.

- Having established the new microscale dead-end filtration methodology the next objective was to demonstrate how this methodology can be employed to assess process interactions affecting primary product recovery using membrane filtration. In particular, it was used to investigate two consecutive process steps: antibody Fab' fragment extraction from *E. coli* cells and their subsequent recovery by dead-end microfiltration. The results are presented in Chapter 4 of the thesis.

- The third objective was to expand the range of operations that can be studied at the microwell scale and entailed the design of a novel, automation compatible, microscale crossflow filtration (CFF) device. Once constructed, the associated methodologies for the operation of the microscale CFF device were developed. Its operation was then compared to the performance of a larger scale CFF module, initially using a model process feed of Baker's yeast with bovine serum albumin (BSA) in phosphate buffer. These results are presented in Chapter 5 of the thesis.

- The final objective was to demonstrate the application of the microscale CFF device in informing bioprocessing options by predicting larger scale performance using an industrially relevant *E. coli* Fab' feedstock. In particular, the impact of DNA hydrolysis by using either exogenous or endogenous nucleases on crossflow

microfiltration processes was investigated. The results are presented in Chapter 6 of the thesis.

Once each of the component elements of the microscale filtration platform has been established their performance characteristics and wider application throughout the biopharmaceutical bioprocessing sector was reviewed. This evaluation is described in Chapter 7 along with recommendations for future work. **Figure 1.12** is a schematic representation of the application of the microscale bioprocessing approach in this thesis for membrane filtration processes, particularly in studying the linked process sequences involving primary recovery.

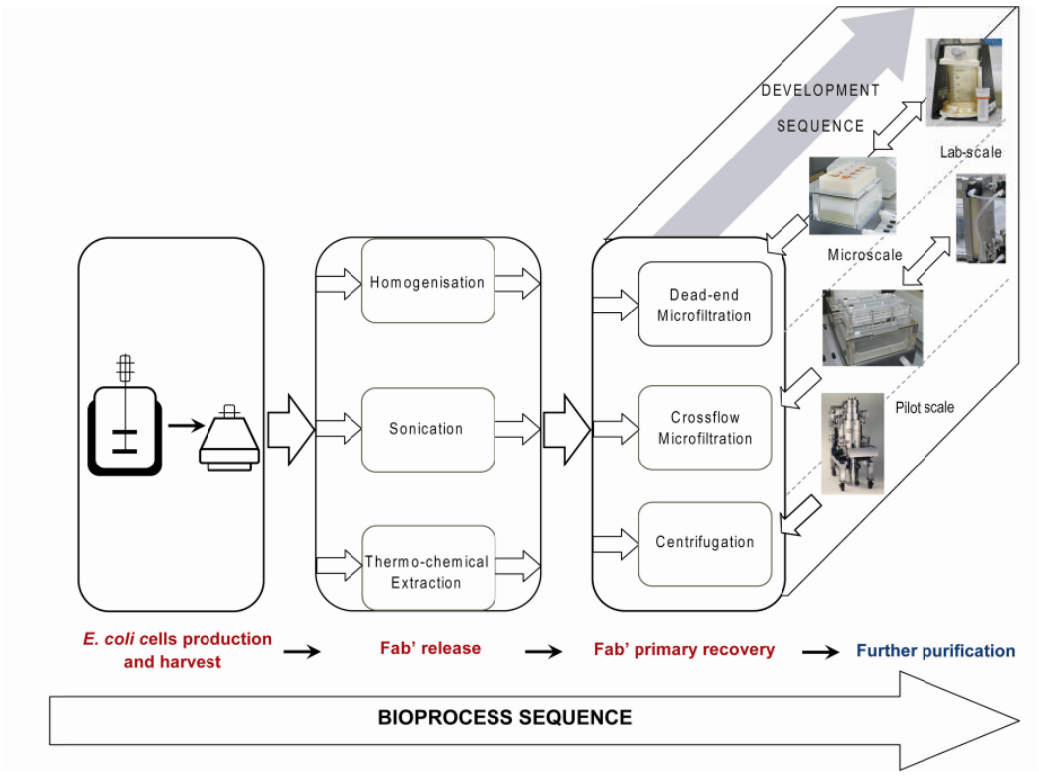

Figure 1.12 Application of the microscale bioprocessing platform for membrane filtration for the investigation of bioprocess routes for the primary recovery of antibody Fab' fragments. (Image credit: Pilot scale centrifuge from www.pneumaticscale.com)

2. Materials and Methods

This chapter describes common materials, routine experimental methodologies and analytical procedures used throughout this work. Details specific to certain experiments are described in the following chapters.

2.1 Materials

Membrane materials were purchased from Millipore (Hertfordshire, UK) and Pall (Portsmouth, UK). All analytical reagents were purchased from Sigma-Aldrich (Dorset, UK) unless otherwise stated and were of the highest purity available. Purified water, conductivity < 0.2 μmS cm^{-1}, from a Millipore Elix 10 water purification system (Hertfordshire, UK) was used in all experiments. The industrial *Escherichia coli* strain W3110 containing plasmid pTTOD A33 was kindly provided by UCB-Celltech (Slough, UK) and was from a working cell bank prepared as described by Bowering et al. (2002). The strain expresses humanised antibody Fab' fragments with each antibody chain preceded by the *E. coli* OmpA signal peptide which directs secretion of the Fab' fragments into the periplasm of the cells (Tustian, 2008). Baker's yeast, *Saccharomyces cerevisiae*, was purchased in powder form from Sigma-Aldrich (Dorset, UK).

2.2 Pilot-scale production of antibody fragments

2.2.1 20 L Fermentation vessel

A 20 L stainless steel, jacketed fermentor (Applikon Biotechnology B.V., Schiedam, The Netherlands) was used in the production of recombinant *E. coli* that expresses antibody Fab' fragments (Section 2.1). The fermentor has a top driven, three-stage, six-bladed Rushton-type impeller, and four-equally spaced baffles. It has ports for sampling, reagent addition and harvest. The main vessel, with the fermentation media, all ports and ancillary lines were steam sterilised in place at 121^{o}C for 20 minutes. The fermentation operation (i.e. control of impeller speed, temperature and pH) was controlled by Applikon's process control software BioXpert. The impeller was on cascade control initially set at 400 rpm (1400 rpm max) and changes according to the measured dissolved oxygen tension (DOT). The DOT probe was calibrated with nitrogen and air for 0% and 100% readings, respectively. Dissolved oxygen was maintained at 30%, using gas blending with enriched oxygen (40:60 O_2:N_2) when necessary. pH was measured with a pH probe that was calibrated off-line at pH 4.0 and 7.0 prior to fermentation. Both DOT and pH probes were sterilised during fermentor sterilisation. Temperature was maintained by passing steam or cooling water through the jacket.

2.2.2 *E. coli* fed-batch fermentation

Recombinant *E. coli* production routinely followed the method previously described by our laboratories based on the earlier work of Tustian (2008). Starter cultures were grown in 2xPY complex media containing 10 μg mL^{-1} tetracycline, 16 g L^{-1} phytone, 10 g L^{-1} yeast extract, and 5 g L^{-1} NaCl shake flasks at 37°C, 200 rpm shaking speed for about 4 hours. These were used to inoculate (10% v/v) shake flasks with SM6G$_c$ defined media containing 112 g L^{-1} glycerol and 10 μg mL^{-1} tetracycline and adjust to pH 6.95. These were then incubated at 30 °C for about 20 hours at 200 rpm shaking

speed. One litre of this defined media shake flask cultures inoculated 10 L of $SM6G_c$ defined media in the fermentor described in Section 2.2.1. DOT was maintained at 30%; pH was maintained at 6.95 using 50% (w/v) ammonia solution and 20% (v/v) H_2SO_4 and temperature at 30 ^oC. After 32 h, the temperature was reduced to 25°C. Glycerol feeds, Mg^{2+}, and PO_4^{2-} were added to the culture at certain intervals when OD_{600} was between 40-90. Isopropyl-β-D-thiogalactopyranosid (IPTG) was then added after approximately 36 hours to induce Fab' production. During the Fab' production phase, glycerol was continuously fed (at feed rates between 10-25 mL h^{-1}) to the fermentor until harvest. The culture was harvested from the fermentor when Fab' started to be secreted into the culture media, which was approximately 36 h after the addition of IPTG. Typical cell growth of this culture is shown in Appendix 1.1. The time profile of the extra- and intra-cellular Fab' content is also shown.

2.2.3 Cell harvest by laboratory scale centrifugation

20-millitre aliquots of the fermentation broth were spun at 4000 rpm for 45 minutes in a bench top centrifuge (Centrifuge 5800, Eppendorf, Germany). The supernatant was removed from the cell paste and both were separately stored as described in Section 2.2.5.

2.2.4 Cell harvest by pilot scale centrifugation

Pilot scale cell harvest was performed using a pilot scale tubular bowl centrifuge (CARR™ P6™ Powerfuge, Pneumatic Scale, Clearwater, FL, USA). Fermentation broth was first collected from the fermentor using 20 L holding vessels.Whole cells were then immediately recovered by centrifugation at a feed rate of 30 L h^{-1} and a bowl speed of 15,000 rpm. The collected cell paste was either used immediately or stored as described in Section 2.2.5.

2.2.5 Storage of cell paste

Harvested cells which were not immediately used for primary recovery experiments were stored in clear bags at -20^{o}C until further use. When required, a portion of the cell paste is obtained and allowed to thaw at room temperature for 1- 4 hours depending on the amount. This sample is referred to as, from here onwards, freeze-thawed samples.

2.3 Methods for Fab' release

2.3.1 Fab' release by continuous homogenisation

Cell disruption was performed to release the Fab' fragments from *E. coli* cells which are either fresh from cell harvest (Section 2.2.4) or freeze-thawed (Section 2.2.5). Cells were first resuspended in 100 mM Tris buffer at the desired pH. Cell disruption by continuous homogenisation was performed using a pilot scale APV Manton-Gaulin Lab 60 (APV International, West Sussex, UK) high pressure homogeniser which was operated at 500 bar and at a constant flowrate of 60 L h^{-1} (or 1 L min^{-1}). At this rate, a 2 L cell suspension was processed through the homogeniser for four minutes before collection in order to achieve homogenisation equivalent to 2-passes. The Lab 60 homogeniser was operated with no temperature control although ethylene glycol was used as coolant. Samples were immediately used in subsequent microfiltration experiments (Section 2.6.2 or Section 2.7.2) or routinely stored overnight at 4^{o}C.

2.3.2 Fab' release by batch homogenisation

Using the cells fresh from cell harvest (Section 2.2.4) or freeze-thawed (Section 2.2.5), cells were resuspended in 100 mM Tris buffer at the desired pH. Batch cell disruption operations were performed using an APV Manton-Gaulin Lab 40 homogeniser (APV International, West Sussex, UK). The homogeniser has a maximum capacity of 40 mL per batch with minimum feed volume of 35 mL. Disruption operations were performed

for 2 passes per batch of cells at 500 bar. At this pressure, maximal Fab' release is achieved in 2 passes. No significant release of Fab' was observed by increasing the number of homogenisation passes (Balasundaram et al., 2009a). Samples were immediately used in subsequent microfiltration experiments (Section 2.5.3, Section 2.6.2 or Section 2.7.2) or routinely stored overnight at 4^{o}C.

2.3.3 Fab' release by thermo-chemical treatment

Using the freeze-thawed cells (Section 2.2.5), the periplasmic Fab' fragments were extracted from the cells by applying a combined heat and chemical treatment. This was done by incubating the cells resuspended in 100 mM Tris / 10 mM EDTA solution, adjusted to the desired pH (pH 7.0, 7.4 or 7.8) using concentrated HCl, and pre-heated to the desired temperature as required. The resuspended biomass concentration varied between 22-52 g_{DCW} L^{-1}. The cell suspensions were filled into a 24-well, round bottom, polypropylene microplate (Whatman-GE, UK), sealed with aluminium film: AlumaSeal^{TM} (Excel Scientific, USA) and incubated for up to 20 hours in a thermomixer (Eppendorf ThermomixerComfort, Eppendorf AG, Germany) at 800 rpm shaking speed. The treated cells were immediately used in subsequent microfiltration experiments (Section 2.5.3).

2.3.4 Fab' release by sonication

Using the freeze-thawed cells (Section 2.2.5), sonication was performed using an MSE Soniprep 150 apparatus (Sanyo Electric, Osaka, Japan) operated at 3 cycles of 20 s on, 10 s off at 8 um amplitude, using 1 mL sample volumes. The sonicator was operated at ambient temperature. Samples were then pooled to make-up at least 8mL of sonicated cells. The pooled samples were immediately used in subsequent microfiltration experiments (Section 2.5.3).

2.3.5 Fab' release by adaptive focused acoustics (AFA)

Fab' fragments were quantified to monitor production during *E. coli* fermentation (Section 2.2.2). For Fab' quantification during this period, cells were disrupted by adaptive focused acoustics (AFA) using the Covaris E210 (Woburn, MA). 1.5 mL of fermentation broth samples in borosilicate glass tubes were placed on a sample rack onto the Covaris' degassed water bath which was maintained at 8^{o}C. A duty cycle of 20%, acoustic radiation intensity of 85W and 500 cycles per burst were used. These settings are known to achieve complete cell disruption comparable with high pressure homogenisation (Perez-Pardo et al., 2011).

2.4 Microwell automation platform: Tecan Genesis™

A Tecan Genesis™ liquid handling platform (Tecan, Reading, UK) was the automation platform used in this work. The lay-out of the platform deck is shown in **Figure 2.1**(A). The key element is the vacuum separation manifold (Te-VacS™) shown in position on the deck in **Figure 2.1**A(1) and in more detail in **Figure 2.1**(B). This is where the automated microwell filtration processes were performed. There are two vacuum block positions in this manifold which are connected to a high-performance vacuum pump via separate extractor and vent lines. Platform operation is controlled and programmed through the Tecan Gemini™ software. A sample Gemini™ program is shown in Appendix 1.2. Actual differential pressures between the atmospheric pressure and the pressure inside the vacuum block were measured by a digital manometer (Manometer 840080 series, SPER Scientific, Scottsdale, AZ) attached via a T-connector to one of the vent lines. Differential pressures were continuously recorded at 60 Hz by a data logging system (Handheld, SPER Scientific) on a PC.

2.5 Microscale dead-end microfiltration

2.5.1 Microscale dead-end filtration device

The custom filter plate used in this study was described previously by Jackson et al., (2006). A picture of the filter plate is shown in **Figure 2.1** (B) while **Figure 2.2** shows a schematic diagram of the set-up for microscale dead-end filtration experiments. The plate dimensions are 128 x 86 x 31 mm and accommodate up to 24, 14 mm diameter wells that can fit removable membrane inserts. Removable collection tubes were obtained by modification of Durapore Ultrafree-CL centrifugal filters (Millipore, UK). The membranes were either pre-fitted within the centrifugal filters or were cut to size and manually fitted into the filter inserts.

2.5.2 Water flux experiments by dead-end filtration

The membrane resistances were determined by measuring the amount of water that permeated through the membrane over a set filtration time. The permeate weights were converted to volume by assuming a density of water of 1.0 g mL^{-1}. The viscosity of water at 23^{o}C [μ = 1.0 x10^{-3} N s m^{-2} (Perry and Green, 1997)] was used in all calculations. The membranes were prepared before use by soaking in deionised water for at least five minutes followed by passage of at least four millilitre of water through the membrane under 65 kPa pressure gradient. Digital pressure measurement was acquired as described in Section 2.4. Replicates were performed in all experiments.

2.5.3 Microfiltration of disrupted *E. coli* cells

Membranes were prepared as described in Section 2.5.2. The volume of feed used in each well was between 400-500 μL, the volumes remaining constant for each parameter tested e.g. temperature, pH etc. Time and permeate mass data were gathered during stepwise filtration at 65 kPa transmembrane pressure. Full details of the stepwise method devised to quantify cake resistance are described in Chapter 3.

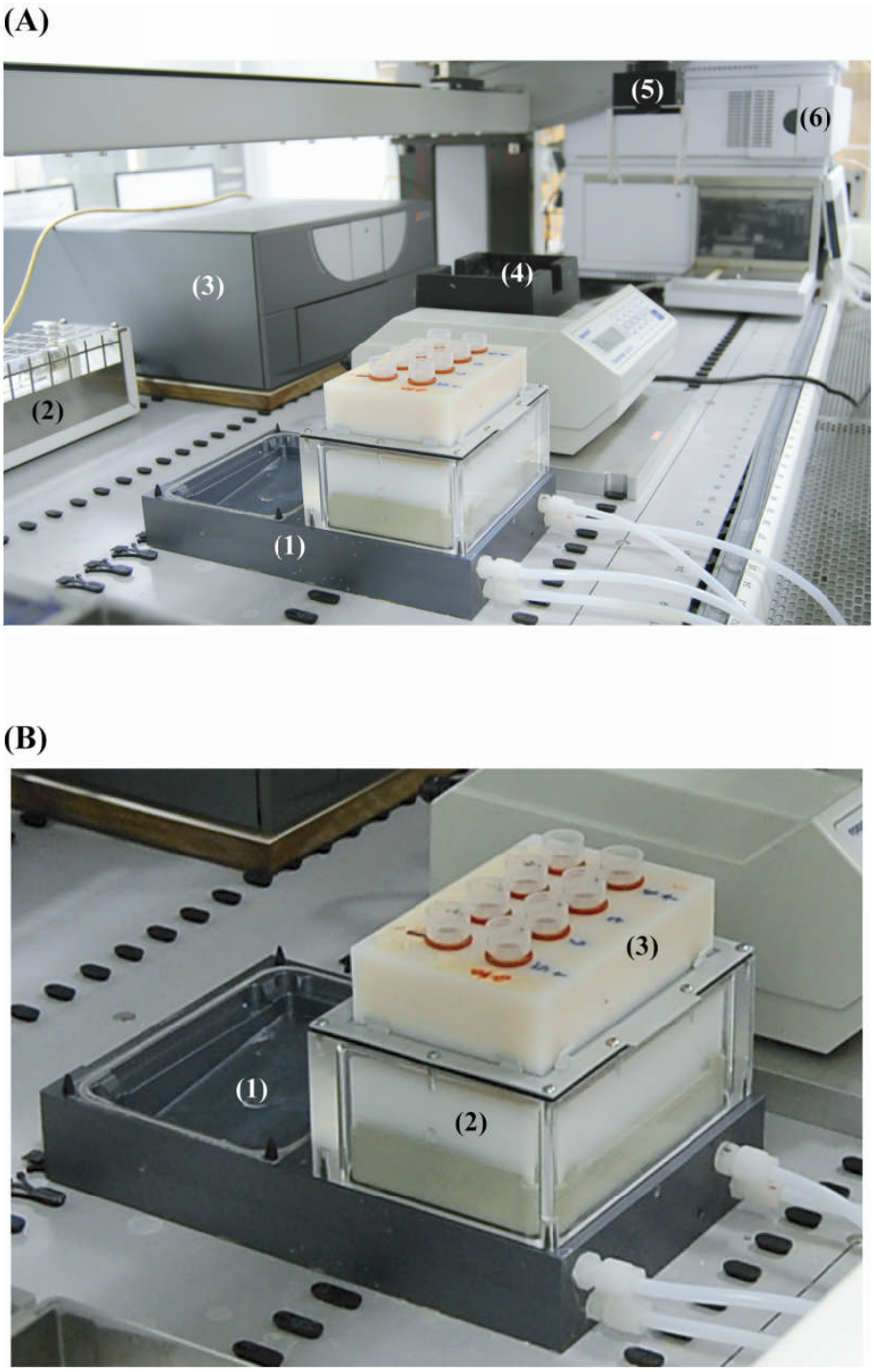

Figure 2.1 Tecan Genesis™ automation platform. (A) View of the deck of the Tecan Genesis™ workstation showing: (1) the vacuum separation manifold (Te-VacS™); (2) UV lamp; (3) plate reader; (4) thermomixer; (5) robotic arm manipulator (RoMa); and (6) HPLC; (B) A close-up view of the vacuum block showing: (1) Position 1 (Te-VacS1); (2) Position 2 (Te-VacS2) with vacuum block; (3) Filter plate holding eight membrane wells.

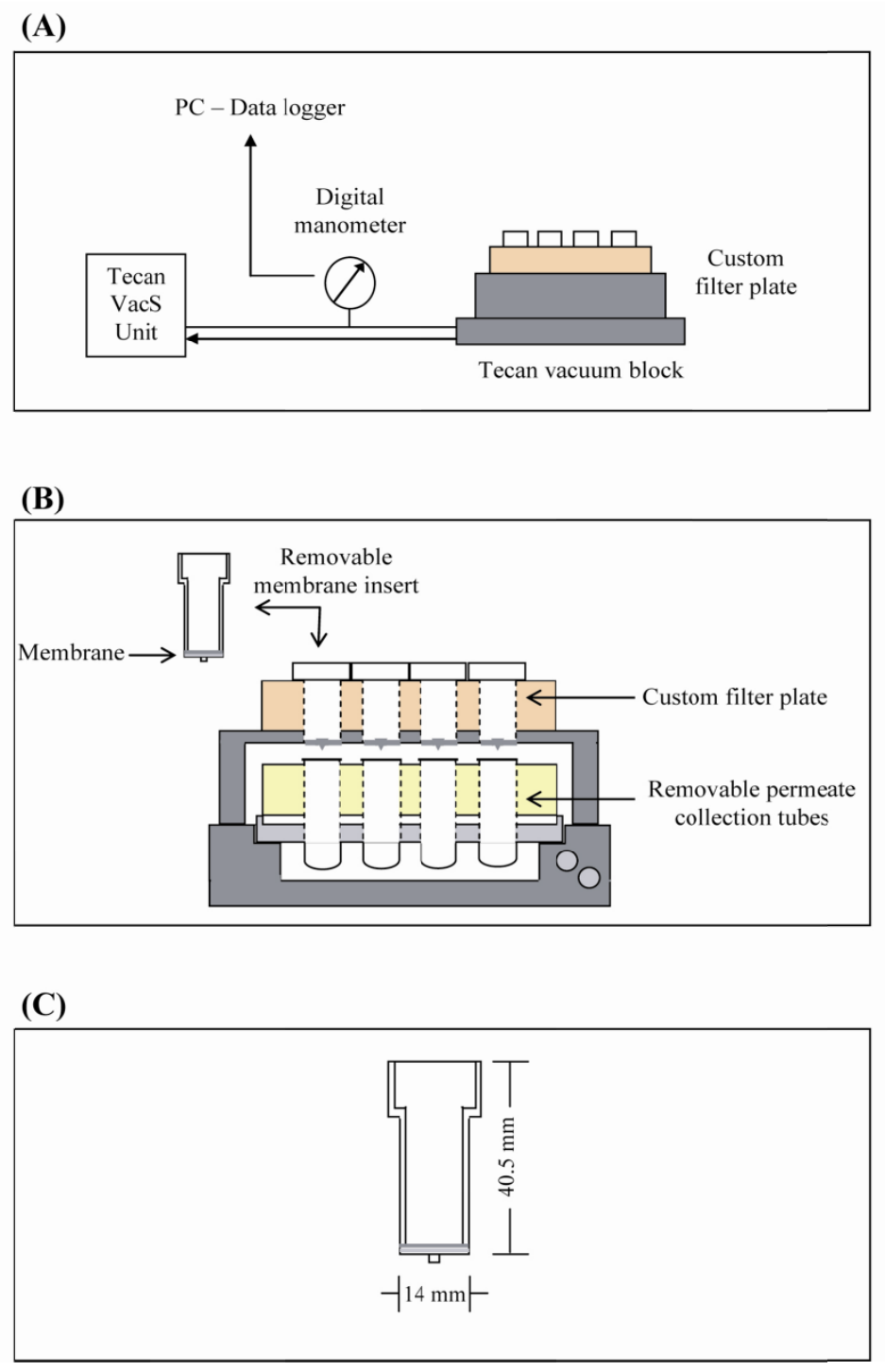

Figure 2.2 Microscale devices for automated microfiltration studies: (A) vacuum manifold equipment located on the deck of a Tecan Genesis™ robotic platform; (B) detailed cross-section of the vacuum block showing filter plate, membrane inserts and collection tubes; (C) dimensions of the membrane insert made of polypropylene material.

2.6 Laboratory scale crossflow filtration

2.6.1 Laboratory scale CFF module

Primary recovery at laboratory scale was performed by crossflow filtration (CFF) using a Millipore Proflux™ M12™ Tangential Filtration System with a Pellicon-2™ Mini membrane module as shown in **Figure 2.3** (0.22 μm rated hydrophilic Durapore poly(vinylidene fluoride) or PVDF, with 0.1 m^2 membrane area, type V-screen). The membrane module is held in a stainless steel Pellicon-2™ mini-holder which is vertically orientated; therefore the feed entered via a bottom port and exited at the top in the retentate port.

2.6.2 Laboratory scale CFF operation

Crossflow filtration experiments were performed at constant transmembrane pressure (ΔP_{TM}) conditions where ΔP_{TM} is defined as:

$$\Delta P_{TM} = \frac{P_F + P_R}{2} - P_P \tag{2.1}$$

where P_F is the feed pressure, P_R is the retentate pressure and P_P is the permeate pressure. The permeate pressure can be neglected while the feed and retentate pressures were measured by digital manometers and logged onto a data acquisition system as described in Section 2.4.

Lab-scale filtration experiments were run in total recycle mode where the retentate and permeate lines were recycled back to the feed reservoir. Permeate was periodically collected from the top permeate port for flux measurements. The permeate flux was determined by monitoring the time (Δt) needed to collect a certain volume of permeate ($V_{\Delta t}$) and can be expressed in terms of LMH or litres per m^2 of membrane area (A_m) per hour. The temperature of the permeate was measured so that the appropriate viscosity

corrections (F) can be applied. These viscosity correction factors were taken from Millipore Maintenance Procedures for Pellicon™ and Pellicon-2™ Cassette Filters. Permeate flux (J_t) was then calculated at different filtration times using Equation (2.2).

$$J_t = \frac{V_{\Delta t} \cdot F}{A_m \cdot \Delta t} \tag{2.2}$$

Normalised flux versus time plots were generated to determine the steady state flux where steady state is defined as the state at which subsequent flux decline is less than five percent per hour.

2.7 Microscale crossflow filtration

2.7.1 Microscale CFF device design

As part of this project a microscale crossflow filtration device was fabricated at the UCL Biochemical Engineering Workshop. Full details of the engineering design and operational features are described later in Chapter 5. In summary, the device consists of a filter plate with a microplate footprint (126 x 86 mm) and was designed so that its operation could be easily integrated with the Tecan vacuum filtration manifold shown in **Figure 2.1** (B). Pictures of the prototype device are shown in **Figure 2.4**.

The filter plate is made out of a cast acrylic sheet (polymethylmethacrylate) and consists of two parts: the top has the feed/retentate channels and the bottom portion has the permeate channels. The two identical filtration channels have a U-shape form with sharp edges and nominal length of 225 mm, channel height of 1.7 mm and channel width of 4.6 mm.

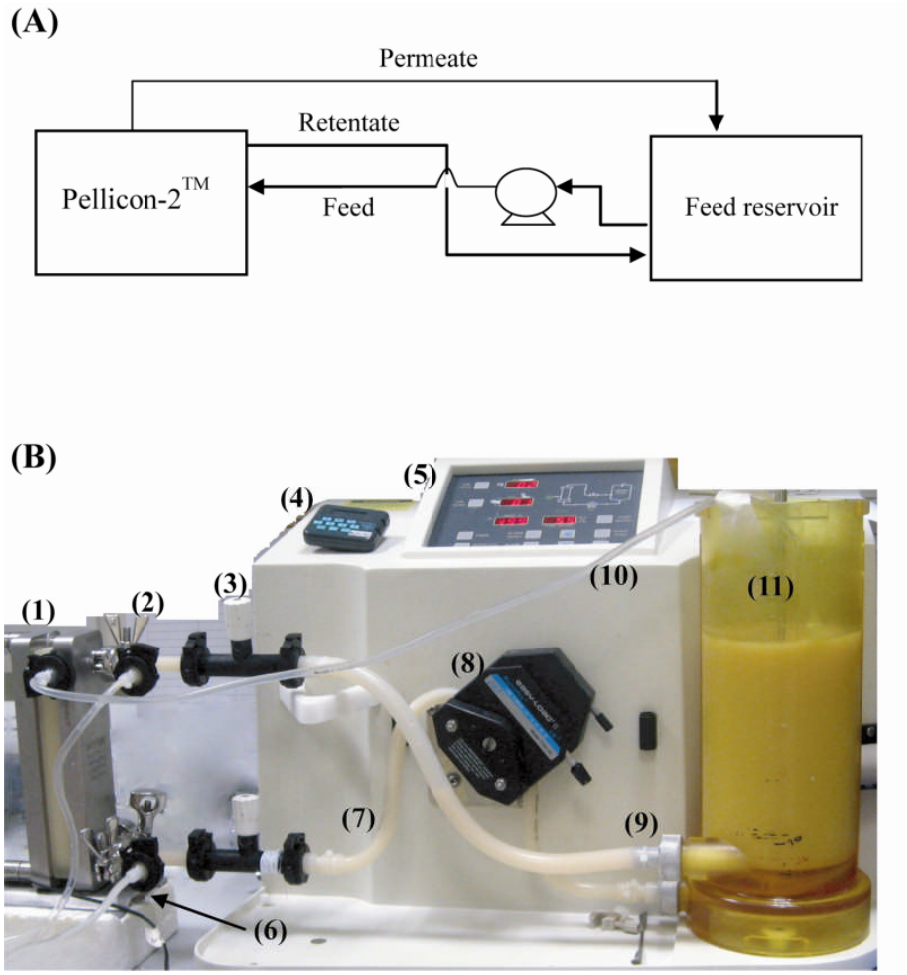

Figure 2.3 Laboratory module used in larger scale CFF experiments: (A) Schematic diagram of the CFF process with permeate recycling; (B) Millipore ProFlux™ M12™ Tangential Filtration System showing: (1) Pellicon-2™ membrane cassette within Pellicon™ stainless steel holder; (2) retentate flow pressure tap; (3) retentate valve; (4) timer; (5) control panel; (6) feed flow pressure tap; (7) feed line to membrane; (8) L/S® Easy-Load® II pump; (9) retentate line to reservoir; (10) permeate line to reservoir; and (11) feed/retentate reservoir.

The available membrane area given this configuration is 100-fold smaller than the larger scale Pellicon-2™ module at 0.001m^2. The bottom plate has o-rings made out of a nitrile o-ring cord with an outside diameter of 1.6 mm (RS Components LTd., Northants, UK), located around the permeate channels to ensure no leakage. The flow in the permeate channel is directed towards an outlet tubing into a permeate reservoir within the vacuum manifold. The test membrane was a 0.22 μm PVDF membrane, cut to shape and sandwiched between the top and bottom plates by a set of screws.

2.7.2 Microscale CFF operation

Microscale CFF experiments were automated by setting and controlling the filtration time and vacuum pressure on the permeate side via the Tecan Gemini™ software. The feeds were pumped to the respective channels by a multi-channel Bredel™ pump with two snap-fit 313X extension pump heads (Watson & Marlow, Cornwall, UK). The retentate line was directed back to the reservoirs. The feed and vacuum permeate pressures were measured using the same digital manometers and data acquisition software as described in Section 2.4. For a given filtration condition (at a specific transmembrane pressure and crossflow rate) filtration runs were performed at different times (30 minutes maximum). After each filtration run, the permeate receiver of each channel was weighed and the temperature noted. The permeate was returned back to the feed reservoirs then the filtration process was repeated for a longer filtration time. The determination of steady state flux by the microscale CFF method is described in detail in Chapter 5.

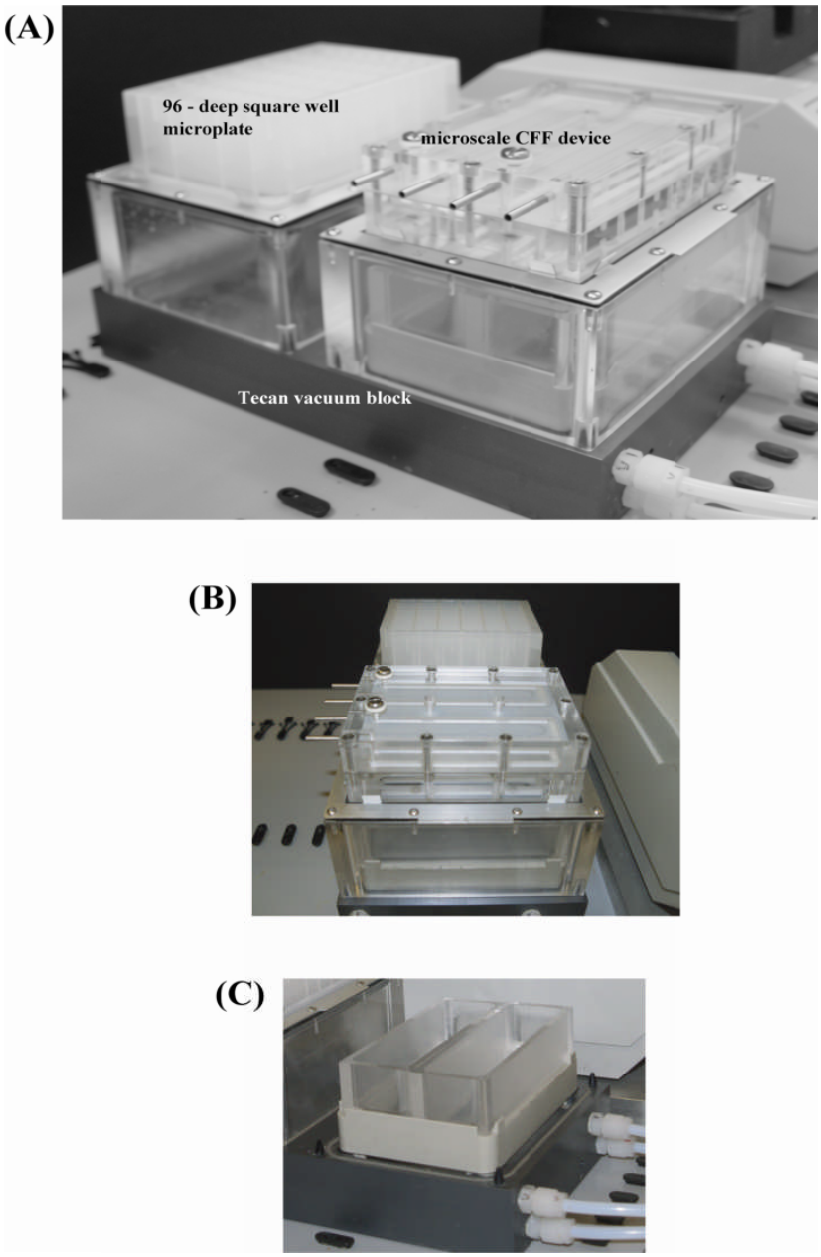

Figure 2.4 Microscale crossflow microfiltration device: (A) isometric view on top of the Tecan vacuum block beside a 96 – deep square well microplate; (B) front view of the microscale device; (C) the two permeate collectors for each channel.

2.8 Quantification of filtration performance

2.8.1 Membrane resistance

Equation 2.3 was used to calculate R_m where ΔP_{TM} is the pressure gradient across the membrane and μ_P is the viscosity of the permeate at the measured temperature. This equation is derived from Equations 1.4 and 1.5 which is based on flux modelling for flow through resistances (Cheryan, 1998). Equation 2.3 is used with water flux experiments, described in Section 2.5.1, wherein the resistance to water flux is attributed to the membrane only.

$$R_m = \frac{\Delta P_{TM}}{\mu_P \dfrac{V_{\Delta t}}{A_m \cdot \Delta t}} \tag{2.3}$$

2.8.2 Normalised water permeability

The normalised membrane permeability (*NWP*) was related to R_m by Equation 2.4. A correction factor is applied based on the viscosity of water at certain temperature. In this case, the reference viscosity was taken at 25 ^{o}C (μ_{25C}).

$$NWP = \frac{1}{R_m \cdot \mu_{25C}} \tag{2.4}$$

2.8.3 Membrane solids rejection

The membrane solids rejection coefficient is defined as:

$$\sigma_s = 1 - \frac{C_{P,s}}{C_{R,s}} \tag{2.5}$$

where $C_{P,s}$ and $C_{R,s}$ are solids content in the permeate and retentate streams, respectively, calculated from the optical density readings at 600 nm (Section 2.9.2).

2.8.4 Transmission

Percentage transmission is defined as:

$$\%T = \frac{C_{P,i}}{C_{R,i}} \times 100 \tag{2.6}$$

where subscript *i* is either Fab'or total soluble protein and C_P and C_R are concentrations in the permeate and retentate streams, respectively determined as described in Section 2.9.3 (for total protein quantification) or Section 2.9.4 (for Fab' quantification).

2.8.5 Apparent transmission

Percentage transmission is defined as:

$$\%T = \frac{C_{P,i}}{C_{F,i}} \times 100 \tag{2.7}$$

where subscript *i* is either Fab'or total soluble protein and CP and CF are concentrations in the permeate and feed streams, respectively determined as described in Section 2.9.3 (for total protein quantification) or Section 2.9.4 (for Fab' quantification).

2.9 Analytical methods

2.9.1 Quantification of biomass concentration (Dry cell weight)

Biomass dry cell weight was determined by centrifuging 1 mL fermentation broth samples in pre-weighed Eppendorf tubes at 13,000 rpm for 30 minutes. The supernatant was discarded and the weight of the wet cells measured before the cell paste was dried in an oven at 100 ^{o}C for ~72 hours until a constant weight was reached. This was then used to determine the dry cell weight (DCW) of each sample. A total of eight measurements were made. The coefficient of variation (CV), which is the ratio of standard deviation to mean, was calculated to be 4 %. Appendix 1.3 provides a

calibration curve of dry cell weights versus wet weight of *E. coli* cells produced as described in Section 2.2.2 and Section 2.2.3.

2.9.2 Quantification of biomass concentration (Optical density)

Fermentation broth samples (Section 2.2.2) or the cell paste (Section 2.2.3) were diluted in deionised water so that the optical density measured by the spectrophotometer (Amersham Biosciences/GE Healthcare, UK) was between less than 1.0 OD units. The optical densities of the samples were measured at a wavelength of 600 nm with a UV-Vis spectrometer. The OD was measured in triplicate and maximum CV of 3 %. Appendix 1.3 shows a calibration curve of the optical density versus dry cell weight for *E. coli* cells.

2.9.3 Quantification of total protein concentration

One millilitre samples of the disrupted cells in Eppendorf tubes were centrifuged (Centrifuge 5800, Eppendorf, Germany) at 13000 rpm for 30 minutes. The total protein content was determined using the Bradford colorimetric assay according to the method by Sigma-Aldrich (technical notes) using their Bradford reagent and calibrated using bovine serum albumin (BSA) protein standard (Sigma-Aldrich, USA). Assays were performed in triplicate and the maximum CV was 3 %. A typical protein calibration curve is shown in Appendix 1.4.

2.9.4 Quantification of antibody Fab' fragment concentration

Fab' concentrations in the supernatant of disrupted cell suspensions and permeates from microfiltration experiments were determined by affinity chromatography using a HiTrap Protein G HP 1 mL column (GE Healthcare, UK) on an Agilent liquid chromatography system (Agilent, USA). Binding and elution buffers (20 mM sodium phosphate) were at pH 7.4 and pH 2.5, respectively, and run through the column at a flowrate of 2 ml min^{-1}. The wavelength used for sample detection was 220nm. The

samples were passed through 0.22 μm syringe filters prior to analysis. Appendix 1.5 and Appendix 1.6 show typical chromatograms and calibration curve, respectively.

2.9.5 SDS PAGE analysis of proteins

Disrupted broth samples, prepared as described in Sections 2.3.1, 2.3.3, and 2.3.4, were centrifuged at 13000 rpm for 30 minutes. The pellets were then discarded and the supernatants used as samples for electrophoresis. SDS PAGE was performed using the Mini-Protean II System (Bio-Rad Laboratories, Inc., Helmel Hempstaed, UK) with gels prepared from Protogel resolving and stacking buffers (National Diagnostics, USA). The preparation of 8% monomer gels and 4% stacking gel were made according to the manufacturer's specification (Protogel protocol, *Methods for SDS-PAGE*). Gel image was captured by GelDoc-It^{TM} imaging system using an Ultraviolet Transilluminator, BioImaging System (UVP Upland, USA).

2.9.6 DNA sample purification

An equal volume of isopropanol was added to clarified samples to precipitate the DNA. The mixtures were immediately centrifuged at 13 000 rpm for 10 minutes. The supernatant was discarded and the pellet washed with 70% ethanol before centrifugation for another 5 minutes. The washed pellet was then dissolved in buffer containing 10 mM Tris-HCL/ 1 mM EDTA at pH 8. One microlitre of Ribonuclease A RNase (Qiagen) was added to each sample to degrade unnecessary RNA and the mixtures were left for 1 hour at 37^{o}C. Material from this preparation step are subsequently called "DNA samples" in this thesis and used for both gel analysis (Section 2.9.7) and nucleic acid quantification (Section 2.9.8).

2.9.7 DNA gel analysis

15 μL of ethidium bromide (500 μg ml^{-1}) was added to a 1% (v/v) agarose gel. Once the gel had set, DNA samples were loaded on each well. A 1 kb DNA ladder (Gene

RulerTM, Fermentas) was used as marker to determine the size of the DNA samples. Electrophoresis was run for 1 hour at 100 volts with 1xTris Borate EDTA electrophoresis buffer (9mM Tris, 9mM boric acid, 1mM EDTA). Images of the gel were taken using a UV gel camera (BioRad Geldoc 2000, BioRad).

2.9.8 Nucleic acid quantification

A nanodrop UV spectrophotometer ND-1000 (Nanodrop, DE, USA) was used to determine the concentration and purity of all DNA samples. The absorbance of each sample was measured at 260 nm and 280 nm. The concentration of DNA (in $\mu g\ mL^{-1}$) was estimated by multiplying the absorbance at 260 nm by a factor of 50 (Sambrook & Russel, 2001). In all cases, the ratio of absorbance at 260 nm and 280 nm was 1.81 ± 0.19, indicating that samples were sufficiently pure to apply this calibration factor.

2.10 Physical methods

2.10.1 Particle size measurement by laser diffraction

Particle size measurement was performed by laser diffraction using a Mastersizer 2000 (Malvern Instruments Ltd., Malvern, UK) with a small volume sample dispersion unit at a detection range of 0.01 – 2000 μm. Samples were added dropwise until the 'obscurance' was within the acceptable range of 10-15%. The output is size distribution in terms of particle volume percentage. d_{10} and d_{90} values were those given by the instrument. The d_{10} (d_{90}) is a value of particle size indicating that 10% (90%) of the total volume of analysed particles has a diameter equal to or less than this reference value. For d_{10} or d_{90} determination, measurements were made in triplicates and the maximum coefficient of variance is 5%.

2.10.2 Viscosity measurement

A Brookfield Cone and Plate DV-II programmable viscometer (Brookfield, Stoughton, MA, USA) was used to quantify the rheological behaviour and viscosity of *E. coli* fermentation broths. Before the sample was loaded, the instrument was set to auto-zero; 500 μL of sample was then loaded on the sample chamber. The re-circulating water bath set at 20^{o}C. The shear rate and shear stress at for at least eight different speeds were read and manually recorded for each sample. A typical shear rate – shear stress curve is shown in Appendix 1.7. To assess reproducibility, the viscosity measurements of three selected samples were repeated. The maximum coefficient of variation for a measured shear stress is 26% while the maximum coefficient of variation for the calculated absolute viscosity is 12%.

3. Creation of an Improved Microscale Dead-end Filtration Methodology‡

3.1 Introduction and aims

The benefits of the microscale bioprocessing approach in speeding development of robust and scaleable processes were described in Section 1.1. To further enable microscale bioprocessing studies the need for creation of new microscale unit operations was highlighted. Special attention is given here to membrane processes. These are widely used in biopharmaceutical product development, yet an area less studied at microscale, but, which could benefit from this approach. Available scale-down membrane devices were summarised in **Table 1.4**. A common feature of these devices is multiple or parallel analysis of processes and the consumption of small quantities of feed material. Among the available platforms, Jackson et al. (2006) were able to show quantitative parallel analysis of dead-end filtration processes using small volumes of feed (< 2 mL) within an automated environment. By incorporating the device within an existing laboratory robotic platform, rapid evaluation of process studies was facilitated. This initial UCL work has demonstrated that data from the microscale device is comparable with data obtained from a larger scale dead-end filtration rig.

---

‡ The methodology presented in this chapter has previously been published as: Rayat ACME, Micheletti M, Lye GJ. (2010). *Evaluation of cell disruption effects on primary recovery of antibody fragments using microscale bioprocessing techniques*. Biotechnology Progress 26:1312-1321.

This chapter will present work done based on the microscale dead-end filtration device developed by Jackson et al. (2006). The aim is to establish an improved microscale dead-end microfiltration method which requires an even more reduced feed volumes and simplified to be more compatible for automated operation, and to demonstrate that this method could capture differences in feeds preparation and operation conditions. **Figure 3.1** illustrates the context of the experimental studies performed in this chapter to achieve the aims, as set above, and the contribution of the chapter in the overall framework and aim of this thesis in the application of microscale bioprocessing platform for membrane filtration. The specific objectives of this chapter are:

- to demonstrate adequate vacuum pressure control within the Tecan vacuum separation manifold (Te-VacS™) over different periods and set differential pressure during vacuum filtration;
- to establish and demonstrate reproducible quantification of automated, microscale dead-end microfiltration data; and
- to establish the suitability of the automated microscale dead-end filtration method in determining microfiltration performance, particularly the specific cake resistance (α).

3.2 Experimental approach

Microscale dead-end microfiltration experiments were performed on the deck of a Tecan Genesis200™ laboratory workstation using the custom filter plate described in Section 2.5.1. Water flux experiments outlined in Section 2.5.2 were performed to determine membrane resistances (R_m); to ascertain the reproducibility of the filtration process using the Te-VacS™ and to assess well-to-well variability. Durapore poly(vinylidene fluoride) PVDF membranes (Millipore) with 0.1, 0.22 and 0.45 μm rating were used throughout this chapter.

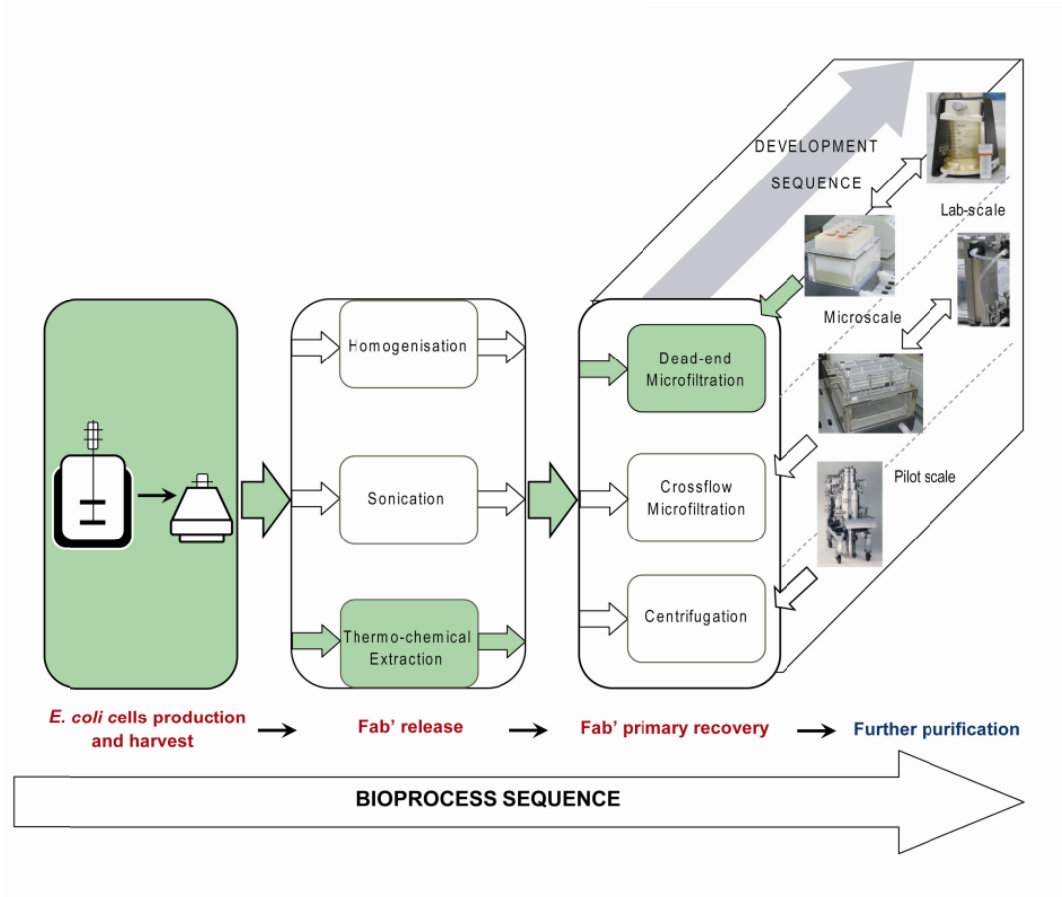

Figure 3.1 Application of microscale bioprocessing platform for membrane filtration for the investigation of bioprocess routes: microscale dead-end microfiltration method development for the primary recovery of antibody Fab' fragments from thermo-chemically extracted *E. coli* cells. (Image credit: Pilot scale centrifuge from www.pneumaticscale.com)

Dead-end microfiltration of thermo-chemically treated *E. coli* cells was initially performed to develop automated experimental procedures allowing further reduction in the volumes of feed used. The *E. coli* cell paste material was previously stored at -20^{o}C and allowed to thaw as described in Section 2.2.5. The cells were then prepared for microfiltration studies as described in Sections 2.3.2 to 2.3.4. The microscale dead-microfiltration method is described in Section 2.5.3 and in more detail in Section 3.3.3. Statistical analysis was performed using Microsoft Office Excel™ Analysis Toolpak™ (ANOVA: single factor).

3.3 Results and discussion

3.3.1 Quantification of clean membrane resistance

To demonstrate reproducible quantification during microscale filtration experiments, initial studies focused on evaluation of R_m for PVDF membranes with different pore sizes. Constant pressure filtration was performed with the feed side exposed to atmospheric pressure and the membrane side to vacuum pressure set within the Tecan Gemini™ software. Since this pressure is automatically measured and logged every second, pressure profiles were generated for each filtration run. Representative pressure profiles during short (30 s) and long (> 15 min) period of pump operation at low (20 kPa) and high (70 kPa) differential pressures are shown in **Figures 3.2**, **3.3**, and **3.4**. These figures demonstrate how quickly the set pressure was achieved once the vacuum pump starts and the stability of the measured pressure at the set value. Integration of these profiles over process time corresponds to the ΔP_{TM} of the respective filtration runs.

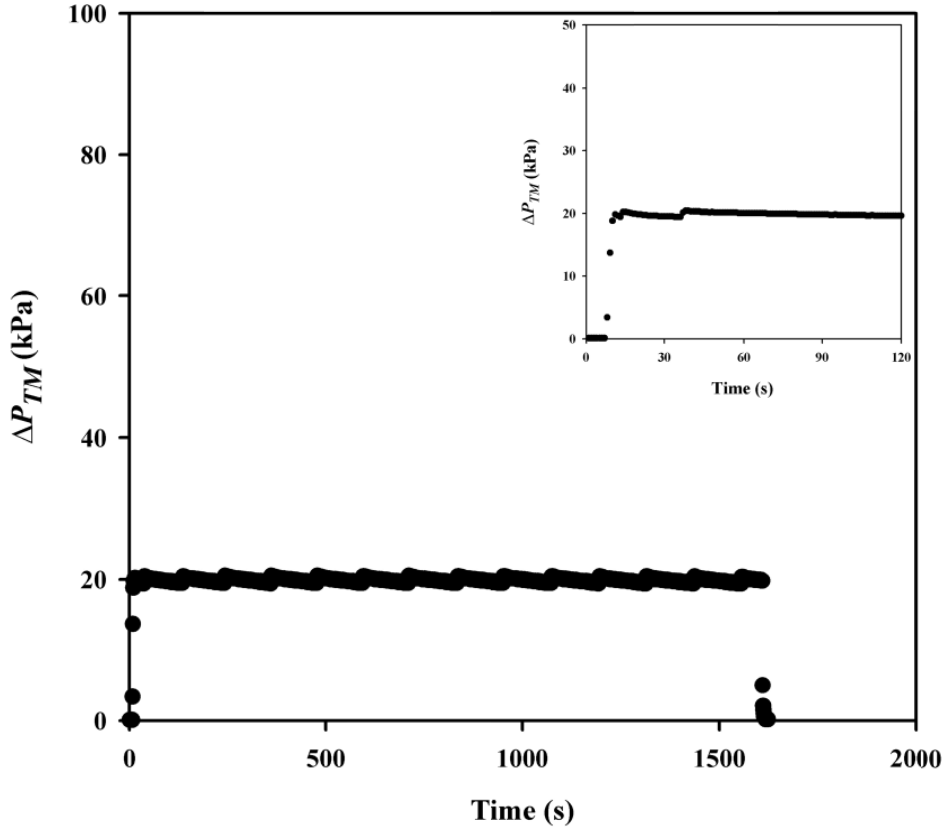

Figure 3.2 Typical pressure profile obtained by setting the pressure difference at 20 kPa for a period of 1600s using the Tecan vacuum manifold. Bottom graph shows the reading for the initial 120s. Experiments were performed as described in Section 2.5.2 using the automation platform and the microscale dead-end filtration device described in Section 2.4 and Section 2.5.1, respectively.

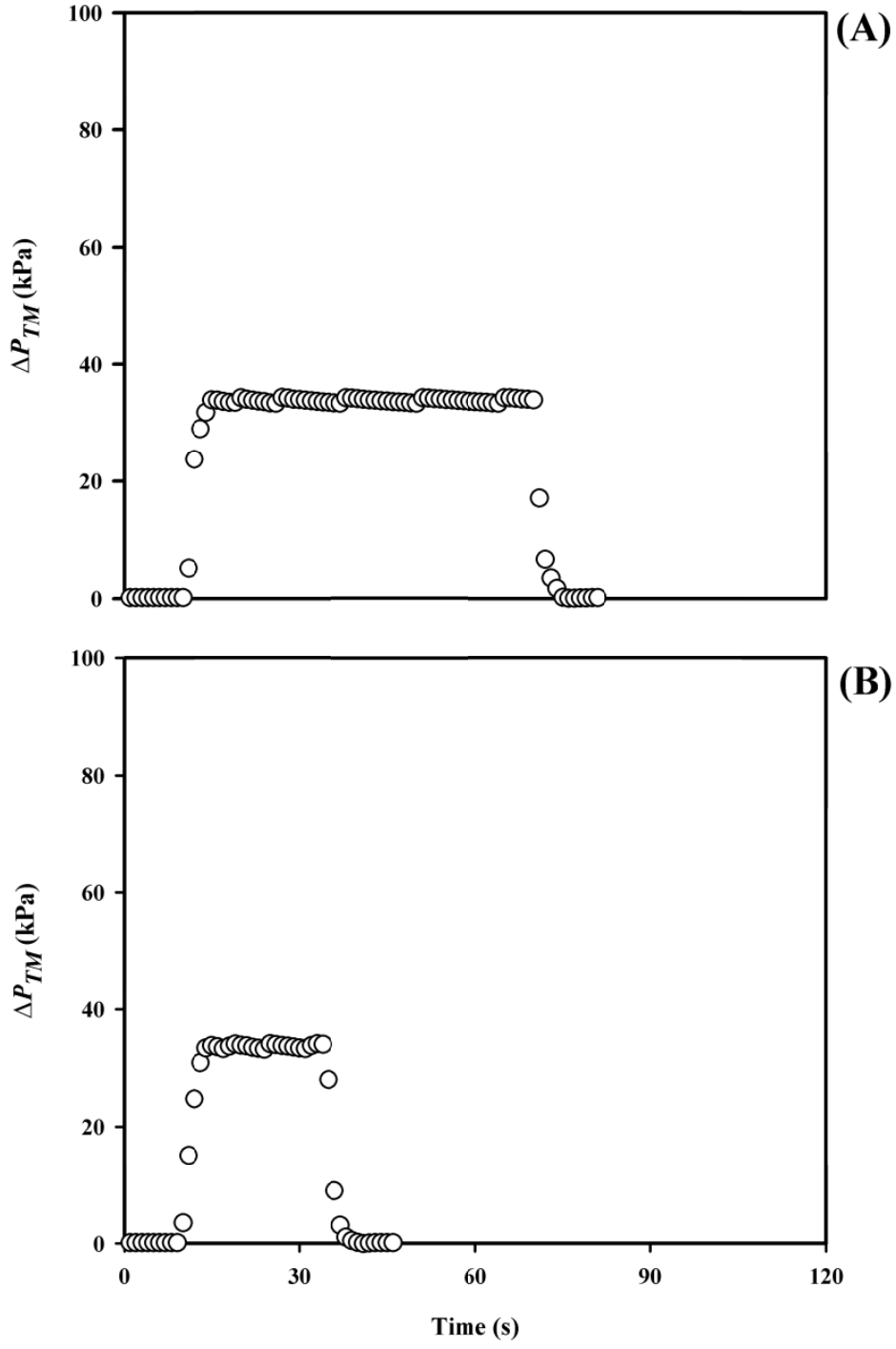

Figure 3.3 Typical pressure profile obtained by setting the pressure difference at 35 kPa for a period of (A) 30s and (B) 60s using the Tecan vacuum manifold. Experiments were performed as described in Section 2.5.2 using the automation platform and the microscale dead-end filtration device described in Section 2.4 and Section 2.5.1, respectively.

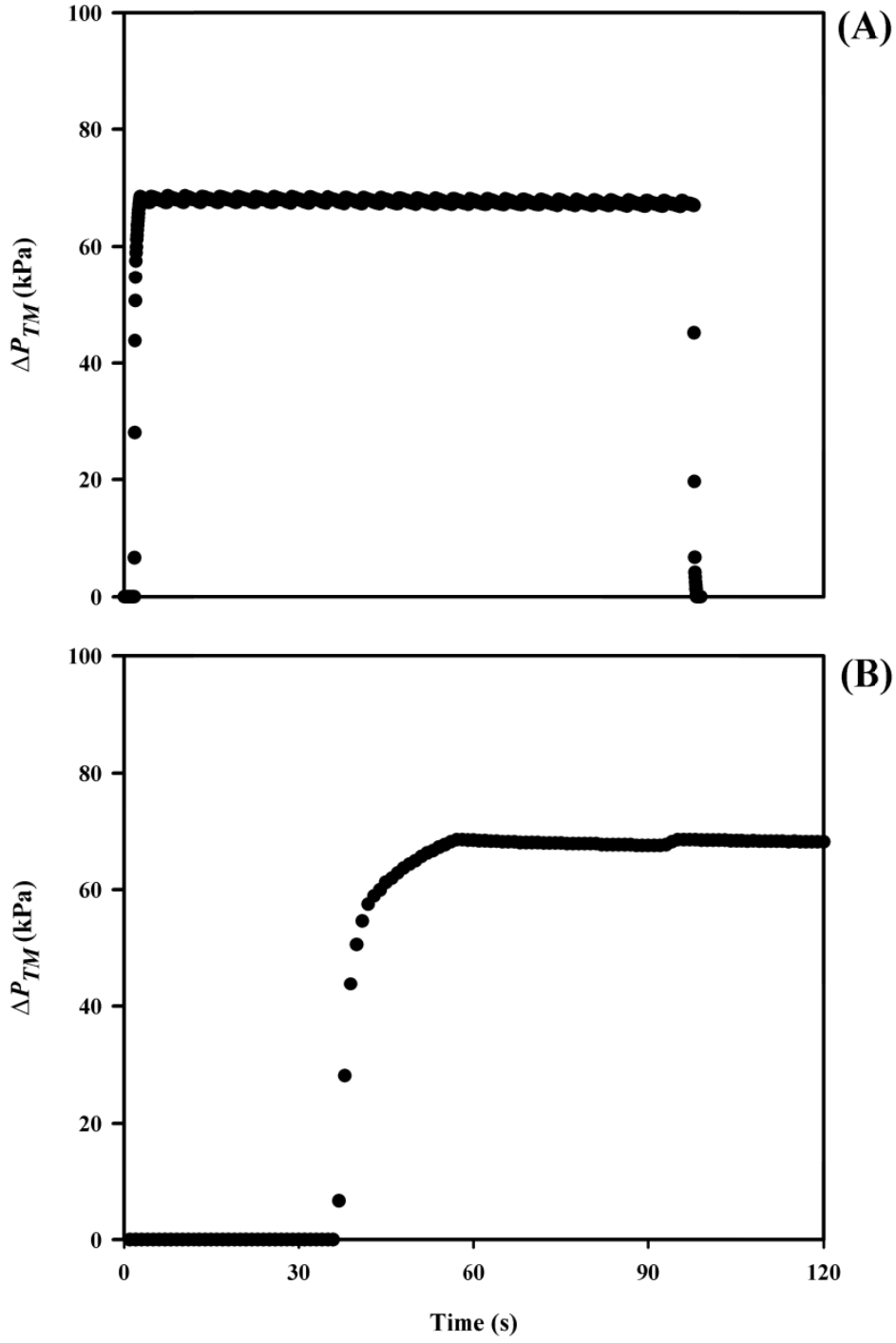

Figure 3.4 Typical pressure profile obtained by setting the pressure difference at maximum (70 kPa) for a period of 2000s using the Tecan vacuum manifold. Bottom graph shows the reading for the initial 120s. Experiments were performed as described in Section 2.5.2 using the automation platform and the microscale dead-end filtration device described in Section 2.4 and Section 2.5.1, respectively.

As indicated in the experimental set-up (**Figure 2.1**), there are two blocks on the Tecan vacuum manifold which are separately connected to the vacuum pump, hence, could be used for alternate filtration runs during automated experiments. To show that the applied pressure in each block is uniform, separate water flux experiments were performed and the R_m values of membranes of the same batch of material were compared. **Figure 3.5** demonstrates that the calculated membrane resistances do not vary between vacuum blocks and are statistically not different (F-test, $p > 0.05$). This is particularly useful as it eliminates the effect of plate position when evaluating or comparing data gathered from the two different blocks.

The variation of R_m values for the same piece of membrane measured in two different wells within the same plate was also determined. The plate orientations in **Figure 3.6** illustrate the positions of the membrane inserts during a single filtration operation. **Figure 3.6** shows that plan B is just the result of the re-arrangement of plan A by rotating the plate 180^o. R_m values of a single plate filtration experiment are shown in **Figure 3.7** and indicate that there is a variation of R_m between the membrane materials in each well. However, the R_m values of the same membrane material remains reasonably constant, and are statistically not different (F-test, $p > 0.05$), even when the membrane insert was placed in a different position on the filter plate.

Table 3.1 summarises the calculated membrane resistances determined in this work. The coefficient of variation between different wells was found to be 6, 3, and 8% for 0.1, 0.22, and 0.45 μm membranes, respectively, and was independent of position on the plate.

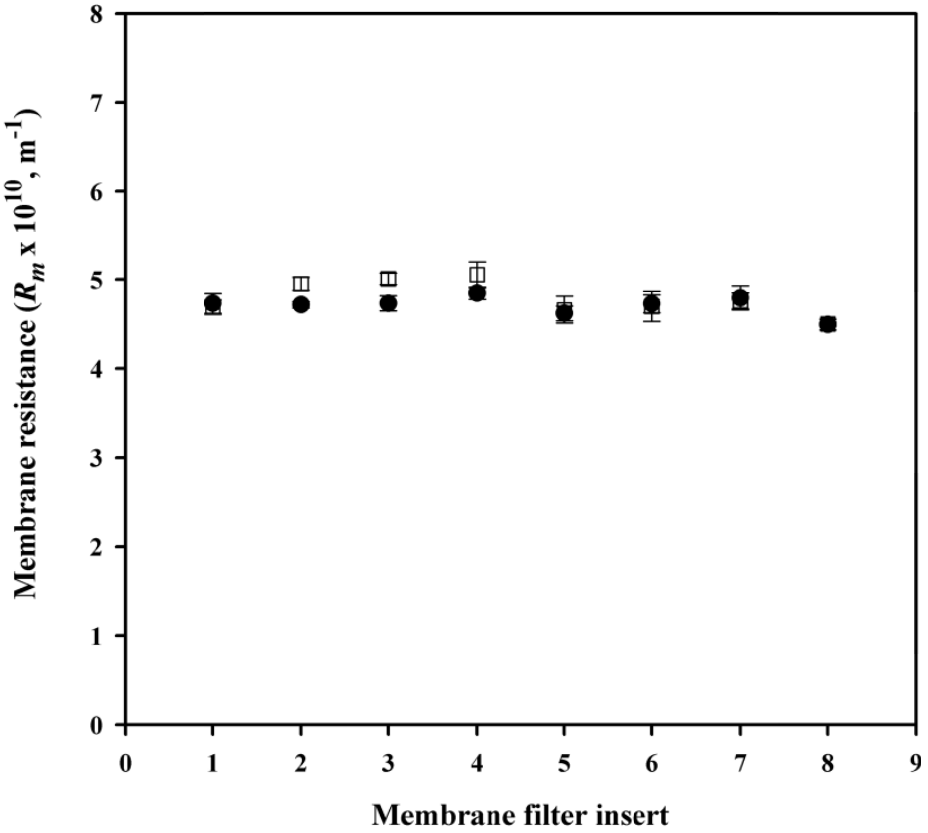

Figure 3.5 Measured membrane resistances of individual membrane insert containing 0.22 μm-rated PVDF membranes on different vacuum block positions: (●) on Te-VacS™ position 1; (□) Te-VacS™ position 2 (symbols overlap with filled circles). The same well position of the membranes on the filter plate was maintained. Error bars, smaller than the data symbol, are one standard deviation about the mean (n=3). Water flux experiments were performed as described in Section 2.5.2 at ΔP_{TM} is 20 kPa using the automation platform and the microscale dead-end filtration device described in Section 2.4 and Section 2.5.1, respectively.

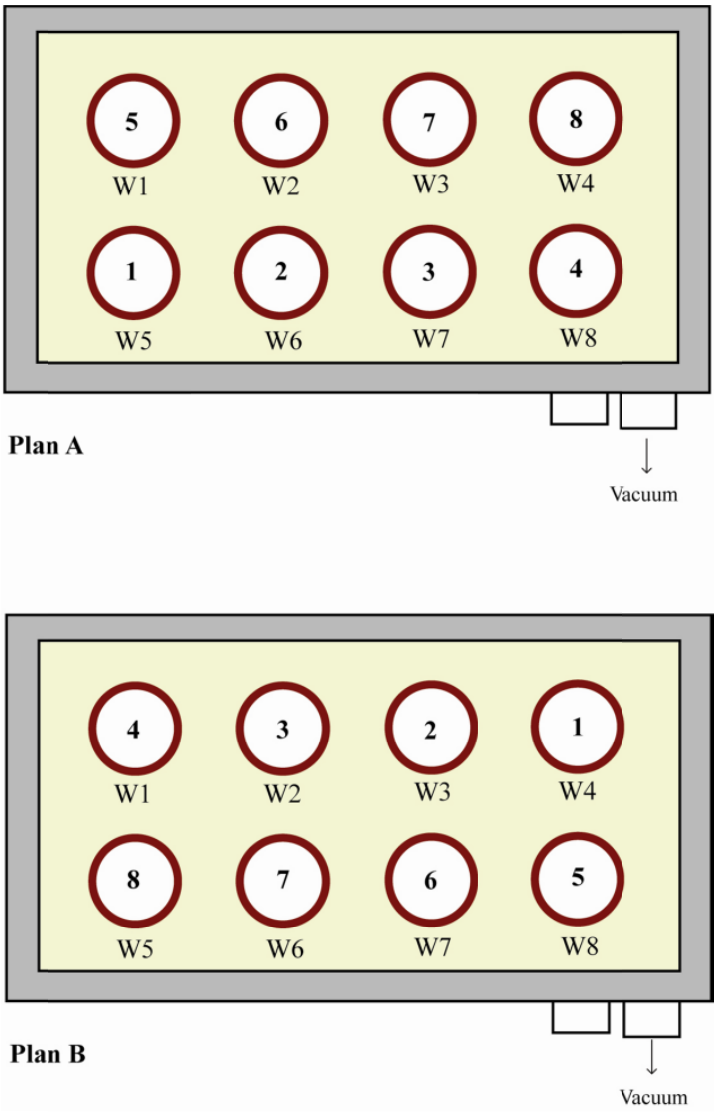

Figure 3.6 Details of the two plate orientations used in water flux experiments on a single plate indicating position relative to vacuum source. The number within the wells indicates a unique membrane insert. For example, membrane 1 in Plan A is in position W5, while in Plan B this same membrane is in W4. Experiments were performed as described in Section 2.5.2 using the automation platform and the microscale dead-end filtration device described in Section 2.4 and Section 2.5.1, respectively.

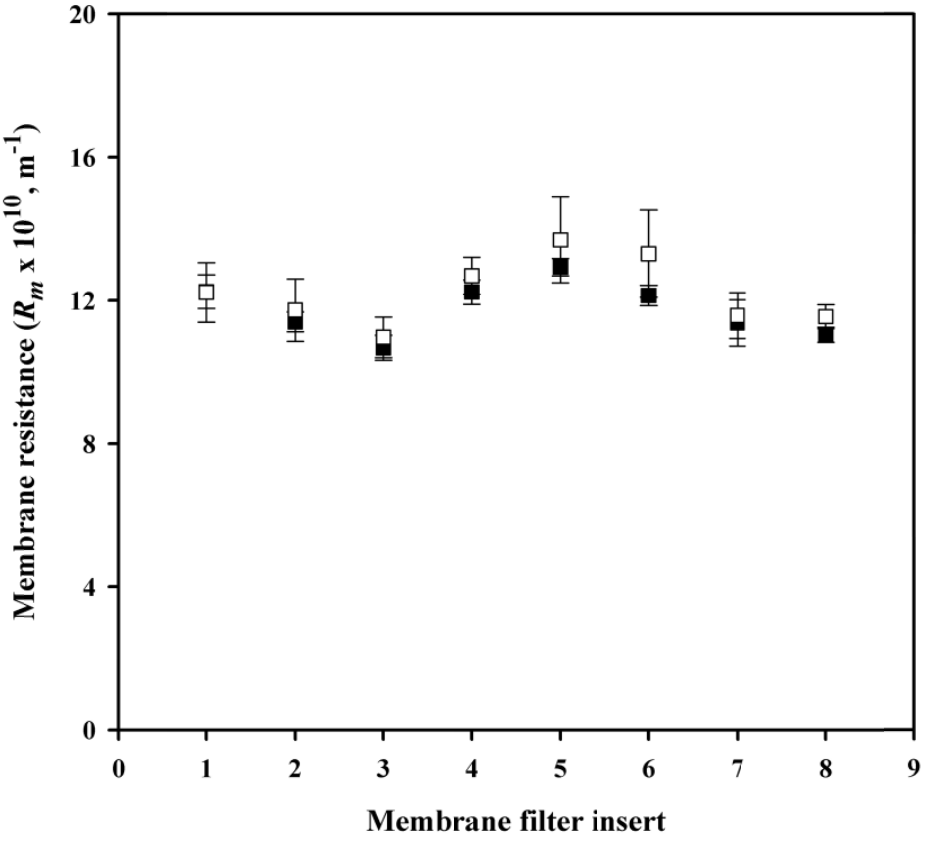

Figure 3.7 Measured membrane resistances for individual membrane inserts obtained by performing water flux experiments on a single plate with inserts arranged according to: plate orientation A (■), and plate orientation B (□) in Figure 3.6. The same vacuum block was used for the different well orientations containing 0.1 μm-rated PVDF membrane on different well positions within a single plate. Error bars are one standard deviation about the mean (n=3). Experiments were performed as described in Section 2.5.2 at ΔP_{TM} is 35 kPa using the automation platform and the microscale dead-end filtration device described in Section 2.4 and Section 2.5.1, respectively.

Table 3.1 Calculated membrane resistances from microscale water flux measurements. All experiments performed as described in Section 2.5.2 using PVDF membranes with an effective filtration area of 0.8 cm^2. Values indicated were calculated according to Equations 2.3 and represent one standard deviation about the mean (n=8).

Source	**Membrane pore size (μm)**	**Sample volume (mL)**	**$\frac{V_s}{A_m}$ ratio (mL cm^{-2})**	**Membrane resistance R_m (x 10^{10} m^{-1})**
This work	0.1	2.20	2.78	12.0 ± 0.9
	0.22			4.8 ± 0.2
	0.45			1.2 ± 0.1
Jackson et al. (2006)	0.22	0.83	1.05	5.2 ± 0.2

The results obtained by Jackson et al. (2006) for a 0.22 μm PVDF membrane are also listed in **Table 3.1** and a difference in R_m values of just 8% is noted. This level of variation is acceptable and could be due to variation in the batches of membranes used. These results, therefore, agree with those obtained by Jackson et al. (2006). Note that in this earlier work, the comparability of the microscale R_m values with data from a larger scale laboratory system, having a membrane area of 3.8 cm^2, has been demonstrated and so this scale comparison is not repeated here. Chandler and Zydney (2004) have also calculated the membrane resistance of 0.45 μm PVDF membrane, having membrane areas between 0.2 – 950 cm^2, to be between 0.8 – 2.4 x 10^{10} m^{-1} which is, on average, the same as the R_m value given in **Table 1.3** for this type of PVDF membrane.

3.3.2 Observations on calculated clean membrane resistances

It can be seen from **Table 3.1** that the average R_m calculated for the 0.1 μm membrane is more than twice the corresponding value obtained with the 0.22 μm membrane and ten times larger than the R_m value obtained with the 0.45 μm membrane. According to the manufacturer's specifications, these membranes should all have the same porosity (~70%) and membrane thickness, hence, can be expected to have similar R_m values. If this is the case, then for the membranes that have been studied here, which all have similar effective area and membrane thickness, it can be expected that membrane resistances should be the same. However, membrane manufacturing characteristics may vary from batch to batch and as does the porosity and morphology of membranes of different pore sizes.

From the Kozeny – Carman equation (Equation 1.11), a small difference in porosity may have a significant effect on the calculated membrane resistance. Furthermore, membranes with different morphology and pore sizes may have different pore internal surface area per unit volume, resulting in the membranes with smaller pore sizes having greater resistance to the flow. In the latter case, the corresponding water flux would be slower resulting in higher values of R_m. This observation is confirmed by the results obtained in this study where the membrane resistance increases with decreasing pore size. As a result of this evaluation, the PVDF membrane with the largest nominal size (0.45 μm) was used in all subsequent work in this chapter.

3.3.3 Improved cake resistance quantification: (1) single plate method

The classical method for determining specific cake resistance (α) values as described in Section 1.4.2.2. This method is also called the dynamic method, as opposed to the steady-state method, wherein filtration data is acquired during actual cake filtration conditions (McGuire et al., 2009). This method was first adapted to an automated

workstation by Jackson et al. (2006). Since the collected permeate is inside the Tecan vacuum block, continuous collection of permeate volume and time data is not possible. In the previous work of Jackson et al. (2006), cake resistance quantification was therefore based on two identical filtration plates being operated in parallel where the collected permeate volume was measured at different time points for each plate. If the filtration process is performed after sufficient initial time, two sets of $\frac{t}{V/A}$ and $\frac{V}{A}$ data would be sufficient to determine α according to Equation 3.1 (derived from Equation 1.12). In order to estimate the specific cake resistance from the data collected using a high throughput methodology, Jackson et al. (2006) suggested to approximate ρ_0 with the dry solids concentration (c) in the feed.

$$\alpha = \frac{\left(\frac{t_2}{\frac{V_2}{A}} - \frac{t_1}{\frac{V_1}{A}}\right)}{\left(\frac{V_2}{A} - \frac{V_1}{A}\right)} \cdot \frac{2\Delta P_{TM}}{\mu_P c} \tag{3.1}$$

Here, this earlier technique is improved to enable quantification of cake resistance from a single plate thus allowing the experimental throughput to be doubled and the volume of feed required halved. In the new method, time and permeate mass data were gathered during stepwise vacuum filtration, a schematic representation of which is shown in **Figure 3.8**. After a filtration time t_1, the filtration process was stopped and the plate containing the permeate collection tubes was removed from the vacuum manifold assembly and replaced with a new plate containing empty collection tubes. The filtration process of the original feed was then resumed at constant applied pressure for an extended time t^*. The volumes were determined from the permeate weights: V_1 (t_1) and V^* (t^*). The two filtration times are indicated by t_1 and t_2 where:

$$t_2 = t_1 + t^* \tag{3.2}$$

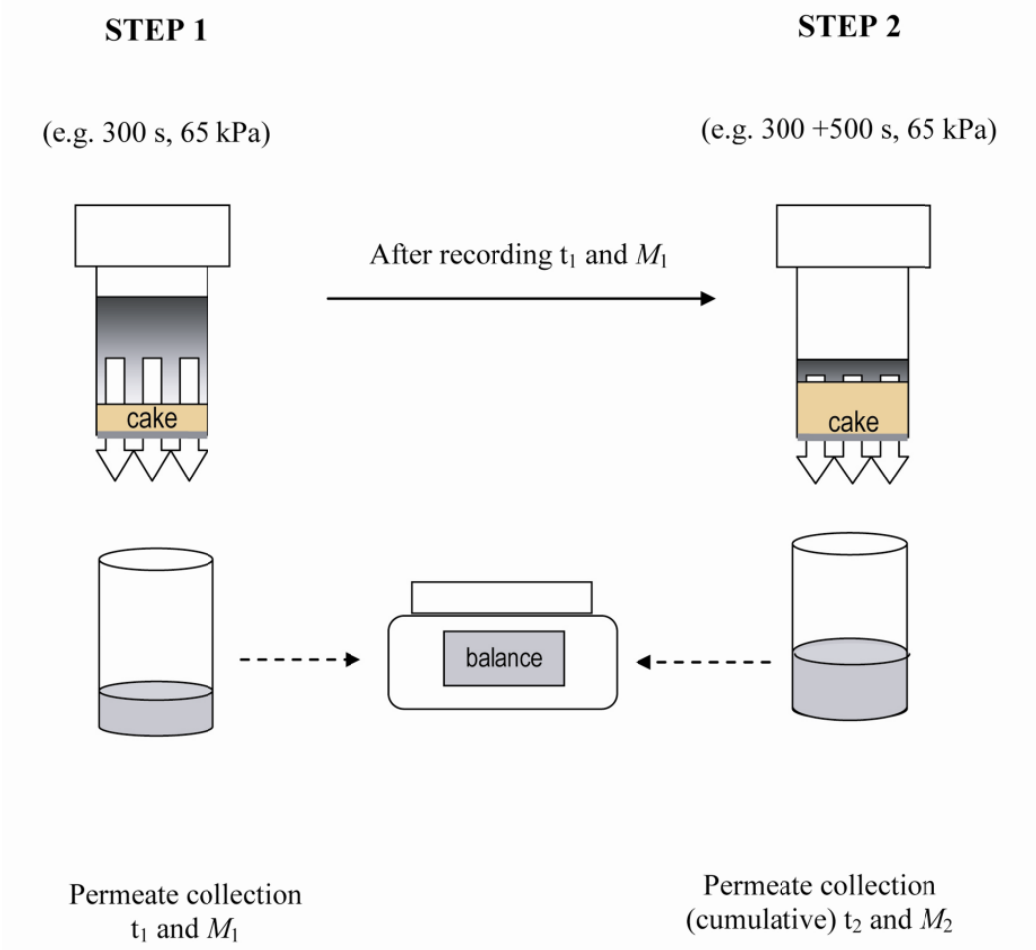

Figure 3.8 Schematic representation for a single well of the two-step microscale dead-end filtration process used for quantification of permeate flux and calculation of specific cake resistance (t = time, M = mass). Experiments were performed on the automation platform described in Section 2.4 using the microscale dead-end filtration device described in Section 2.5.1, and according to Section 2.5.3 and Section 3.3.3.

The cumulative volume of permeate V_2 can be obtained from Equation 3.3. Thus, from the same filter plate, two cumulative volumes of permeate at two different filtration times were collected. The resulting data points were then used in Equation 3.1 to calculate α values.

$$V_2 = V_1 + V^* \tag{3.3}$$

This method assumes that the cake, initially formed during the first filtration step, was not significantly altered when the pressure was released. In order to validate this assumption and the improved step-wise procedure, the permeate flux for one 800s long filtration run was compared with the flux obtained from the cumulative volumes of filtrate when the filtration process was terminated at t_1= 300s and then resumed for an additional t^*=500s. **Figure 3.9** shows the typical permeate flux variation with process time using a feed of thermo-chemically extracted *E. coli* cells. The difference between the two fluxes obtained using the previously described method was found to be 9%. This resulted in a difference of 13% between the calculated specific cake resistances. Statistically, this variation is not significant ($p > 0.05$) which confirms the utility of the new method.

Calculated α values for two different process feedstocks are shown in **Figure 3.10**. Both feedstocks were prepared by thermo-chemical extraction of *E. coli* cells. This figure compares the α values determined by the two-plate method described by Jackson et al. (2006) and the single plate, two-step method described here. The variations of α values using these two methods for both process feeds in **Figure 3.10** are statistically not significant ($p>0.05$). Therefore, the single plate method developed here can reliably be used in subsequent microscale dead-end microfiltration experiments for specific cake resistance determination.

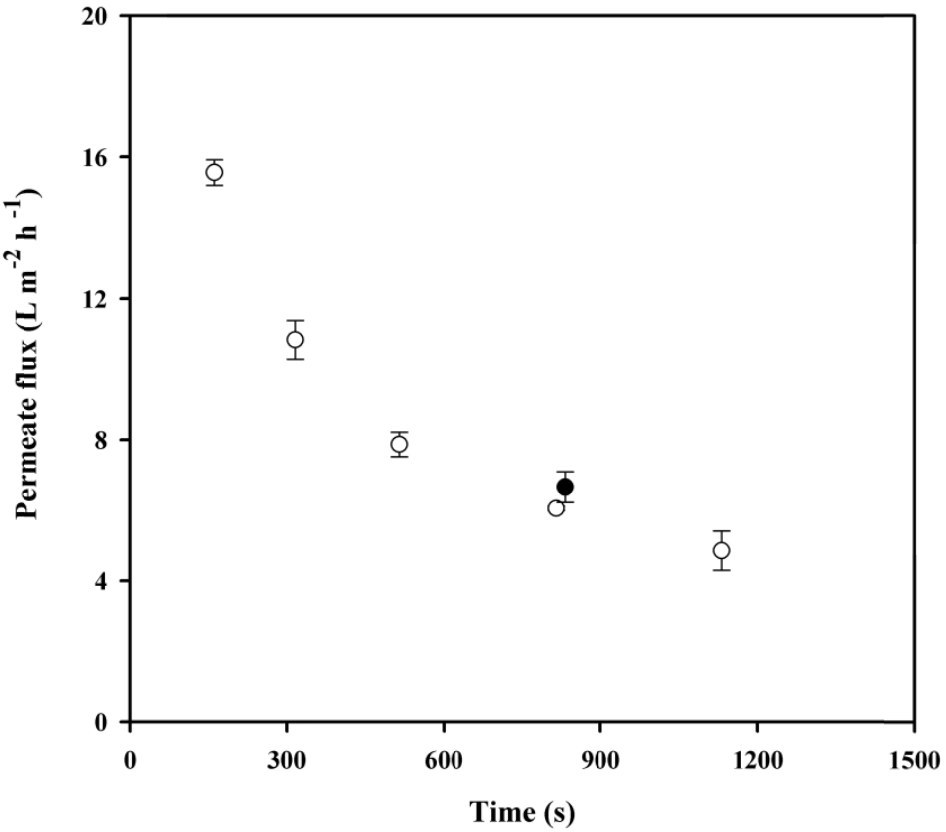

Figure 3.9 Quantification of permeate flux versus time for dead-end microfiltration of thermo-chemically extracted *E. coli* cells. The filled circle data point was acquired by the two-step filtration method (300s + 500s) shown in Figure 3.8. Extraction performed according to Section 2.3.3 at 50^{o}C for 16 h, pH 7.4 with 32 g_{DCW} L^{-1} solids loading. Filtration experiments performed according to Section 3.3.3 at ΔP_{TMP}= 65 kPa using 0.45 μm PVDF membrane. Error bars represent one standard deviation about the mean (n=4).

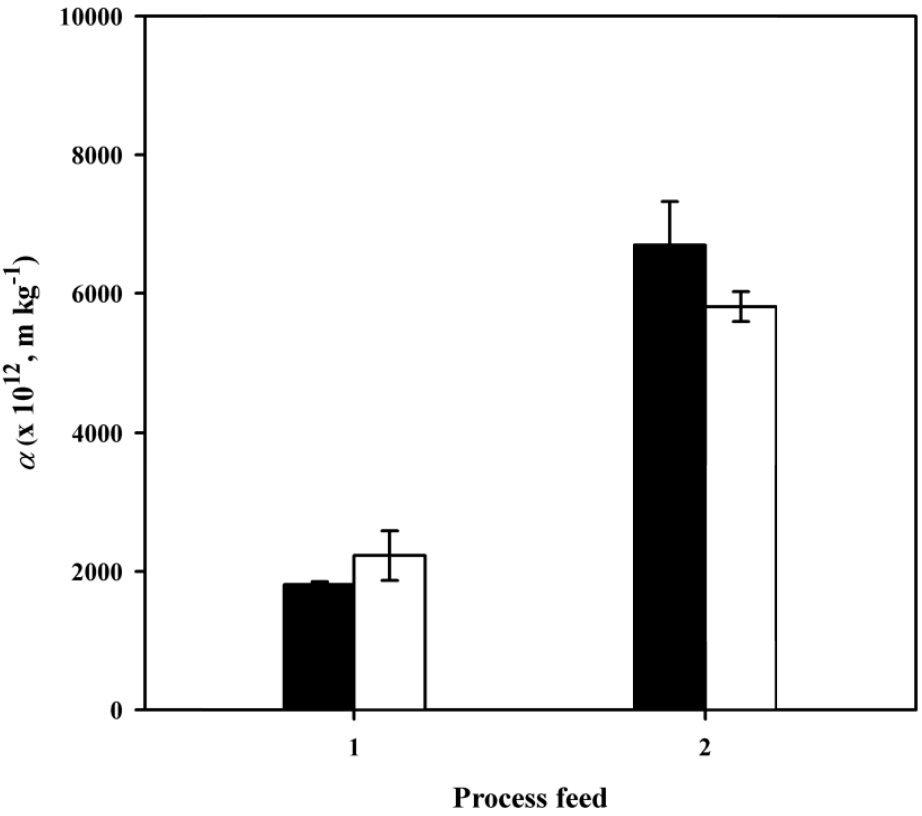

Figure 3.10 Comparison of calculated specific cake resistances (α) of thermo-chemically extracted *E. coli* cells by the two- plate method employed by Jackson et al. (2006) (■) and the improved single-plate method developed in this work (□). Process feed 1 has solids loading of 32 g_{DCW} L^{-1}, extracted with 100 mM Tris/ 10 mM EDTA buffer at pH 7.4 at 50^{o}C for 16 h. Process feed 2 has a solids loading of 27 g_{DCW} L^{-1}, extracted with 100 mM Tris/ 10 mM EDTA buffer at pH 7.0 at 50^{o}C for 2 h. Microscale dead-end filtration was performed at ΔP_{TMP}= 65 kPa, using 0.45 μm PVDF membranes as described in Section 3.3.3. α values were calculated according to Equation 3.1. Error bars represent one standard deviation about the mean (n=4).

3.3.4 Application of the single plate microscale filtration method

The previous section demonstrated a new automated microscale dead-end filtration method for quantitative evaluation of the microfiltration performance of cell suspensions such as *E. coli* cells. This section shows how this new method is able to capture differences in microfiltration performance, as indicated by α values, for different feed stream preparations. Experiments were performed as in Section 3.3.3 and used thermo-chemically treated *E. coli* cells with Tris-EDTA, for a range of pH values, as extraction buffer. It is expected that the different conditions of Tris-EDTA plus heat treatment will result in suspensions with different soluble components (Weir and Bailey, 1997). Therefore, the specific cake resistance is also expected to change depending on the characteristics of the cell suspension.

The results of these experiments are summarised in **Table 3.2**. Experiments investigating the effect of extraction time from 2 h to 16 h (Expt. 1) showed that these two feeds give α values that are statistically different (F-test, $p<0.05$). Another filtration experiment (Expt. 2) was performed where three feeds were prepared under the same extraction conditions except for the pH (either pH 7.0, 7.4 or 7.8). Results again indicate that slight differences in extraction pH lead to significant difference (F-test, $p<0.05$) in filtration performance as indicated by the specific cake resistances. These results clearly illustrate that the α values of thermo-chemically treated *E. coli* cells are affected by the way the Fab' extraction process is performed. Although the results can not be directly explained at present, these show the capability of the microscale dead-end device and the associated methodology in depicting the microfiltration performance of various feeds.

Table 3.2 Application of the single plate, two-step microscale filtration method. Filtration experiments were performed as described in Section 3.3.3 at ΔP_{TMP}= 65 kPa, using 0.45 μm PVDF membranes. Values indicated were calculated according to Equations 3.1 and represent one standard deviation about the mean ($2 \leq n \leq 4$).

Expt.	**Solids loading** (g_{DCW} L^{-1})	**Extraction conditions**			α (x 10^{12} m kg^{-1})	**Variation between α values**
		^{o}C	pH	h		
(1)	27	60	7.4	2	4796 ± 2625	Statistically different ($p < 0.05$)
				16	1498 ± 146	
(2)	32	55	7.0	20	503 ± 90	Statistically different ($p < 0.05$)
			7.4		396 ± 43	
			7.8		964 ± 182	

3.3.5 Improved cake resistance quantification: (2) steady-state method

In the preceding section, the dynamic method of measuring the average specific cake resistance was described and an improved method for quantification of α values shown. This section will discuss a second method that has been used to further simplify and expedite the experimental procedure.

Some research groups, as initially reported by Nakanishi et al. (1987) and followed by several others like Chandler and Zydney (2004), Meireles et al. (2004) and Foley (2006b), have used what they call the 'steady state' method to determine α values. In this approach, a suspension of known solids concentration is allowed to form a cake layer over a membrane. When all the solids are deposited onto the cake, a buffer or a saline solution is passed through the pre-formed cake. The filtrate flux is then recorded

until such time that it reaches a constant value (hence the term 'steady state'). To explore α values at various ΔP_{TM} , different experimental approaches were performed by these authors. For example, Foley (2006b) suggested stepping up the pressure after steady state is achieved at each lower pressure. Filtration continues at the higher pressure until steady state is again reached at which point, the filtrate is returned to the filtration cell, the pressure is further increased, and the cycle continues until the highest operating pressure studied. Chandler and Zydney (2004) on the other hand, used freshly formed cake for each pressure measurement.

The specific cake resistance is then determined by Equation 3.4 with R_m being the clean membrane resistance. This equation is derived by integrating Equation 1.12 at steady state conditions.

$$\alpha = \frac{\frac{\Delta P_{TM}}{\mu_P J_{\Delta t}} - R_m}{\frac{cV_{\Delta t}}{A_m}} \tag{3.4}$$

Recently, this method was criticised since it was argued that it does not accurately describe cake formation during filtration but rather a compression process by flow of liquid through a cake (Tien and Ramarao, 2008), i.e. it describes cake consolidation instead of cake filtration. Key differences lie in the different compressive stresses experienced by the cakes during filtration and consolidation processes. The cake formed *in situ* during filtration is subjected to a range of compressive stress from zero at the cake-suspension interface to the applied total pressure at the cake-membrane interface (Tien and Ramarao, 2008). During cake compression on the other hand, the compressive stress at the cake-suspension interface is greater than zero and should therefore be known. The process of determining this, however, is reported to be complex. To support this argument, McGuire et al. (2009) more recently performed microfiltration experiments with Baker's yeast using both the dynamic and steady state

methods to determine α values. They found that the steady state methods produce larger α values than the dynamic method, by between 30-120%, and concluded that the steady state method should not be used in determining α values. The over-estimation of the α values increases proportionally with ΔP_{TM}.

In this context, the application of the automated microscale methodology described in Section 3.3.3 becomes more appropriate for microfiltration studies if the purpose is rapid experimental determination of α values. The microscale dead-end filtration device and the methodology that was designed allows ease of experimentation even with multiple feeds and with small volumes. If it is necessary to determine the dependence of specific cake resistance with pressure, actual microfiltration experiments should be performed at the desired pressure range and measure α by Equation 3.1. Indeed, when the steady state method was attempted to be used with the microscale device in filtering heat-treated *E. coli* suspensions, it was found that it was not possible to obtain a pre-formed cake for a reasonable duration of filtration since the liquid (from a total feed volume of 300 μL) does not fully permeate through the cake even at the highest setting of pressure difference (70 kPa).

It might even be possible to simplify the microscale process further by performing single step, single plate filtration. According to Tien and Ramarao (2008), as long as sufficiently long filtration time has elapsed, or α values are large, R_m can be ignored in Equation 1.13. Calculation of α values could then be simply achieved by a set of t and V data from a single step, single plate filtration experiment. To test this proposition, this method was performed, using thermo-chemically extracted *E. coli* cells, and the resulting α values compared with the two-step, single plate method described in Section 3.3.3. Results are shown in **Figure 3.11**. Statistical analysis shows that these two methods give α values that are not significantly different (F-test, $p > 0.05$). This method

thus further reduces the amount of feed required for microfiltration experiments and simplifies the experimental procedure, making it even easier for automated methodology to be applied.

3.3.6 Observations on actual R_m and α values of biological feeds

During cake filtration, the actual membrane resistance may not be the same as the clean membrane resistance. Tien and Ramarao (2008) explain that R_m will increase due to the presence of the cake layer over the membrane. The membrane resistance increases during filtration and will increase with increasing applied pressure (Teoh et al., 2006). The correlation between the membrane resistance and applied pressure is even more pronounced if surface adsorption is the main mechanism of clogging (Teoh et al., 2006). According to Equation 1.12, the actual membrane resistance can be determined in this case from the y-intercept of the plot of $\frac{t}{V/A}$ against $\frac{V}{A}$.

An inspection of these plots in the published literature (e.g. Okamoto et al., 2001; Hodgson et al., 1993) shows that some biological samples used in dead-end microfiltration studies show plots that have very steep slopes resulting in negative values of the y-intercept. In this case, Equation 1.12 could not be used to determine actual values of R_m. This behaviour was also seen with the *E. coli* samples used here where plots of $\frac{t}{V/A}$ against $\frac{V}{A}$ of the process feeds show negative y-intercept values. This seems to be a phenomenon common to biofiltration (i.e. filtration of biological materials: cells, cell debris components etc. in broth, buffer or saline).

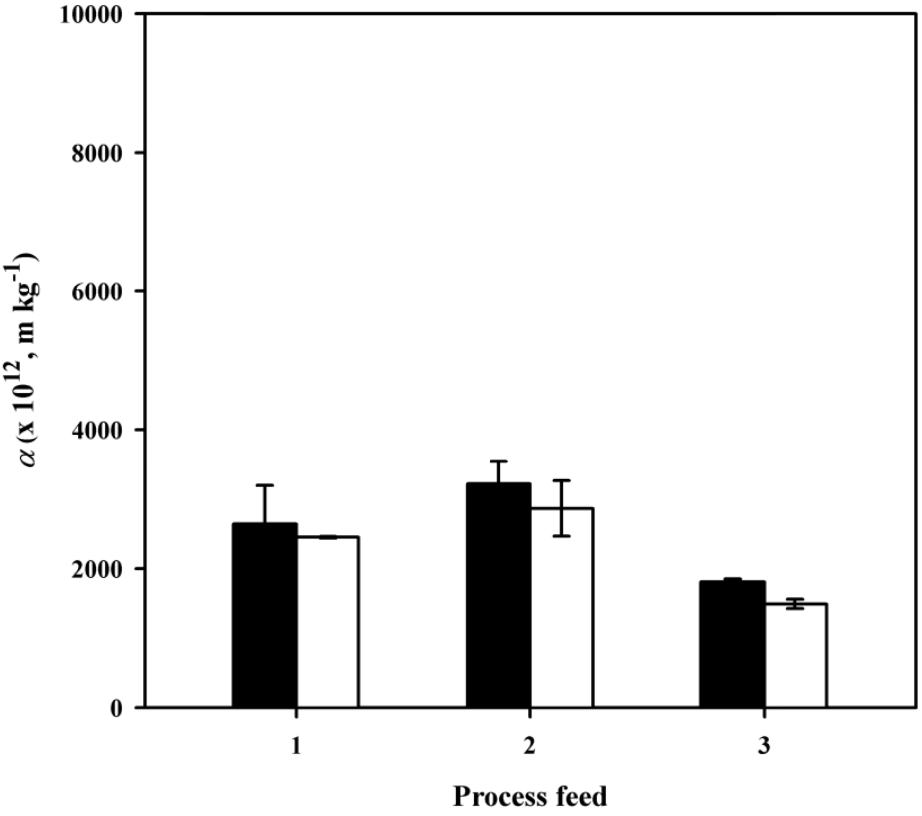

Figure 3.11 Comparison of calculated specific cake resistances of thermo-chemically extracted *E. coli* cells by the single plate method developed in this work. (■) Filtration was performed by the two-step method described in Section 3.3.3 , where pressure was temporarily released at t_1 to measure V_1 then resumed to continue to t_2. (□) Filtration was performed by the method suggested in Section 3.3.5, for a sufficiently long time (40 minutes) with no interruption. Fab' extraction with 100 mM Tris/ 10 mM EDTA buffer at pH 7.4 for 16 h. Process feed 1 concentration is 22 g_{DCW} L^{-1}, extracted at 35°C. Process feed 2 concentration is 32 g_{DCW} L^{-1}, extracted at 35°C. Process feed 3 concentration is 32 g_{DCW} L^{-1}, extracted at 50°C. Microscale dead-end filtration was performed at ΔP_{TMP}= 65 kPa, using 0.45 μm PVDF membranes as described in Section 3.3.3. α values were calculated according to Equation 3.1. Error bars represent one standard deviation about the mean ($2 \leq n \leq 3$).

Membrane filtration of non-biological particles like polystyrene latex, talc, $CaCO_3$, kaolin etc., show α values less than 1 x 10^{12} m kg^{-1} (Grace, 1953b; Tiller, 1953; McCarthy et al., 1999). On the other hand, biofiltration experiments have resulted in α values that are usually greater than 1 x 10^{12} m kg^{-1}. Some have really high α values of the order $\geq 10^{14}$ m kg^{-1} like *E. coli* and *C. Glutamicum* (Jackson et al., 2006; Okamoto et al., 2001; Ohmori and Glatz, 1999). The most common cell material used in dead-end microfiltration studies is yeast for which reported α values are of the order of 1 x 10^{11} m kg^{-1} (Nakanishi et al., 1987; McCarthy et al., 1998; Chandler and Zydney, 2004). Thus when investigating microfiltration behaviour with yeast, the plots of $\frac{t}{V/A}$ against $\frac{V}{A}$ are not very steep and will show positive y-intercept values as expected.

The negative y-intercept values obtained from the studies using other microorganisms aside from yeast could indicate that actual membrane resistances is a function of time or permeate volume depending on the fouling mechanism. Although the actual R_m values may not be calculated without knowing the exact correlation of $R_m = f(t)$ or $R_m = f(V)$ that can be substituted in the R_m in Equation 1.11, plots of $\frac{t}{V/A}$ against $\frac{V}{A}$ still provide valuable insights on the microfiltration behaviour of biological feeds by providing reasonable estimates of α values as well as an indication of the fouling effect of the feed suspension on the membrane through the sign of the y-intercept.

3.4 Conclusions

The aim of this chapter was to describe the development of a microscale dead-end microfiltration method (Section 3.3.3) which is compatible for operation within an automated workstation, requires small volumes of feed and enables parallel experimentation. The quantitative reproducibility of the microscale experiments on the Te-VacS™ was demonstrated (Section 3.3.1). The reasonable sensitivity of the

microscale dead-end filtration device and associated methodology in capturing the different microfiltration performance of various feeds was also established (Section 3.3.4). It was also shown that the developed method suitably reflects the theoretical considerations in evaluating α values (Section 3.3.5). Finally, by analysis of the largely different microfiltration performance between non-biological and biological feeds, and the difference between yeast (as a common model process feed) and other microbiological systems (Section 3.3.6) as feeds in microfiltration studies, the case for the microscale bioprocessing approach for microfiltration is even more emphasized. Because of the very small feed requirement (~500 μL) for microscale dead-end microfiltration, it is now possible to study feed-specific microfiltration performance instead of relying on model yeast feeds which may not necessarily represent the microfiltration behaviour of these industrially relevant feedstocks. This type of investigation is illustrated in Chapter 4 in the evaluation of the impact of the type of unit operations and conditions of Fab' extraction on Fab' fragments recovery by microfiltration.

4. Evaluation of Microscale Filtration Methodology for Primary Recovery of Antibody Fragments‡

4.1 Introduction and aims

In the previous chapter, a single-plate filtration method to investigate microfiltration performance, particularly the quantification of specific cake resistance (α), was established. This chapter, as illustrated in **Figure 4.1**, demonstrates the application of this method (Section 3.3.3) and the microscale dead-end fitration device (**Figure 2.2**) to study the interaction between intracellular product release and subsequent recovery by dead-end microfiltration. The product of interest is an antibody Fab' fragment produced in *E. coli*. Recombinant proteins overexpressed in *E. coli* are often produced in the form of inclusion bodies especially proteins containing complex disulfide bonds or mammalian proteins requiring post-translational modification for activity (Choi and Lee, 2004). This is due to its cytoplasm having a reducing environment that does not permit disulfide bonds formation resulting in the aggregation of certain disulfide bond-rich proteins such as antibody fragments. To overcome this situation, complex proteins can be engineered to be secreted in the periplasm where correct formation of disulfide bonds can be facilitated (Baneyx and Mujacic, 2004).

---

‡ The majority of the methodologies and results presented in this chapter have previously been published as: Rayat ACME, Micheletti M, Lye GJ. (2010). *Evaluation of cell disruption effects on primary recovery of antibody fragments using microscale bioprocessing techniques*. Biotechnology Progress 26:1312-1321.

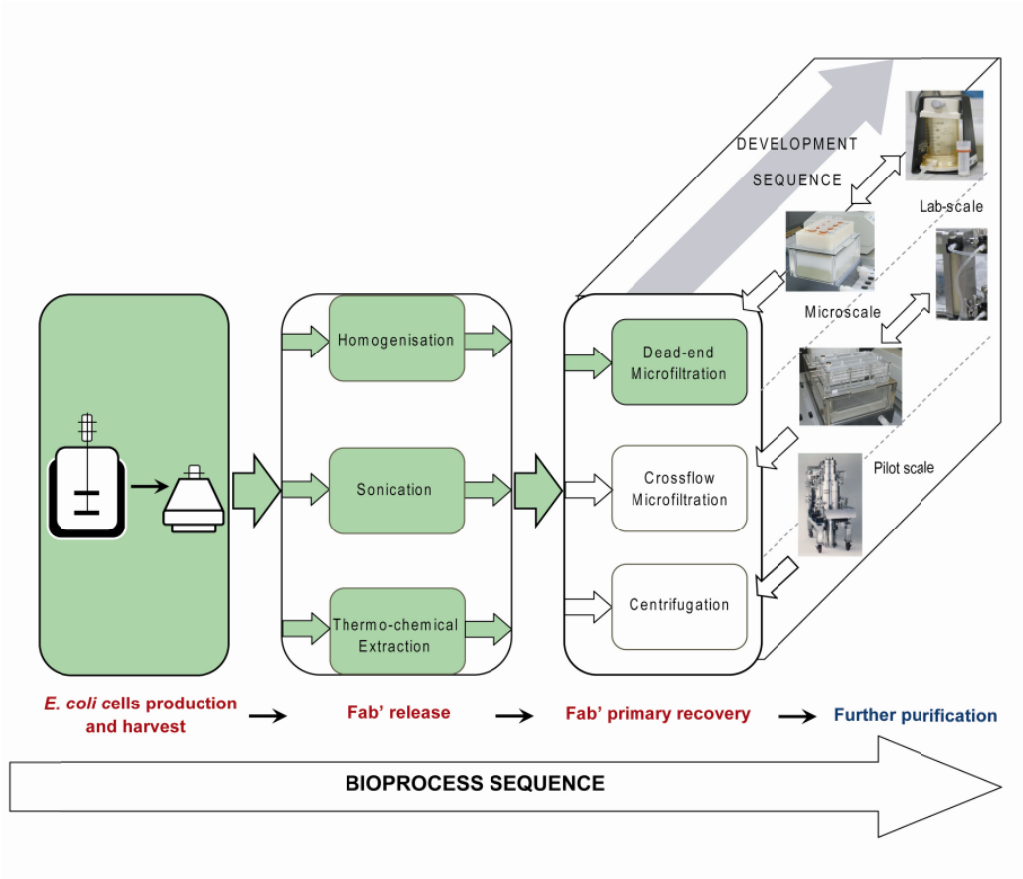

Figure 4.1 Application of microscale bioprocessing platform for membrane filtration for the investigation of bioprocess routes: evaluation of the microscale dead-end microfiltration methodology to study the impact of Fab' release on primary recovery of antibody Fab' fragments.(Image credit: Pilot scale centrifuge found at www.pneumaticscale.com)

Process recovery for intracellular products such as Fab' involves additional unit operations to release the products from the cells before recovery by solid-liquid separation can be performed. The extraction of intracellular products requires cell disruption wherein the cellular structure is broken apart and product is released (Middelberg, 1995). For antibody fragments, industrial-scale product extraction involves disruption of host cells by chemical lysis or by mechanical disruption techniques (Spitali, 2009).

Following cell rupture, solid-liquid separation is required and is usually performed using centrifugation or microfiltration. The choice of cell disruption method is usually based on the optimisation of the amount of product recovered from the cell while less attention is paid to the characterisation of the process stream properties. However, such properties have been shown to have a strong impact on the subsequent unit operations (Siddiqi et al., 1995; van Hee et al., 2004; Clarkson et al., 1993). Cell disruption methods are known to substantially affect subsequent recovery operations due to variations in contaminant concentrations, differences in particle size distribution and surface properties (Quirk and Woodrow, 1984; van Hee et al., 2006). Furthermore, the effect of pH, ionic strength and preconditioning of the feed before filtration processes have also been reported to influence performance (Ohmori and Glatz, 1999; Okamoto et al., 2001).

The aim the chapter is to show how the methodology developed in Chapter 3 can be employed to assess process interactions affecting primary product recovery using membrane filtration. Specifically, the objectives of this chapter are:

- to demonstrate the application of the microscale dead-end filtration device (Section 2.5.1) to investigate two consecutive bioprocess steps: antibody Fab'

fragment extraction from *E. coli* cells and their subsequent recovery by microfiltration;

- to study the impact of the choice of cell disruption operation on the microfiltration performance of disrupted *E. coli* suspensions;
- to demonstrate a two-step microscale process sequence: thermo-chemical extraction and dead-end microfiltration; and
- to study the impact of extraction and filtration conditions on optimisation of the linked unit operations.

4.2 Experimental Approach

Cell paste previously prepared according to Section 2.2.2 – 2.2.3 and stored at -20^{o}C was first thawed at room temperature. The periplasmic Fab' fragments were then extracted either by high pressure homogenisation, thermo-chemical extraction or sonication. These are described in Sections 2.3.2, 2.3.3 and 2.3.4, respectively.

Microscale dead-end microfiltration experiments were performed, according to Section 2.5.3, on the deck of Tecan Genesis200™ using the custom filter plate described previously in Section 2.5.1. All experiments were replicated ($n \geq 2$). Membrane materials used were either Durapore poly(vinylidene fluoride) PVDF membranes (Millipore, Hertfordshire, UK) or Supor polyethersulfone (PES) membranes (Pall, Portsmouth, UK) with 0.1, 0.22 or 0.45 μm rating.

Prior to and after microfiltration, samples were collected for total protein and Fab quantification by spectrophotometry (Section 2.9.3) and HPLC (Section 2.9.4). Samples

were also collected before microfiltration for SDS PAGE analysis and particle size described in Sections 2.9.5 and 2.10.1, respectively.

Statistical analysis was performed using Microsoft Office Excel™ Analysis Toolpak™ (Anova: single factor). Design Expert 7 (Stat-Ease, MN, USA) was used to analyse multiple factor interactions.

4.3. Results and discussion

4.3.1. Impact of cell disruption technique on filtration performance*

Choice of various cell disruption operations will result in differences in product and impurity profiles which may affect subsequent primary recovery operations like microfiltration (Balasundaram et al., 2009a). To examine this here, three methods were investigated: high pressure homogenisation (Section 2.3.2), sonication (Section 2.3.4) and a combined heat and chemical extraction (Section 2.3.3). Homogenisation is one of the most common process scale cell disruption methods (Balasundaram et al., 2009a) while sonication is often the preferred cell disruption method at the laboratory scale (Wenger et al. 2008). For antibody fragments in particular, thermo-chemical extraction is used at industrial process scale for the release of periplasmic Fab' fragments (Spitali, 2009). This latter extraction process is readily compatible with the microwell format and so was established in this study.

Table 4.1 shows the Fab' and total soluble host cell protein (HCP) content of the differently disrupted cell suspensions. As expected, the homogenised sample yielded the highest Fab' content however it also has the highest amount of HCP released. This high HCP load is known to cause a burden for the subsequent downstream processing steps and is considered a significant disadvantage for large scale operation.

* Acknowledgements are due to: R. Hanif, for providing the homogenised *E.coli* cells; A. Wong, my student, for her assistance in the sonication experiments as part of her project under the Nuffield Foundation Science Bursary in 2008.

Table 4.1 Impact of various laboratory and microscale *E. coli* cell disruption operations on protein composition of Fab' suspensions.

Cell disruption operation*	**Total host cell protein (mg L^{-1})**	**Fab' content (mg L^{-1})**	**Purity****
Homogenisation (H)	>5700	> 1062	~20%
Sonication (S)	3500	312	10%
Thermo-chemical extraction (T)	1000	197	20%

**Disruption conditions:* (H) – solids load of 30 g_{DCW} L^{-1} in 100 mM Tris-HCL pH 7.0, 2-pass at 500 bar (according to Section 2.3.2); (S) – solids load of 22 g_{DCW} L^{-1} in 100 mM Tris/ 10 mM EDTA pH 7.0, 3 x 20s cycle (according to Section 2.3.4); (T) – solids load of 22 g_{DCW} L^{-1} in 100 mM Tris/ 10 mM EDTA pH 7.0 for 16h at 50^{o}C (according to Section 2.3.3). **The indicated purity of Fab' is with respect to total protein content.
Bradford assay and Protein G chromatography were performed to quantify total protein and Fab' content, respectively (according to Section 2.9.3-2.9.4).

Figure 4.2 illustrates the microscale specific cake resistance values, α, subsequently measured using each of these different upstream cell disruption operations. As expected, these values are about five times higher than previously reported α values for non-disrupted *E.coli* cells. The results show that the homogenised samples have an average α of almost an order of magnitude larger than the thermo-chemically treated cells (this corresponds to a two-fold decrease in permeate flux). On average, the α value of the sonicated samples is also four times larger than the heat-extracted cells and is approximately half that of the homogenised samples.

When the particle size data of the respective feed samples were investigated, results showed rather different particle size distributions. **Figure 4.3** illustrates these size distributions. Sonicated samples showed the presence of only one population size while the heat-extracted cells resulted in a bi-modal distribution. The latter can be explained by the presence of smaller debris, probably consisting of fragments of broken outer membrane, and by larger cellular debris.

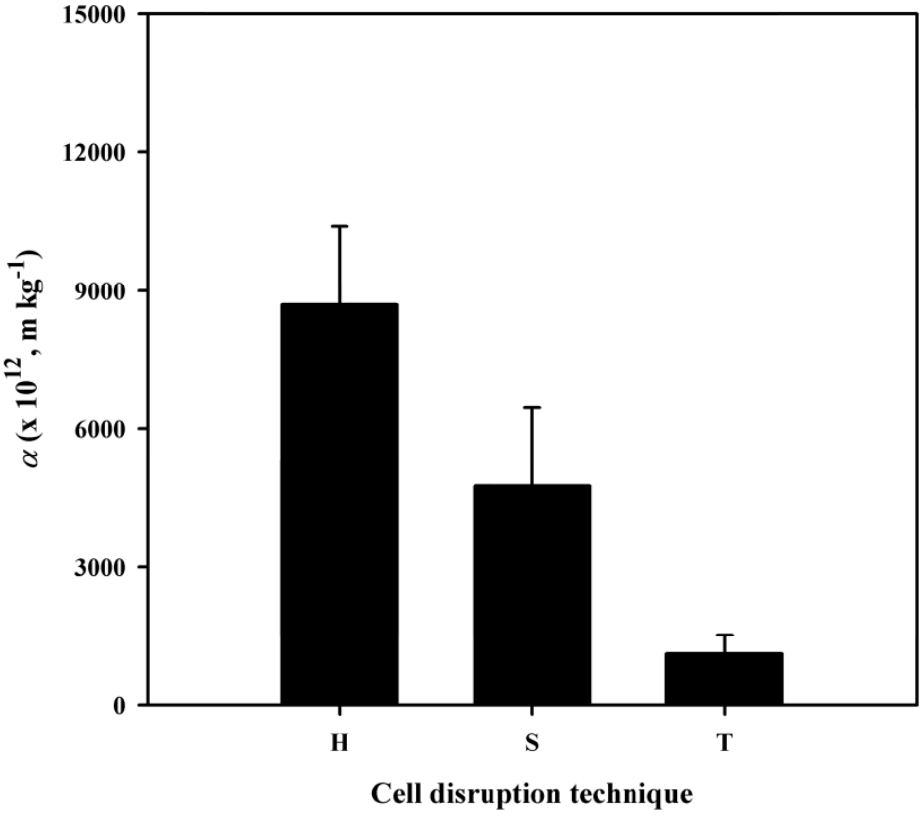

Figure 4.2 Quantification of specific cake resistance following different *E. coli* cell disruption methods: (H) homogenisation, (S) sonication, and (T) thermo-chemical extraction. (H) Homogenisation performed according to Section 2.3.2 using disruption conditions*:* solids load of 30 g_{DCW} L^{-1} in 100 mM Tris-HCL pH 7.0, 2-pass at 500 bar; (S) Sonication was according to Section 2.3.4 using solids load of 22 g_{DCW} L^{-1} in 100 mM Tris/10 mM EDTA pH 7.0, 3 x 20 s cycle; (T) Thermo-chemical extraction was performed according to Section 2.3.3 using solids load of 22 g_{DCW} L^{-1} in 100 mM Tris/10 mM EDTA pH 7.0 for 16 h at 50^{o}C . Filtration was performed according to Section 3.3.3 at ΔP_{TMP}= 65 kPa using PVDF 0.45 μm membrane. Error bars represent one standard deviation about the mean (n=3).

The d_{10} for both heat-extracted and sonicated samples was found to be 1μm while d_{90} values were 23μm and 9 μm for the thermo-chemically extracted and sonicated samples, respectively. Typical particle sizes for similar *E. coli* homogenates show a d_{90} of around 4μm or smaller (Balasundaram et al., 2009a). In this case, d_{90} for the homogenate sample is 1 μm. These differences in particle size data partly explain the outcome of the microfiltration process presented in **Figure 4.2**. During microfiltration, suspensions with smaller particle sizes (such as the homogenate suspensions used in this work) will form a more compact cake structure resulting in a higher specific cake resistance (Grace, 1953b).

SDS-PAGE results presented in **Figure 4.4**[*] (lanes 1, 2, and 6) confirmed that homogenised and sonicated samples (lanes 1 and 2) contain a larger quantity of impurities than the thermo-chemically extracted cells (lane 6). Note that the homogenised sample is from a cell suspension with a cell dry weight of 30 $g_{DCW}\ L^{-1}$ while the sonicated and heat extracted samples had cell content of 22 $g_{DCW}\ L^{-1}$. Thus, comparing the two samples from cell suspensions with the same level of cell content, **Figure 4.4** shows that the thermo-chemically extracted sample (lane 6) is relatively "cleaner" than the sonicated sample (lane 2). On the other hand, the sonicated sample, although from a sample of lower cell content, appears to have similar profile and level of contaminants as the homogenised sample. These results illustrate that cell disruption operations (as in homogenisation and sonication) will lead to the release of more contaminating proteins. This is in contrast to the permeabilising action to the cell membrane by the heat-extraction step which appeared to have resulted in the limited release of contaminants. As shown later in Section 4.3.2, the presence of these contaminating solutes (mostly host cell proteins) may have a profound negative effect on the microfiltration performance of the *E. coli* cell suspensions.

P. Morris is acknowledged for her assistance in the gel analysis in Figure 4.4.

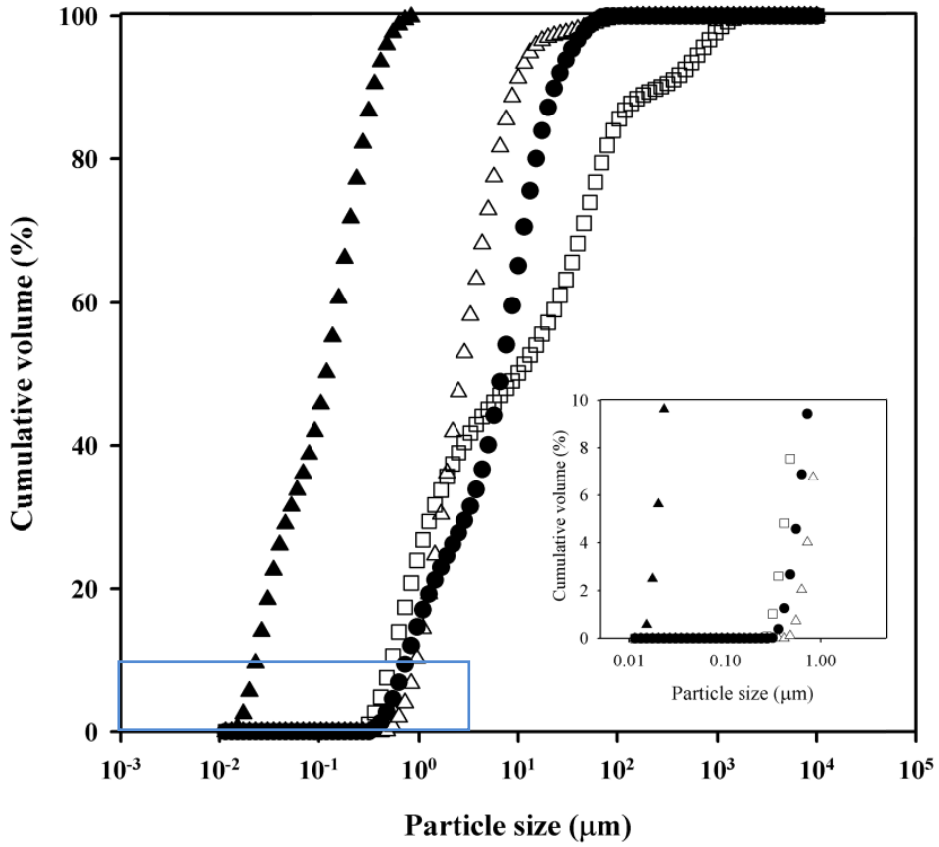

Figure 4.3 Particle size distribution of disrupted *E. coli* cells by: (▲) homogenisation; (△) sonication; (●) thermo-chemical extraction. PSD profile of whole *E. coli* cells in fermentation media (□) is also shown for reference. Disrupted cell suspensions prepared as described in Figure 4.2. Particle size measurement was performed using dynamic light scattering according to Section 2.10.1. Inset shows the size distribution of the bottom (smaller) 10% of the particles.

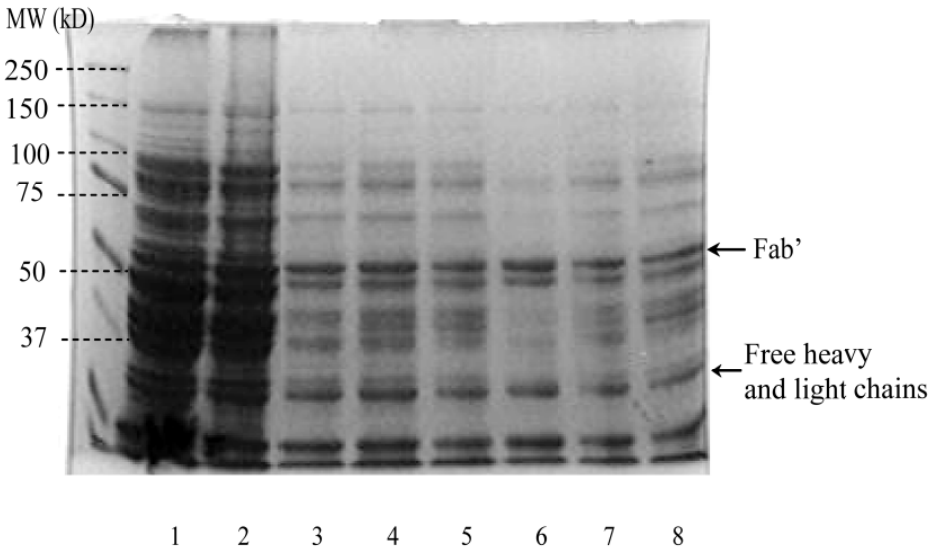

Figure 4.4 SDS PAGE analyses of *E. coli* suspensions following different cell disruption operations. Lane 1: homogenised sample – solids load of 30 g_{DCW} L^{-1} in 100 mM Tris-HCL pH 7.0, 2-pass at 500 bar; Lane 2: sonicated sample – solids load of 22 g_{DCW} L^{-1} in 100 mM Tris/10 mM EDTA pH 7.0, 3 x 20s cycle; Lanes 3-5: thermo-chemical extraction at 35^{o}C for 16h, 2h, 1min respectively - solids load of 22 g_{DCW} L^{-1} in 100 mM Tris/10 mM EDTA pH 7.0; Lanes 6-8: thermo-chemical extraction at 50^{o}C for 16 h, 2 h, 1 min respectively - solids load of 22 g_{DCW} L^{-1} in 100 mM Tris/10 mM EDTA pH 7.0. Homogenisation, sonication and thermo-chemical extraction were performed according to Sections 2.3.2, 2.3.4 and 2.3.3, respectively. SDS PAGE was performed according to Section 2.9.5.

From **Table 4.1**, **Figure 4.2** and **Figure 4.3**, it can also be observed that sonicated samples do not match the properties of the homogenised samples in terms of Fab' yield, total protein release, and microfiltration performance. This emphasises that sonicated samples are not representative of homogenised material either in terms of composition or particle size distribution. Consequently, the outcome of processes conducted using sonication at laboratory scale will not accurately represent the process scale outcomes using homogenised materials. In contrast, the microscale thermo-chemical extraction method does give comparable results to pilot scale (10 L) thermo-chemical Fab' extraction (unpublished data, Alison Tang, UCL).

A final consideration for process characterisation is the release of incorrectly assembled or unfolded Fab' which provide difficult purification challenges further downstream. The thermo-chemical extraction step was designed to destabilise the outer membrane of the *E. coli* cells and release only the components present in the periplasmic space (Weir and Bailey, 1997). The high pressure homogenisation and sonication methods may provide higher Fab' yields but they also contain larger proportions of incorrectly assembled or unfolded Fab', as well as many other contaminating proteins, from the cytoplasm. It is common that fermentation processes will produce a proportion of these unfolded, incorrectly assembled or incomplete Fab' (Baneyx and Mujacic, 2004; Spitali, 2009). These Fab' species are also included in the quantification of Fab' content (for example as in **Table 4.1**) since the Protein G assay used (Section 2.9.4) detects both the complete, functional Fab' species as well as the incomplete and non-functional antibody fragments (Bowering et al., 2002). Thus, even if it appears that the homogenised and thermo-chemically extracted samples have similar purities based on **Table 4.1**, it is the preparation from the periplasmic extraction which will contain the highest purity of correctly assembled, disulphide bond-rich antibody Fab' fragments. Further analysis of the Fab' species were not done in this work. However, with increased interest on the understanding of antibody fragments, analytical techniques

have now emerged in order to quantify specific species. For example, Roque et al. (2005) have studied affinity chromatography using Protein L resin which could differentiate between species of antibody fragments. From **Table 4.1,** the Fab' content obtained thermo-chemical extraction is the lowest among the three Fab' release methods. Yield improvement for Fab' release using thermo-chemical extraction may be achieved by coupling this method with mild homogenisation (Spitali, 2009).

Overall, the results in this section indicate that a trade-off between quantity and quality of product release and subsequent efficiency of recovery should be considered in deciding the preferred process route. Although some cell disruption methods were shown to be more efficient in releasing the product, the properties of the suspension may not be beneficial for the subsequent unit operation in the downstream process sequence. This observation emphasises the need for a whole bioprocess approach, linking upstream and downstream process operations, when assessing different bioprocess flowsheet options.

4.3.2 Impact of disruption conditions on Fab' recovery by microfiltration

One of the advantages of the microscale approach is the ability to link different operations together in a defined process sequence thus allowing investigation of unit operation interactions. Consequently, the effects of different conditions during thermo-chemical extraction on the microfiltration performance of *E. coli* cells were investigated in detail as indicated in **Figure 4.5.** This enables the effects of a range of extraction conditions to be investigated for their impact on the filterability of the resulting suspensions.

4.3.2.1 Influence of cell concentration and extraction pH

It was deemed important to first study the effect of cell concentration as this is one of the factors which may affect the release of intracellular products during a chemical

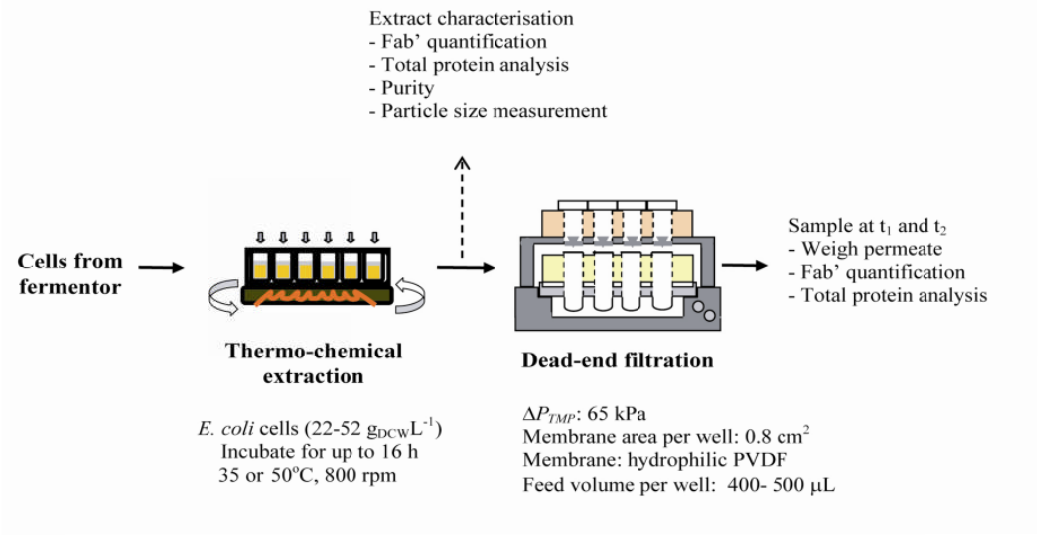

Figure 4.5 Microscale process sequence for automated evaluation of impact of Fab' thermo-chemical extraction conditions on subsequent microfiltration performance of disrupted *E. coli* cells. Process was automated on the deck of a Tecan Genesis robotic platform.

extraction step (Choe and Middleberg, 2001). At the same time, a narrow pH range was studied to test the sensitivity of Fab' recovery with small pH variations which may occur during processing. Statistical analysis showed that the pH of the Tris-EDTA solution does not have a significant effect (F-test, $p>0.05$) on Fab' release over the pH range 7.0 - 7.8. **Figure 4.6** shows the Fab' concentration obtained at the different cell loadings. The Fab' concentration increased with increasing cell loading, however, the amount of Fab' released per gram of cell was found to decrease with increasing biomass concentration. The thermo-chemically treated cell suspensions were subsequently used in microfiltration experiments to characterise their filterability in terms of cake resistance. **Figure 4.7** shows the calculated α values and the corresponding Fab' transmission after undergoing sequential extraction and filtration. Statistical analysis (F-test, $p<0.05$) shows that pH has a significant effect on α values while the cell concentration or solids loading does not have a significant effect. This result is in contrast to the effects of pH and cell loading on the release of Fab' fragments during the preceding extraction step (**Figure 4.6**) and illustrates the need to consider the impact of a process parameter like pH on subsequent downstream operations. The α values of heat-extracted cells were also affected by the interaction effects between pH and solids loading. On the other hand, Fab' transmission data have been shown to have a negative correlation with α, the magnitude of correlation depending on the solids concentration.

Particle size distribution analysis (PSD) of these thermo-chemically extracted cells (**Figure 4.8**) showed the presence of a bimodal size distribution; one peak for particles having diameters smaller than 2 μm and the other for diameters larger than 2 μm. Typical dimensions of *E. coli* are 0.5 by 2 μm (Miao et al., 2003). The data obtained indicates that particle size distributions are very similar for the different cell suspensions at the same cell concentration even at different pH values. The particle size

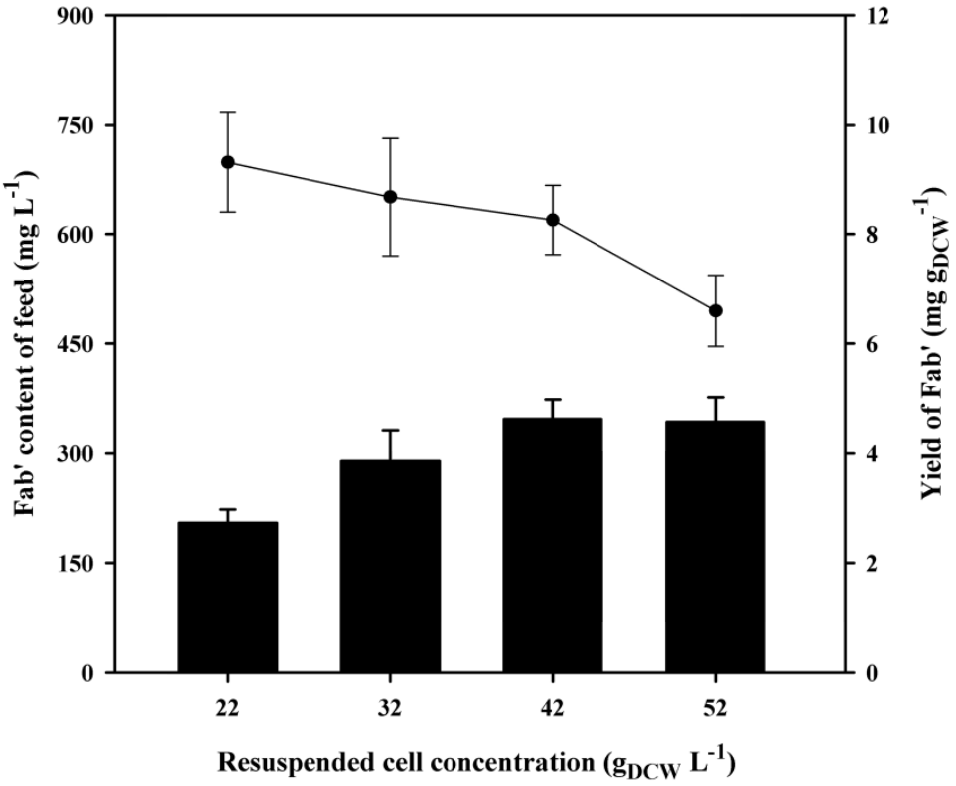

Figure 4.6 Impact of cell concentration on Fab' release from thermo-chemically extracted *E. coli* cells. (■) Fab' content; (●) Yield of Fab'. Periplasmic extraction in 100 mM Tris/10 mM EDTA solution, pH 7.0-7.8, at 50^{o}C for 16 h as described in Section 2.3.3. Error represent one standard deviation about the mean (n=3).

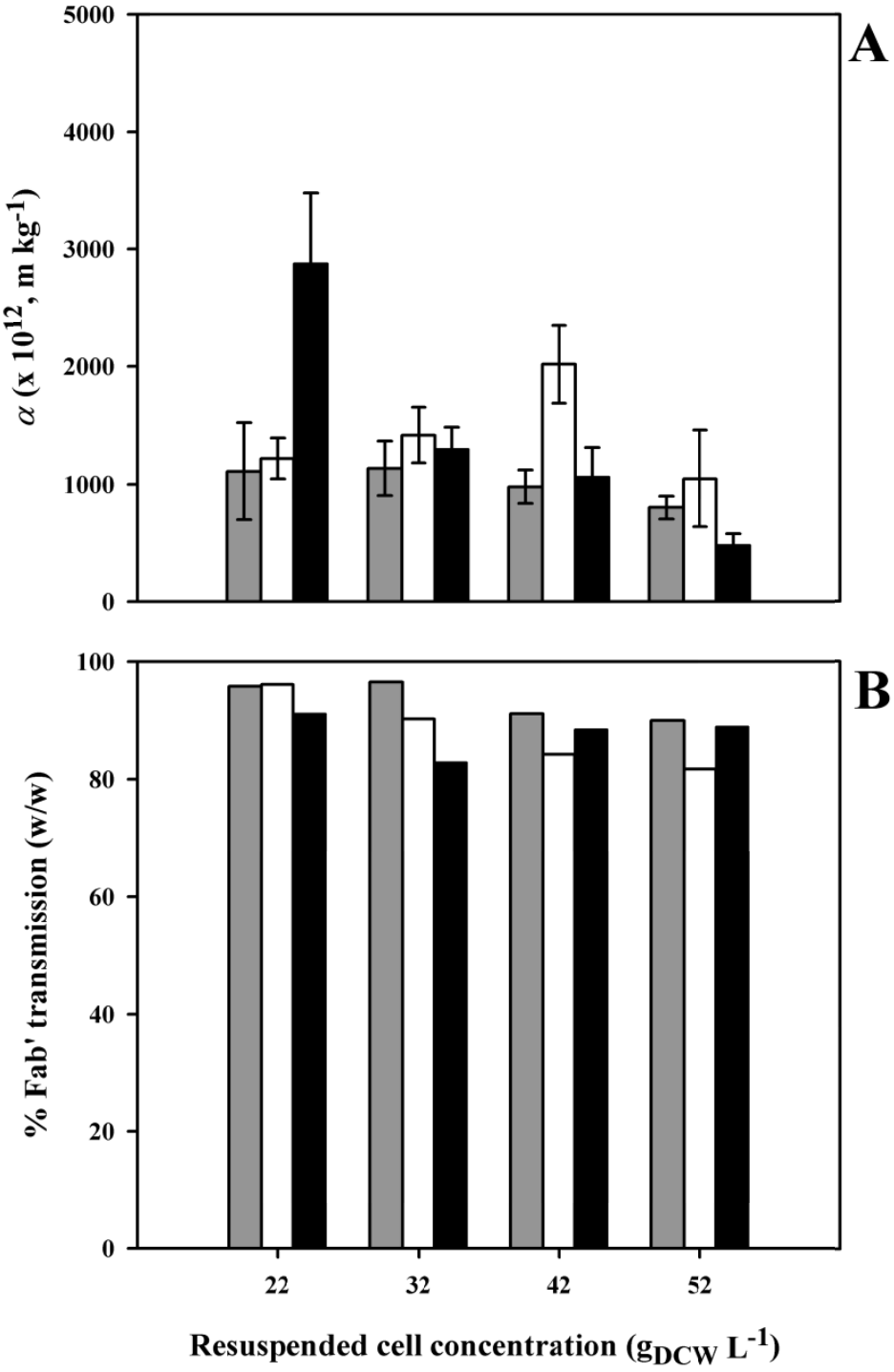

Figure 4.7 Impact of cell concentration on (A) calculated specific cake resistance and (B) apparent permeate transmission of thermo-chemically extracted *E.coli* cells. Extraction in 100 mM Tris/10 mM EDTA solution, at 50^{o}C for 16 h: (■) pH 7.0; (□) pH 7.4; (■) pH 7.8 as described in Section 2.3.3. Filtration was performed at ΔP_{TMP}= 65 kPa using a PVDF 0.45 μm membrane as described in Section 3.3.3. Error bars represent one standard deviation about the mean (n=3).

distribution of the untreated cells resuspended in the original fermentation broth shows that the whole cells tend to form more aggregates than the treated ones (**Figure 4.8 A**). The untreated whole cell suspensions have 50% of particles larger than 10 μm while only 30% of the heat-extracted cells are larger than 10 μm (**Figure 4.3**). The treated cell suspensions have therefore smaller size aggregates than the untreated whole cells indicating the probable effect of Tris-EDTA on cell-cell interactions.

Tris is known to alter the outermembrane permeability of *E. coli* cells resulting in a limited release of components from the cell envelope (Irvin et al., 1981). On the other hand, EDTA treatments have been reported to alter cell surface properties by changing the morphological structure of the outermembrane surface, releasing polyliposaccharides and increasing envelope permeability (Bayer and Leive, 1977). These cell surface properties are known to affect both cell-cell as well as cell-solutes interactions in a suspension (van Hee et al., 2006) and so will impact on filtration performance in a number of ways. Hodgson et al. (1993) have demonstrated that a modified extracellular matrix on the cell surface reduced the specific cake resistance of the Gram-negative marine bacterium SW8. This kind of effect of cell surface changes on filtration performance was also found in this study where the α values for whole cells in the fermentation media are several orders of magnitude larger than the heat-extracted, Tris-EDTA treated cells.

The microfiltration performance of these cells (**Figure 4.7**) may have also been affected by the presence of different components in solution. These are the solutes that were released from the cells together with the antibody Fab' fragments. Considering that solution components affect cell-cell and cell-protein/solute interactions as well as the cells' state of aggregation (Ohmori and Glatz, 1999), it is clear that these components may consequently affect the cake structure being formed and therefore the permeate

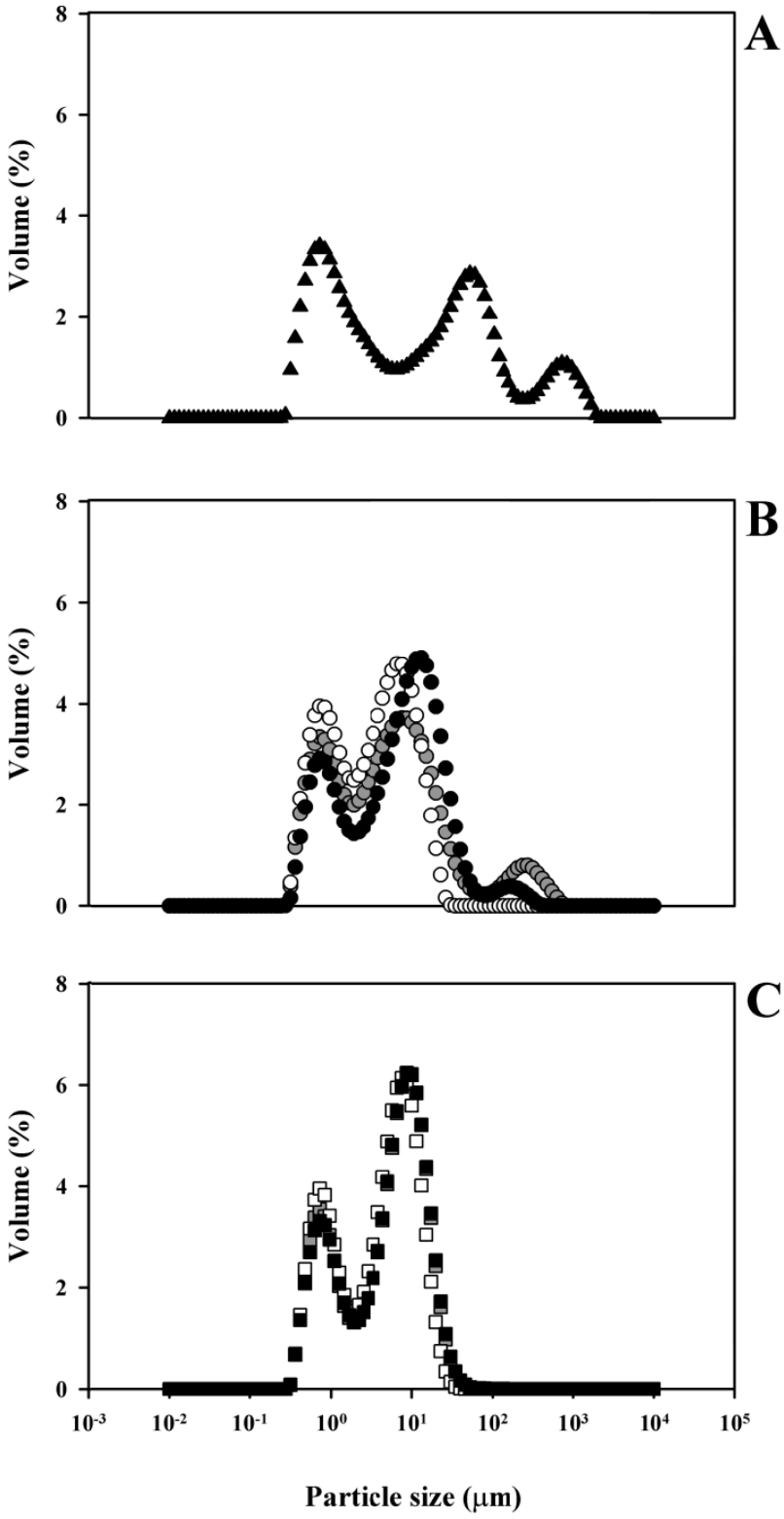

Figure 4.8 Particle size distributions of *E. coli* cell suspensions before and after thermo-chemical extraction. (A) Whole cells; (B) and (C) Thermo-chemically extracted cells as described in Section 2.3.3 at 50°C for 16 h with dry cell loading of (B) 22 and (C) 32 g_{DCW} L^{-1}: (●,■) pH 7.0; (○,□) pH 7.4; (●,■) pH 7.8.

flux during filtration. If these interactions have a large influence on the cake formation process, they will also affect the packing and cake porosity.

The cake porosity is known to largely influence the cake resistance (Foley, 2006b) and is likely to impact on the permeation of Fab' fragments through the filter cake (van Reis and Zydney, 2007). The cake structure has also affected the apparent transmission which is the ratio of Fab' concentration in the permeate to the concentration of Fab' in the feed (Equation 2.7). The Fab' transmission was 80% (w/w) which is low in comparison to the high permeation expected of proteins and other soluble components through microporous membranes. This may be due to the treated cell suspension having an environment that (a) causes the formation of a cake layer that become impermeable to the Fab' fragments or (b) results in the adsorption of Fab' onto the remaining cells or cell debris. A number of studies cite reduced protein transmission during microfiltration due to adsorption onto cell debris (Ohmori and Glatz, 1999; Le et al., 1984; Yamasaki et al., 1993).

4.3.2.2 Influence of extraction temperature and time

In order to understand further the mechanism of the heat extraction process, similar microscale experiments were performed to examine the effects of temperature and time on Fab' recovery. The time profiles of Fab' and protein release for two extraction temperatures (35 and 50^{o}C) and two cell concentrations (22 and 32 g_{DCW} L^{-1}) are shown in **Figure 4.9**. For both solids loading, the Fab' release from cells in Tris-EDTA solution increases with time. Results show that Fab' release was relatively fast since Fab' concentration values measured after one minute incubation were already higher than half the concentration values for the longest incubation time (16 h). Fab' content was also higher at the higher extraction temperature although the maximum difference in Fab' fragments concentration between the two temperatures is only 9%.

A similar profile of fast release of total protein content can be observed at the lower extraction temperature. However at 50^{o}C, the protein content decreases with time. The disappearance of these proteins is also evident in the SDS PAGE gel shown in **Figure 4.4** (lanes 8 and 6). Fab' fragments are reported to be thermally stable (Weir and Bailey, 1997) hence they are not degraded at 50^{o}C. The heat extraction step employed here is also designed to cause denaturation of the more labile host cell proteins causing them to precipitate from solution and further decrease the HCP load on subsequent chromatographic downstream process steps. These precipitated proteins are therefore not detected during the total protein assay and SDS PAGE because the samples used were from clarified supernatants of the extracted cell suspensions.

The cell suspensions extracted at 2 h and 16 h at temperatures of 35^{o}C and 50^{o}C were next used as feeds to subsequent microfiltration operations. The measured α values with these cell suspensions are shown in **Figure 4.10**. The results show that α decreases as the extraction time and extraction temperature were increased. The reduction in specific cake resistance corresponds to the lower contaminating soluble protein levels in the cell extracts from 50^{o}C, a further indication that contaminating proteins present in solution were contributing factors in the microfiltration of the heat-extracted *E. coli* cells. At the lower temperature, Fab' and protein release is not as efficient hence, the contaminating protein profiles were different for the two extraction temperatures investigated as illustrated in **Figure 4.4**.

The differences in the release of cellular components during heating of *E. coli* cell suspensions can be explained by the mechanism of heat destruction of the outer cell membrane. The effect of heating on *E. coli* W3110 cells has already been reported. Katsui et al. (1982) found that release of outermembrane components such as lipids and polyliposaccharides was induced by heating the cells (at 55^{o}C) in Tris buffer. The pattern of release obtained is similar to the Fab' release shown in **Figure 4.10** wherein

the initial rapid release of these components was followed by a secondary release at a slower rate. It is noteworthy that the authors did not detect a substantial release after incubating the cells at 37^{o}C. Tsuchido et al. (1985) reported that increasing the concentration of Tris buffer above 100 mM enhances its toxic effect on both the intact and heated cells. This may explain the differences in the released soluble components at the two temperatures investigated. With the higher concentrations of Tris-EDTA used here it can be expected that the release of cellular components, particularly from the periplasmic space, is more efficient at 50^{o}C than at 35^{o}C. These results show that there is a clear advantage in increasing the temperature of extraction to 50^{o}C even if the lower temperature at 35^{o}C may release similar amounts of Fab' fragments at extended extraction periods. The advantage is the cleaner preparation of the extracts which results in better filterability (and therefore more efficient recovery) of the extracted cell suspensions at the higher temperature. As Bowering et al. (2002) also noted, Fab' is released after 10 minutes but the extended time period at a higher temperature (60^{o}C in their study) allows for the complete degradation of incomplete Fab'. In this case, it was also shown that this prolonged extraction time not only improved the purity by eliminating these contaminating proteins and non-functional Fab' fragments, but more importantly the process produced an extract that has better filterability and therefore, improved the recovery from the linked process sequence.

4.3.3 Impact of filtration conditions on Fab' recovery by microfiltration

Sections 4.3.1 and 4.3.2 have shown how a preceding unit operation, such as cell disruption, could impact on the performance of a subsequent dead-end microfiltration process. This section will now present results on the impact of the operating conditions employed during the microfiltration of disrupted *E. coli* cells. Operating conditions investigated include the type of membrane material, pore size, and the transmembrane pressure.

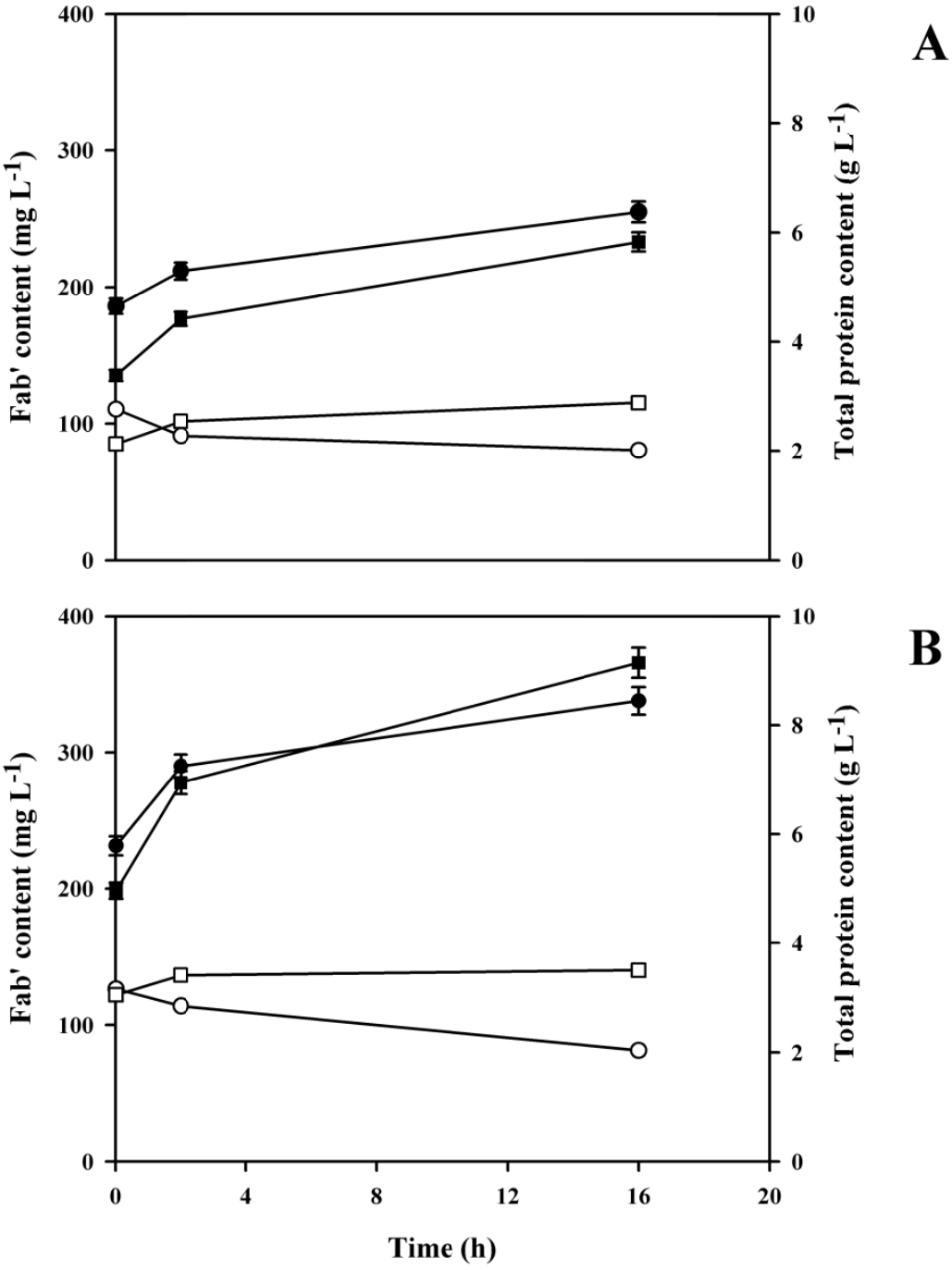

Figure 4.9 Impact of heat extraction temperature and time on Fab' and total protein release from thermo-chemically extracted *E. coli* cells. Periplasmic extraction with solids loads of (A) 22 and (B) 32 g_{DCW} L^{-1} in 100 mM Tris/10 mM EDTA at pH 7.4 performed as described in Section 2.3.3. Open data points represent protein content while filled data points are Fab' content. (■,□) 35°C extraction temperature and (●,○) 50°C extraction temperature.

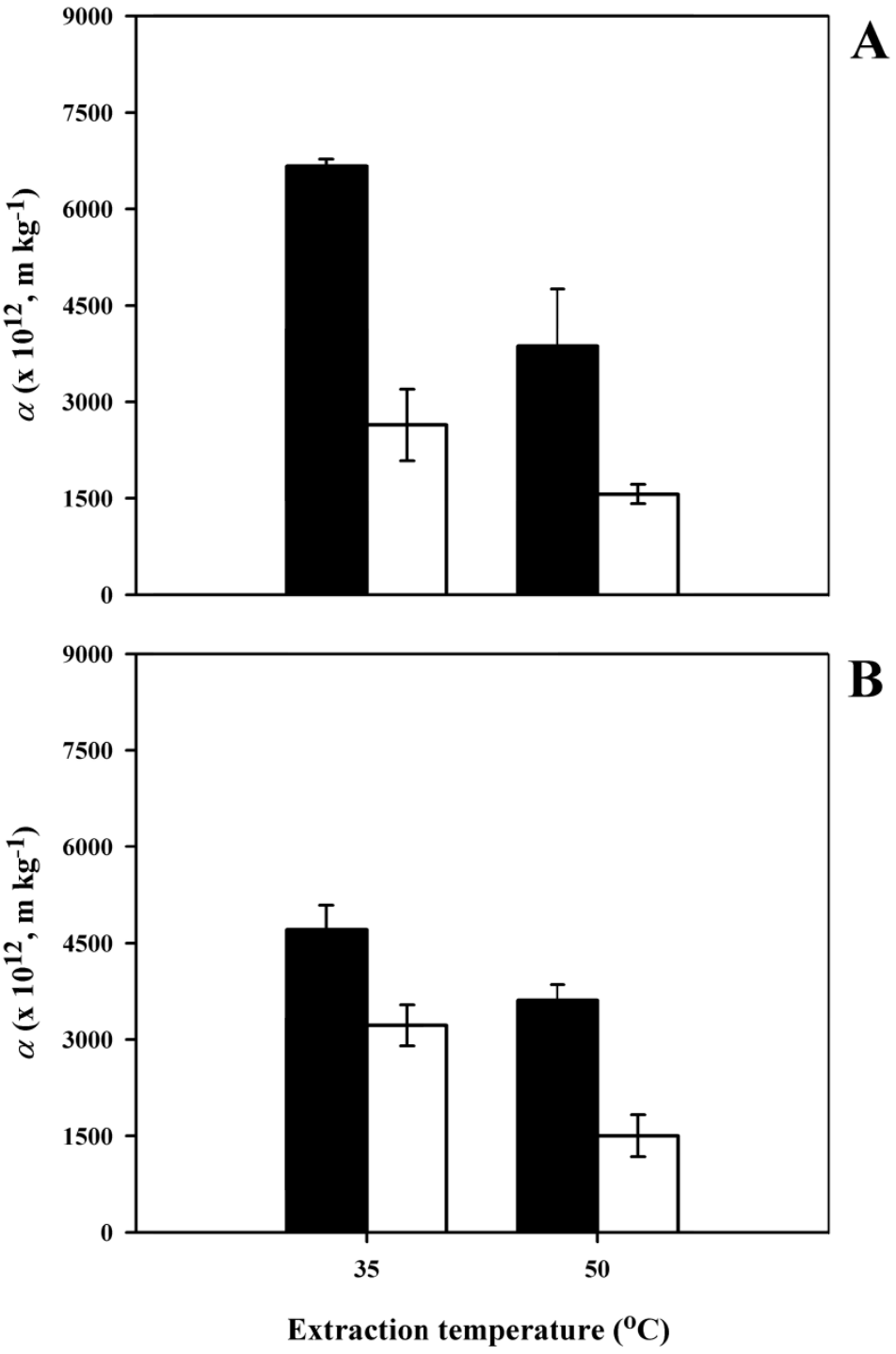

Figure 4.10 Impact of heat extraction temperature and time on calculated specific cake resistance of thermo-chemically extracted *E.coli* cells. Periplasmic extraction with solids load of (A) 22 and (B) 32 g_{DCW} L^{-1} in 100 mM Tris/10 mM EDTA at pH 7.4 for 2 h (■) and 16 h (□) as described in Section 2.3.3. Filtration was performed at ΔP_{TMP}= 65 kPa using PVDF 0.45 μm membrane as described in Section 3.3.3. α values were calculated according to Equation 3.4 Error bars represent one standard deviation about the mean (n=3).

4.3.3.1 Influence of membrane material

In Section 1.4, a selection of various types of membrane material and pore sizes together with their common usage were presented. The choice of the most appropriate membrane material and correct pore size is important in ensuring high permeate flux, minimal product adsorption and therefore reduced product loss. Thus in this section, the use of different pore sizes and membrane material is investigated.

It was shown in **Table 3.1** that the membrane resistances of PVDF membranes rated 0.1, 0.22 and 0.45 μm differ by as much as 90%. The one with the smallest membrane resistance, 0.45 μm, was therefore used in the rest of Chapter 3 and in the previous sections here in Chapter 4. When PVDF membranes with smaller pore ratings were used in the microfiltration of thermo-chemically heat treated cells (data not shown), results illustrated no significant difference in the microfiltration performance, both in terms of specific cake resistance and Fab' transmission. The difference in membrane resistance as a result of the difference in pore size (and possibly porosity and internal surface area, as discussed in Section 3.3.2) is therefore not a key factor in the microfiltration of *E. coli* cells. This is in agreement with the mechanism and assumptions used in cake filtration studies, particularly in deriving Equation 1.12 where membrane resistance is assumed negligible compared to cake resistance (Teoh et al., 2006).

Microfiltration of the same heat treated cells was performed using a different membrane material namely 0.45 μm-rated hydrophilic polyethersulfone (PES) membrane filters. Results are shown in **Table 4.2**. The membrane resistance of the PES membrane is 1.5 ± 0.3 x 10^{10} m^{-1}, which is similar to the membrane resistance of a PVDF membrane of the same pore rating. The measured membrane resistance is also similar to the one reported in literature for PES (McGuire et al., 2009).

Table 4.2 Specific cake resistances (α) of cell disrupted *E. coli* cells using 0.45 μm PES filters. Conditions for (A): cell loading of 32 g_{DCW} L^{-1}, incubation was at 50°C for 16 h as described in Section 2.3.3. Conditions for (B) is: 22 g_{DCW} L^{-1} as described in Section 2.3.4. Filtration was performed at ΔP_{TMP}= 65 kPa as described in Section 3.3.3. α values calculated according to Equation 3.1. Values inside brackets are percent difference to PVDF data with negative values indicating lower values.

Cell disruption technique		**α (x 10^{12} m kg^{-1})**	**Fab' transmission (%, w/w)**
(A) Thermo-chemical extraction	pH 7.0	673 ± 132 [-41%]	88 [-8%]
	pH 7.4	1009 ± 156 [-29%]	86 [-4%]
	pH 7.8	1140 ± 36 [-12%]	82 [-1%]
(B) Sonication		4201 ± 632 [-4%]	98 [-2%]

In comparison with the microfiltration performance using hydrophilic PVDF membranes, the specific cake resistances from PES filters are smaller. Statistical analysis shows that this difference is significant (F-test, $p<0.05$) at pH 7.0 and 7.4. Both manufacturers of these two filters mention that the filters offer low protein binding. So on the basis of specific cake resistances, it was expected that transmission through PES filters will give slightly larger transmission of Fab'. However, the PES data shown in **Table 4.2** are slightly smaller than Fab' transmission through PVDF filters.

It is believed that this lower transmission is primarily due to the binding of Fab' fragments on the PES membrane. As part of the protocol in HPLC analysis (described in Section 2.9.4) samples have to be filtered using syringe filters. The same result was also observed by the Fab' concentration data (not shown) from the supernatant of the feeds prior to filtration. An inspection of Fab' concentrations from these supernatants

show that, using PES syringe filter, concentrations are 2-9% lower compared to PVDF-filtered samples even if the samples come from the same pool of supernatant.

Table 4.2 also shows the result of microfiltration using PES membranes for disrupted *E. coli* cells suspensions by sonication. In contrast to the thermo-chemically extracted cells, the disrupted cells from sonication gave comparable microfiltration performance with either PES or PVDF membranes. As discussed in Section 4.3.1, the sonicated and heat extracted samples differ in their Fab and total soluble protein content. This may explain why these two cell suspensions have different microfiltration behaviour using PVDF or PES membranes. Thermo-chemically extracted cells may have properties that resulted in a different interaction with PVDF than PES membranes. On the other hand, the sonicated samples may have properties that neither interact with PVDF or PES membranes, thus the microfiltration behaviour is the same even with different membrane type. These properties include cell-cell interaction type resulting in a certain cell – membrane interaction, or soluble component interactions with the membranes.

4.3.3.2 Influence of transmembrane pressure

Being a pressure driven process (Section 1.4), membrane microfiltration depends on a transmembrane pressure difference (ΔP_{TM}) to achieve the separation and permeation of the desired solute from the undesired components in a suspension. The relationship of permeate flux versus ΔP_{TM} is commonly known to be positively correlated. However, during microfiltration of microbial cell suspensions, there is a phenomenon called filter cake compressibility which may also influence the permeate flux. Foley (2006b) explains that the packing structure of compressible cakes cannot sustain the viscous drag caused by the pressure gradient in the fluid at the particle-fluid interface. A new stable packing structure is required and this is achieved, in the case of microbial suspensions, by particle re-arrangement either with or without particle deformation. The re-arrangement or deformation of particles may also result in the change in cake

porosity, thereby influencing not only the permeate flux but also the transmission of permeable components. Thus it is necessary to investigate the relationship of α versus ΔP_{TM} since this will provide the basis for determining the extent of compressibility of microbial suspensions.

One of the practical problems associated with the determination of cake compressibility is the number of experiments required, which translates to a certain amount of feed volume. The amount required is even greater when the microfiltration behaviour of several feed preparations is examined (Sections 4.3.1 and 4.3.2). In this regard, a method was developed (Section 3.3.5) where a single plate microscale dead-end filtration experiment is performed for an adequate period of time. The method was shown to conform to cake filtration theory, while enabling experimentation with minimal amount of feed. The single plate, single-step method was used here to determine the α versus ΔP_{TM} behaviour of thermo-chemically treated cells (**Figure 4.11**).

As shown in **Figure 4.11**, the specific cake resistances of feeds with different cell loading and extraction conditions increase with transmembrane pressure. The linear relationship ($r^2 > 0.98$) indicates the compressible nature of thermo-chemically extracted *E. coli* cells which is in agreement with findings in literature for *E. coli* suspensions (Riesmeier et al., 1989). The figure also illustrates that the extent of dependence of α with ΔP_{TM} is affected by the feed preparation (in this case, the extraction temperature).

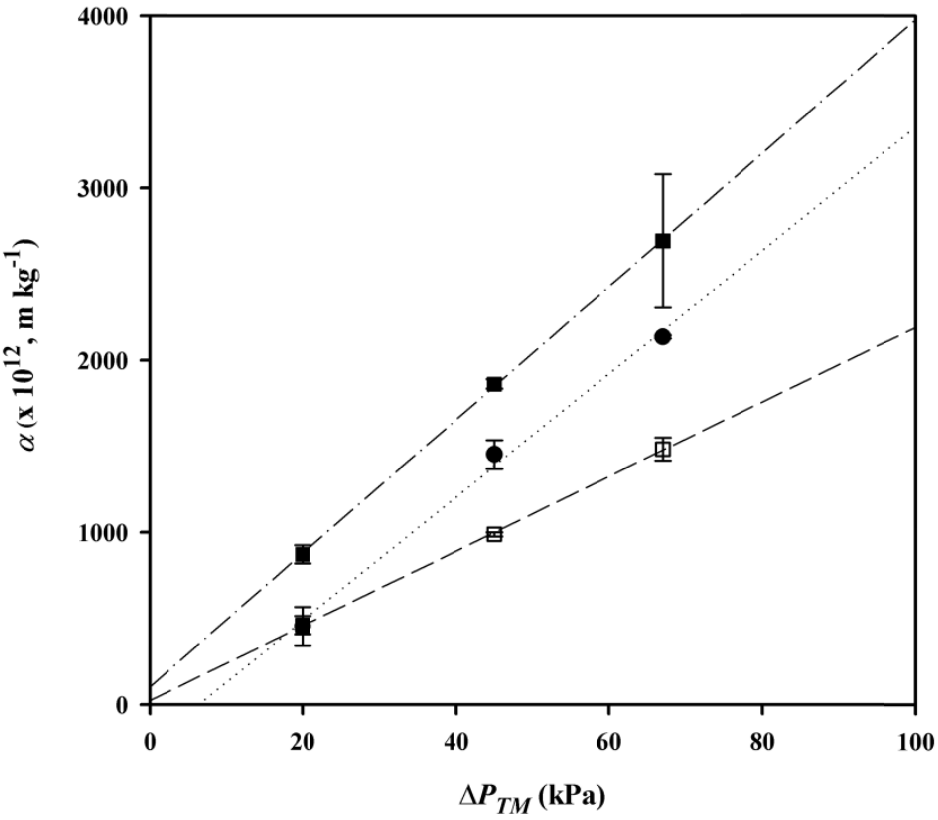

Figure 4.11 The effect of transmembrane pressure on specific cake resistance (α) values. Thermo-chemically extracted cells were prepared as described in Section 2.3.3. (●) 22 g_{DCW} L^{-1}, 35°C extraction temperature; (■) 32 g_{DCW} L^{-1}, 35°C extraction temperature; (□) 32 g_{DCW} L^{-1}, 50°C extraction temperature. Lines: (-·-); (····); (----) are regression lines. Filtration was performed according to Section 3.3.5. α values were calculated using Equation 1.12.

4.4 Conclusions

In this chapter, microscale methods for *E. coli* thermo-chemical extraction and filtration (**Figure 4.5**) were established and effectively used to gather quantitative engineering data for the primary recovery of antibody fragments in a linked process sequence. Using these techniques, it has been shown that thermo-chemically extracted cell suspensions gave better microfiltration performance than the disrupted cell suspensions prepared by homogenisation or sonication (**Figure 4.2**). Although the latter disruption methods were more efficient in releasing the Fab' product (**Table 4.1**), the quality of the feed, in terms of the levels of contaminating host cell protein and misformed Fab' fragments, was poorer and hence detrimental for the subsequent downstream processing step. The conditions of thermo-chemical extraction such as pH, extraction temperature and time, not only affect the yield of the extracted Fab' but also impacts on the microfiltration performance (Section 4.3.2). Finally, the differences in microfiltration behaviour using different membrane types were compared. It was demonstrated that depending on the type of cell disruption method, there may or may not be any difference in filtration behaviour using either PVDF or PES membranes (Section 4.3.3).

Overall these results demonstrate how microscale bioprocessing techniques can identify early key issues related to operation of linked bioprocess sequences. The parallelization of microscale experiments and integration within an automated platform allowed the acquisition of process information with relative ease and reproducibly, thus providing the possibility to explore and optimise a broader spectrum of process conditions than is normally possible manually. Specifically, this approach facilitated a better understanding of the mechanism of the Fab' extraction process which can then be used in the design and optimisation of the primary recovery sequence. In the following chapter, the microscale approach is extended to show a novel design and automated microscale methodology for the rapid evaluation of crossflow microfiltration operation.

5. Design and Evaluation of a Microscale Crossflow Filtration Device‡

5.1 Introduction and aims

A unique feature of the automated microscale approach is the potential to establish linked bioprocess sequences in order to rapidly investigate the effect of upstream process conditions on downstream operation efficiency. The previous chapters have described an example of this highlighting the impact of Fab' extraction conditions on microscale dead-end filtration performance. Dead-end membrane filtration is commonly used for small volume laboratory applications or with single-use processes. In contrast, crossflow filtration (CFF) processes are more frequently recommended for larger scale process applications (Belfort et al., 1994; Yavorsky et al., 2003). As shown in Section 1.5 very few studies to date have examined microscale CFF devices which mimic the operation of larger-scale processes. The best example has been to use a miniature rotating disc-membrane device to simulate the performance of a larger scale diafiltration process (Guijun et al., 2010). However, this approach is not readily amenable to parallel experimentation and automation. The creation of a novel crossflow device which is appropriately designed for operation and integration within a robotic laboratory platform will gain the benefits of increased number of experimental variables that could be investigated and facilitate the study of linked

‡ Majority of the results presented in this chapter is to be submitted for publication as: Rayat, ACME, Craig, A, Lye, GJ, Micheletti, M. (2011). A novel microscale crossflow filtration device for the rapid evaluation of microfiltration processes.

bioprocess sequences. To date, the full potential of crossflow microfiltration has not yet been fully exploited commercially due to the difficulty in describing and modelling process performance *a priori*. Several attempts have been made to model the crossflow microfiltration operation in order to predict process performance particularly in terms of the steady state permeate flux. Belfort et al. (1994) reports that there are models which combine mass and momentum transport equations and are solved with sophisticated numerical techniques. The complexity of the phenomena occurring during crossflow microfiltration meant that no unified framework could accurately describe the process. Due to this, and partly because of the complicated analyses required to solve the models, these were not used in actual design or online prediction of the process performance (Belfort et al., 1994). Given this background, the merit of extending the microscale approach to crossflow microfiltration is evident. It is precisely this kind of unit operations that could greatly benefit by this approach: where models could not satisfactorily describe and predict process performance, adequate data from microscale experiments could be quickly collected covering a wide range of conditions for prediction of larger-scale processes (Titchener-Hooker et al., 2008).

The aim of this chapter, therefore, is to design a novel microscale crossflow filtration (CFF) device and to show its capability to test process conditions relevant to larger scale operations. This device will complement the developments on microscale upstream operations (Jackson et al., 2006) and constitute a valuable option to the already available microscale unit operations. **Figure 5.1** illustrates the context of the creation of this device within the overall aim of this thesis.

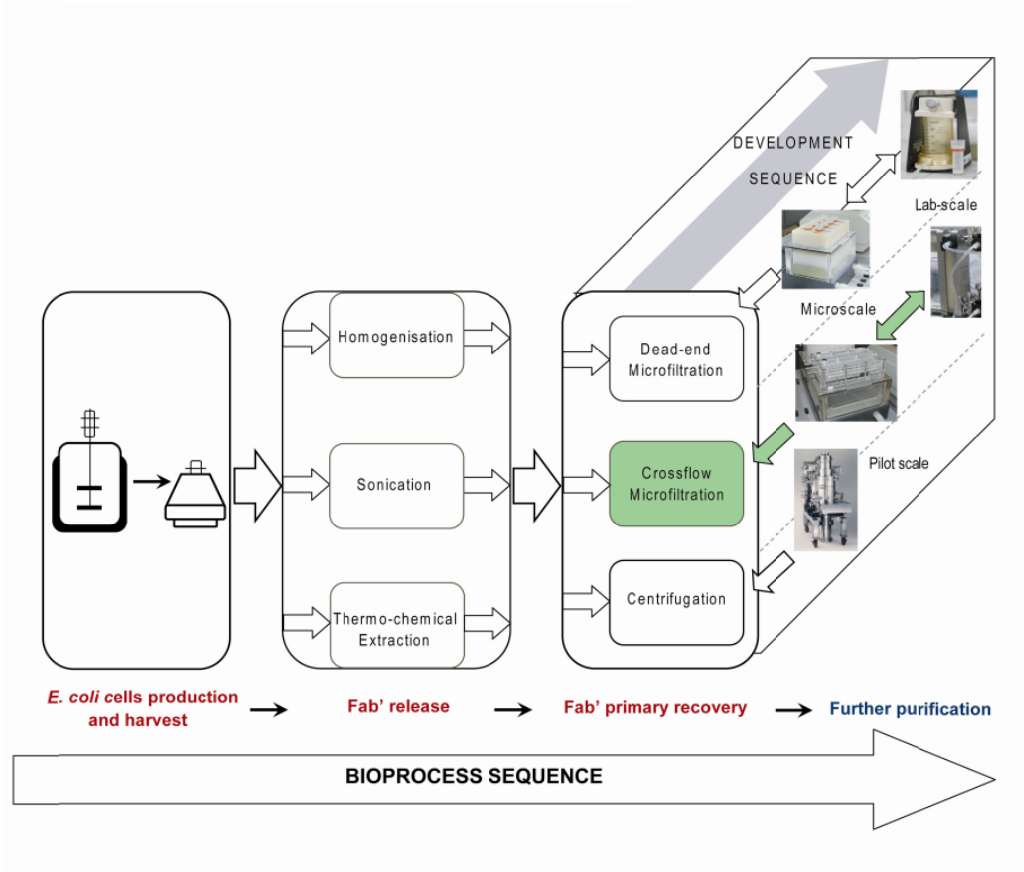

Figure 5.1 Application of microscale bioprocessing platform for membrane filtration for the investigation of bioprocess routes: creation of microscale crossflow filtration device and method development. (Image credit: Pilot scale centrifuge from www.pneumaticscale.com)

The specific objectives are as follows:

- to determine key design considerations and criteria for mimicking commercially available flat-sheet based membrane filtration modules that is able to operate in parallel on a Tecan™ platform;
- to design, fabricate, and evaluate the design performance of the microscale CFF device based on these criteria;
- to establish an automated microscale CFF methodology for predicting larger-scale microfiltration operation for steady state flux determination; and
- to establish the comparability of the microfiltration performance (steady state flux) when using the microscale CFF device to that of the larger-scale laboratory CFF module.

5.2 Microscale CFF design criteria

It is important to achieve consistent results across scales for scale-down or scale-up mimics of unit operations. These mimics have been widely employed for the validation of processes, trouble shooting, and process optimisation studies (van Reis et al., 1997). Van Reis et al. (1997) have listed the important parameters that must be considered for different CFF systems. Among the different operating parameters, the fluid dynamics in the membrane modules is considered an important factor in the effective operation of crossflow microfiltration (Belfort et al., 1994). It is therefore essential to maintain the same hydrodynamic conditions when scaling-up or scaling-down CFF operations.

For flat-sheet membrane module designs as will be used here, such as the Pellicon-2™ (Millipore, Hertfordshire, UK) (**Figure 5.2**), a key criterion for scale translation (scale-up or scale-down) is to maintain a constant channel length (van Reis et al., 1997).

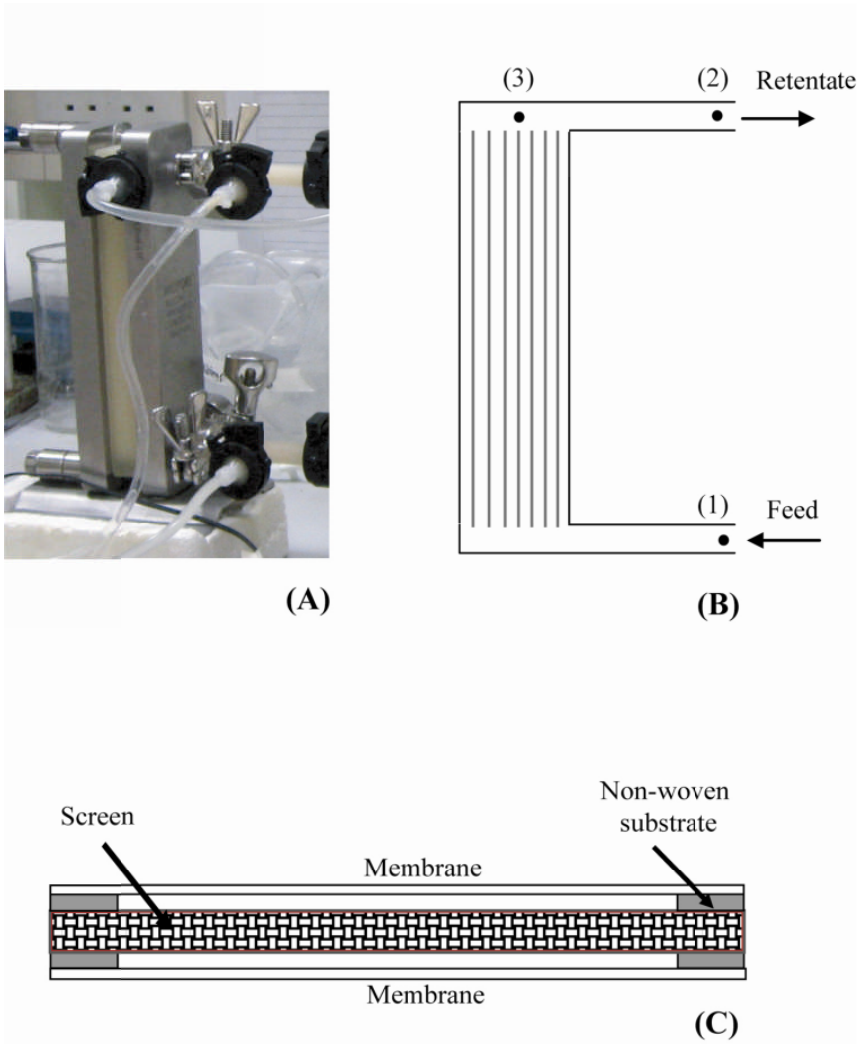

Figure 5.2 The laboratory CFF module used in larger scale crossflow filtration experiments: (A) Pellicon-2™ Mini sandwiched between stainless steel holders; (B) illustration of the membrane configuration within the module and the different ports for (1) feed and (2) retentate pressure measurements, and (3) permeate sampling; (C) schematic representation of the cross section of the module showing a suspended screen between membranes (screen illustration courtesy of Millipore).

Friction along the channel length causes the hydraulic fluid pressure to decrease along the channel. As a result, the permeate flowrate through the membrane also decreases along the channel. Both of these actions result in an increase in concentration of solutes. Therefore when channels of filtration cassettes have different lengths, there will be a variation between their fluid velocity and concentration profiles, resulting in filtration performances that are not comparable. Using this approach to scale translation, the membrane area could be increased by designing parallel membranes within a membrane module or increasing the width of the membrane while maintaining the length.

Another key design factor in scale translation is the channel height (van Reis et al., 1997). In the Pellicon-2™ system effective channel height is mainly controlled by the module design and channel height compression (as a result of flow through parallel feed/retentate channels). Compression, in turn, is a function of physical deformation of the membrane, spacer screen, encapsulant and gaskets (van Reis et al., 1997). These two scale translation criteria, channel (hydraulic) length and channel height, are fundamental to the design aspect of the microscale device established in Section 5.4.1.

5.3 Experimental approach

The microscale crossflow microfiltration device shown in **Figure 5.3** was fabricated in-house in the Department of Biochemical Engineering at UCL. Preliminary evaluation involved performing water flux experiments to test the device for leaks and reproducibility of performance. Following these initial tests, crossflow microfiltration experiments were performed first with a model biological process feed consisting of Baker's yeast.

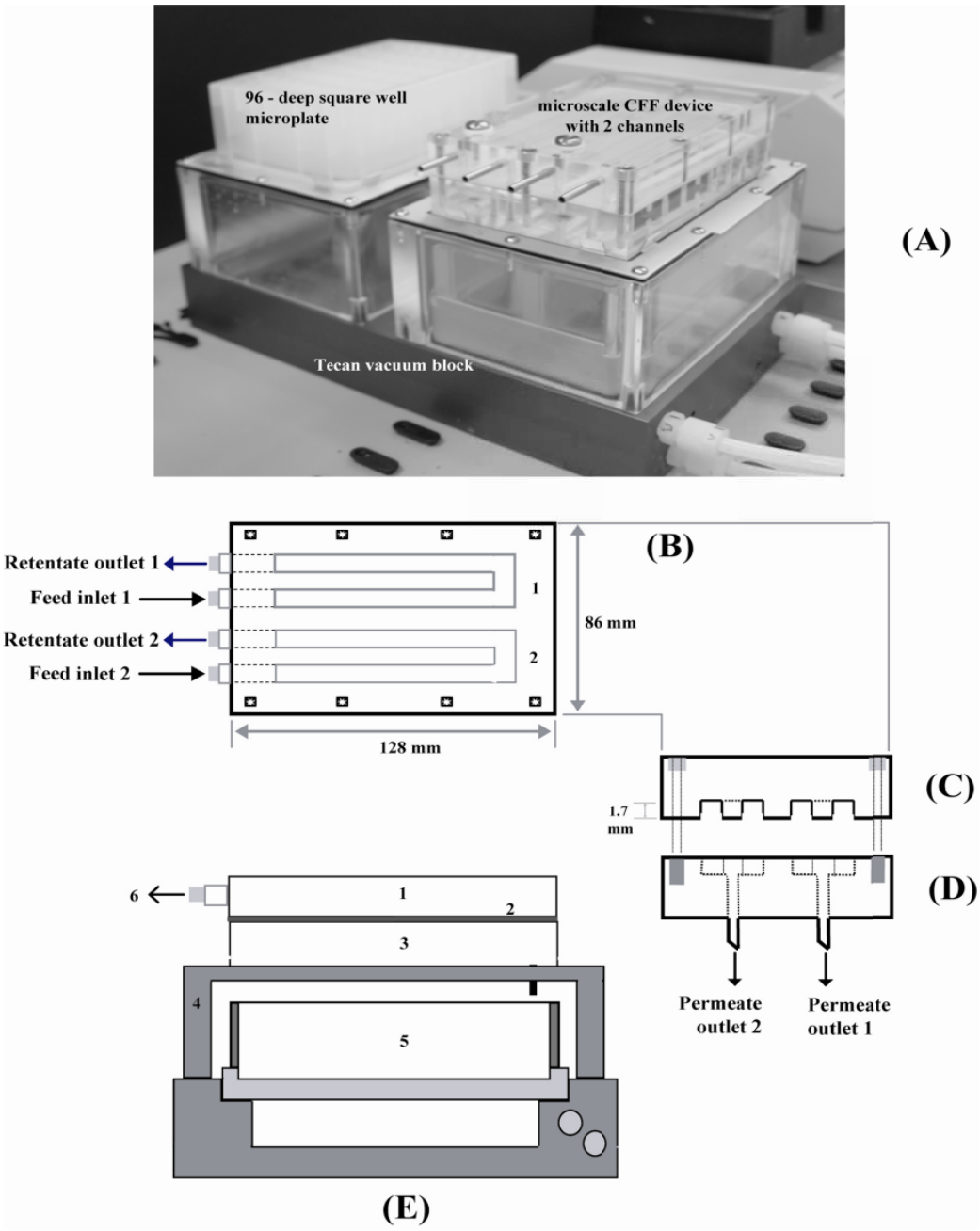

Figure 5.3 Details of the microscale crossflow microfiltration device designed in this work: (A) on top of the Tecan vacuum block beside a 96 – deep square well microplate; (B) Top view of the membrane module; and right side view of membrane module showing (C) feed/retentate channels and (D) permeate channels; (E) Detailed cross section of the vacuum block showing (1) top plate (feed/retentate channels), (2) membrane, (3) bottom plate (permeate channels and o-rings), (4) Tecan holder, (5) permeate receiver, and (6) feed/retentate ports.

Active Baker's yeast from *Saccharomyces cerevisiae* was purchased in powder form from Sigma-Aldrich (Dorset, UK) and was added with bovine serum albumin (BSA) to 10 mM sodium phosphate buffer at pH 6.4. Yeast and BSA concentrations were approximately 30 g L^{-1} dry weight and 6 g L^{-1}, respectively. Once prepared, the yeast suspension was used immediately for the crossflow microfiltration experiments.

Laboratory scale crossflow microfiltration experiments were performed using a Millipore Proflux™ M12™ Tangential Filtration System (Section 2.6.1) and operated according to the procedure described in Section 2.6.2. Microscale crossflow microfiltration experiments were performed using the novel device as shown in **Figure 5.3** and operated according to Section 2.7.2. Details of the CFF methodology are described in Section 5.4.3. Statistical analysis of permeate flux data from both membrane modules was performed using Microsoft Office Excel™ Analysis Toolpak™ (Anova: single factor).

5.4 Results and discussion

5.4.1 Design considerations

An important consideration in the design of the microscale CFF device (**Figure 5.3**) is the Tecan platform on which the device is to be operated. Two things are affected as a result of this. One is the physical design of the filter plates. The length of the filter channels were limited by the available length within a standard microtitre plate. Also, since the filtration process has to be performed under negative applied pressure this influenced the methodology of CFF operation on the Tecan platform.

The main principle followed while designing the microscale CFF device is the linear scaling concept; adopted to simulate the process performance of the Pellicon-2™

system. As earlier mentioned in Section 5.2, it is important to consider the channel length because of its effect on the axial pressure drop (ΔP_{axial}), and therefore the velocity and concentration profiles along the channel. In addition, the hydrodynamics inside the channels, mainly affected by the design of the channel height and width, should also be kept similar. Therefore, the CFF channels were designed so that the resulting total hydraulic length would result in ΔP_{axial} along the channel that is similar to the pressure drop experienced in laboratory scale membrane modules with open or suspended screens. The U shape channel was designed so as to give the necessary length to meet the expected ΔP_{axial} since the total length of the plate (12 cm) is shorter than the 21 cm channel length of the lab-scale module. The channels in the microscale and larger scale device have rectangular cross-sections.

The actual membrane material is placed on the bottom side of the feed/retentate channel while the top side is the etched portion of the acrylic sheet that forms the channel (**Figure 5.3 (C)**). Consideration was given to the practical fabrication limitations to ensure that the height of the channels would be uniform along the lengths of both channels on the filter plate. While the channel height should be made similar in magnitude as that of the Pellicon-2™ membrane, if not smaller, a smaller channel height could result in improved hydrodynamics at a given crossflowrate and this could compensate for the lack of turbulence promoter in the microscale device. Based on these practical and theoretical considerations, the design specifications for the channel height and width were selected. The ΔP_{axial} and wall shear rate (γ_{wall}) were calculated for a range of fluid velocities at a given channel hydraulic length using Equations 5.1 – 5.8.

$$\Delta P_{axial} = f \cdot \left(\frac{S \cdot L}{A_c} \right) \cdot 0.5 \cdot \rho_F v \tag{5.1}$$

$$f = 24\, Re^{-1} \quad \text{(laminar)} \tag{5.2}$$

$$f = 0.133 Re^{-0.25} \quad \text{(turbulent)} \tag{5.3}$$

$$Re = \frac{\rho_F \cdot v \cdot D_H}{\mu_F} \tag{5.4}$$

$$D_H = \frac{2 \cdot h \cdot w}{h + w} \tag{5.5}$$

$$S = 2(w + h) \tag{5.6}$$

$$A_c = w \cdot h \tag{5.7}$$

$$\gamma_{wall} = \frac{h \cdot \Delta P_{axial}}{8 \mu_F L} \tag{5.8}$$

Equation 5.1 is the Fanning equation which relates the axial pressure drop and velocity in a channel and straight pipe. Equations 5.2 and 5.3 can be used to calculate the friction factors for a given channel geometry in laminar or turbulent flow, respectively (Mulder, 1996). In the equations, *Re* is the Reynolds number for which *Re < 2000* indicates that fluid flow is laminar while flows with *Re > 3000* are in the turbulent region (Bird et al., 2001). D_H is the hydraulic diameter, *S* is the circumference or wetted perimeter, *L* is the channel length, A_c is the cross-sectional area of the channel, ρ_F and μ_F are the density and viscosity of the process stream, respectively, *v* is the fluid velocity, *w* is the channel width and *h* is channel height.

Table 5.1 summarises the important dimensions of the Pellicon-2™ Mini- system, the basis of the design of the microscale CFF device and the actual microscale device dimensions. Some of the information regarding the Pellicon-2™ system was estimated from established Millipore data sheets and actual module dimensions, including auxiliary tubing. The calculations to estimate these entries are shown in Appendix 2.1.

Table 5.1. Design features of the laboratory scale and microscale crossflow microfiltration systems.

Parameter	Pellicon™ 2-Mini (V-screen)	Microscale CFF		Remarks on Microscale Design
		Design	Actual	
Screen/channel type	Suspended screen	Open/U-shaped		Design specification 1
Length (cm)	21	18.5	21.5	Design specification 2
Width (cm)	5.6	0.5	0.46	Design specification 3
Height (cm)	2.2	0.1	0.17	Design specification 4
Membrane area (cm^2)	1000	9	10	Design output: a result of spec 2,3
Channels per device	5*	1	1	Design specification 5
Membranes per device	10*	1	1	Design specification 6
Parallel experimentation per device	No	Yes***	Yes***	Design specification7
Hydraulic length (cm)	85**	37.5	55	Design output: a result of spec 1-4
Active membrane length (cm)	16.5	18.5	21.5	Design specification 8
Active membrane width (cm)	60*	0.5	0.46	Design specification 9
Axial pressure drop (bar)	< 0.4 (typical)	0.01-1.8	< 0.2	Design output: a result of spec 1-4
Crossflow velocity (cm s^{-1})	25 (typical)	10-500	30-50	Operating variable

* estimated from given information in published Millipore technical data sheets
** estimated from given information in published Millipore technical data sheets and dimensions including holder and tubing before/after pressure taps
*** two independent channels per filter plate

The Pellicon-2™ Mini system was chosen as the larger scale crossflow filtration module to be mimicked in this work because its design allows it to be linearly scaled-up to pilot scale (from the available 0.1 m^2 for Pellicon-2™, this can be scaled up to 2 m^2 and even up to 80m^2, information found at www.millipore.com).

5.4.2 Preliminary experiments

Initial experiments with the microscale CFF device involved checking for the presence of leaks and performing water flux quantification. Actual ΔP_{axial} measured during these water flux experiments was 30 mbar which is in good agreement with the calculated ΔP_{axial} value (27 mbar) using Equation 5.1. This is also comparable with the measured ΔP_{axial} for the larger scale module which was 40 mbar. This indicates that the designed hydraulic length of the channels in the microscale CFF device, in the form of a U shape, matches the hydraulic length of the larger scale module.

Data from water flux experiments were used to calculate membrane resistances using Equation 2.3. A typical flux versus transmembrane pressure (ΔP_{TM}) curve obtained from the microscale CFF water flux experiments is shown in **Figure 5.4**. The slope represents the normalised water permeability (NWP) and is related to the membrane resistance R_m by Equation 2.4. It can be observed from **Figure 5.4** that the measured membrane resistance is constant across the range of ΔP_{TM} values examined.

Table 5.2 compares the calculated R_m values, calculated for the two channels of the microscale device, and previous data obtained for the same membrane material but using the microscale dead-end filtration method (Section 3.3.1). The R_m values for both channels are comparable and are also similar to the ones previously reported for this 0.22 μm PVDF membrane. The clean membrane resistance is a property inherent to the membrane and therefore should not change with the mode of membrane filtration used (i.e. crossflow as opposed to dead-end mode).

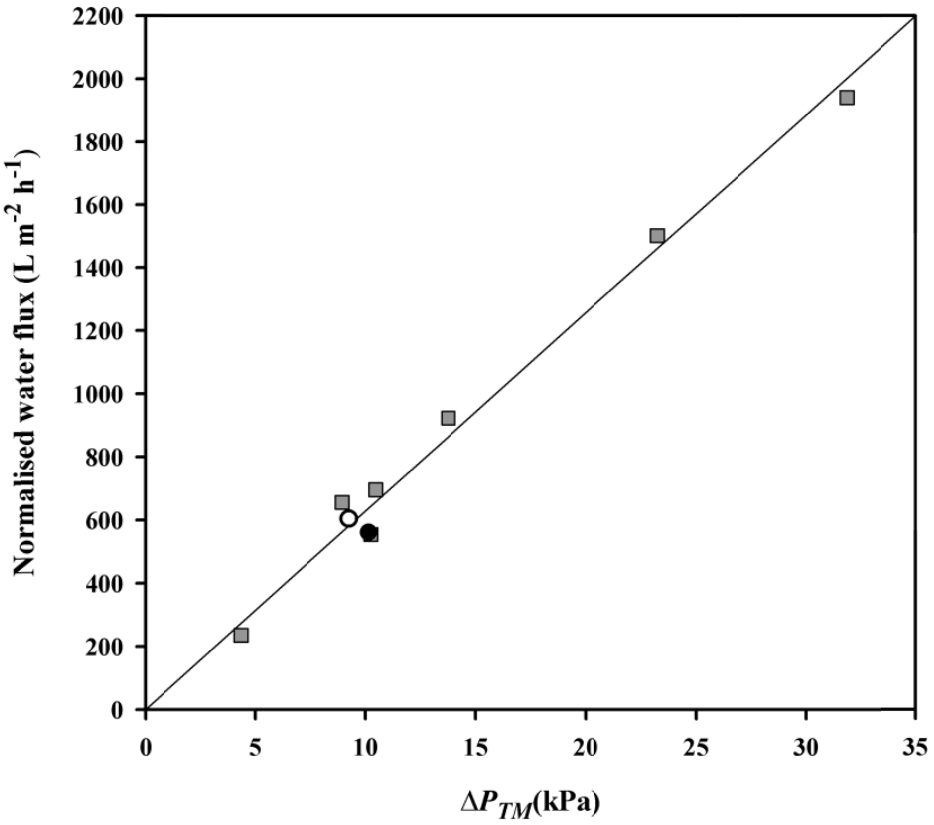

Figure 5.4 Typical permeate data from water flux experiments with the microscale CFF module. (■) Data from one membrane channel at different ΔP_{TM}; (●,○) Repeats using two different membranes. Experiments used the microscale CFF device described in Section 2.5.1 and were performed as described in Section 2.7.2. Solid line represents linear fit ($r^2 = 0.99$)

Table 5.2 Comparison of calculated membrane resistances from water flux experiments using microscale crossflow and dead-end filtration devices. Error bar represents one standard deviation about the mean (n≥ 3).

Membrane type; pore size	**PVDF 0.45 μm**	**PVDF 0.22 μm**
Experimental System	**R_m (x 10^{10} m^{-1})**	
Channel 1 Crossflow	0.9	5.2 ± 0.7
Channel 2 Crossflow	1.0	5.8 ± 0.6
Dead-end filtration	1.2 ± 0.1	4.8 ± 0.2*

*from Section 3.3.1

In contrast to the microscale data, it was found that the larger scale device yields a larger membrane resistance by approximately one order of magnitude. The R_m of the Pellicon-2™ Mini (V-screen) was determined to be 5 x 10^{11} m^{-1}. Membranes of the same type should normally give similar clean membrane resistances. However, communication with the membrane manufacturer's (Millipore) technical support has confirmed that the PVDF membranes purchased as disc membranes (used for the microscale CFF device) were the same as the PVDF membranes inside the Pellicon-2™. Three reasons are thought to cause this difference in R_m: (1) variations in membrane thickness; (2) variation in membrane porosity; and (3) additional hydraulic resistance being measured together with the membrane resistance. The manufacturing variations of the membranes inside the module could result in thickness differences as large as 50% (Millipore Technical Support). Based on the Kozeny-Carman relationship (Equation 1.11), this could result in as much as 50% difference in the measured R_m between these membranes. Considering there are, at least, 10 membranes inside the Pellicon-2™ module (**Table 5.1**), it is quite possible to achieve such high membrane resistance overall.

A Millipore technical specialist (personal communication) also mentioned that membranes for the lab-scale Pellicon-2™ system and the bioscience cut discs (used in the microscale devices) may also have slight differences in the bubble point pressure

(PB). The membranes in the lab-scale module have higher PB than the cut discs (28 psi as opposed to 22 psi). The bubble point test is normally used to measure the maximum pore size in a given membrane (Mulder, 1996). The test measures the pressure required to blow air through a wet membrane. The relationship between this pressure and pore diameter (*d*) is given by the Laplace equation in Equation 5.9.

$$PB = \frac{4 \cos \theta}{d} \sigma \tag{5.9}$$

where *d* is the pore diameter, σ the surface tension at the liquid/air interface, and θ is the contact angle. A higher PB means a smaller pore diameter. From previous membrane resistance calculations, smaller pore diameter gives larger membrane resistance.

In addition, the difference between the calculated R_m values could be due to the lab-scale module containing spacer screens whereas the channels in the microscale CFF device do not have these. Membrane resistance for a similar module, Pellicon™ (Durapore 0.45 μm PVDF), has been reported to be 4.0 x 10^{11} m^{-1} (Hooper et al. 1998), a value close to the one obtained in this study for Pellicon-2™ which they have reported to be affected by the additional hydraulic resistance caused by the spacer screens.

5.4.3 Steady state flux determination

Based on the results obtained in Section 5.4.2 the microscale CFF device provides reproducible and comparable process data for the two membrane channels in water flux experiments. Before the device could be used to evaluate filtration performance of cellular suspensions, a comparable crossflow filtration methodology had to be first established to determine steady state flux for each of the lab-scale and microscale systems. The steady state flux, J_{ss}, is usually obtained by running crossflow microfiltration experiments at constant ΔP_{TM} conditions. J_{ss} is a key membrane filtration performance criterion as it provides information required for scaling-up filtration

processes (Bacchin et al., 2006). Information on the required membrane area is important in evaluating the capital and operating costs required in setting up a filtration process.

For the lab-scale Pellicon-2™ system, flux determination follows established experimental procedures as permeate samples can be collected at defined time intervals throughout the filtration run. **Figure 5.5** shows an example of permeate flow rate versus time data obtained in this larger scale system. It shows that a steady state permeate flow is achieved within one hour of operation.

With the microscale CFF assembly the permeate receiver is inside the Tecan vacuum block (**Figure 5.3**) the amount of permeate can only be measured upon termination of the filtration run. As a result, permeate measurements were made over several sequential filtration runs which terminated at different times. Each measurement thus represents the cumulative amount of permeate collected from the start of the filtration run. In this way the flux measurements do not represent the "true" instantaneous flux at a specific filtration time. In order to measure the "real" flux, the difference between permeate values for two different filtration times need to be used.

To analyse the microscale data, the cumulative permeate values are first plotted for each filtration time. The resulting plot resembles a logarithmic function showing a steep rise in cumulative permeate during the initial stages of filtration followed by a slower rate towards the end. An example of this plot is shown in **Figure 5.6**. This type of plot showing normalised permeate values with respect to time can then be used to determine the actual steady state flux. This steady state condition is represented by the slope of the portion of this plot after the steep rise in cumulative permeate. This linear part (usually after t = 0.2 h) represents where the change in permeate with time is already constant, hence demonstrating a steady state flux.

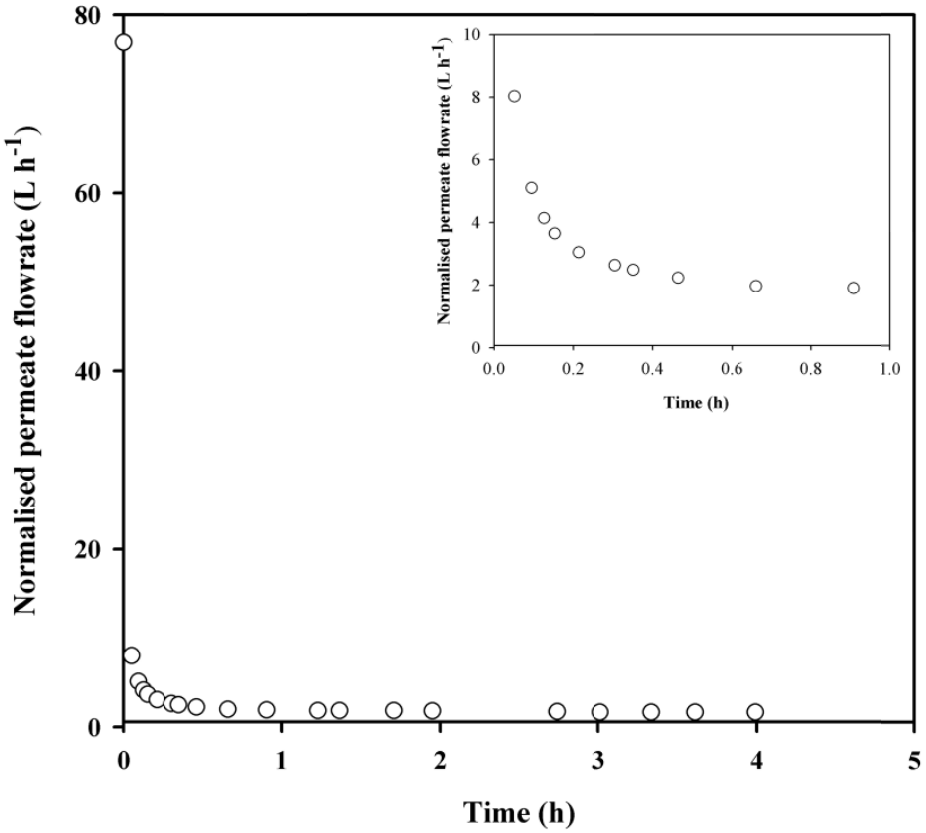

Figure 5.5 Typical permeate flowrate data from lab-scale crossflow microfiltration experiments with Baker's yeast and BSA. Crossflow rate = 80 L h^{-1}, ΔP_{TM} = 100 kPa, A_m = 0.1 m^2 using 0.22μm PVDF membrane. Experiments were performed as described in Section 2.7.2. Data points were calculated using Equation 2.3. The steady state flux is then calculated using Equation 2.2. Inset shows in detail the permeate flowrate during the first hour of operation.

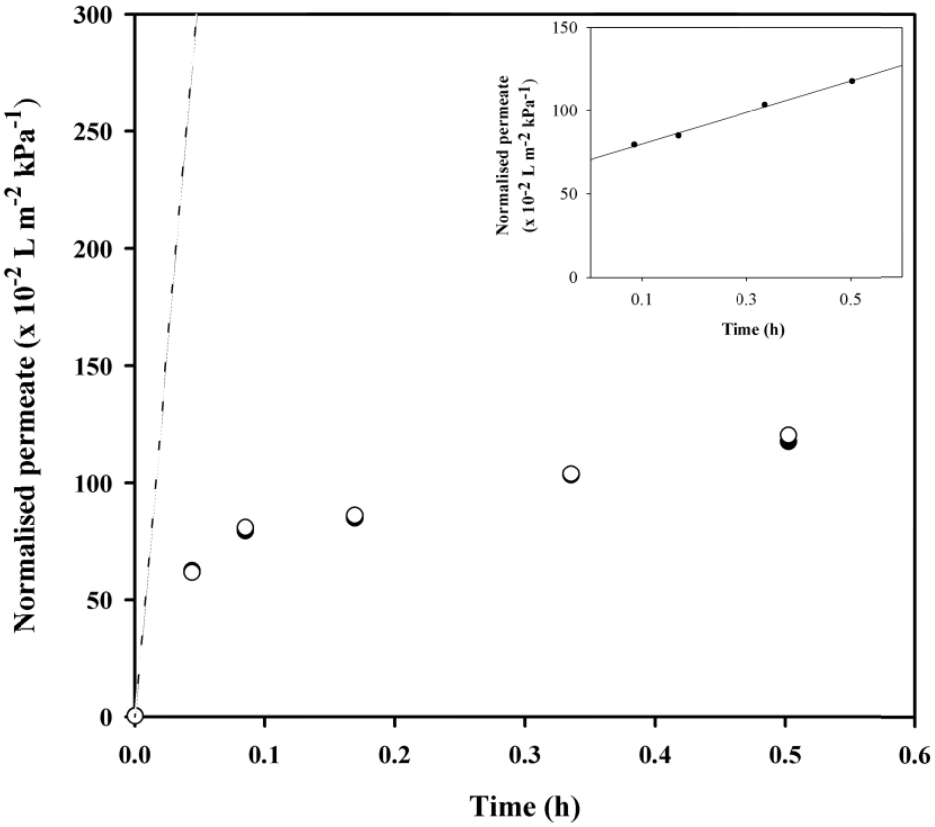

Figure 5.6 Typical permeate flowrate data from microscale crossflow microfiltration experiments with Baker's yeast and BSA. Crossflow rate = 8 L h^{-1}, $\Delta P_{TM.ave}$ = 22 kPa, A_m = 0.001 m^2 using 0.22μm PVDF membrane. (●,○) Data from channels 1 and 2, respectively. Dashed line represents water flux data using R_m values in Table 5.2. Inset shows regression analysis data of the last four points from Channel 1 (●). r^2=0.99, slope = 0.984 L m^{-2} kPa^{-1} h^{-1}.

Table 5.3 shows how the microfiltration data points in **Figure 5.6** were derived. The steady state flux is calculated from Equation 5.10. The slope in this equation is the slope of the line as indicated in the inset of **Figure 5.6**. The linearity was judged by a value of the regression coefficient, $r^2 \geq 0.95$. **Figure 5.6** shows the regression analysis of the data set from Channel 1. From the slope data, J_{ss} is 21.6 L m^{-2} h^{-1}.

$$J_{ss} = slope \cdot \Delta P_{TM.ave} \tag{5.10}$$

The water flux line in **Figure 5.6** was estimated using Equation 5.11 and using the R_m value given in Table 5.1 for 0.22 μm PVDF membrane.

$$\frac{V_{\Delta x}}{A_m \Delta P_{TM}} = \frac{\Delta x}{\mu_P R_m} \tag{5.11}$$

For the Baker's yeast/BSA feed stream, **Figure 5.6** shows that the permeate flow almost instantaneously deviates from the water flux line (dashed line). This type of filtration behaviour is an indication that the resistance could be due to surface or pore adsorption building up at the onset of the filtration run in addition to the membrane resistance (Field et al., 1995). The cumulative permeate flow over time quickly slowed down. In general, steady state fluxes were achieved in less than thirty minutes in the crossflow microfiltration experiments in this work.

Table 5.3 Sample calculation for the microscale microfiltration data points plotted in Figure 5.6. Data is shown for the final three points in the figure as indicated. For each filtration time [A], the feed [*f*] and permeate [*p*] pressures were measured. The ΔP_{TM} [B] were then calculated. At each filtration time [A], the amount of permeate [E] is calculated by subtracting the weight of the receiver [C] from the measured weight of permeate+receiver [D]. The mass of permeate is converted to volume by dividing with the permeate density [G]. The correction factor [H] is applied to calculate the normalised permeate [J] to account for flow differences due to differences in temperature [F].

Filtration time (h) [A]	**Feed pressure (kPa)** [*f*]	**Permeate pressure (kPa)** [*p*]	**ΔP_{TM} (kPa)** $B = \frac{f + r}{p}$ [B]	**Permeate + receiver (g)** [D]	**Permeate (g)** $E = D - C$ [E]	**Permeate temperature (^{o}C) [F]**	**Correction factor** [H]	**Normalised permeate (L kPa^{-1} m^{2})** $J = \frac{\left(\frac{E}{G}\right) \cdot \left(\frac{H}{1000}\right)}{B \cdot I}$ [J]
0.169	5.3	19.6	22.2	95.6	17.1	19.5	1.138	**85**
0.335	5.3	19.7	22.3	99.6	21.1	19.8	1.130	**103**
0.502	5.2	19.7	22.3	102.8	24.3	20.4	1.114	**118**
	Retentate pressure [*r*]	---	Receiver (g) [C]	78.5	Permeate density,(g mL^{-1}) [G]	1.0	A_m, (m^2) [I]	0.001

5.4.4 Characterisation of the fluid dynamics in the membrane systems

As mentioned previously in Section 5.4.1, maintaining the same fluid dynamic conditions in different membrane systems is crucial to achieve consistent crossflow microfiltration performance across the scales. In this work, this was achieved by appropriately designing the geometry of the microscale CFF device to ensure that the axial pressure drop (ΔP_{axial}) and the wall shear rate (γ_{wall}) were similar to those typical of the larger scale Pellicon-2™ system. This section illustrates the establishment of the comparable fluid dynamics between the crossflow microfiltration devices at the two different scales.

The γ_{wall} obtained during a crossflow microfiltration experiment can be estimated using Equation 5.12.

$$\gamma_{wall} = \frac{1.5Q}{w \cdot \left(\frac{h}{2}\right)^2} \tag{5.12}$$

If the Hagen-Poiseuille equation for horizontal flow is used in Equation 5.12 for Q, Equation 5.8 is obtained. The effective channel height (h) can then be determined for each membrane system. In the Pellicon-2™ system, the effective channel height was calculated using Equation 5.13, derived from the momentum balance (Appendix 2.2) along the membrane module, under the assumptions of laminar flow, full rectangular channels and by taking into account the vertical upward direction of the flow.

$$h = \left[\frac{\mu_F \cdot Q \cdot L \cdot C}{\rho_F \cdot w \cdot \left(\frac{\Delta P_{axial}}{\rho_F} + g \cdot L \right)} \right]^{1/3} \tag{5.13}$$

In Equation 5.13, C is a constant, and is equal to 12 for Millipore devices (Technical document from Millipore Technical Support), Q is the feed volumetric flowrate, g is the

acceleration due to gravity, μ_F and ρ_F are the viscosity and density of the process fluid, respectively.

In the microscale CFF device the effective channel height can be determined by Equation 5.14, which takes into account the main horizontal flow direction in the device.

$$h = \left[\frac{\mu_F \cdot Q \cdot L \cdot C}{w \cdot \Delta P_{axial}} \right]^{1/3} \tag{5.14}$$

These equations were initially derived for single-phase flow in non-porous walls, and only represent a simplification of the complex multi-phase flow phenomena occurring in membrane processes in porous walls. Therefore, it is emphasized that Equations 5.13 and 5.14 can only be used to provide estimates of wall shear rate (γ_{wall}) and not actual values.

It is noteworthy that the Pellicon-2™ system was operated at crossflow rates less than or equal to 135 L h^{-1} which is within the range of recommended by the manufacturer (30 – 210 L h^{-1}). Actual flowrates depend on the feed properties such as cell concentration and viscosity. Typical crossflow flowrates for whole cell filtration are 30-70 L h^{-1} (Millipore data sheets). These recommended crossflow rates correspond to typical shear rates between 3000 - 10000 s^{-1} calculated according to Equations 5.12 and 5.13. Initial experiments with Baker's yeast suspension showed that experimental shear rates achieved were between 3900-9900 s^{-1}. During crossflow microfiltration of Baker's yeast in the Pellicon-2™, it was observed that neither the crossflow rate nor the ΔP_{TM} significantly changed the measured permeate flux. This is illustrated in **Figure 5.7**. Although in the lab-scale system the shear rate is coupled with the ΔP_{TM}, the corresponding increase in ΔP_{TM} for an increase in shear rate of 7000 s^{-1} is just 70 mbar. To further increase the ΔP_{TM}, the back pressure needs to be increased.

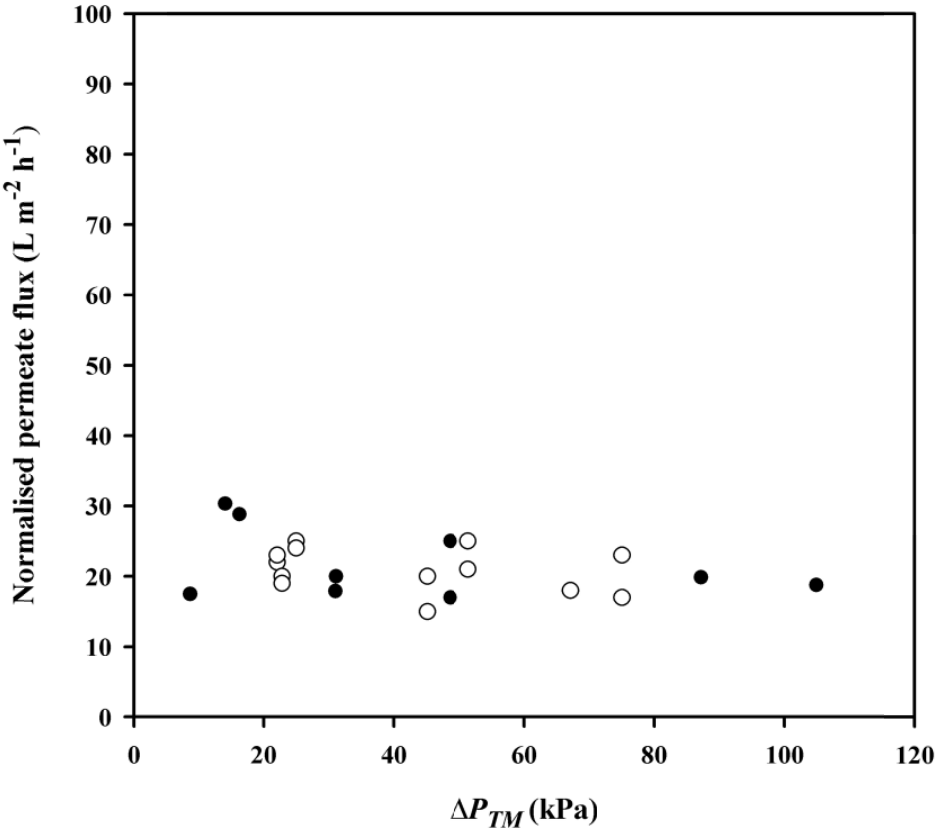

Figure 5.7 Effect of ΔP_{TM} during crossflow microfiltration (0.22 μm PVDF) of Baker's yeast with BSA in phosphate buffer. Large scale data points (●) were obtained with a Millipore Pellicon-2™ membrane module operated at crossflow rates recommended by the manufacturer (80-135 L h^{-1}). Microscale data points (○) were obtained from the two channels in the microscale CFF device which was operated at crossflow rates of 8 and 14 L h^{-1}. Maximum CoV for large scale and microscale data is 26% and 24% ($n \geq 2$). Experiments performed according to Section 2.6.2 and Section 2.7.2, respectively.

For the microscale CFF device, in order to have comparable process conditions with the larger scale system, it was important to also determine the range of crossflow rates that could provide similar shear rates at the small scale. The effect of crossflow rate using the microscale device was investigated for a range of transmembrane pressures and the results are presented in **Table 5.4.** γ_{wall} is 3000, 7000 and 13000 s^{-1} at crossflow rates 3, 8 and 14 L h^{-1}, respectively. These shear rates are similar to the range obtained in the Pellicon-2™ system. However, as **Table 5.4** indicates, the microscale device should be operated at crossflow rates larger than 3 L h^{-1} since only the faster crossflow rates (8 and 14 L h^{-1}) show a similar trend with the lab-scale system where there are no significant changes in the permeate flux across the range of ΔP_{TM} used. These data are plotted together with the lab-scale data in **Figure 5.7**.

Table 5.4 Effects of ΔP_{TM} and crossflow rate using the microscale CFF device (A_m = 0.001 m^2) on permeate flux during crossflow microfiltration (0.22 μm PVDF) of Baker's yeast with BSA in phosphate buffer.

Crossflow rate (L h^{-1})	**Nominal ΔP_{TM} (kPa)**	**J_{ss} (L m^{-2} h^{-1})**	**Coefficient of Variation**	**Variation between J_{ss} values**	**Variation between J_{ss} values**
3	20	7	9	Statistically different ($p<0.05$)	
3	40	18	21		
3	60	2	28		
8	20	21	9	Not statistically different ($p>0.05$)	Not statistically different ($p>0.05$)
8	50	18	20		
8	70	18	0		
14	20	24	3	Not statistically different ($p>0.05$)	
14	50	23	12		
14	70	20	21		

Section 5.4.2 established that the microscale device has ΔP_{axial} similar to that of the lab-scale module during water flux experiments. In this section, the examination of the fluid flow characteristics between the two crossflow microfiltration devices at different scales have shown that for actual microfiltration experiments using Baker's yeast/BSA, the microscale CFF device has to be operated at shear rates $\geq$ 7000 s^{-1} (corresponding to $\geq$ 8 L h^{-1}) to match the microfiltration performance of the lab-scale module. On this basis, the microscale CFF device is suggested to be operated at crossflow rates $\geq$ 8 L h^{-1} in order to confidently predict the microfiltration performance of the lab-scale module at the same ΔP_{TM}.

5.4.5 Scale comparison of the crossflow microfiltration of Baker's yeast

From the characterisation of the membrane systems in Section 5.4.4, comparison of filtration performance between the two systems can now be made on the basis of matched ΔP_{TM} and optimal range of operational shear rates for each of the membrane systems (i.e. for the Pellicon-2™ and microscale CFF device, shear rates of at least 3000 s^{-1} and 7000 s^{-1}, respectively). Microfiltration data using Baker's yeast and BSA obtained from experiments with matched operating conditions at the lab- and microscale will now be discussed in this section.

The crossflow microfiltration of Baker's yeast cells achieved a high degree of clarification, resulting in a solids rejection coefficient of one in all the experiments. As shown in Figure 5.7, data from the microscale CFF device are in good agreement with data obtained from the lab-scale membrane module. At both scales, ΔP_{TM} did not affect the normalised permeate flux values. The observed independence of the crossflow microfiltration performance of Baker's yeast on ΔP_{TM} is not in agreement with the commonly accepted notion of proportional flux increase with ΔP_{TM} (Bacchin et al., 2006). Previous studies have shown that flux increases with increasing transmembrane pressures and crossflow rates (and hence, crossflow velocity). However, most of the

studies were performed at low pressures, low feed concentration and high velocity (Cheryan, 1998; Bacchin et al., 2006). Any deviation from these conditions results in pressure-independent fluxes, even at quite low pressures (Cheryan, 1998). In this regard, it is important to note that the feedstocks used in this study is characterised by high cell concentrations (in this work, about 30 g L^{-1} dry cell weight, corresponding to 100 g L^{-1} wet weight) and by the presence of macromolecules (soluble BSA).

The measured fluxes also appear to be independent of crossflow rates at both scales. This observation could be explained by the module design where laminar flow conditions occur for both the larger-scale Pellicon-2™ system and the microscale CFF device. Laminar flow systems such as these are reported to not benefit by an increase of crossflow velocity as much as turbulent flow systems (Cheryan, 1998). This further suggests the resulting hydrodynamic conditions during crossflow microfiltration at these flow rates may not be significantly different in each device thus producing similar filtration performance.

Overall, the results obtained clearly indicate that the microscale CFF operation is a good mimic of the Pellicon-2™ system, as shown by the permeation flux results obtained for Baker's yeast. The flux data from the microscale is consistent with the data obtained from the larger scale module to within ± 10%. This is considered to be an adequate simulation of the flux data at larger scale considering that variation of manufactured membranes could result to 30% difference in filtration performance for small filters (Roush and Lu, 2008).

Note that the presence of screens in the Pellicon module was ignored in this work. Spacer screens were reported to improve fluxes in ultrafiltration (Da Costa et al., 1991). However, it was found that for microfiltration, the presence of flow barriers, such as the spacer screens, have no beneficial impact on steady state fluxes (Kromkamp et al.,

2005). This was also observed in the outcome of this work wherein the microscale device consistently produced similar microfiltration performance as the Pellicon-2™ even if the microscale CFF device had no screens. **Table 5.5** shows a summary of attributes of crossflow microfiltration modules for both scales.

Table 5.5 Summary of attributes of the Pellicon-2™ Mini crossflow filtration system (lab-scale) and the novel microscale crossflow filtration device.

Attributes	**Lab-scale**	**Microscale**
Turbulence promoters	Present (suspended screens)	None (open channel)
ΔP_{TMP} and ΔP_{axial}	Coupled	Not coupled
Pressure driving force	Positive (gauge)	Negative (gauge)
Membrane orientation	Vertical	Horizontal
Membrane area	A	0.01A
Channel width	B	0.007B
Nominal channel (path) length	C	0.9C
Nominal channel height	D	4D
Membrane resistance	E	0.1E
Process volume requirements	F	0.1F
Typical axial pressure drop (kPa)	$\leq$ 30	< 30
Shear rates (s^{-1})	3,000-10,000	4,000-10,000

5.5 Conclusions

In this chapter, the design (**Table 5.1** and **Figure 5.3**), characterisation (Sections 5.4.2 and 5.4.4) and testing of a novel microscale crossflow filtration device for the automated evaluation of the primary recovery of biological process feeds, in this case, a model feed of Baker's yeast in phosphate buffer has been demonstrated. An associated microscale crossflow filtration methodology was established for operation of this novel device on a Tecan™ robotic platform (**Table 5.3** and **Figure 5.6**). Preliminary evaluation showed a high level of consistency between the two channels of the device and reproducibility between filtration runs (**Table 5.2**). This has allowed parallel experimentation in investigating the microfiltration performance of the process feed. A comparison of the crossflow microfiltration performance at two scales illustrates that the device mimics the performance of the Pellicon-2™ membrane module in terms of hydrodynamics and transmembrane pressure (Section 5.4.4) and as a result achieved comparable steady state permeate flux values (**Figure 5.7**). This was achieved with a microscale device which has a 100-fold smaller membrane area and obtained a 10-fold reduction in process feed volumes. The next chapter will demonstrate the application of the microscale CFF device in investigating bioprocess options for the primary recovery of a complex biological feedstock *E. coli* Fab'.

A. Craig is acknowledged for the fabrication of the microscale CFF device that was designed in this work.

6. Microscale Technology Evaluation of the Impact of DNA Hydrolysis on Primary Recovery Operations‡

6.1 Introduction and aim

The design and development of a novel microscale crossflow filtration (CFF) device as well as the associated microscale methodologies were shown in Chapter 5. Initial evaluation of this device showed its capability to mimic the crossflow operation of a larger scale filtration module, specifically for the determination of steady state permeate flux of a model feed system (**Figure 5.7**). The creation of this device complemented the microscale dead-end filtration strategies established in Chapter 3 and their application in an automated manner demonstrated in Chapter 4. This final results chapter will now illustrate the application of the microscale CFF device to bioprocess development with a particular focus on the primary recovery by crossflow microfiltration of antibody Fab' fragments produced in *E. coli*.

6.1.1 Background microscale information

Microscale data in Chapters 3 and 4 have shown that dead-end microfiltration can provide high quality process stream of antibody Fab' fragments. The permeate has no detectable particulates and the data demonstrated that the filtration process has a certain level of selectivity towards Fab' fragments over other host cell proteins enabling primary purification (Section 4.3).

‡ Majority of the results presented in this chapter is to be submitted for publication as: Rayat, ACME et al. (2011). Impact of DNA Hydrolysis in the Primary Recovery of Antibody Fab' Fragments from an Industrial *E. coli* Strain.

However, fluxes achieved were very low (<10 L m^{-2} h^{-1}) even with the use of the best Fab' release method (thermo-chemical extraction). The flux of the homogenised sample is twice as small as the thermo-chemically extracted *E.coli* Fab' suspension (Section 4.3.1). A major reason for this is the large hydraulic resistance of the filter cake which formed during the dead-end microfiltration process.

The problem of cake formation can be avoided by running the filtration process in crossflow mode. In this regard, it is expected that crossflow microfiltration will provide improved fluxes due to reduced cake formation. It is also expected that CFF will handle higher cell concentrations of suspensions than dead-end microfiltration. Crossflow microfiltration is therefore employed in this chapter as an alternative to dead-end filtration and centrifugation as means for primary clarification and recovery of antibody Fab' fragments.

6.1.2 Selection of Fab' extraction method

Section 4.3.1 illustrated that the method of cell disruption influences the microfiltration performance of *E. coli* Fab' suspensions. In this chapter, the chosen cell disruption method is homogenisation for two reasons. Firstly, homogenisation is widely used as a cell disruption method at process scale, including in the isolation of antibody Fab' fragments (Balasundaram et al., 2009a; Spitali, 2009). Secondly, given the poor performance of the *E. coli* homogenate in dead-end filtration (Section 4.3.1), it is thought that the benefits of using CFF will be best demonstrated when using difficult-to-filter feedstocks such as the *E. coli* homogenate.

However, a known disadvantage of homogenisation as a cell disruption method is the concurrent release of chromosomal DNA along with the host organism's cellular proteins and the desired recombinant product. The release of chromosomal DNA during

this process results in an increase of the viscosity of the process stream; the higher viscosity consequently impacts the subsequent processing steps (Boynton et al., 1999).

6.1.3 DNA hydrolysis for process feedstock conditioning

Viscosity is an important rheological parameter which affects unit operations such as centrifugation and filtration (Perry and Green, 1997). In a study by Balasundaram and co-workers (2009b), it was shown that a more efficient centrifugation process may follow after a reduction in viscosity of the feed stream. In membrane filtration, reduction of viscosity of the feed stream affects the process in two ways. First, the reduced viscosity of the process stream across a filtration channel will result in a higher Reynolds number (Equation 5.4) leading to an increased turbulence of the process stream and also a higher wall shear rate (Equation 5.8). The result is a hydrodynamic situation wherein cell deposition could be limited, thus reducing cake formation leading to improved permeate flux. In addition, a reduced viscosity of the feed stream may result in the reduction of viscosity of the permeate stream, in which case the flow through the membrane is enhanced, thus also increasing the flux. As shown in Equation 1.4, the permeate flux is inversely proportional with permeate viscosity.

DNA hydrolysis has been suggested to alleviate the effect of increasing viscosity due to the release of chromosomal DNA during homogenisation. DNA digestion could serve as a feed pre-conditioning step for unit operations after homogenisation. Auto-hydrolysis of host DNA can be achieved by endogenous nucleases such as the co-expression of Staphylococcal nuclease (Boynton et al., 1999; Cooke et al., 2003; Balasundaram et al., 2009b) or by the addition of exogenous nucleases (e.g. Benzonase® nuclease) to hydrolyse chromosomal DNA (Lee et al., 2004). The degradation of these nucleic acids improved unit operations such as centrifugation (Balasundaram et al., 2009b) and crossflow microfiltration (Lee et al., 2004). Additionally, the benefit extends to the regulatory point of view as DNA hydrolysis

prevents the inclusion of heterologous genetic sequences in biopharmaceutical products, the presence of which could introduce undesirable immune responses (Cooke et al., 2003).

6.1.4 Aim and specific objectives

Given the aforementioned background, this chapter aims to demonstrate the utility of the novel microscale CFF device, described in Chapter 5, in informing bioprocessing options by predicting larger scale performance using an industrially relevant *E. coli* Fab' feedstock. In particular, the impact of DNA hydrolysis by using either exogenous (Benzonase®) or endogenous (Staphyloccocal) nucleases on crossflow microfiltration processes will be investigated. **Figure 6.1** illustrates the context of this study in the development of a bioprocess route for the primary recovery of antibody Fab' fragments.

Specifically, the objectives of this final chapter are to:

- investigate the impact of DNA hydrolysis on the characteristics of the bioprocess suspension (viscosity, Fab' content, purity);
- to investigate the impact of DNA hydrolysis on crossflow microfiltration performance criteria such as: the steady state permeate flux, Fab' product transmission and purity of the desired process stream;
- to use the information from the microscale CFF experiments in order to establish the best process condition for *E. coli* Fab' CFF; and
- to compare the large-scale primary recovery operations of CFF and centrifugation as bioprocess options.

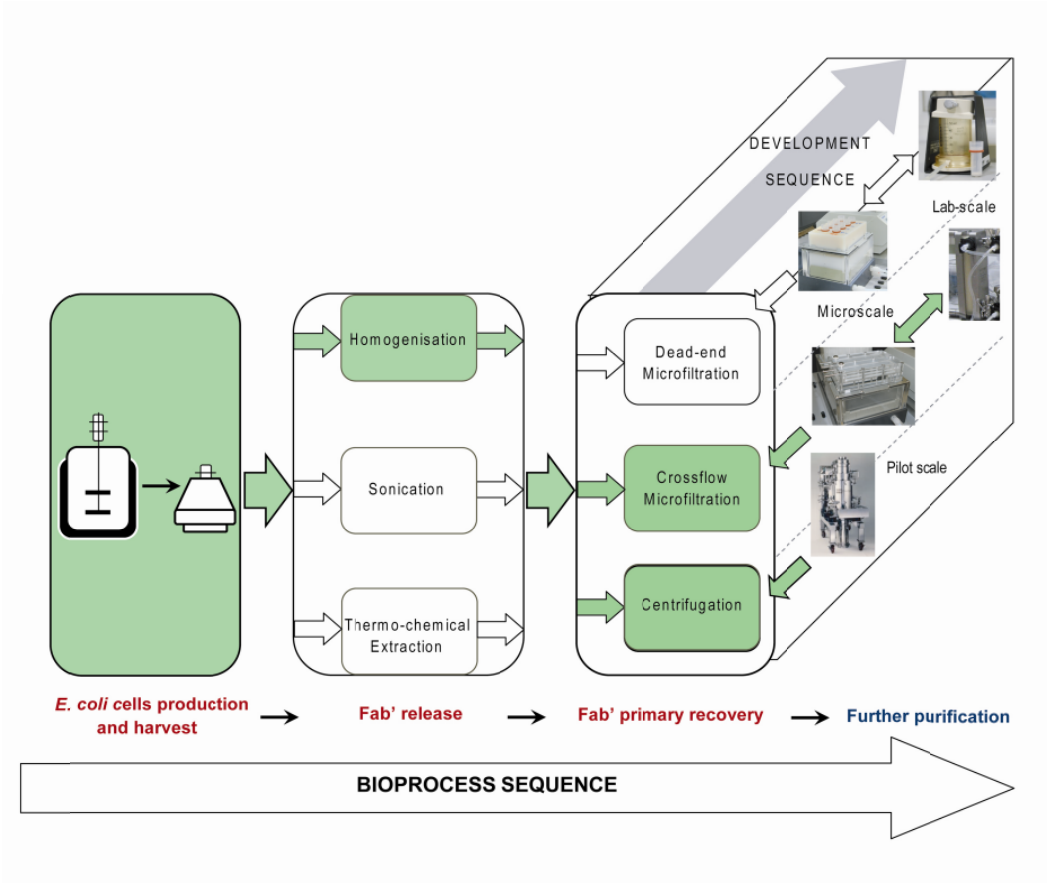

Figure 6.1 Application of microscale bioprocessing platform for membrane filtration for the investigation of different options for the primary recovery of antibody Fab' fragments. (Image credit: Pilot scale centrifuge from www.pneumaticscale.com)

6.2 Experimental approach

6.2.1 *E. coli* strains and fermentation

Two *E. coli* expression systems were used. One is the control strain (described in Section 2.1) which produces periplasmic antibody Fab' fragments only, hereafter referred to as Control. The other is a cell engineered *E. coli* strain which co-expresses Staphylococcal nuclease together with the Fab' fragments, hereafter referred to as SNase. These two strains undergo a series of processing steps as illustrated in **Figures 6.1** and **6.2**.

The plasmid construction and cell engineering of *E.coli* Fab' to co-produce Staphylococcal nuclease has been reported by Balasundaram and co-workers (2009a). An IncQ plasmid was used to express the protein Staphylococcal nuclease B (nucB) with the OmpA signal sequence added for secretion into the periplasm. In this way, the nuclease can only access the chromosomal DNA in the cytoplasm once cell disruption procedure has taken place (Balasundaram *et al.,* 2009b). Cell cultivation and harvest was the same for both strains and was performed according to Section 2.2.2 and 2.2.4, respectively. When cell pastes were used instead of freshly harvested broth, freeze-thawing procedures were performed according to Section 2.2.5.

6.2.2 Fab' extraction and DNA digestion

The Fab' fragments were extracted from the cells by high pressure homogenisation as described in Section 2.3.1 or Section 2.3.2. In this sudy, the extraction buffer used was 10 mM sodium phosphate at pH 7.0. After homogenisation, the cells were either used immediately for the Fab' recovery (Section 6.2.3) and analytic steps (Section 6.2.4) or routinely stored overnight at 4^{o}C until further use.

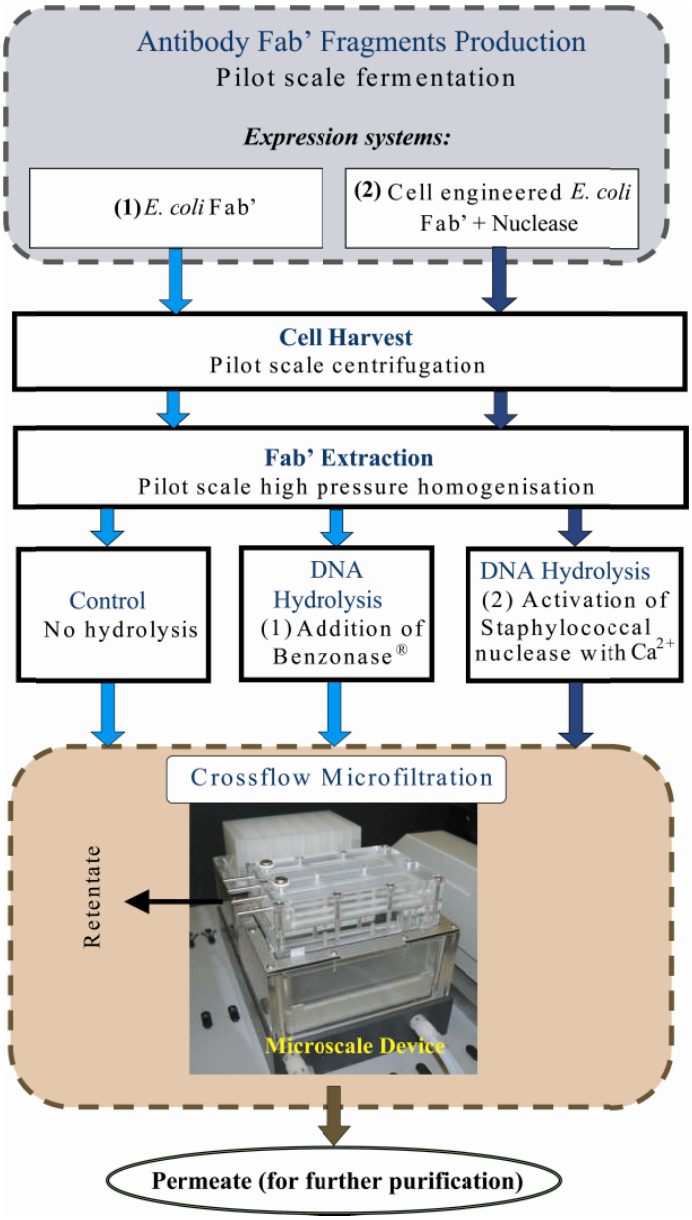

Figure 6.2 Bioprocesss flowsheet used in the study of crossflow microfiltration process as an option for primary recovery of antibody Fab' fragments in *E. coli*.

For the cell homogenates that are to be processed immediately, Benzonase® nuclease (Merck KGaA, Darmstadt, Germany) was added to some of the homogenates from the control strain (see **Figure 6.2**). Benzonase® nuclease ($\geq$ 90% (w/w) purity, 250 unit uL^{-1}) came in buffered glycerol solution containing 20 mM Tris HCl, pH 8.0, 2 mM $MgCl_2$, and 20 mM NaCl. The amount of Benzonase® added was varied up to a maximum of 17.5 μL Benzonase® per $mg_{DCW.}$ These samples are referred to as BNase. Alternatively, 10 mM $CaCl_2$ was added to the SNase homogenates. The cell homogenates (Control, BNase, and SNase) were incubated for two hours at room temperature and then used for Fab' recovery experiments. **Table 6.1** describes the various feedstocks prepared from these cell homogenates.

6.2.3 Fab' recovery

6.2.3.1 Microscale dead-end microfiltration

Microscale dead-end microfiltration experiments were performed, according to Section 3.3.3, using the custom filter plate described previously in Section 2.5.1. The type of membrane material used was Durapore poly(vinylidene fluoride) PVDF membranes (Millipore, Hertfordshire, UK) with pore size of 0.22 μm.

Table 6.1 Descriptions of the different bioprocess feedstocks used in this chapter.

Name	Description
Whole broth	*E. coli* cell suspension from fermentation harvest
Control	Homogenised *E. coli* (expressing periplasmic Fab only)
#X BNase e.g.10X BNase	Homogenised *E. coli* (expressing periplasmic Fab' only) plus10 times X Benzonase®. X= 0.5 μL Benzonase® per mg_{DCW}
SNase	Homogenised *E. coli* (expressing periplasmic Fab' and co-expressed Staphylococcal nuclease)
Fresh	Refers to cells or cell pastes which were freshly harvested from fermentation broth
Freeze-thawed	Refers to cells or cell pastes which were stored frozen in -20°C after fermentation harvest

6.2.3.2 Crossflow microfiltration

Laboratory scale crossflow microfiltration experiments were performed using a Millipore Proflux™ M12™ Tangential Filtration System (Section 2.6.1) and operated according to Section 2.6.2. Microscale crossflow microfiltration experiments were performed using the novel device previously described in Chapter 5. Microscale CFF was performed according to the methodology given in Section 5.4.3.

6.2.3.3 Pilot scale centrifugation

Fab' fragments were recovered from the supernatant of a centrifugation process using a pilot scale tubular bowl centrifuge (CARR™ P6™ Powerfuge System, Pneumatic Scale Corp., Clearwater, FL, USA). The process runs at a feed rate of 30 L h^{-1} at 15,000 RPM.

6.2.4 Characterisation of process streams

Before and after each Fab' recovery step (Section 6.2.3), samples were collected for total protein and Fab' quantification by spectrophotometry (Section 2.9.3) and HPLC (Section 2.9.4), respectively. Samples were also collected for DNA gel analysis (Section 2.9.7), DNA quantification by spectrophotometry (Section 2.9.8), and viscosity measurement (Section 2.10.2).

Statistical analysis was done using Microsoft Office Excel™ Analysis Toolpak™ (Anova: single factor) and where necessary, Design Expert 7 (Stat-Ease, MN, USA) was used to analyse multiple factor interactions.

6.3 Results and discussion

6.3.1 DNA hydrolysis in homogenised *E. coli* strains

6.3.1.1 Effect of nuclease digestion on DNA fragments

The hydrolytic action of Benzonase® nucleases or Staphylococcal nucleases on the DNA in homogenised *E. coli* cell suspensions is shown in **Figure 6.3**. The sizes of chromosomal DNA fragments in the Control are mostly between 250 to 2000 base pairs (bp) as indicated by the greater intensity of the gel bands within these DNA molecular weights. For the 35X BNase and SNase samples, theDNA sizes are less than 250 bp. The wells in each lane also appear to contain some DNA samples. The samples in the wells are assumed to be intact DNA with sizes much greater than 10 kbp. Boynton et al. (1999) have indicated the samples left in the wells of their DNA agarose gel are the undigested chromosomal DNA with sizes of 23 kbp.

The corresponding DNA concentrations by spectrophotometry are shown on top of each lane in **Figure 6.3**. The measured DNA concentrations are decreasing with respect to the amount of Benzonase® added. SNase has the smallest measured DNA content. It is expected, from material balance, that DNA quantification will show similar concentrations of DNA albeit with smaller fragments due to nuclease digestion of DNA in the samples. However, based on the quantification performed here, there seems to be a loss of DNA material as shown by the decreasing concentration of measured DNA.

One explanation of the apparent loss of DNA is that smaller fragments of DNA may not have been efficiently recovered during DNA analysis. It is thought that it is during the alcohol precipitation step that the smaller fragments of DNA are lost. Since this step is known to recover nucleic acids larger than 100 nucleotides (equivalent to 50 bp) (Strege and Lagu, 1991). Also, during this process, the smaller fragments could take a longer

time to precipitate. Note that the same incubation time was used in the precipitation step during DNA recovery from the samples (Section 2.9.6).

6.3.1.2 Effect of process shear on DNA fragments

To some extent, the number of homogenisation passes also affected the DNA fragment sizes. The DNA gel (not shown) of the control homogenate after the first pass shows a markedly denser smearing above 2000 bp, corresponding to larger DNA fragments, in comparison with the Control in **Figure 6.3** which went through 2-passes of homogenisation. This observation conforms to the widely known observation that genomic DNA degrades due to shear forces during processing.

6.3.1.3 Influence of cell age on DNA hydrolysis

The cell homogenates described above, except for SNase, are from freshly harvested material. In a research setting, it is not unusual to freeze cells for storage after fermentation harvest. For example, experiments in Chapters 3 and 4 used cell pastes which were previously frozen and stored at -20^{o}C. However, a freeze-thawing process could alter the physico-chemical properties of the cells which in turn could also impact process performance. In comparison with fresh Control homogenates, freeze-thawed Control homogenate samples have smaller fragments of DNA with the intensity of the DNA gel suggesting molecular weights between 250 and 1000 bp (Appendix 3.1 Lanes 2 and 3). In all cases, some traces of intact DNA can be seen in the wells of the DNA gel although it is obvious in the DNA gel using the freeze-thawed control samples (Appendix 3.1) that DNA digestion by Benzonase® treatment clearly reduces the amount of the DNA fragments; this is indicated by the observed reduction in intensity of the well as Benzonase® concentration increases.

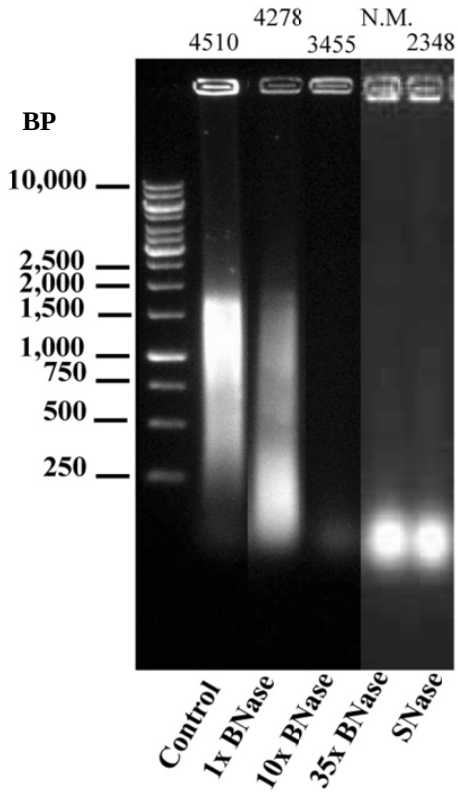

Figure 6.3 Agarose gel showing the hydrolysis of chromosomal DNAs in homogenised *E. coli* cells as described in Table 6.1. Fresh cells were used with wet cell concentration of 30% (w/w). Homogenisation performed according to Section 2.3.1. DNA hydrolysis according to Section 6.3.1. DNA sample preparation according to Section 2.9.6. Agarose gel electrophoresis performed according to Section 2.9.7. The number on top of each lane represents the quantified DNA concentration ($\mu g\ mL^{-1}$) by spectrophotometry (Section 2.9.8.). N.M. – not measured. BP – base pairs.

6.3.1.4 Influence of cell concentration on DNA hydrolysis

Compared to the above mentioned freeze-thawed Control homogenate which has 30% wet cell weight, a freeze-thawed Control homogenate with 15% wet cell weight has DNA fragments between 250 – 750 bp. No distinct differences can be seen between samples with or without treatment with Benzonase® at the lower cell concentration (Appendix 3.2).

6.3.2 Impact of DNA hydrolysis on viscosity of *E. coli* homogenates

6.3.2.1 Effect of nuclease digestion on viscosity

The purpose of performing DNA hydrolysis on the cell homogenates is to achieve a reduction of viscosity in the samples. **Figure 6.4** shows that there is a corresponding decrease in viscosity as DNA is progressively hydrolysed as indicated in **Figure 6.3**. Figure 6.4 also shows the viscosity of whole *E.coli* broth which is almost half the viscosity of the Control homogenate. This is a confirmation that the release of DNA in the Control homogenate is the cause of the rise in viscosity.

Each viscosity measurement presented in **Figure 6.4** is the slope of a plot of shear stress versus shear rate (see example in Appendix 3.3). This type of viscosity determination is acceptable since the samples exhibit the properties of a Newtonian fluid in the shear rates achieved in the unit operations used in this work. A Newtonian fluid is one having a linear relationship between the shear stress and the shear rate (Perry and Green, 1997). The constant of proportionality is the absolute viscosity of the fluid. Newtonian fluids have apparent viscosities which do not change with the shear rate. **Figure 6.5** confirms that in all samples, the apparent viscosity is constant at shear rates > 50 s^{-1}. Calculated shear rates under actual crossflow filtration conditions in this chapter exceeds 1000 s^{-1}.

6.3.2.2 Influence of cell age

Figure 6.4 also showed that freeze-thawed samples have lower viscosity than fresh samples. This corresponds to the smaller size of DNA fragments for the freeze-thawed cells shown in Section 6.3.1. However, the ratio of viscosities is the same between the Control and the BNase samples with lower Benzonase® concentration (< 30X) for both the fresh and freeze-thawed samples. This implies that further reduction of the viscosity of these samples is a result of freeze-thawing. The relative viscosity of the hydrolysed samples with respect to the viscosity of the Control appears to have a linear relationship with the concentration of Benzonase® as shown in **Figure 6.6**. In this plot, the relative viscosities of the freeze-thawed 30X BNase and SNase samples were calculated with respected to the fresh Control.

Freeze-thawing does not seem to have an effect on the viscosity of samples with the highest concentration of Benzonase as well as the sample with Staphylococcal nuclease. This is illustrated by the similar viscosities of fresh and freeze-thawed samples for 30X BNase and SNase. This may be due to these samples having an almost complete DNA hydrolysis, such that no further hydrolysis is caused by the freeze-thaw process. In practical terms, the linear relationship shown in **Figure 6.6** would be useful in extrapolating the extent of viscosity reductions for higher concentrations of Benzonase® in homogenised *E. coli* Fab' suspensions.

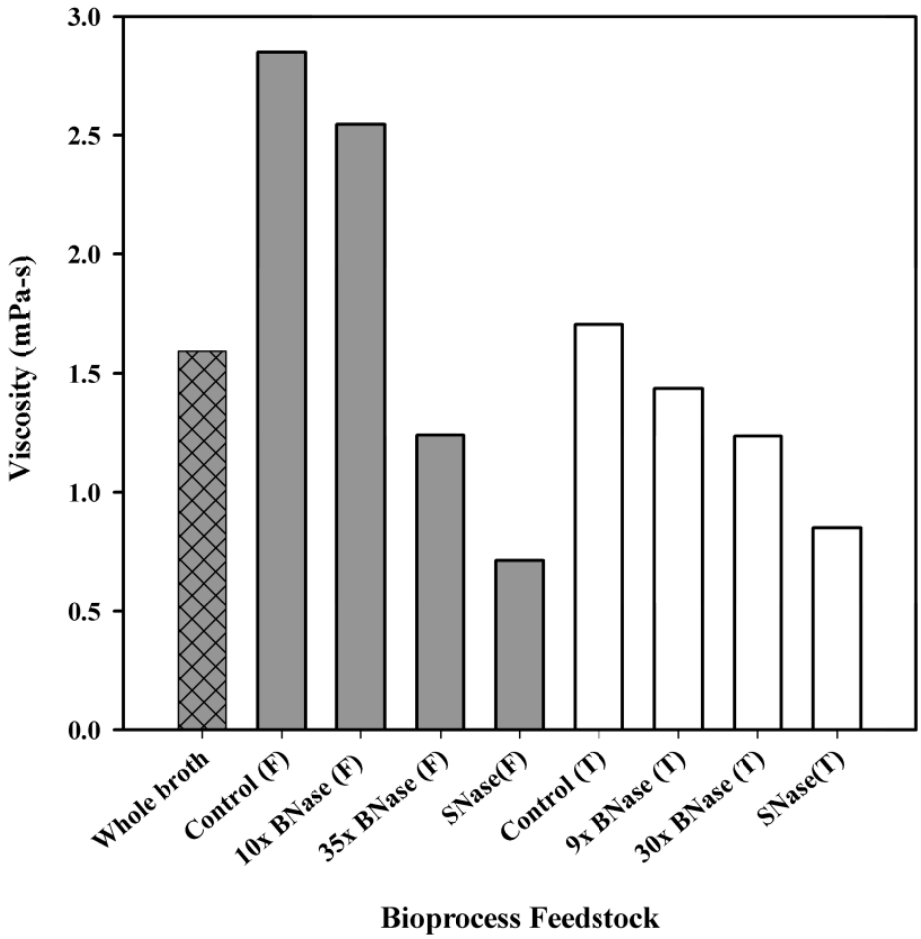

Figure 6.4 Absolute viscosity (μ_i) of *E. coli* feedstocks as defined in Table 6.1. (■, F): fresh harvest; (□, T): freeze-thawed cells; (☒) whole *E.coli* broth; Wet cell concentration is 30% (w/w). Homogenisation performed according to Section 2.3.2. DNA hydrolysis according to Section 6.2.2. Absolute viscosity was taken as the slope of the plot of shear stress against shear rate for each sample (e.g. Appendix 3.3). Rheological properties were measured according to Section 2.10.1.SNase (F) data was taken from Balasundaram et al. (2009b).

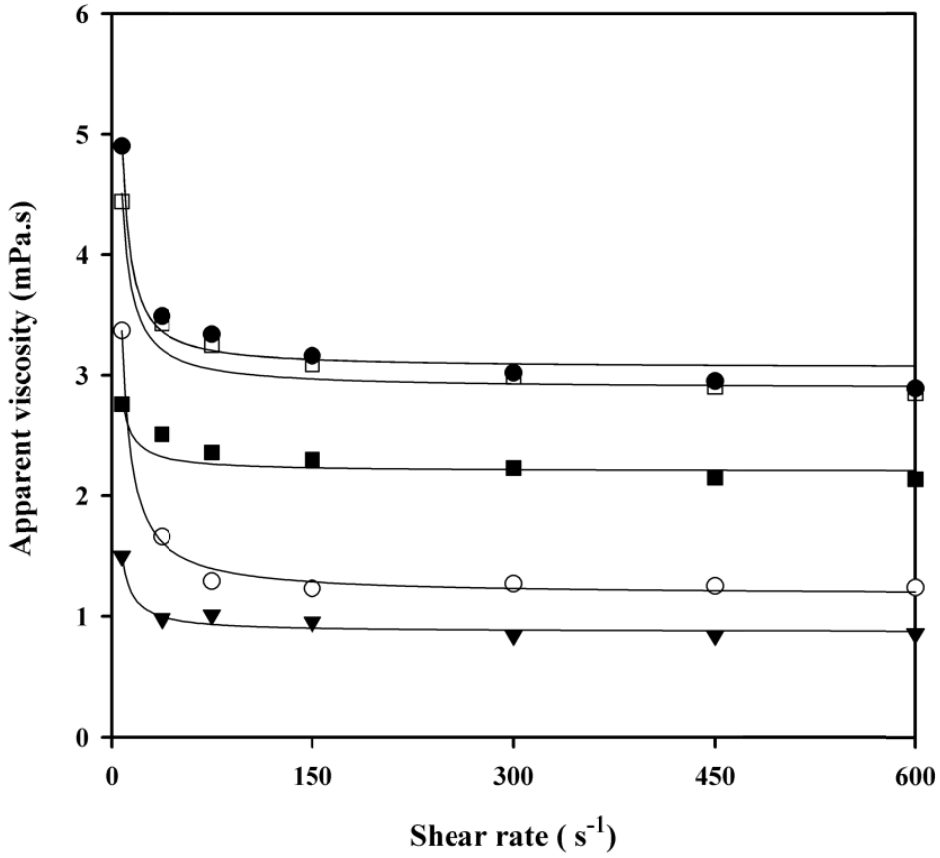

Figure 6.5 Rheological properties and apparent viscosity of selected homogenised *E. coli* process feedstocks. Feedstocks as described in Table 6.1. (●) Control; (□) 1X BNase; (■) 10X BNase; (○) 35X BNase; (▼) SNase. Coefficient of variation for apparent viscosity measurements is 14%. Wet cell concentration is 30% (w/w). Homogenisation performed according to Section 2.3.2. DNA hydrolysis according to Section 6.2.2. Rheological properties were measured according to Section 2.10.2.

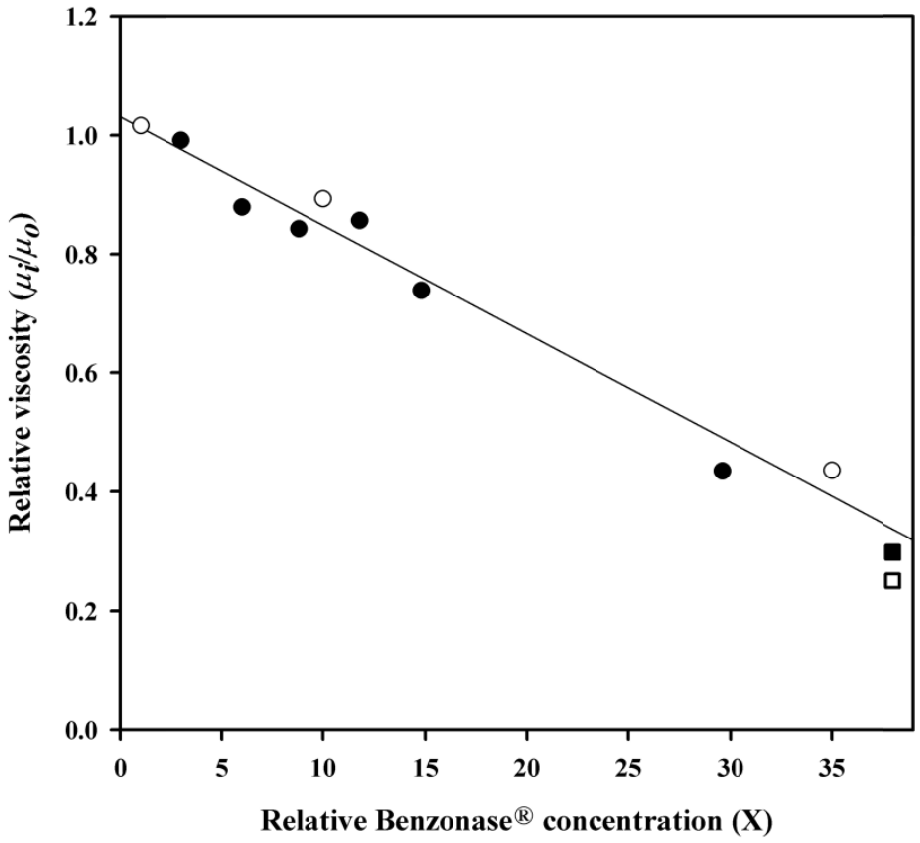

Figure 6.6 Ratio of absolute viscosity (μ_i) of *E. coli* feedstocks to the absolute viscosity (μ_o) of the Control. μ_o is 2.85 mPa.s (fresh); μ_o is 1.70 mPa.s (freeze-thawed); (○,●) BNase. Relative concentration is a factor of X = 0.5 μL Benzonase® per mg_{DCW}; (■,□) SNase. Feedstocks as described in Table 6.1. Open symbols are fresh samples, filled symbols are freeze-thawed. Wet cell concentration is 30% (w/w). Homogenisation performed according to Section 2.3.2. DNA hydrolysis according to Section 6.2.2. Absolute viscosity is taken as the slope of the plot of shear stress vs. shear rate for each sample (e.g. Appendix X). Rheological properties were measured according to Section 2.10.2. SNase (F) data is taken from Balasundaram et al. (2009b).

6.3.2.3 Influence of cell concentration

The effect of cell concentration on the viscosity of homogenised *E. coli* cells is shown in Table 6.2. The table shows that a higher cell concentration (in this case, 50% increase) also increases the suspension viscosity. Moreover, there seems to be little effect of DNA hydrolysis on viscosity at the lower cell concentration since the suspension viscosities are within a small range of 0.92-1.07 mPa.s, similar to the viscosity of water at ambient temperature. At the higher cell concentration, the effect of DNA hydrolysis is more pronounced. The differences in viscosities between these two cell concentrations are much less than for the cell homogenates with larger concentrations of Benzonase® which suggests that DNA digestion at the higher concentrations of Benzonase® is efficiently reducing the viscosity of the samples.

Table 6.2 Effect of a two-fold increase in cell concentration on viscosity of homogenised *E. coli* from freeze-thawed cell paste. Experiments performed according to Section 2.10.2. Feedstocks as described in Table 6.1.

Feedstock	**$\mu_{15\%}$ (mPa.s)**	**% Difference**
Control	1.07	60
3X BNase	0.96	76
6X BNase	0.94	59
9X BNase	0.92	56
12X BNase	1.02	43
15X BNase	0.92	37
30X BNase	0.93	33

$\%\text{Difference} = \frac{\mu_{30\%} - \mu_{15\%}}{\mu_{15\%}} \cdot 100$;

($\mu_{15\%}$ is absolute viscosity at 15% wet weight (w/w or 45 g_{DCW} L^{-1})

6.3.3 Impact of DNA hydrolysis on Fab' and protein release

6.3.3.1 Influence of DNA digestion on Fab' release

It is important that the addition of exogenous Benzonase® nucleases should not affect the extracted Fab'. Analysis of the Fab' content of disrupted *E. coli* suspensions (30% wet cell weight) which were freshly harvested from fermentation and immediately followed by homogenisation show that the addition of Benzonase® does not affect the Fab' content. On average, Fab' content is 986 ± 64 μg mL^{-1} for the Control and BNase samples.

6.3.3.2 Influence of cell age on Fab' release

Benzonase® addition also did not affect the Fab' content of the homogenised suspensions from freeze-thawed cell paste having 15% wet cell weight. However, the Fab' content from these samples, which are on average 915 ± 73 μg mL^{-1}, is much higher than the expected Fab' content of about 500 μg mL^{-1} (based on the amount of Fab' from the sample above with 30% wet cell weight). In a separate study using freeze-thawed samples containing 45% wet cell weight, the corresponding Fab' content is 2800 μg mL^{-1} (unpublished data, Bangaru Balasundaram, UCL). These two freeze-thawed samples have about 21 mg g_{DCW}^{-1} of Fab' content while the homogenised samples from fresh cells have a Fab' content of only about 11 mg g_{DCW}^{-1}.

At first glance, it appears that the freeze-thaw process caused an increase in Fab' content. However, considering that homogenisation is a very efficient method for disrupting the cells it is logically expected that the method will be efficient in releasing the periplasmic antibody Fab' fragments. Besides, the freeze-thawing process occurred before cell disruption and so its physical effects should only be minimal. The difference in Fab' content is therefore attributed to the difference in "available" Fab' in the

solution, unbound from the cell debris. Antibody Fab' fragments could have interacted with the cell debris causing some of the Fab' fragments to be left bound to the debris and therefore not recovered in the clarified liquid during solid-liquid separation. This has also been observed during the recovery of Fab' by centrifugation. Bowering (2004) reported that Fab' fragments preferentially partition to the heavy phase, incurring losses to the supernatant. The cells which were freeze-thawed will have different cell surface properties than the fresh cells. From the obtained result, it appears that the acquired surface properties of the freeze-thawed cells caused the diminished Fab'-cell debris interaction, leaving more Fab' available in solution for primary recovery. This result, together with the lower viscosity found in Section 6.3.2.2, gives freeze-thawing an advantage over the use of freshly harvested cells. This benefit of the freeze-thaw process, specifically in increasing the product yield, has been exploited in the manufacture of recombinant antibodies (Sehdev and Spitali, 2006).

6.3.3.3 Total protein content of **E. coli** *homogenates*

The total soluble protein content of the homogenised samples represents the level of host cell protein (HCP) contaminants in the *E. coli* Fab' suspensions. Analysis of the HCP levels (data not shown) demonstrated that the Control homogenates have significantly larger total protein content (18% larger) compared with BNase samples. Control homogenates from freeze-thawed cells have lower measured total soluble protein content (300 mg g_{DCW}^{-1}) compared to the Control homogenates from freshly harvested cells (491 mg g_{DCW}^{-1}). The freeze-thawing process has been reported to cause damage in some proteins, particularly for long periods of frozen storage (> 24h), which resulted in a decrease in measured protein content (Bakir and Hamamci, 1997).

6.3.3.4 Fab' and HCP content of E. coli *with co-expressed Staphylococcal nuclease*

It is important to mention that the Fab' content from the cell engineered *E. coli* strain used in this study (freeze-thawed SNase) is about 80 μg mL^{-1} (wet cell weight of 30%). This corresponds to a Fab' content of 0.9 mg g_{DCW}^{-1} or 23 times smaller than the Fab' content of the Control homogenates from freeze-thawed cells. It is 12 times smaller than the Fab' content of the Control homogenates from fresh cells. Fresh SNase has a Fab' content of 40 μg mL^{-1} (Balasundaram et al., 2009b). The total protein content of the cell engineered strain (SNase) is similar to the Control with less than 4% difference.

If the cell engineered strain is to be used for large-scale production of antibody Fab' fragments, the Fab' yield would need to be improved. The freeze-thawing process has already resulted in a two-fold increase in Fab' for the SNase sample. The improvement in Fab' yield for the SNase sample is important yet it is not the main focus of this work. Furthermore, Section 6.3.2 demonstrated that freeze-thawed SNase homogenates have similar rheological properties as fresh SNase. Therefore, the freeze-thawed SNase homogenates will continue to be used in the subsequent Fab' recovery operations demonstrated in the next sections.

6.3.4 Comparison of microscale and large scale CFF performance

In this section, a comparison is made between the microscale and larger scale crossflow microfiltration performance using the Control and the SNase homogenates. The performance criteria used in assessing the scale comparison are the permeate flux, Fab' transmission and total soluble protein transmission. Results are shown in **Figure 6.7** with scale translation based on a matched ΔP_{TM} at 22 kPa and on matched shear rates. The figure clearly shows that the microscale device mimics the performance of the larger scale module. Percent differences between microscale and large scale values

were up to ± 25% for the permeate flux, up to ± 7% for Fab' transmission, and up to ± 11% for protein transmission. These differences are considered acceptable considering that membrane differences, particularly evident at microscale, can reach up to 30% due to lot-to-lot variation (Section 3.3.1).

Having established confidence in the capability of the microscale CFF device to mimic larger scale performance, the following section will present the results of the microscale evaluation of the impact of DNA hydrolysis on the crossflow microfiltration performance of homogenised *E. coli* cells. Based on the results shown in Sections 6.3.1-6.3.3, only homogenates from fresh cells (apart from SNase) were used for the subsequent microscale CFF study. In particular, only the Control, 1X and 10X BNase samples were used. The 35X BNase was not further used since it is assumed that it will provide similar process behaviour as the SNase given the similar DNA profiles and viscosities of these two feedstocks as illustrated in **Figure 6.3** and **Figure 6.6**.

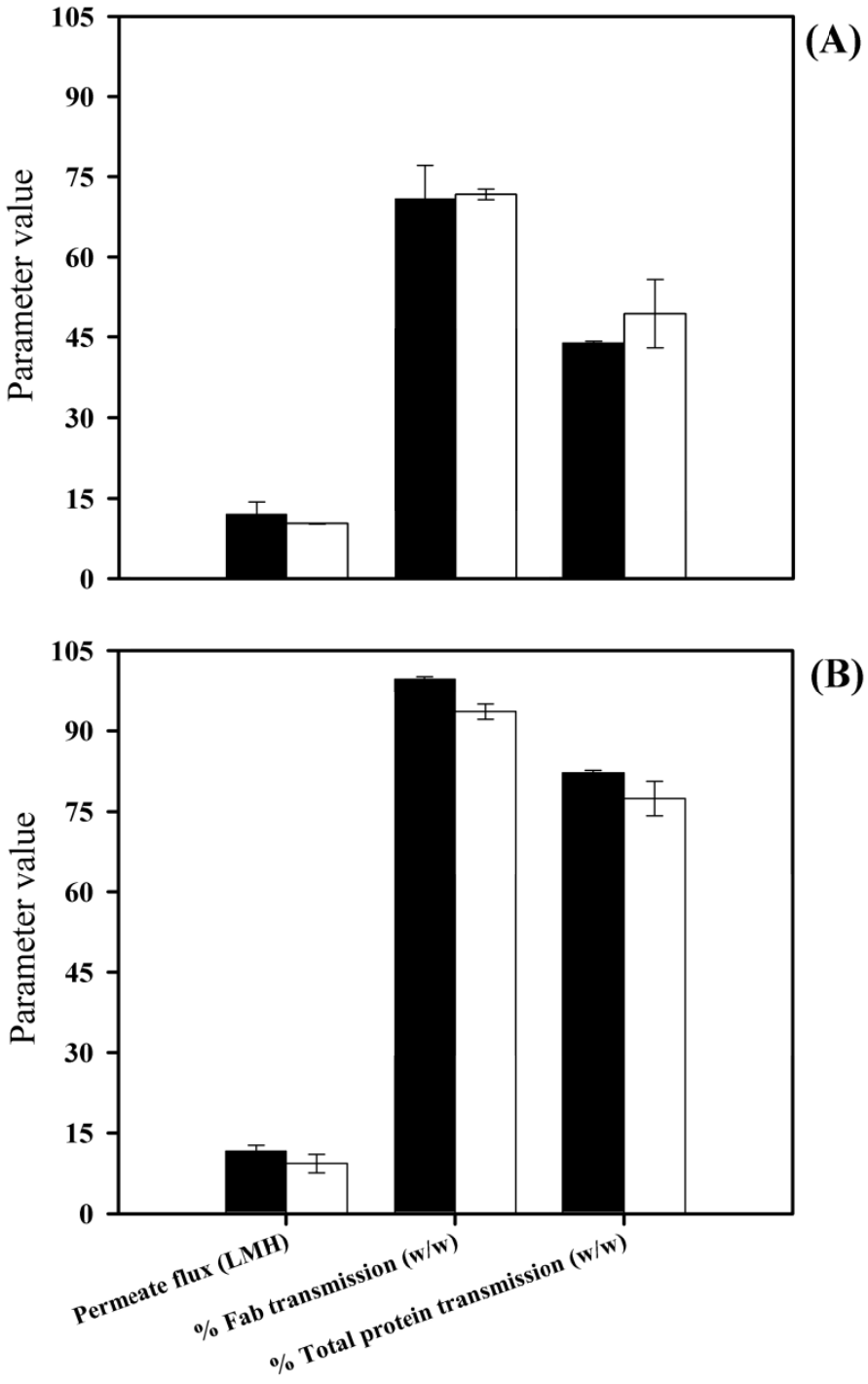

Figure 6.7 Comparison of crossflow microfiltration performance of *E. coli* Fab feedstocks using the lab-scale Pellicon 2 Mini - Millipore TFF System (■) and the novel microscale CFF device described in Section 5.4.1 (□). Feedstocks are: (A) Control; and (B) SNase, as described in Table 6.1. Homogenisation performed according to Section 2.3.1. DNA hydrolysis performed according to Section 6.2.2. ΔP_{TM} is 22 kPa. Crossflow velocities are 80 and 14 L h^{-1} for the lab-scale and microscale systems, respectively. Membrane used is 0.22 μm PVDF. Large-scale CFF operation was performed according to Section 2.6.2 and microscale CFF operation according to Section 5.4.3.

6.3.5 Microscale CFF study of *E. coli* homogenates: flux behaviour

Filtration studies are performed by operating under constant transmembrane pressure (ΔP_{TM}) when data is required for scaling-up filtration processes (Bacchin et al., 2006). The steady state flux which could be measured at constant ΔP_{TM} conditions provides the membrane area requirement to run a process. The size of the membrane area impacts on the economics of the filtration process (Shukla and Kandula, 2009).

6.3.5.1 Impact of DNA hydrolysis on flux

The steady state permeate fluxes of the different homogenised feeds are presented in **Figure 6.8**. Compared to the flux (< 5 L m^{-2} h^{-1}) obtained during dead-end microfiltration of a similar *E. coli* homogenate (Section 4.3.1.), the fluxes obtained during crossflow microfiltration are greater than 10 L m^{-2} h^{-1}. Higher fluxes were achieved even if the cell concentration used during CFF is almost 3-fold larger than the one used during dead-end microfiltration.

It can also be observed from **Figure 6.8** that the fluxes are similar for all *E. coli* homogenates. This result was unexpected since **Figure 6.4** clearly shows that samples with hydrolysed DNA by Benzonase® addition or Staphylococcal nuclease co-expression have smaller viscosities compared with the Control. The differences in process stream viscosities were expected to result in some benefit on permeate fluxes for the hydrolysed feeds where samples with the lower viscosity were expected to have higher fluxes due to the expected increase in shear rate based on Equation 5.12. However, a close inspection of the calculated shear rates shows that this is not the case.

The calculated shear rates during microfiltration of the homogenised feeds were very similar. The calculated Reynolds number also indicate laminar flow regime for all the process feeds used while the actual measured pressure drops along the membrane path length were also similar for the feedstocks used (ΔP_{axial} ~ 10 kPa). ΔP_{axial} indicates fluid

velocity within the channels in the microscale CFF device and similar ΔP_{axial} meant similar fluid velocities of the samples. These flow indicators (shear rate, Reynolds numbers, ΔP_{axial}) establish that similar hydrodynamic conditions were achieved during the crossflow microfiltration of the different homogenised *E. coli* samples and could explain the similarity of the permeate fluxes which were achieved during microscale CFF. The results confirm the reported limitations of flat sheet membrane systems in manipulating permeate fluxes in terms of fluid hydrodynamics (Cheryan, 1998). As mentioned in Section 5.4.5 these types of membrane system generally operate in the laminar region where increased fluid velocity do not represent a corresponding increase in permeate flux, particularly at higher cell concentrations.

In their study, Lee et al. (2004) have reported the improved microfiltration (with buffer exchange) efficiency of inclusion body (IB) extracts with the addition of Benzonase®. The crossflow microfiltration device used was a ceramic monotube, with pulsed backwashing employed throughout the diafiltration process. However, in their study, the hydrolysis was achieved after 12-14 h of incubation in Benzonase® which resulted in DNA fragments sizes of ~ 500 bp only (compared to the 2 h incubation used here, with DNA fragments < 2000 bp in the presence of intact chromosomal DNAs, **Figure 6.3**). Thus, the flux improvement in the work of Lee and co-workers (2004) cannot be attributed alone to the use of Benzonase®.

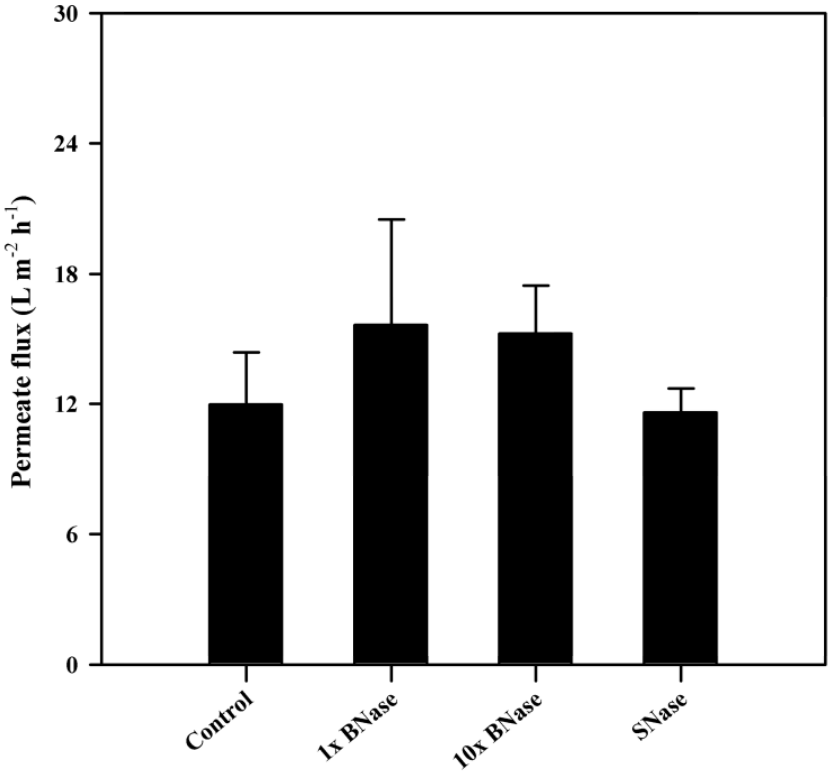

Figure 6.8 Steady state permeate fluxes during microscale crossflow microfiltration of *E. coli* Fab' homogenates. Bioprocess feedstocks as defined in Table 6.1. Error bars indicate one standard deviation about the mean (n=2). Homogenisation performed according to Section 2.3.1. DNA hydrolysis according to Section 6.2.2. Microscale CFF operation according to Section 5.4.3. Crossflow rate at 14 L h^{-1}, ΔP_{TM} = 22 kPa and A_m is 0.001 m^2.Membrane used is 0.22 μm PVDF.

6.3.5.2 Impact of transmembrane pressure on flux

The transmembrane pressure (ΔP_{TM}) maintained during the crossflow microfiltration experiments in Section 6.3.5.1 was 22 kPa. When the ΔP_{TM} was increased to 70 kPa, the permeate fluxes of each of the homogenised samples did not significantly change from the fluxes obtained at the lower ΔP_{TM}. This is similar to the behaviour of a high cell density Baker's yeast suspension illustrated in Chapter 5 which was explained as due to the high concentrations used (30 g_{DCW} L^{-1} and 90 g_{DCW} L^{-1}, respectively for Baker's yeast used in Chapter 5 and *E. coli* suspensions used in this chapter). At high concentrations, operating conditions such as ΔP_{TM} and velocity do not significantly affect the steady state flux (Cheryan, 1998). The same was also shown in the seminal study by Patel (1987) in which the pressure-independence behaviour was attributed to concentration polarization effects as well as the low turbulence achieved by the filtration module.

Equation 6.1 shows a hydrodynamic model developed by Schulz and Ripperger (1989) which relates the back-transport behaviour with equation of cake filtration theory in Equation 1.11. One basis of the model is the mass balance of the retained material (cake) on the membrane. The model assumes the hydraulic resistances of most cakes are larger than the membrane resistance thus making R_m negligible, and that the rate of back-transport from the membrane to the bulk stream is proportional to the velocity gradient on the membrane and also to the layer thickness. It was shown in Section 3.3.6 that the hydraulic resistance of biological filter cakes, including filter cakes of *E. coli* Fab', are significantly larger than published membrane resistances, thus the model is applicable in this case.

$$J_{ss} = \sqrt{\frac{K_1 \cdot \Delta P_{TM} \cdot (\rho_c - c_B) v}{\mu_P \cdot \alpha \cdot D_H \cdot c_B}} \tag{6.1}$$

Equation 6.1 is specifically applied to the steady state case and laminar flow. In this equation, J_{ss} is the steady state flux, K_1 is the constant of proportionality for laminar flow, ΔP_{TM} is the transmembrane pressure, ρ_c is the density of the cake layer, c_B is the concentration in the bulk stream, v is the crossflow velocity, μ_P is the viscosity of the permeate, α is the specific cake resistance, D_H is the hydraulic diameter. As shown in Equation 6.1, J_{ss} is not proportional to ΔP_{TM} or v but rather it is proportional to $\Delta P_{TM}^{0.5}$ and $v^{0.5}$.

From Equation 6.1 it can be illustrated that for a 2-fold increase in permeate flux, at least a 4-fold increase in transmembrane pressure is required. Considering that *E. coli* cells are compressible, including *E. coli* homogenates as shown in Section 4.3.3.2., it is expected that α will correspondingly increase with ΔP_{TM}. Given the opposing effects of ΔP_{TM} and α, it is therefore not expected to significantly increase with ΔP_{TM}.

Analysis of the transient flux data (e.g. that of the SNase sample in Appendix 3.4 and also **Figure 5.5** for Baker's yeast) show how the fluxes of these relatively high cell density feeds immediately deviate from the expected water flux behaviour at the beginning of the filtration run. These could mean that membrane adsorption (surface or pore) takes place quickly since the start of the filtration process and resulted in an immediate drop in permeation fluxes compared to the expected clean membrane water flux. The same filtration behaviour can be observed with data from the microscale device (e.g. SNase sample in Appendix 3.5 and Baker's yeast in **Figure 5.6**) where it can be observed, even by visual observation of the slope of the line, that the rate at which the permeate passed through the membrane rapidly reached a constant value which is away from the water flux line (dashed lines). The results, together with the observed pressure-independent behaviour, suggest that when using complex feedstocks such as the ones used in this work, surface or pore adsorption as well as concentration

polarisation may be dominating the microfiltration process. This is not an unreasonable deduction given that the concentration of macromolecules and of colloidal particles in these complex process feeds could be high enough to result in this phenomenon. It is important to note that the experiments conducted do not provide information on irreversible fouling, which, if present, would further corroborate the observed pressure-independent behaviour of the permeate flux.

6.3.6 Microscale CFF study of *E. coli* homogenates: Fab' recovery

Aside from permeate flux, another key microfiltration performance criteria is the recovery of the desired product in the process stream of interest. In this case, the key process stream is the permeate and the key performance indicator is the Fab' transmission which is related to Fab' recovery.

6.3.6.1 Impact of DNA hydrolysis on Fab' transmission

Figure 6.9 illustrates the behaviour of Fab' transmission as a function of Benzonase® content or presence of Staphylococcal nuclease in the homogenised *E. coli* cell suspensions. Statistical analysis indicates that the DNA hydrolysis, either by Benzonase® treatment or co-expression of Staphylococcal nuclease, has a significant effect on Fab' transmission ($p < 0.05$). In the case of the SNase, **Figure 6.9** shows that SNase has better Fab' transmission than the Control. On the other hand, the BNase feeds have demonstrated lower Fab' transmission. The differences in transmission behaviour of the feedstocks with and without Benzonase® could be due to the Benzonase® treatment further enhancing the Fab'-cell debris interaction.

As shown in **Figure 6.9**, the transmission of Fab' using the control sample is around 70%. As a soluble product, it was expected that Fab' will not be rejected during microfiltration and should be mostly, if not fully, recovered in the permeate. Since this is not the case, one explanation would be that Fab' fragments interact with the cell

debris. This was already observed in the results shown in Section 4 during microfiltration and was implied in Section 6.3.3.2 when freeze-thawed cells of the same concentration showed a higher measured Fab' concentration than freshly harvested cells. During CFF, some of the Fab' fragments, which were otherwise in solution, could have adsorbed onto the cell debris particles which formed a cake during the crossflow microfiltration process. It appears that this could have happened when using the Control as shown by the low Fab' transmission (~70%). The addition of Benzonase® seems to have exacerbated this Fab'-cell debris interaction as indicated by the decreased Fab' transmission (< 70%) compared to the Control.

On the other hand, the SNase feedstocks appears to have none of this interaction since Fab' transmission was almost 100%. Note that the SNase feedstocks have relative lower Fab' content than the control feedstocks (as shown in Section 6.3.3). If there was Fab'-cell debris interaction, the loss of (transmitted) Fab' in the permeate will be more pronounced. However, this was not observed. It is therefore assumed that even if the Fab' content has been optimised to match the Fab' content of the control samples, the transmission of Fab' in the SNase will still be better than Control.

6.3.6.2 Impact of transmembrane pressure on Fab' transmission

Increasing the transmembrane pressure (ΔP_{TM}) from 22 kPa to 75 kPa did not significantly change the Fab' transmission in the different feedstocks ($p > 0.05$). This confirms the deductions made on the observed permeate flux and on Fab' transmission. Given that concentration polarization of particulate debris was recognised as a reason for the pressure-independent flux behaviour demonstrated in Section 6.3.5, and that Fab'-cell debris interaction was the cause of transmission performance illustrated in Section 6.3.6.1, it follows that Fab' transmission is also pressure-independent.

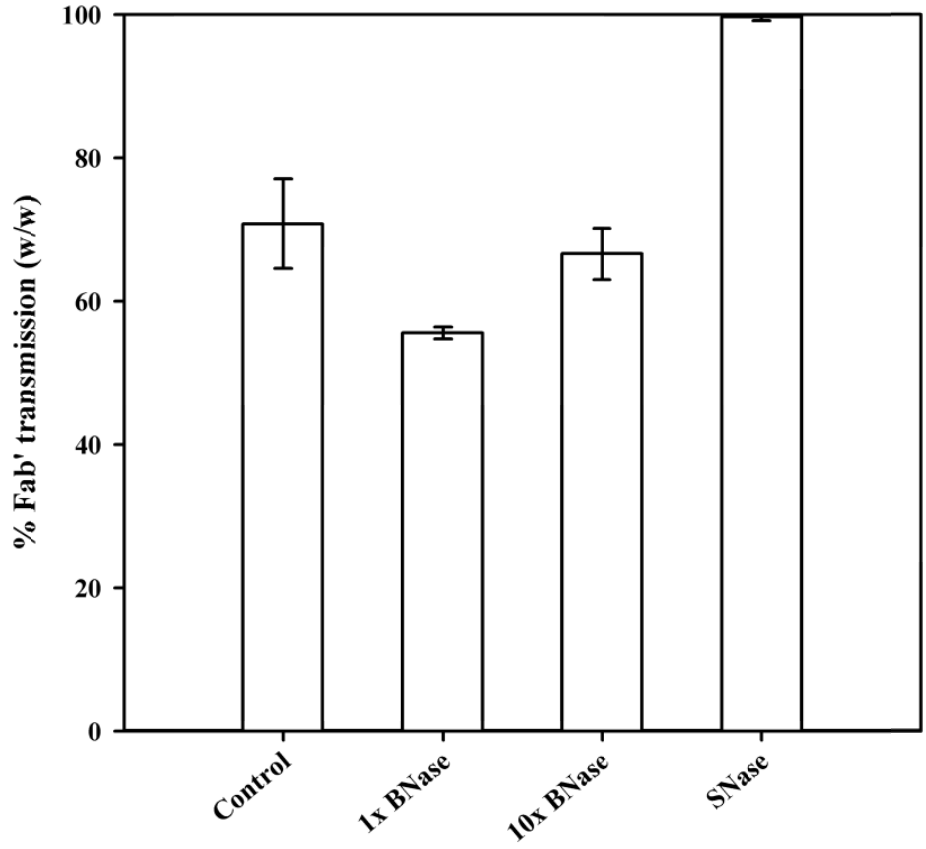

Figure 6.9 Fab' transmission levels obtained during microscale crossflow microfiltration of *E. coli* Fab' homogenates. Bioprocess feedstocks as defined in Table 6.1. Error bars indicate one standard deviation about the mean (n=2). Homogenisation performed according to Section 2.3.1. DNA hydrolysis according to Section 6.2.2. Microscale CFF operation according to Section 5.4.3. Crossflow rate at 14 L h^{-1}, ΔP_{TM} = 22 kPa and A_m is 0.001 m^2.Membrane used is 0.22 μm PVDF. Fab' quantification according to Section 2.9.4.

6.3.7 Microscale CFF study of *E. coli* homogenates: total protein recovery

The total protein recovery in the permeate stream is another important microfiltration performance indicator. Taken together with Fab' transmission, total protein recovery indicates the selectivity of the crossflow microfiltration process. **Figure 6.10** presents the total soluble protein transmission for all feed samples for the two ΔP_{TM} conditions used. Analysis of the data in this figure demonstrates a small positive correlation of protein transmission with Benzonase® treatment under the two ΔP_{TM} conditions.

However, the SNase feedstock demonstrated a different CFF behaviour in terms of protein recovery. At the lower ΔP_{TM}, a higher protein transmission is observed; while at the higher ΔP_{TM}, the protein transmission of the Control is not significantly different than the protein transmission of the SNase feed ($p > 0.05$).

It is clear from **Figure 6.10** that, notwithstanding the impact of DNA hydrolysis, an increase in ΔP_{TM} results in a decrease in total protein transmission. The importance of a low recovery of total soluble protein has already been described in Chapter 4. Specifically, the removal of host cell proteins (HCP) in the overall Fab' recovery is essential since these proteins could precipitate under the conditions used in chromatographic separation and purification of the Fab' fragments (Spitalli, 2009). In protein A chromatography, HCP were found to cause precipitation, with the precipitates being a risk to the in-process sterile filters or reduce resin lifetime (Vunuum et al., 2009). Therefore, the removal of HCP during the early primary recovery steps is valuable for the whole bioprocess sequence.

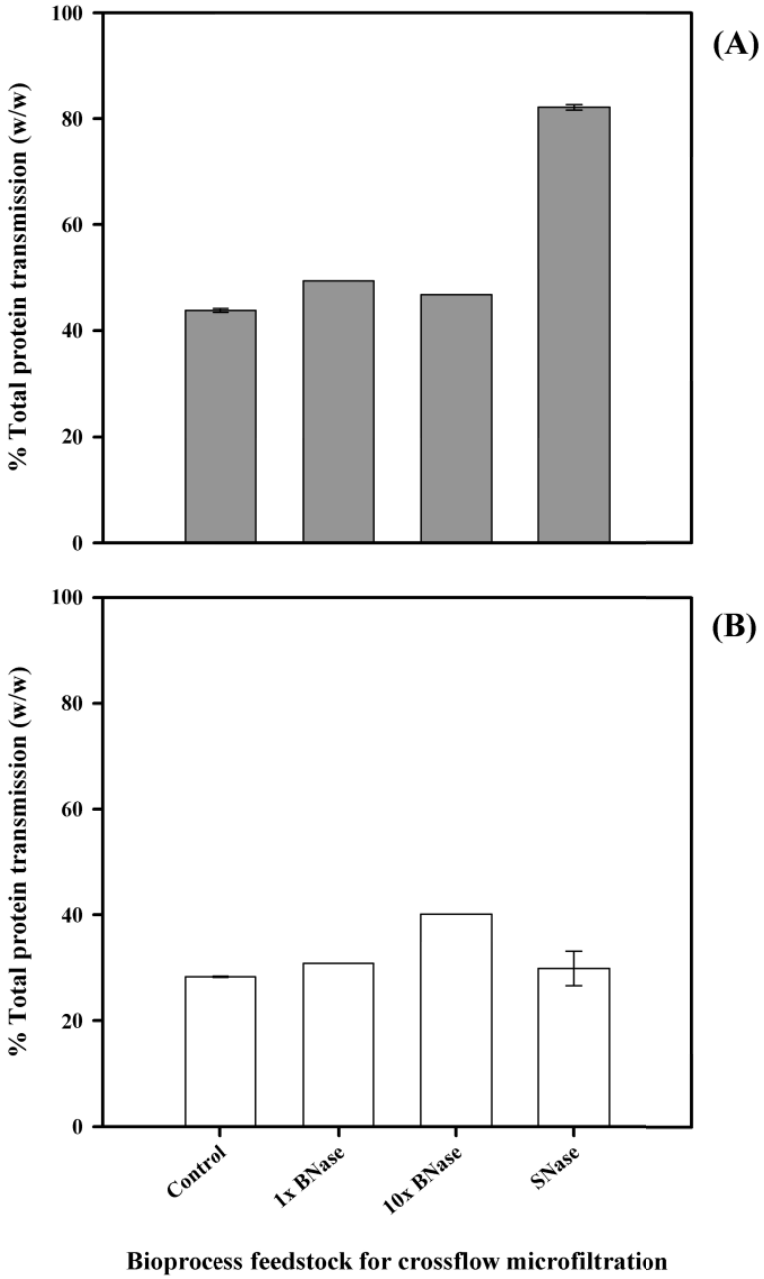

Figure 6.10 Total soluble protein transmission obtained during microscale crossflow microfiltration of *E. coli* Fab' homogenates under ΔP_{TM} (A) 22 kPa and (B) 75kPa. Bioprocess feedstocks as defined in Table 6.1. Error bars indicate one standard deviation about the mean (n=2). Homogenisation performed according to Section 2.3.1. DNA hydrolysis according to Section 6.2.2. Microscale CFF operation according to Section 5.4.3. Crossflow rate at 14 L h^{-1}, and A_m is 0.001 m^2.Membrane used is 0.22 μm PVDF. Total protein quantification according to Section 2.9.3.

6.3.8 Microscale CFF study of *E. coli* homogenates: DNA removal

It is important for biopharmaceutical products to have chromosomal DNA levels at a minimum. The US FDA has set the residual DNA levels to less than 100 picogram per dose (Cooke et al., 2003). Since chromosomal DNA is negatively charged, it is routinely separated from the Fab' product by anion exchange chromatography after Fab' capture (Spitali, 2009). **Figure 6.11** shows the transmission levels of chromosomal DNA during crossflow microfiltration of the homogenised *E. coli* homogenates. The figure illustrates an interaction between key effects of DNA hydrolysis by Benzonase® treatment and the operating transmembrane pressure during crossflow microfiltration. On the other hand, the homogenate feed with co-expressed nuclease (SNase) has lower DNA transmission than the Control. The differences between the samples are significant ($p < 0.05$) and with a larger observed difference at the lower ΔP_{TM} (22 kPa).

Figure 6.12 shows the agarose gel of the CFF samples. This clearly indicates a reduction in DNA content in the permeates compared to the feeds as illustrated by the reduced intensity of the smear in the DNA gel. It is important to point out that even without DNA hydrolysis, the Control demonstrates a considerable reduction in DNA levels in the permeate as illustrated in **Figure 6.11** and **6.12**. Furthermore, in **Figure 6.12**, the lane corresponding to the permeate of the Control evidently shows a decrease in the larger (intact) DNA fragments which were thought to be left inside the wells of the lanes in the DNA gel. This suggests that the crossflow microfiltration process facilitated the retention of the larger DNA fragments.

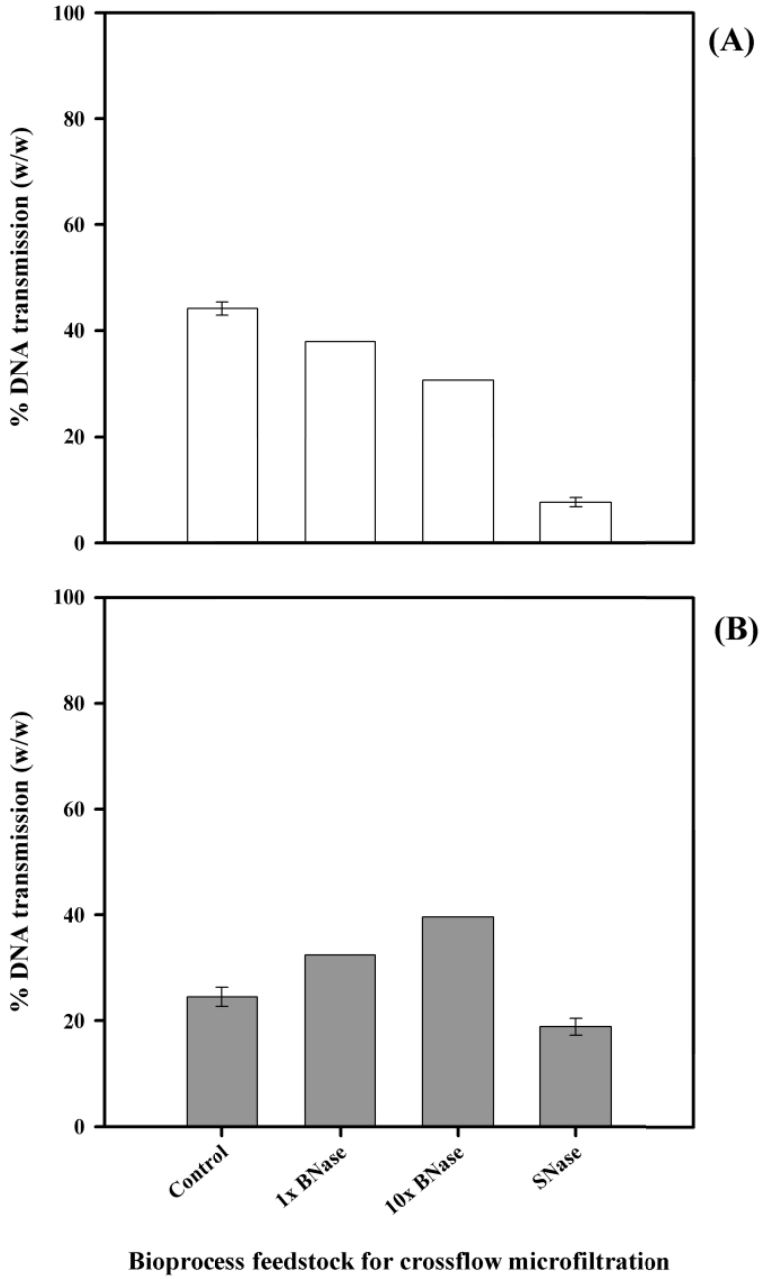

Figure 6.11 DNA transmission obtained during microscale crossflow microfiltration of *E. coli* Fab homogenates under ΔP_{TM} (A) 22 kPa and (B) 75kPa. Bioprocess feedstocks as defined in Table 6.1. Error bars indicate one standard deviation about the mean (n=2). Homogenisation performed according to Section 2.3.1. DNA hydrolysis according to Section 6.2.2. Microscale CFF operation according to Section 5.4.3. Crossflow rate at 14 L h^{-1}, and A_m is 0.001 m^2.Membrane used is 0.22 μm PVDF. DNA sample preparation according to Section 2.9.6. DNA quantification was performed using nanodrop spectrophotometer according to Section 2.9.8.

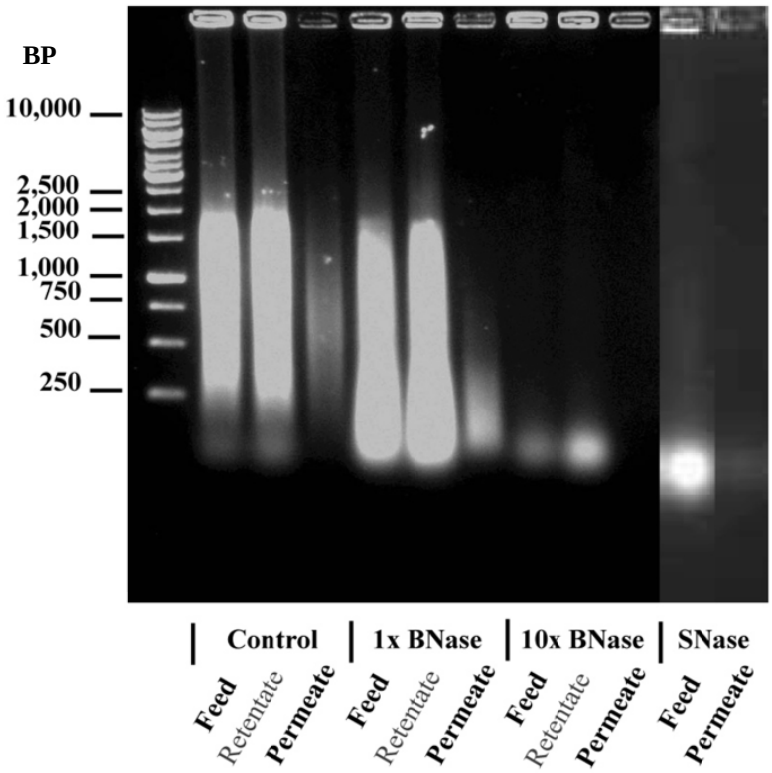

Figure 6.12 Agarose gel showing chromosomal DNAs from the different process streams following crossflow microfiltration of *E. coli* homogenate feedstocks as defined in Table 6.1. Homogenisation performed according to Section 2.3.1. DNA hydrolysis according to Section 6.2.2. Microscale CFF operation according to Section 5.4.3. Crossflow rate at 14 L/h, and A_m is 0.001 m^2.Membrane used is 0.22 μm PVDF. DNA sample preparation according to Section 2.9.6. Agarose gel electrophoresis performed according to Section 2.9.7. BP – base pairs.

The transmission of DNA at the lower ΔP_{TM} follows a similar pattern, although at smaller levels, to that of the Fab' transmission. It is possible that there was some Fab'-DNA interaction during the CFF process due to their opposing charges. At the operating pH (pH 7.0), Fab' has a slightly positive charge since the isoelectric point of Fab' is pI 8.0 (Humphreys et al., 2004; Spitali, 2009). In addition to this, DNA-cell debris interaction is also possible because DNA transmission levels were lower than Fab' transmission levels. In general, the very low transmission of DNA (< 50%) from the different feedstocks is advantageous for the next chromatographic operations for reasons previously described.

The DNA transmission data completes the crossflow microfiltration criteria for assessing overall performance. Taken as a whole, the results on permeate flux, Fab' transmission, total soluble protein transmission and DNA transmission indicate that the best crossflow microfiltration conditions would be at the higher ΔP_{TM} (in this case, 75 kPa). At this condition, permeate flux and Fab' levels are at best while DNA and total soluble protein contents in the permeate are at their lowest. In the last section, the results of a large scale CFF operation based on this best condition will be shown in tandem with pilot scale centrifugation data.

6.3.9 Comparison of clarification methods for *E. coli* Fab' homogenates

The results described in the previous sections were obtained by using the novel microscale CFF device developed in this work (shown in Chapter 5). The experiments were performed to gain an understanding of the crossflow microfiltration behaviour of the different homogenised *E. coli* Fab' samples with or without DNA hydrolysis. Based on the information from the preceding section, large scale crossflow microfiltration and pilot-scale centrifugation experiments were performed for both Control and SNase feedstocks.

Table 6.3 shows the component profile of the clarified Fab' solution from the permeate of the large scale CFF process. In the same table, the component profile of clarified Fab' solution from a pilot scale centrifuge is also shown. From visual inspection of the two solutions, it was noticed that the Fab' solution from CFF is clear and transparent while the Fab' solution from the centrifugation process is turbid. The turbidity of the Fab' solution from centrifugation is expected. It is commonly known that centrifugation is usually followed by depth filtration as a secondary clarification step to obtain particle-free solutions in the harvest of therapeutic monoclonal antibodies and related proteins (See **Figure 1.5**). It is evident from **Table 6.3** that the centrifugation process recovered most Fab' than crossflow microfiltration. However, it could also be observed that the Fab' solution from the crossflow microfiltration process has lower levels of contaminating protein and chromosomal DNA.

Table 6.3 Comparison of clarified *E. coli* Fab' profiles from large scale experiments of crossflow microfiltration and centrifugation.

Clarification method	**Control**			**SNase**		
	Fab' (μg mL^{-1})	**DNA** (μg mL^{-1})	**Total protein** (mg mL^{-1})	**Fab'** (μg mL^{-1})	**DNA** (μg mL^{-1})	**Total protein** (mg mL^{-1})
Crossflow microfiltration[1]	679	476	13	58	160	10
Centrifugation[2]	1074	4183	39	83	1251	28

[1] According to section 2.6.2 using Pellicon 2-Mini, ΔP_{TM} is 100 kPa, crossflow rate of 80 L h^{-1}, 0.22 μm PVDF

[2] According to section 2.2.4 using Carr Powerfuge, feed flow rate of 30 L h^{-1}

The operating condition for CFF was based on information from the results of microscale experiments in Sections 6.3.6 – 6.3.8. although the actual ΔP_{TM} is higher (100 kPa in the large scale experiment compared to the 75 kPa in microscale). Despite this, the flux obtained and transmission levels achieved were similar to the microscale data indicating that the pressure-independent behaviour extends up to 100 kPa in this case. On the other hand, the operating condition for the pilot scale centrifugation process was already under optimal conditions (Balasundaram et al., 2009b). The feed flowrate, currently at 30 L h^{-1}, is at the low end of applicable feed rates. Processing larger volumes of feed will therefore require a considerable length of processing time. Increasing the flowrate, however, has its own disadvantage since it is widely known that increasing feed rates in centrifugation will result in a decrease in the clarification efficiency.

6.4 Conclusions

The aim of this chapter was to demonstrate the utility of a novel microscale CFF device in obtaining bioprocessing information by predicting the performance of larger scale crossflow microfiltration module. Specifically, the impact of DNA hydrolysis on crossflow microfiltration processes was investigated.

Initially, the impact of DNA hydrolysis on the physical properties of the different *E. coli* homogenate feedstocks was investigated (**Table 6.1**). It was shown (Section 6.3.1) that the addition of Benzonase® nuclease or the co-release of Staphylococcal nuclease from cell engineered *E. coli* Fab' digested DNA molecules into smaller fragments (**Figure 6.3**). The DNA hydrolysis facilitated the decrease in viscosity (**Figure 6.4**) of the different homogenate feedstocks (**Table 6.1**). DNA hydrolysis using Benzonase® nuclease did not affect the degree of release of the Fab' fragments (Section 6.3.3). It was demonstrated (Sections 6.3.1-6.3.3) that freeze-thawing resulted in a decrease in

viscosity of the Control and BNase samples (low concentration), an increase in Fab' content, and a decrease in total protein content. However, freeze-thawed SNase homogenates have been demonstrated to have similar rheological properties as fresh SNase (**Figure 6.4**) and so have been used in the further study of primary recovery of Fab' fragments.

A good prediction of the larger-scale crossflow microfiltration module was demonstrated (**Figure 6.7**) by the novel microscale CFF design using the *E. coli* Fab' homogenates (Control and SNase) and so the microscale CFF device was used in the detailed analysis of the impact of DNA hydrolysis on crossflow microfiltration processes (Sections 6.3.5-6.3.8).

Crossflow microfiltration of the different *E. coli* Fab' homogenates showed that DNA hydrolysis does not significantly affect the permeate flux (**Figure 6.8**). However, DNA hydrolysis significantly impacts on the levels of Fab' transmission (**Figure 6.9**) and total soluble protein transmission (**Figure 6.10**). The SNase feedstocks had the highest levels of Fab' transmission and total soluble protein transmission at the lower ΔP_{TM} investigated. Both the permeate flux and the Fab' transmissions of the homogenates were independent of pressure but the total protein transmission decreased with an increase in ΔP_{TM}. The transmission of DNA was found to be affected by both the extent of DNA hydrolysis and ΔP_{TM} (**Figure 6.11** and **Figure 6.12**).

Lastly, based on the results of the microscale evaluation of the crossflow microfiltration behaviour of *E. coli* Fab' homogenates, the best operating condition was identified. This information was used to operate a large-scale crossflow microfiltration experiment and compared with pilot-scale centrifugation (**Table 6.3**).

As a whole, this chapter demonstrated the application of the microscale crossflow microfiltration device in investigating the CFF behaviour of industrially relevant, complex feedstocks. The use of the microscale approach in crossflow microfiltration has clearly facilitated the acquisition of bioprocess information that enabled the process comparison of larger-scale unit operations. The microscale approach also aided in recognizing the mechanisms of the crossflow microfiltration performance of the different homogenates, with or without DNA hydrolysis (e.g. Fab'-cell debris and Fab'-DNA interactions could have influenced transmission levels). However, the nature and mechanism of how these interactions occur during microfiltration is not well understood and the current study was not designed to cover such investigation. The microscale devices developed in this work can be used in future research to study these interactions.

In conclusion, DNA hydrolysis improved the crossflow microfiltration performance of *E. coli* Fab' homogenates. Centrifugation has shown a higher recovery of Fab' fragments however, it has also recovered most contaminating proteins and DNA. Both Fab' content and the levels of contaminating components should be considered in deciding which process route to proceed. In the whole bioprocess approach described in Section 1.2, a wider view of the impact of certain process stream profiles will enable to choose the process option that is best not only for a specific process step but for the overall bioprocess sequence. The microscale CFF device used in this work has provided extensive data on crossflow microfiltration which will allow the broad and exhaustive evaluation necessary for a whole bioprocess approach.

The assistance of the following people is acknowledged for their contributions to the work produced in this chapter: Dr. B.Balasundaram, formerly a postdoctoral researcher at UCL Biochemical Engineering and A. Affandy for the joint experimental work in the production of *E. coli* Fab' homogenates, DNA quantification and gel analysis, viscosity measurements and pilot scale centrifugation experiment.

7. Conclusions and Future Work

7.1 Summary and overall conclusions

The overall aim of this thesis was to establish a microscale bioprocessing platform for the investigation of both dead-end and cross flow filtration (CFF) operations and the impact of upstream operations on filtration performance (Section 1.6). A key consideration in this work is the compatibility of these microscale filtration platforms with laboratory automation, specifically the Tecan™ laboratory robotic platform (**Figure 2.1**). The establishment of a microscale filtration platform contributes to the whole bioprocess development approach (Section 1.1.) within the context of biopharmaceutical product development. The goal of the whole bioprocess is to understand each unit operation or step within a bioprocess sequence (in this case: membrane filtration) and to determine the impact of each of these steps in subsequent unit operations. The combination of microscale bioprocessing with laboratory automation allows the rapid evaluation of the unit operations within a bioprocess sequence (Micheletti et al., 2006). Microscale bioprocessing enables the study of wider design space, specifically facilitated by its high-throughput and low-volume features. The time- and cost-effectiveness of the high throughput process development approach to obtain process and product understanding is increasingly being recognised (Bhambure et al., 2011).

The primary recovery of humanised antibody Fab' fragments was used as a case study for the evaluation of the microfiltration methodologies established in this work. Fab' fragments have only been recently approved for therapeutic applications; therefore a defined production process has yet to become widely established (Shukla and Thömmes, 2010). There is thus an opportunity to contribute to the understanding and development of different processes and unit operations for antibody Fab' fragments currently in the development pipeline.

The membrane filtration processes investigated in this work were dead-end microfiltration and cross flow microfiltration processes for the primary recovery of antibody Fab' fragments. The first two results chapters (Chapter 3 and 4) have focused on dead-end microfiltration process. The last two results chapters (Chapter 5 and 6) have focused on the crossflow filtration process.

A series of objectives were outlined (Section 1.6) in order to achieve the overall aim of establishing a microscale platform for the investigation of these processes for the primary recovery of antibody Fab' fragments. The organization of these objectives followed these general steps:

1. the determination of scale down criteria;
2. the design and creation of the microscale filtration device based on (1);
3. the design of associated microscale filtration methodology that is compatible with laboratory automation;
4. the evaluation of the device and methodology in studying filtration processes; and
5. the application of the device and methodology.

The microscale dead-end filtration device has previously been created and investigated by Jackson et al. (2006). In this thesis, the methodology associated with the microscale

dead-end filtration device has been further developed. Thus, for the dead-end filtration process, steps 3 to 5 above were re-established. Chapter 3 has demonstrated a single-plate/two-step methodology in determining the specific cake resistance (α) of antibody Fab' fragments during dead-end microfiltration (Section 3.3.3). The method has reduced the sample volume to half of that used by Jackson et al. (2006). A single-plate/single-step methodology was also demonstrated that could facilitate the reduction of sequences for automation thus simplifying the experimental determination of pressure-dependence of α (Section 3.3.5). Chapter 4 established the application of the new microscale methodology for dead-end filtration in assessing a linked bioprocess sequence comprising of the Fab' release step followed by recovery by dead-end microfiltration. The impact of cell disruption techniques, and specific operating conditions to release the Fab' fragments from *E. coli* cells on the specific cake resistances were illustrated (Section 4.3).

Establishment of the crossflow filtration option required the creation of a completely novel device which is automation compatible. Therefore, in the case of the microscale CFF option, steps 1 to 5 of the generic steps earlier described were performed. In Chapter 5, the scale down basis was identified (Section 5.2), and the design process and the characteristics of the novel device were presented (Section 5.4.1). A microscale crossflow methodology was developed (Section 5.4.3 - 5.4.4) and the preliminary evaluation of the device plus methodology was demonstrated using a model feed (Section 5.4.5). It was shown that the microscale CFF device has comparable performance in terms of steady state permeate flux of the model feed system within ± 10% difference (**Figure 5.7**). This was achieved with a ten-fold reduction in volume and a 100-fold reduction in membrane area.

Chapter 6 has illustrated: (1) the scale comparison of the microscale CFF device with the larger scale CFF module using the industrially relevant *E. coli* Fab' feedstocks

(Section 6.3.4); (2) the application of the microscale CFF device in studying the effect of DNA hydrolysis on crossflow microfiltration (Section 6.3.5 – 6.3.8); and (3) the utility of the microscale CFF device in the rapid identification of key process information (e.g. operating conditions such as ΔP_{TM}) (Section 6.3.9). The identification of key scale up condition (e.g. ΔP_{TM}) enabled the analysis of process stream profiles of different options of larger-scale unit operations for primary Fab' recovery (Section 6.3.9).

The above results demonstrate the accomplishment of the overall aim of the thesis to establish a microscale bioprocessing platform for membrane filtration processes. In the following section the implications of using the microscale filtration platform and the wider application of the devices are illustrated.

7.2 Broader implications and applications

There are several implications which could be derived from the course of developing and evaluating the microscale bioprocessing platform for membrane filtration presented in this thesis. Two key implications are related to the whole bioprocess approach in analysing bioprocesses and the re-evaluation of existing theories and models for membrane microfiltration, specifically those applied to crossflow microfiltration.

7.2.1 Enabling whole bioprocess analysis

The application of the microscale devices and methodologies in the study of dead-end filtration and crossflow filtration processes has manifested the importance of a "whole bioprocess" approach in the bioprocess development. In Chapter 4, an essential finding is the divergent effects of the Fab' release step and the dead-end microfiltration step on overall recovery of antibody Fab' fragments (Section 4.3.1). This finding highlighted the need for an extensive evaluation of bioprocess sequences in product recovery optimisation and not to only focus on a single unit operation. With the aid of the

microscale dead-end filtration device it was demonstrated that the key issues affecting the linked process sequence could be identified. In Chapter 6, the microscale crossflow microfiltration study on the effect of DNA hydrolysis demonstrated the divergent effects of different crossflow microfiltration conditions as well as the conditions (nuclease source, concentration) for DNA hydrolysis on the profile of the process streams. The data obtained (Section 6.3.5 - 6.3.8) revealed the necessary trade-offs to consider, such as the level of product recovery and the contaminant profile, in selecting bioprocess routes as well as in deciding to improve producer strains through cell engineering.

The usefulness of the microscale membrane devices presented here has so far been mostly applied to the study of the effect of upstream unit operations, such as fermentation and cell disruption, on membrane filtration processes. This kind of investigation can be extended further downstream of primary recovery, that is on the capture and purification of the process streams to get the desired therapeutic protein. For example, the microscale membrane filtration devices can be applied in combination with studies using automated microscale chromatographic purification which has already been shown as a strategy for process development (Wenger et al., 2007; Coffman et al., 2008; Kramarczyk et al., 2008). Since the parameters for scale translation and the required automation for these two unit operations have already been established, together with known microscale fermentation strategies, a rapid evaluation of the “whole bioprocess” sequence (**Figure 1.2**) is now possible. As the development of the microscale devices for each unit operations are refined, greater confidence in the “whole bioprocess” approach is also expected to develop.

7.2.2 Enabling deeper understanding of microfiltration processes

The relatively small-volume feed requirement, the parallel and automation-compatible experimentation of the microscale filtration devices mean that a wider scope of experimental design space can be investigated using industrially-relevant, complex biological feedstocks. The amount of data which could be generated from microscale bioprocessing studies would enable the re-evaluation of available theories and models on membrane filtration processes specially those concerning complex biological feedstocks. As demonstrated in Section 3.3.6, there is a large difference in the dead-end microfiltration of non-biological and biological feeds. Biological feedstocks could also differ, depending on the complexity of the soluble components (macromolecules, colloids, etc.) and the interaction of these components with the cellular debris. Cake filtration analysis may now be performed in view of the interacting effects of surface adsorption of soluble material in suspension (which in turn may affect R_m) and the cell debris-protein interaction on the measured specific cake resistance (α) of specific feedstocks, instead of using model feeds to characterise and predict dead-end microfiltration behaviour.

The observed pressure-independence of the permeate fluxes of the yeast (Section 5.4.5) and *E. coli* Fab' suspensions (Section 6.3.5) were unusual, but plausible. The current available experimental data as well as crossflow filtration theories were limited in their application to the current data because of the complexity of the feed characteristics and therefore, in explaining the crossflow microfiltration behaviour. Note that most of the deterministic models only apply to narrow definitions of the feed suspensions which do not capture the complexity of most biological feeds.

Current crossflow filtration models are mostly derived for application to ultrafiltration processes with only a few fundamental studies dedicated to the understanding of crossflow microfiltration processes. However, the microfiltration behaviour of crossflow

processes has the added dimensions of the debris-debris, debris-protein, protein-membrane and debris-membrane interactions which are more than the usual solute-solute-membrane interaction that dominate ultrafiltration processes. The use of the microscale CFF device will facilitate the better understanding of the mechanism of the crossflow microfiltration processes of complex feeds.

Given the constraints in resources during process development, it is best to determine a property of a bioprocess feedstock that reflects the collective impact of the different physical properties of the components in a feed suspension for microfiltration. As shown in Section 4.3.2, the specific cake resistance, α, reflects even the slightest changes in the solution components of *E. coli* Fab' extracts as a result of slight change in extraction condition (e.g. pH). Therefore, α can be a better predictor of the filtration behaviour of feed suspensions.

From dead-end filtration experiments, insights on the dependence of the specific cake resistance on solution properties could be obtained. Combined with CFF microfiltration experiments, an exhaustive view of the microfiltration behaviour is obtained and therefore, better information can lead to better process design.

Finally, it would be interesting to see how a certain feed's dead-end microfiltration performance can actually predict the crossflow microfiltration behaviour. The amount of feed volume necessary for microscale dead-end filtration is very small (~40x smaller) compared to the required volume for microscale crossflow filtration thus there is a complementary benefit in understanding a certain feedstock's microfiltration performance using the dead-end and crossflow filtration modes of operation.

The context of this work was within biopharmaceutical product development but it is envisioned that the microscale membrane filtration methodologies could be applied to

any membrane filtration processes using complex biological feeds (e.g. other biotechnological processes such as separation of extracellular enzymes from cells, fractionation of complex molecules based on size, etc). Although, some slight modification of microscale methodologies maybe required. Further work such as these are presented in the next section.

7.3 Recommendations for future research

After highlighting the outcome of the work performed in this thesis (Section 7.1) and demonstrating the broader implications and applications of the microscale membrane filtration devices (Section 7.2), this section will present the necessary work in the short term in order to get a complete characterisation of the microscale microfiltration systems developed in this work.

- The microscale dead-end microfiltration methodology which was developed and evaluated in Chapter 3 can be further assessed by applying it in the study of dead-end microfiltration behaviour of other complex biological feeds, perhaps using different industrially relevant expression systems (e.g. mammalian cells, *Pichia pastoris*), which would cover a broad range of filtration characteristics. These can provide insights whether, for example, there is a need to replenish easily filterable (high flux) feeds in the feed/retentate wells or if the length of filtration time to get over the “initial phase of filtration” is the same for the different materials. The former requires a strategy for feeding without disturbing the cake formation, and the latter is important specifically for the two-step/single plate methodology (Section 3.3.3) where it necessary to determine after how long should the first-step filtration period to run.

- Further experiments can be made, in relation to the above, to assess different membrane types and membrane pore sizes. Again, with particular focus initially on the applicability of the microscale methodology for initial process selection.

- Further experiments can be made in relation to Section 4.3.1, specifically using the linked sequence at microscale of thermo-chemical extraction and dead-end filtration, in order to understand the release mechanism of Fab' and HCP. A detailed study on the impact of the different component profiles on microfiltration performance can be performed. The aim is to enhance understanding of the extraction processes and the impact on succeeding microfiltration operation.

- Further studies similar to those described in Section 4.3.2.2 should be performed to determine the impact of combining heat with sonication or homogenisation on the specific cake resistance and compare the dead-end microfiltration performance with heat extracted *E. coli* Fab'. A broad range of temperatures can be studied, including the heat extraction method, so that a complete picture of the impact of cell disruption method can be achieved. This is to enable the analysis of the different process trade-offs which may emerge.

- Additionally, the heating profile at microscale should be studied to determine if this also mimics the heating profile at larger scale. The focus should not only be on the temperature profiles but also on the component analysis (e.g. Fab', total soluble protein, DNA).

- The microscale crossflow microfiltration device (**Figure 5.2**) was designed without turbulence promoters or screens. These screens are present in the larger-scale module (**Figure 5.1**). In order to understand how the promoters affect the microfiltration performance of complex feeds, studies should be performed to evaluate the effect of the turbulence promoters, in their current design, inside the larger scale device. A hydrodynamic description, as well as a description relating to

mass transfer may be determined so that this can be related to the conditions achieved at microscale which do not have turbulence promoter.

- Further studies to optimise the crossflow method to further reduce the required feed volume should be performed. It is important to determine whether this minimum volume is feed-specific.

- In relation to the above, crossflow microfiltration experiments should be performed using other expression systems such as those described for dead-end microfiltration (e.g. mammalian cells, *Pichia pastoris*). These experiments will provide insights on the robustness of the microscale CFF methodology.

- Investigate if the CFF performance of the cell engineered *E. coli* co-expressing Staphylococcal nuclease changes when Fab' expression of this strain has been optimised.

- Based on the results in Section 4.3 and 6.3, there is a need to increase the Fab' yield from microfiltration. It is thought that Fab' interact with the cell debris and are therefore adsorbed on or trapped within the cake being formed during CFF/dead-end microfiltration. Thus, it is necessary to investigate how to reduce Fab'-cell debris interaction during dead-end or crossflow microfiltration by studying the impact of pH, ionic strength, freeze-thawing, heating etc.

- In order to enhance the dead-end and crossflow microfiltration device design and to improve its compatibility with automation the following work is required:

    - To explore ways of pumping fluid which is representative of large scale operation and determine how this can be integrated within the laboratory robotic platform (Tecan™);

- To re-design the crossflow microfiltration device to reduce the channel heights to further increase possible range of shear rates. A second prototype has been designed and Fabricated with slightly different dimension in feed/retentate channel height (smaller) and permeate channel height (smaller, not inclined downwards). However, this has not yet been evaluated.

- To re-design the dead-end and crossflow microfiltration devices to improve permeate collection. In particular, the collectors could be made of materials that are conductive like that of the Tecan™ tips. The conductivity of the material can be used to detect liquid volume electronically. Together with the quantification of the permeate for the product or total protein, the measured conductivity could also be used as an indicator of a change in soluble contents or concentration in the permeate.

- Given the large amount of data generated by using the microscale dead-end and crossflow filtration devices (e.g. time, pressures, permeate volumes, contaminant and product profiles, etc.) it would be helpful to have a data processing tool which allows the capture of raw data from the laboratory robotic platform and will convert the data to useful process attributes (e.g. flux, volume versus time, flux versus pressure relationships, etc.). This data processing/data analysis tool will enable the rapid navigation within the experimental design space and will readily provide the information to decide on process adjustments and evaluate specifications.

- Lastly, in order to have a broad range of crossflow microfiltration operation conditions, a microscale mimic of other crossflow modules will be valuable. For example, modules which operate under turbulent regime will provide a comparison on the crossflow characteristics and performance of the *E. coli* Fab'' feedstock used here. The crossflow microfiltration module mimicked in this work operates under laminar-flow with flat-sheet membranes. The limitations ascribed to the crossflow

processes described here only reflect the limitations of the module itself, not necessarily of the crossflow operation as a whole. Thus, having microscale mimics of different modules with different hydrodynamic characteristics will enable to gather information that will provide a better understanding of the crossflow microfiltration processes of feedstocks derived from biological materials.

References

Allen TM. 2002. Ligand-targeted therapeutics in anticancer therapy. Nature Reviews Cancer 2:750-763.

Andersen DC, Reilly DE. 2004. Production technologies for monoclonal antibodies and their fragments. Current Opinion in Biotechnology 15:456-462.

Anicetti V. 2009. Biopharmaceutical Processes: A Glance into the 21st Century. BioProcess International 7(S1), p 4-11.

Bacchin P, Aimar P, Field RW. 2006. Critical and sustainable fluxes: Theory, experiments and applications. Journal of Membrane Science 281:42-69.

Bakir U, Hamamci H. 1997.The effect of freeze-thawing on the release of intracellular proteins from *Escherichia coli* by means of a bead mill. World Journal of Microbiology and Biotechnology 13 (4): 475-477.

Balasundaram B, Harrison S, Bracewell DG. 2009a. Advances in product release strategies and impact on bioprocess design. Trends in Biotechnology 27:477-485.

Balasundaram B, Nesbeth D, Ward JM, Keshavarz-Moore E, Bracewell DG. 2009b. Step change in the efficiency of centrifugation through cell engineering: co-expression of *Staphylococcal nuclease* to reduce the viscosity of the bioprocess feedstock. Biotechnology and Bioengineering 104:134-142.

Baneyx F, Mujacic M. 2004. Recombinant protein folding and misfolding in *Escherichia coli*. Nature Biotechnology 22:1399-1408.

Bayer ME, Leive L. 1977. Effect of ethylenediaminetetraacetate upon Surface of *Escherichia coli*. Journal of Bacteriology 130:1364-1381.

Belfort G, Davis RH, Zydney AL. 1994.The behavior of suspensions and macromolecular solutions in crossflow microfiltration. Journal of Membrane Science 96:1-58.

Betts JI, Baganz F. 2006. Miniature bioreactors: current practices and future opportunities. Microbial Cell Factories 5. Art. 21.

Bhambure R, Kumar K, Rathore AS. 2011. High-throughput process development for biopharmaceutical drug substances. Trends in Biotechnology 29:127-135.

Birch J, Rancher A. 2006. Antibody production.Advanced Drug Delivery Reviews 58: 671– 685.

Bird RB, Stewart WE, Lightfoot E.N. 2001. Transport phenomena. New Jersey: John Wiley and Sons.

Bowering LC, Bracewell DG, Kesharvarz-Moore E, Hoare M, Weir ANC. 2002.Comparison of techniques for monitoring antibody fragment production in *E. coli* fermentation cultures. Biotechnology Progress 18:1431-1438.

Bowering LC. 2004. Microbial Systems for the Manufacture of Therapeutic Antibody Fragments.BioProcessInternational , p 40-47.

Boynton ZL, Koon JJ, Brennan EM, Clouart JD, Horowitz DM, Gerngross TU, Huisman GW. 1999. Reduction of cell lysate viscosity during processing of poly(3-hydroxyalkanoates) by chromosomal integration of the staphylococcal nuclease gene in *Pseudomonas putida*. Applied and Environmental Microbiology 65:1524-1529.

Brekke OH, Løset GA. 2003. New technologies in therapeutic antibody development. Current Opinion in Pharmacology 3:544-550.

Chandler M, Zydney A. 2004. High throughput screening for membrane process development. Journal of Membrane Science 237:181-188.

Cheryan M. 1998. Ultrafiltration and Microfiltration. Boca Raton: CRC Press.

Chhatre S, Bracewell DG, Titchener-Hooker NJ. 2009. A microscale approach for predicting the performance of chromatography columns used to recover therapeutic polyclonal antibodies. Journal of Chromatography A 1216:7806-7815.

Choe W, MiddelbergAPJ. 2001. Direct chemical extraction of a recombinant viral coat protein from *Escherichia coli* at high cell density. Biotechnology and Bioengineering.75:451-455.

Choi JH, Lee SY. 2004. Secretory and extracellular production of recombinant proteins using *Escherichia coli*. Applied Microbiology and Biotechnology 64:625-635.

Clarkson AI, Lefevre P, Titchener-Hooker NJ. 1993. A study of process interactions between cell disruption and debris clarification stages in the recovery of yeast intracellular products. Biotechnology Progress 9:462-467.

Coffman JL, Kramarczyk JF, Kelley BD. 2008. High-throughput screening of chromatographic separations: I. Method development and column modeling. Biotechnology and Bioengineering 100:605-618.

Cooke GD, Cranenburgh RM, Hanak JAJ, Ward JM. 2003. A modified *Escherichia coli* protein production strain expressing staphylococcal nuclease, capable of auto-hydrolysing host nucleic acid. Journal of Biotechnology 101(3):229-239.

Curling J. 2009.The Development of Antibody Purification Technologies In: Gottschalk U editor. Process Scale Purification of Antibodies. Hoboken, New Jersey: John Wiley & Sons, Inc. 25-45.

Da Costa AR, Fane AG, Fell CJD, Franken ACM. 1991. Optimal channel spacer design for ultrafiltration. Journal of Membrane Science 62:275-291.

Dennis MS, Zhang M, Meng YG, Kadkhodayan M, Kirchhofer D, Combs D, Damico LA. 2002. Albumin Binding as a General Strategy for Improving the Pharmacokinetics of Proteins. Journal of Biological Chemistry 277:35035-35043.

Dimasi JA, Grabowski HG, Vernon J. 2004. R&D costs and returns by therapeutic category. Drug Information Journal 38: 211-223.

Farid S. 2006. Established bioprocesses for producing antibodies as a basis for future planning. Advances in Biochemical Engineering, Biotechnology 101:1-42.

Farid SS. 2009. Process Economic Driver in Industrial Monoclonal Antibody Manufacture, In: Gottschalk U, editor. Process Scale Purification of Antibodies. Hoboken, New Jersey: John Wiley & Sons, Inc. p 239-262.

Field RW, Wu D, Howell JA, Gupta BB. 1995. Critical Flux Concept for Microfiltration Fouling. Journal of Membrane Science 100:259-272.

Foley G, Macloughlin PF, Malone DM.1995.Membrane fouling during constant flux Cross-flow microfiltration of dilute suspensions of active dry yeast. Separation Science and Technology30:383-398.

Foley G. 2006a. Dimensional analysis of crossflow microfiltration data. Separation Science and Technology 41:3169-3185.

Foley G. 2006b. A review of factors affecting filter cake properties in dead-end microfiltration of microbial suspensions. Journal of Membrane Science 274:38-46.

Ghidossi R, Veyret D, Moulin P. 2006. Computational fluid dynamics applied to membranes: State of the art and opportunities. Chemical Engineering and Processing 45:437-454.

Goochee CF. 2002. The roles of a process development group in biopharmaceutical process startup. Cytotechnology38:63-76.

Grace HP. 1953a. Resistance and Compressibility of Filter Cakes. Chemical Engineering Progress 49:303-318.

Grace HP. 1953b. Resistance and Compressibility of Filter Cakes .2.Under Conditions of Pressure Filtration. Chemical Engineering Progress 49:367-377.

Grant Y, Matejtschuk P, Dalby PA. 2009. Rapid Optimization of Protein Freeze-Drying Formulations Using Ultra Scale-Down and Factorial Design of Experiment in Microplates. Biotechnology and Bioengineering 104:957-964.

Guijun M, Jean A, Spyridon G, Ranna EP, Alan C, Mike H, Yuhong Z. 2010. Mimic of a large-scale diafiltration process by using ultra scale-down rotating disc filter. Biotechnology Progress 26:466-476.

Ho RJY, Gibaldi M. 2003. Biotechnology and Biopharmaceuticals: Transforming Proteins and Genes into Drugs. Hoboken, New Jersey: John Wiley & Sons, Inc.

Hodgson PH, Leslie GL, Fane AG, Schneider RP, Fell CJD, Marshall KC. 1993. Cake resistance and solute rejection in bacterial microfiltration: The role of the extracellular matrix. Journal of Membrane Science 79:35-53.

Hooper LA, Hollein HC, Slater CS. 1998. Microfiltration of *Streptomyces rimosus*: cell harvesting process studies. Separation Science and Technology 33:1747-1765.

Humphreys DP, Heywood SP, King LM, Bowering LC, Turner JP, Lane SE. 2004. Engineering of *Escherichia coli* to improve the purification of periplasmic Fab' fragments: changing the pI of the chromosomally encoded PhoS/PstS protein. Protein Expression and Purification 37:109-118.

Humphreys DP. 2003. Production of antibodies and antibody fragments in *Escherichia coli* and a comparison of their functions, uses and modification. Current Opinion in Drug Discovery & Development 6:188-196.

Irvin RT, Macalister TJ, Costerton JW. 1981. Tris(Hydroxymethyl)Aminomethane buffer modification of *Escherichia coli* outer-membrane permeability. Journal of Bacteriology 145:1397-1403.

Jackson NB, Liddell JM, Lye GJ. 2006. An automated microscale technique for the quantitative and parallel analysis of microfiltration operations. Journal of Membrane Science 276:31-41.

Jefferis R. 2005. Glycosylation of Recombinant Antibody Therapeutics. Biotechnology Progress 21:11-16.

Katsui N, Tsuchido T, Hiramatsu R, Fujikawa S, Takano M, Shibasaki I. 1982. Heat-induced blebbing and vesiculation of the outer-membrane of *Escherichia coli*. Journal of Bacteriology 151:1523-1531.

Kelley B. 2007. Very large scale monoclonal antibody purification: The case for conventional unit operations. Biotechnology Progress.23:995-1008.

Kelley B. 2009. Industrialization of mAb production technology: The bioprocessing industry at a crossroads. mAbs 1:443-452.

Keskinler B, Akay G, Bayhan YK, Erhan E. 2002. Effect of ionic environment on the crossflow microfiltration behaviour of yeast suspensions. Journal of Membrane Science 206:351-360.

Kramarczyk JF, Kelley BD, Coffman JL. 2008. High-throughput screening of chromatographic separations: II. Hydrophobic interaction. Biotechnology and Bioengineering 100:707-720.

Kromkamp J, Bastiaanse A, Swarts J, Brans G, van der Sman RGM, Boom RM. 2005. A suspension flow model for hydrodynamics and concentration polarisation in crossflow microfiltration. Journal of Membrane Science 253:67-79.

Kromkamp J, Faber F, Schroen K, Boom R. 2006. Effects of particle size segregation on crossflow microfiltration performance: Control mechanism for concentration polarisation and particle fractionation. Journal of Membrane Science 268:189-197.

Ladisch M. 2001. Bioseparations Engineering: Principles, Practice, and Economics. New York: John Wiley and Sons, Inc.

Le MS, Spark LB, Ward PS. 1984. The separation of aryl acylamidase by cross flow microfiltration and the significance of enzyme cell debris interaction. Journal of Membrane Science 21:219-232.

Lebreton B, Brown A, van Reis R. 2008. Application of high-performance tangential flow filtration (HPTFF) to the purification of a human pharmaceutical antibody fragment expressed in *Escherichia coli*. Biotechnology and Bioengineering 100:964-974.

Lee CT, Morrealle G, Middelberg APJ. 2004. Combined in-fermenter extraction and cross-flow Microfiltration for Improved Inclusion Body Processing. Biotechnology and Bioengineering 85:103-113.

Liddell JM. 2009. Production strategies for antibody fragment therapeutics. BioPharm International p. 1-9.

Lye GJ, Ayazi-Shamlou P, Baganz F, Dalby PA, Woodley JM. 2003. Accelerated design of bioconversion processes using automated microscale processing techniques. Trends in Biotechnology 21:29-37.

Mazor Y, Blarcom TV, Mabry R, Iverson BL, Georgiou G. 2007. Isolation of engineered, full-length antibodies from libraries expressed in *Escherichia coli*. Nat Biotech 25:563-565.

McCabe W, Smith J, Harriot P. 2005. Unit Operations of Chemical Engineering. New York: McGraw-Hill.

McCarthy AA, Gilboy P, Walsh PK, Foley G. 1999. Characterisation of cake compressibility in dead-end microfiltration of microbial suspensions. Chemical Engineering Communications 173:79-90.

McCarthy AA, O'Shea DG, Murray NT, Walsh PK, Foley G. 1998. Effect of cell morphology on dead-end filtration of the dimorphic yeast *Kluyveromyces marxianus* var. marxianus NRRLy2415.Biotechnology Progress 14:279-285.

McGuire I, Coyle K, Foley G. 2009. Specific cake resistance of yeast suspensions measured by dynamic and steady state methods. Journal of Membrane Science 344:14-16.

Meireles A, Molle C, Clifton MJ, Aimar P. 2004. The origin of high hydraulic resistance for filter cakes of deformable particles: cell-bed deformation or surface-layer effect? Chemical Engineering Science 59:5819-5829.

Meltzer TH, Jornitz MW (eds.) 1998. Filtration in Biopharmaceutical Industry. New York: Marcel Dekker, Inc.

Miao JW, Hodgson KO, Ishikawa T, Larabell CA, Legros MA, Nishino Y. 2003. Imaging whole *Escherichia coli* bacteria by using single-particle x-ray diffraction. Proceedings of the National Academy of Sciences of the United States of America 100:110-112.

Micheletti M, Lye GJ. 2006. Microscale bioprocess optimisation. Current Opinion in Biotechnology 17:611-618.

Middelberg APJ. 1995. Process-scale disruption of microorganisms. Biotechnology Advances 13:491-551.

Modise CM, Shan HF, Neufeld RD, Vidic RD. 2005. Evaluation of permeate flux rate and membrane fouling in dead-end microfiltration of primary sewage effluent. Environmental Engineering Science 22:427-439.

Mulder M. 1996. Basic Principles of Membrane Technology.Dordrecht: Kluwer Academic Publishers.

Nakanishi K, Tadokoro T, Matsuno R. 1987. On the specific resistance of cakes of microorganisms. Chemical Engineering Communications 62:187-201.

Ohmori K, Glatz CE. 1999. Effects of pH and ionic strength on microfiltration of *C. glutamicum*. Journal of Membrane Science 153:23-32.

Okamoto Y, Ohmori K, Glatz CE. 2001. Harvest time effects on membrane cake resistance of *Escherichia coli* broth. Journal of Membrane Science 190:93-106.

Patel PN, Mehaia MA, Cheryan M. 1987. Crossflow membrane filtration of yeast suspensions. Journal of Biotechnology 5:1-16.

Perez-Pardo MA, Ali S, Balasundaram B, Mannall GJ, Baganz F, Bracewell DG. 2011. Assessment of the manufacturability of *Escherichia coli* high cell density fermentations. Biotechnology Progress (In Press).

Perry R, Green D. 1997.Perry's Chemical Engineer's Handbook.McGraw-Hill.

Potgieter TI, Cukan M, Drummond JE, Houston-Cummings NR, Jiang Y, Li F, Lynaugh H, Mallem M, McKelvey TW, Mitchell T, Nylen A, Rittenhour A, Stadheim TA, Zha D, d'Anjou M. 2009. Production of monoclonal antibodies by glycoengineered*Pichiapastoris*. Journal of Biotechnology 139:318-325.

Quirk AV, Woodrow JR. 1984.Investigation of the parameters affecting the separation of bacterial enzymes from cell debris by tangential flow filtration. Enzyme and Microbial Technology 6:201-206.

Rao S., Hou Y., Agroskin Y., Pohl C. mAb heterogeneity characterization. Genetic Engineering & Biotechnology News (GEN) 31(6), p 46-47. 15-3-2011. New York.

Rayat ACME, Micheletti M, Lye GJ. 2010. Evaluation of cell disruption effects on primary recovery of antibody fragments using microscale bioprocessing techniques. Biotechnology Progress 26:1312-1321.

Riesmeier B, Kroner KH, Kula MR. 1989. Tangential filtration of microbial suspensions: filtration resistances and model development. Journal of Biotechnology 12:153-172.

Ripperger S, Altmann J. 2002. Crossflow microfiltration - state of the art. Separation and Purification Technology 26:19-31.

Romero CA, Davis RH. 1991. Experimental verification of the shear-induced hydrodynamic diffusion model of crossflow microfiltration. Journal of Membrane Science 62:249-273.

Roque AC, Taipa M, Lowe CR. 2005. An artificial protein L for the purification of immunoglobulins and Fab fragments by affinity chromatography. Journal of Chromatography A 1064:157-167.

Roush DJ, Lu Y. 2008. Advances in primary recovery: centrifugation and membrane technology. Biotechnology Progress 24:488-495.

Russotti G, Osawa AE, Sitrin RD, Buckland BC, Adams WR, Lee SS. 1995. Pilot scale harvest of recombinant yeast employing microfiltration - acase study. Journal of Biotechnology 42:235-246.

Sambrook, J. &Russel, D. W. 2001. Molecular Cloning: A Laboratory Manual, 3rd ed. New York: Cold Spring Harbor Laboratory Press.

Schulz G, Ripperger S. 1989. Concentration polarization in crossflow microfiltration. Journal of Membrane Science 40:173-187.

Shukla AA, Hubbard B, Tressel T, Guhan S, Low D. 2007. Downstream processing of monoclonal antibodies - application of platform approaches. Journal of Chromatography B 848:28-39.

Shukla AA, Kandula JR. 2009. Harvest and recovery of monoclonal antibodies: cell removal and clarification, In: Gottschalk U, editor. Process Scale Purification of Antibodies. New Jersey: John Wiley & Sons, Inc. p 53-78.

Shukla AA, Thömmes Jr. 2010. Recent advances in large-scale production of monoclonal antibodies and related proteins. Trends in Biotechnology 28:253-261.

Siddiqi SF, Bulmer M, Ayazi-Shamlou P, Titchener-Hooker N. 1995. The effects of fermentation conditions on yeast cell debris particle size distribution during high pressure homogenisation. Bioprocess and Biosystems Engineering 14:1-8.

Sinclair A. 2009. Design and optimization of manufacturing In: Gottschalk U editor. Process Scale Purification of Antibodies. Hoboken, New Jersey: John Wiley & Sons, Inc. 263-292.

Sinclair, A. and Monge, M. 2008. Disposable Technologies Implementation: Understanding and Managing Risks. BioPharm International 21(12).

Song LF, Elimelech M.1995.Theory of Concentration Polarization in Cross-Flow Filtration. Journal of the Chemical Society-Faraday Transactions 91:3389-3398.

Song LF. 1998. Flux decline in crossflow microfiltration and ultrafiltration: mechanisms and modeling of membrane fouling. Journal of Membrane Science 139:183-200.

Spitali M. 2009. Downstream processing of monoclonal antibody fragments, In: Gottschalk U, editor.Process Scale Purification of Antibodies. New Jersey: John Wiley & Sons, Inc. p 349-372.

Strege MA, Lagu AL. 1991. Anion-exchange chromatography of DNArestriction fragments. Journal of Chromatography 555:109-124.

Strohl WR. 2009. Therapeutic monoclonal antibodies: past, present and future, In: An Z, editor. Therapeutic Monoclonal Antibodies: From Bench to Clinic. Hoboken, New Jersey: John Wiley & Sons, Inc. p 3-50.

Tait AS, Aucamp JP, Bugeon A, Hoare M. 2009.Ultra scale-down prediction using microwell technology of the industrial scale clarification characteristics by centrifugation of mammalian cell broths. Biotechnology and Bioengineering 104:321-331.

Teoh SK, Tan RBH, Tien C. 2006. Analysis of cake filtration data - A critical assessment of conventional filtration theory. AICHE Journal 52:3427-3442.

Tien C, Ramarao BV. 2008. On the analysis of dead-end filtration of microbial suspensions. Journal of Membrane Science 319:10-13.

Tiller FM. 1953. The role of porosity in filtration - numerical methods for constant rate and constant pressure filtration based on Kozenylaw. Chemical Engineering Progress 49:467-479.

Titchener-Hooker NJ, Dunnill P, Hoare M. 2008.Micro biochemical engineering to accelerate the design of industrial-scale downstream processes for biopharmaceutical proteins. Biotechnology and Bioengineering 100:473-487.

Tsuchido T, Katsui N, Takeuchi A, Takano M, Shibasaki I. 1985. Destruction of the outer-membrane permeability barrier of *Escherichia coli* by heat treatment. Applied and Environmental Microbiology 50:298-303.

Tustian AD, Salte H, Willoughby NA, Hassan I, Rose MH, Baganz F, Hoare M, Titchener-Hooker NJ. 2007. Adapted ultra scale-down approach for predicting the centrifugal separation behavior of high cell density cultures. Biotechnology Progress 23:1404-1410.

Tustian, AD. 2008.An engineering study of key interactions within the process for antibody fragment production. EngD Thesis. University of London. UCL Department of Biochemical Engineering.

van Hee P, Elumbaring ACMR, van der Lans RGJM, van der Wielen LAM. 2006. Selective recovery of polyhydroxyalkanoate inclusion bodies from fermentation broth by dissolved-air flotation. Journal of Colloid and Interface Science 297:595-606.

van Hee P, Middelberg APJ, van der Lans RGJM, van der Wielen LAM. 2004. Relation between cell disruption conditions, cell debris particle size, and inclusion body release. Biotechnology and Bioengineering 88:100-110.

van Reis R, Goodrich EM, Yson CL, Frautschy LN, Dzengeleski S, Lutz H. 1997. Linear scale ultrafiltration. Biotechnology and Bioengineering 55:737-746.

van Reis R, Leonard LC, Hsu CC, Builder SE. 1991. Industrial-scale harvest of proteins from mammalian-cell culture by tangential flow filtration. Biotechnology and Bioengineering 38:413-422.

van Reis R, Zydney A. 2007. Bioprocess membrane technology. Journal of Membrane Science 297:16-50.

vandezande P, Gevers LEM, Paul JS, Vankelecom IFJ, Jacobs PA. 2005. High throughput screening for rapid development of membranes and membrane processes. Journal of Membrane Science 250:305-310.

Wenger MD, DePhillips P, Braceivell DG. 2008. A microscale yeast cell disruption technique for integrated process development strategies. Biotechnology Progress 24:606-614.

Wenger MD, DePhillips P, Price CE, Bracewell DG. 2007. An automated microscale chromatographic purification of virus-like particles as a strategy for process development. Biotechnology and Applied Biochemistry 47:131-139.

Wier, A.N.C. and Bailey, N.A. 1997. Process for obtaining antibodies utilizing heat treatment. United States Patent 5665866

Wiley DE, Fletcher DF. 2003. Techniques for computational fluid dynamics modelling of flow in membrane channels. Journal of Membrane Science 211:127-137.

Woo SC, Anton PJM. 2001. Direct chemical extraction of a recombinant viral coat protein from *Escherichia coli* at high cell density. Biotechnology and Bioengineering 75:451-455.

Yamasaki H, Lee MS, Tanaka T, Nakanishi K. 1993. Characteristics of crossflow filtration of Pullulanbroth. Applied Microbiology and Biotechnology 39:26-30.

Yavorsky D, Blanck R, Lambalot C, Brunkow R. 2003. The clarification of bioreactor cell cultures for biopharmaceuticals. Pharmaceutical Technology, p 62-70.

Yigzaw Y, Piper R, Tran M, Shukla AA. 2006. Exploitation of the adsorptive properties of depth filters for host cell protein removal during monoclonal antibody purification. Biotechnology Progress 22: 288-296.

Zaman F, Allan CM, Ho SV. 2009. Ultra scale-down approaches for clarification of mammalian cell culture broths in disc-stack centrifuges. Biotechnology Progress 25:1709-1716.

Appendices

Appendix 1

This section has the cited Appendices from **Chapter 2.**

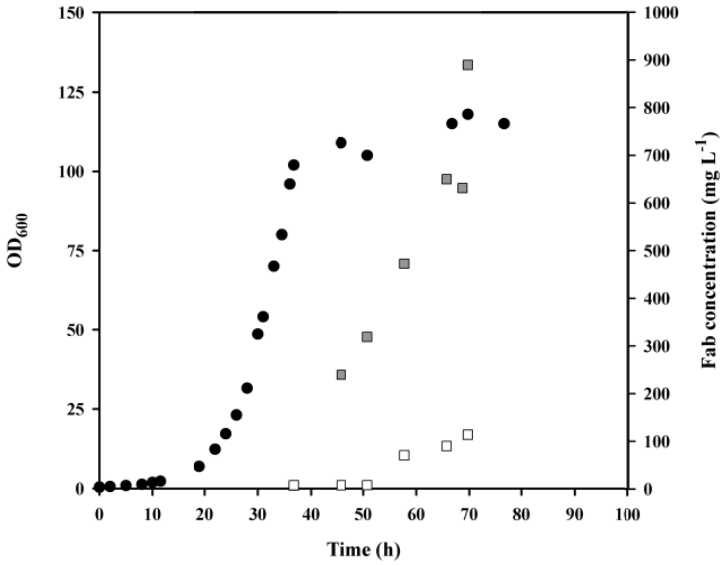

Appendix 1.1 Fermentation profile during production of antibody Fab' fragments from *E.coli*. Filled circles are biomass. Squares are concentrations of Fab' inside the cell (filled) and Fab' fragments excreted in the medium.

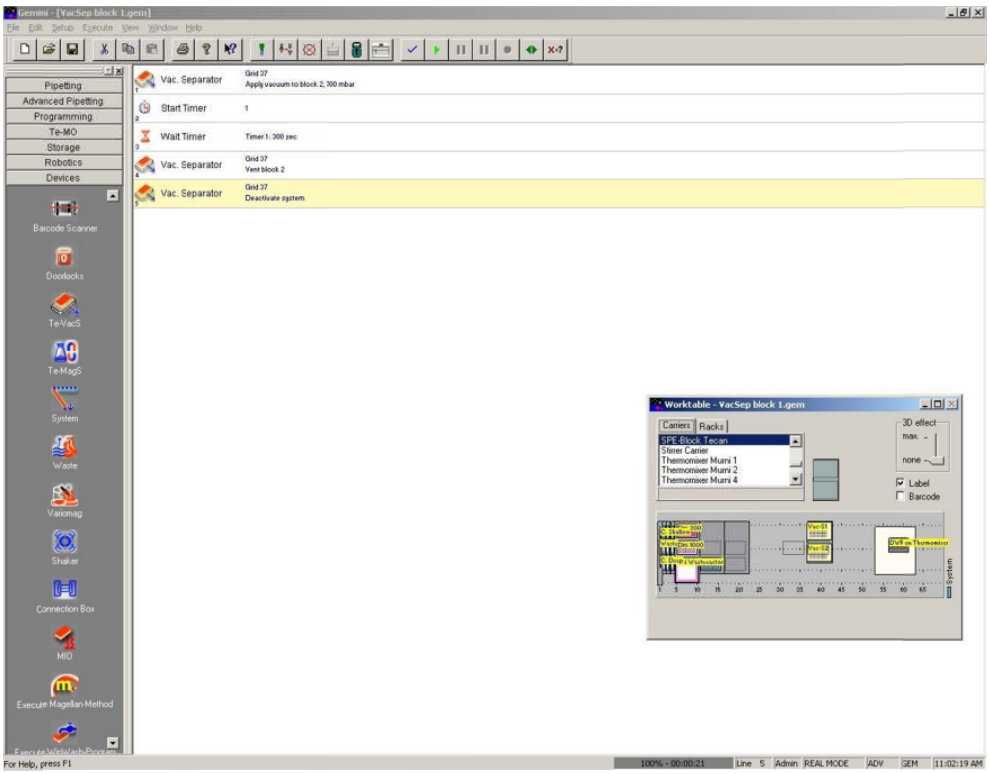

Appendix 1.2 Sample Tecan Gemini™ program for the automated operation of the vacuum separator (Te-VacS) on the deck of the Tecan.

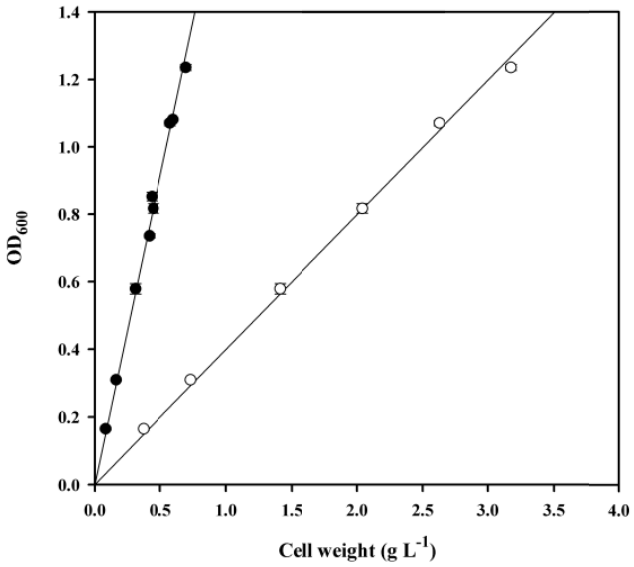

Appendix 1.3 Optical density measurements corresponding to dry cell (●) and wet cell (○) concentrations.

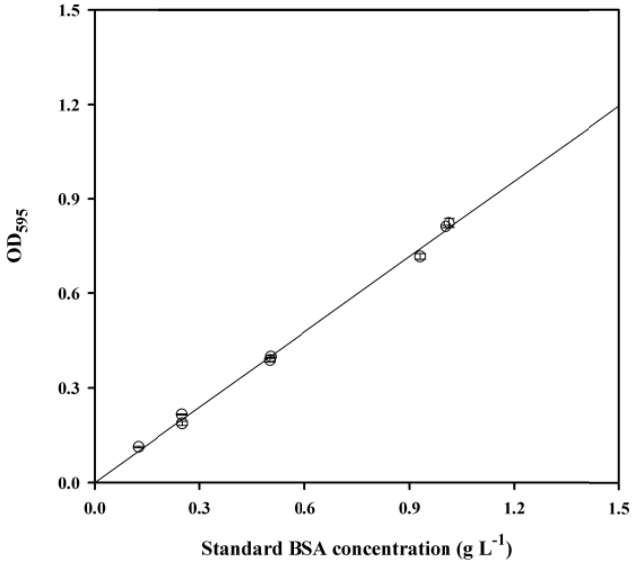

Appendix 1.4 Typical total protein calibration curve.

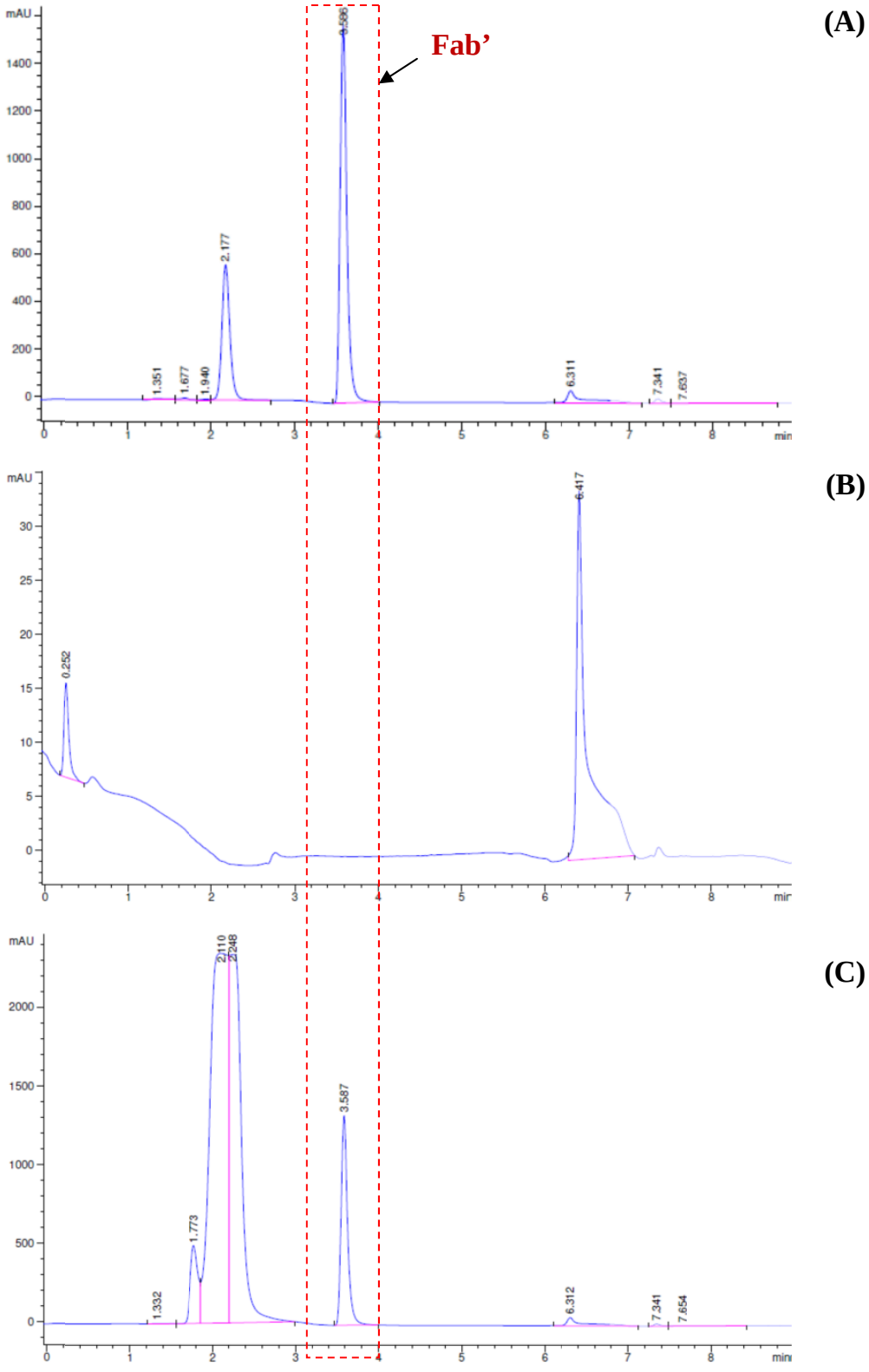

Appendix 1.5 Typical chromatograms of: (A) Fab' standard prepared by and according to Tustian (2008); (B) blank sample composed of the binding buffer 20 mM sodium phosphate at pH 7.4 ; and (C) Fab' lysate from thermo-chemical extraction.

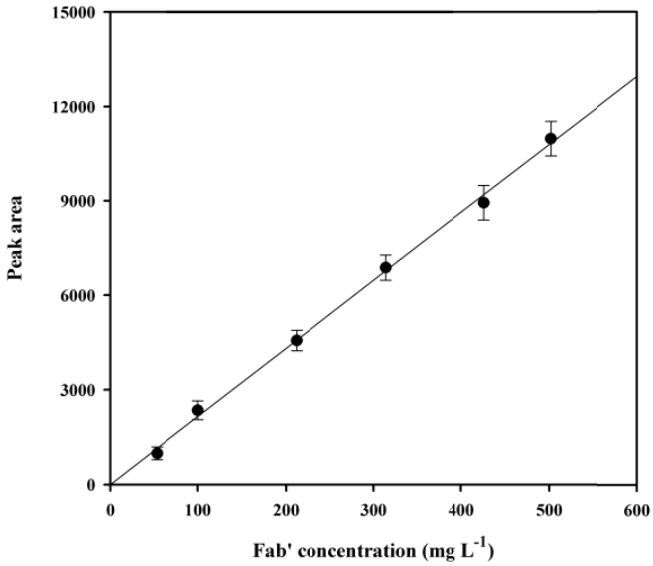

Appendix 1.6 Typical calibration curve of the Fab' standard.

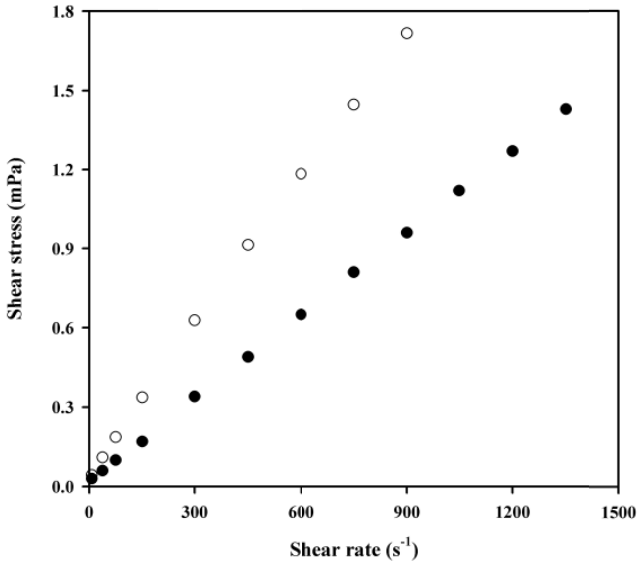

Appendix 1.7 Typical shear stress-shear rate curve showing a linear relationship (r^2>0.95) which depicts Newtonian fluid behaviour. Samples are from freeze-thawed cells with concentrations of 15% (●) and 30% (○) wet cell weight (w/w).

Appendix 2

This section has the cited Appendices from **Chapter 5.**

Appendix 2.1 Estimation of Pellicon-2™ dimensions

Parameter	Pellicon-2™ Mini (V-screen)
Total membrane area (cm^2)	1000
Nominal width (cm)	5.6
Channels per device	5*
Membranes per device	10*
Active membrane length (cm)	16.5
Total active membrane width (cm)	60*

$$Total\ active\ membrane\ width = \frac{Total\ membrane\ area}{Active\ membrane\ length} = \frac{1000}{16.5} = 60$$

$$Number\ of\ channels = \frac{Total\ active\ membrane\ width}{Nominal\ width \text{ x } 2} = \frac{60}{5.6\ x\ 2} = 5$$

$$Membranes\ per\ device = No.channels \text{ x } 2\ (Parallel\ membranes) = \ 10$$

Appendix 2.2 Momentum balance to derive Equation 5.13

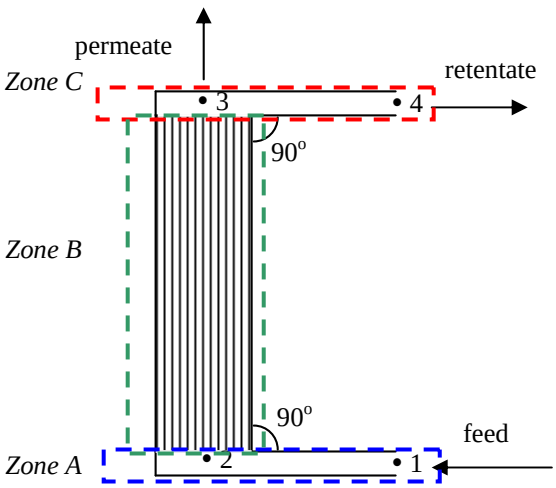

For flow through channels (rectangular ducts) where flow is against gravity, the Bernoulli equation appears as:

$$\frac{p_2}{\rho_2}+\frac{\upsilon_2^{\,2}}{2}+gz_2=\frac{p_3}{\rho_3}+\frac{\upsilon_3^{\,2}}{2}+gz_3+l_f \qquad\qquad l_{f.straight}=\frac{2f\upsilon^2L}{D}$$

Assumption: density is constant, thus volumetric flowrates are $Q_2 \sim Q_3$, so that velocities are $v_2 \sim v_3$.

$$\frac{p_2}{\rho_2}=\frac{p_3}{\rho_3}+gz_3+\frac{2f\upsilon_2^{\,2}L}{D}$$

Assume flow is laminar (Hagen-Poisuille): $$f=\frac{16}{\mathrm{Re}_H}=\frac{16}{\frac{\rho\upsilon D}{\mu}}=\frac{16\mu}{\rho\upsilon D}$$

β is the angle between the duct axis and horizontal (in this case 90°);

$$-(\sin\beta)L=z_3 \quad ; \quad \frac{p_2}{\rho_2}=\frac{p_3}{\rho_3}+gz_3+\frac{2f\upsilon_2^{\,2}L}{D} \quad ; \quad \frac{p_2-p_3}{\rho_F}+g(\sin\beta)L=\frac{2\left(\frac{16\mu_F}{\rho_F\upsilon D}\right)\upsilon^2L}{D}$$

$$\frac{p_2-p_3}{\rho_F}+g(\sin\beta)L=\frac{2\left(\frac{16\mu_F}{\rho_F D}\right)\left(\frac{Q}{\pi D^2/4}\right)L}{D}=\frac{128\mu_F QL}{\rho_F\pi D^4}$$

$$\frac{p_2 - p_3}{\rho_F} + g(\sin\beta)L = \frac{128\mu_F QL}{\rho_F \pi D^4}$$

for laminar flow: $D=D_E$, equivalent diameter

$$D_E = \left(\frac{128ab^3}{\pi C}\right)^{1/4}$$

Therefore:

$$\frac{p_2 - p_3}{\rho_F} + g(\sin\beta)L = \frac{128\mu_F QL}{\rho_F \pi\left(\left(\frac{128ab^3}{\pi C}\right)^{1/4}\right)^4}$$

$$\frac{\Delta P_{axial}}{\rho_F} + g(\sin\beta)L = \frac{\mu_F QL}{\frac{\rho_F ab^3}{C}}$$

$$\frac{\Delta P_{axial}}{\rho_F} + g(\sin\beta)L = \frac{\mu_F QLC}{\rho_F ab^3}$$

$$b = \left[\frac{\mu_F QLC}{\rho_F a\left(\frac{\Delta P_{\text{axial}}}{\rho_F} + g(\sin\beta)L\right)}\right]^{1/3}$$

Since β=90°C; sinβ=1 and setting b=h then it can be re-written as:

$$h = \left[\frac{\mu_F QLC}{\rho_F a\left(\frac{\Delta P_{\text{axial}}}{\rho_F} + gL\right)}\right]^{1/3}$$

which is the equation shown in Equation 5.13.

Appendix 3

This section has the cited Appendices from **Chapter 6.**

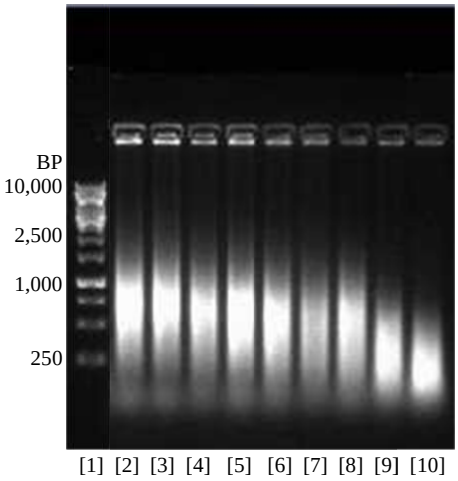

Appendix 3.1 Agarose gel showing the hydrolysis by Benzonase® of chromosomal DNAs in freeze-thawed homogenised (30% w/w) *E. Coli* cells: Lanes: [1] – MW marker ; [2, 3] freeze-thawed Control; [4,5] 3X BNase; [6] 6X BNase; [7] 9X BNase; [8] 12X BNase; [9] 15X BNase; [10] 30X BNase. Homogenisation performed according to Section 2.3.2. DNA hydrolysis according to Section 6.3.1. DNA sample preparation according to Section 2.9.6. Agarose gel performed according to Section 2.9.7. BP – base pairs.

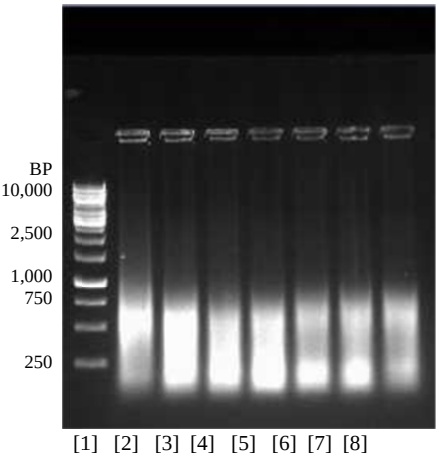

Appendix 3.2 Agarose gel showing the hydrolysis by Benzonase® of chromosomal DNAs in freeze-thawed homogenised (15% w/w) *E. Coli* cells: Lanes: [1] – MW marker ; [2] freeze-thawed Control; [3] 3X BNase; [4] 6X BNase; [5] 9X BNase; [6] 12X BNase; [7] 15X BNase; [8] 30X BNase. Homogenisation performed according to Section 2.3.2. DNA hydrolysis according to Section 6.3.1. DNA sample preparation according to Section 2.9.6. Agarose gel performed according to Section 2.9.7. BP – base pairs.

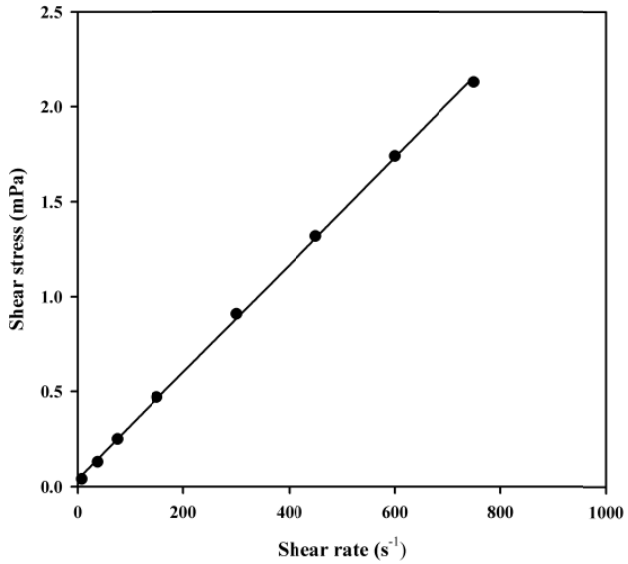

Appendix 3.3 An example of a shear stress-strain plot used as basis for determining absolute viscosities in Figure 6.4. Sample is fresh Control, homogenised according to Section 2.3.3. Rheological properties were measured according to Section 2.10.2

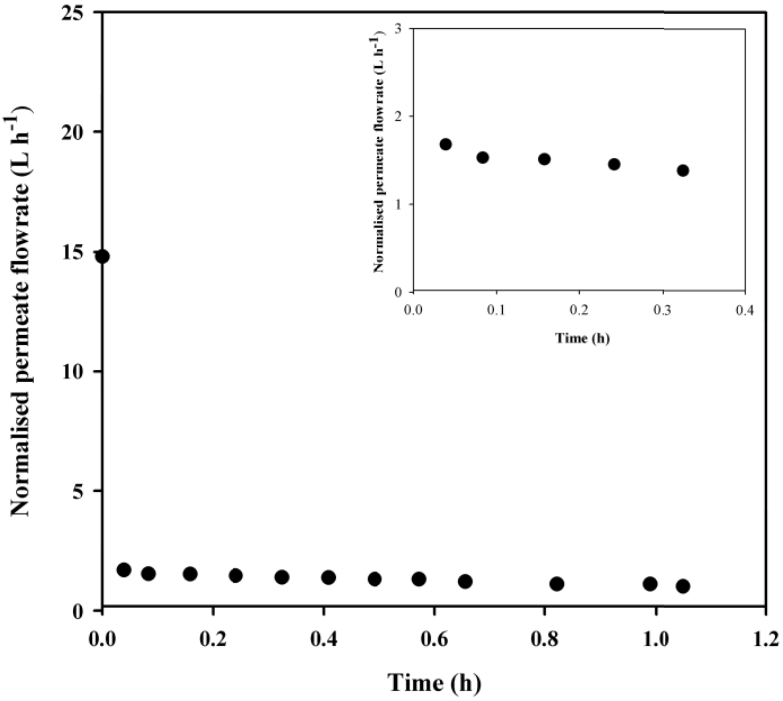

Appendix 3.4 Typical permeate flowrate data from lab-scale crossflow microfiltration experiments withSNase. Crossflow rate = 80 L h^{-1}, ΔP_{TM} = 22 kPa, A_m = 0.1 m^2 using 0.22μm PVDF membrane. Experiments were performed as described in Section 2.7.2. Data points were calculated using Equation 2.3.

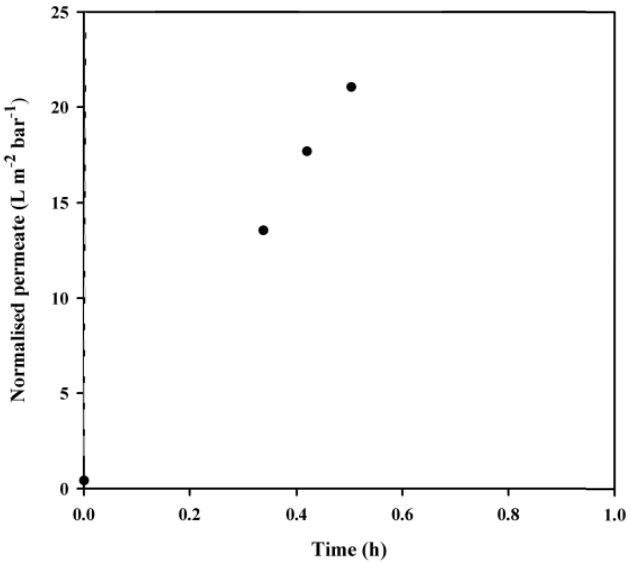

Appendix 3.5 Cumulative permeate data from microscale crossflow microfiltration experiments with SNase (Channel 2). Crossflow rate = 14 L h^{-1}, $\Delta P_{TM.ave}$ = 22 kPa, A_m = 0.001 m^2 using 0.22μm PVDF membrane. Dashed line (near Y-axis) is water flux line.